A GENERALIZED SOLUTION TO THE THIN-WIRE ELLIPTICAL-CYLINDRICAL HELICAL-BEAM ANTENNA PROBLEM

by

AYORINDE, AYOTUNDE ABIMBOLA

B.Sc. (Hons.), M.Sc., MIET

A Thesis submitted to the School of Postgraduate Studies

University of Lagos for the award of the degree of

Doctor of Philosophy (Ph.D.) in Electrical Engineering

Supervisors –

Professor S.A. Adekola; Professor of Electrical Engineering, C. Eng., FAS, FIET, FASA, FNSE, FAEng.

Dr. A.I. Mowete; Associate Professor of Electrical Engineering, MNSE

Department of Electrical & Electronics Engineering
University of Lagos, Lagos, Nigeria

2008

SCHOOL OF POSTGRADUATE STUDIES
UNIVERSITY OF LAGOS

CERTIFICATION

This is to certify that the Thesis:

"A GENERALIZED SOLUTION TO THE THIN-WIRE ELLIPTICAL-CYLINDRICAL HELICAL-BEAM ANTENNA PROBLEM"

Submitted to the
School of Postgraduate Studies
University of Lagos

For the award of the degree of
DOCTOR OF PHILOSOPHY (Ph. D)
is a record of original research carried out

By

AYORINDE, AYOTUNDE ABIMBOLA
in the Department of Electrical & Electronics Engineering

AYORINDE, AYOTUNDE ABIMBOLA		11/12/2008
AUTHOR'S NAME	SIGNATURE	DATE
PROF S.A. ADEKOLA		11.12.08
1ST SUPERVISOR'S NAME	SIGNATURE	DATE
IKE MOWETE		11/12/2008
2ND SUPERVISOR'S NAME	SIGNATURE	DATE
OLUWOLE ADEGBENRO		11 12 08
1ST INTERNAL EXAMINER	SIGNATURE	DATE
PROF MUSBAU A. SALAU		11-12-2008
2ND INTERNAL EXAMINER	SIGNATURE	DATE
PROF. G.A. ADEGBOYEGA		11/12/08
EXTERNAL EXAMINER	SIGNATURE	DATE
FASHANU, T.A (Dr.)		11/12/08
SPGS REPRESENTATIVE	SIGNATURE	DATE

© Copyright by

AYORİNDE, Ayotunde Abimbola

2008

Dedication

TO MY PARENTS

BISIRIYU OLABODE AYORINDE (OF BLESSED MEMORY),

AND

WINIFRED AKANKE AYORINDE

for their love and very highly appreciated sacrifices towards my education.

A GENERALIZED SOLUTION TO THE THIN-WIRE ELLIPTICAL-CYLINDRICAL HELICAL-BEAM ANTENNA PROBLEM

by

AYORINDE, AYOTUNDE ABIMBOLA

B.Sc. (Hons.), M.Sc., MIET

Abstract

This thesis develops a generalized formulation, based on the electromagnetic potential theory and the thin-wire concept, of the radiation problem of thin-wire elliptical-cylindrical helical-beam antenna, which, heretofore, had been unavailable in the open literature. The generalized formulation enunciated embodies an integro-differential operator equation, which links an incident plane electromagnetic field to the distribution of induced current on the helical arm in the formulation of the radiation integrals for the elliptical-cylindrical helical-beam antenna. A generalized solution of the problem is effected through the use of a powerful analytical tool (the method of moments) in conjunction with the Galerkin procedure. It is shown that the generalized solution immediately extends over the analytical and numerical treatments of the radiation problems associated with eight fundamental thin wire antenna configurations, namely, circular helix, planar helix (zig-zag structure), multi-turn elliptical loop, single-turn elliptical loop, multi-turn circular loop, single-turn circular loop, vertical linear element and horizontal linear element. In other words, the solutions of the problems of thin-wire antennas of regular geometrical shapes have been brought under one umbrella.

A systematic application of the generalized solution to the problem of a novel "exclusion-mode" helix, in which the conventional ground plane is excluded from the feeding arrangement, clearly reveals the important roles played by the components featuring in the conventional feeding mechanisms of helical antenna, via comparative analyses. In particular, it is demonstrated

that when the helical antenna is fitted on a small ground plane modelled by wire grids; the resulting composite antenna is typified by lower input impedance, higher input power, and improved radiation characteristics, when compared with the exclusion case. This suggests, therefore, that the small wire-grid ground plane serves not only as a counterpoise for the helix antenna, but also to enhance antenna performance characteristics.

Further applications of the generalized solution facilitate novel characterizations of centre-fed helix, loop-backed helix, as well as a helix mounted on a large ground plane, which constitutes the original helical antenna problem, as formulated by Kraus, (1947).

In addition, the thesis extends the generalized solution to the analysis and design of planar array of helical antennas, towards providing a radiation-pattern-shaping procedure, of interest to practical applications requiring specific pattern directivity performances. It is noteworthy that the validity of the generalized solution is established through comparison with various published results on special cases.

Acknowledgements

First, I want to express my profound appreciation to Professor Sulaiman Adeniyi Adekola, who, not only suggested the topic, but also painstakingly supervised the research work reported in this thesis; it was the Professor that nurtured my fledgling career in academics by encouraging me to stay in the university system after my Masters degree programme in 1992. In addition to giving free access to his rich library, he also generously allowed me to use his personal office for the first two years of my employment by the University of Lagos (Unilag), which was a rare privilege. It is worthy of note that he provided me with residential accommodation on campus for seven continuous years, thereby ensuring my rapid integration into the university system. For all these good gestures and for his fatherly roles since the demise of my father 1993, I remain most grateful to him.

Next, it is a great pleasure to thank Dr. Alex Ike Mowete, who co-supervised the thesis. Remarkably, he introduced me to the field of electromagnetics when he taught my class Electric and Magnetic Fields in 1987 at the Department of Electrical Engineering, University of Lagos (Unilag). He later supervised my final-year project, and since then, had taken me as his family member to the extent that he funded the production of eighty copies of the application for approval for title of thesis and supervisors submitted to the Postgraduate School. Sir, I thank you most sincerely for thoroughly co-supervising my thesis and also for your regular counsel to me.

It is with deep gratitude that I acknowledge the contributions of Professor Kanmi Aderogba, formerly a Professor of Mathematics at the University of Lagos, but now of the University of Cambridge, England, for his guidance, support and counsel on several occasions. To say the least, I greatly valued our interactions while in Unilag, and your continued interest in my career. My indebtedness also goes to Dr. O.U. Okereke of Abubakar Tafawa Balewa University (ATBU) Bauchi, for facilating my National

Service at the ATBU, and more importantly, for providing the computer subroutines utilized for my M.Sc. research work.

After thanking my academic advisers, I am obliged to show my sincere gratitude to Mr. Ephraim Oluwatogbekele Agunbiade (1922 1992) of blessed memory, who shaped my outlook towards life during my formative years by way of strict discipline and daily preaching of the word of God. As fondly called, Master, may your gentle soul continue to rest in perfect peace, amen.

I must not forget to mention a number of families that supported me in various forms since my arrival in Lagos 1984. These include the Lawals, Idowus, Oyelowos, Adebayos, Okelolas, Adeseyojus and the Abioyes. While carrying out Ph.D. research work, I received regular encouragement, of which I am very grateful, from the following persons: Engr. & Mrs. S.A. Adetunji, Mr. & Mrs. E.A. Raji, Dr. & Mrs. R.O. Masha, Mr. & Mrs. T.W. Carrena, Engr. & Mrs. Ayo Cardoso, Sir Ladi Sowemimo, Mrs. E.A. Adeola, and my darling aunty, Mrs. Doyin Odunuga.

My full appreciation goes to all members of staff of the Department of Electrical & Electronics Engineering, Unilag, for their cordial and rewarding relationships with me. I am also obliged to some members of the 1990 graduating set of the Department of Electrical Engineering, Unilag, (of which the author was one) who have continued to maintain close contact with me. In particular, Seyi Makinde, who has been of great assistance to me, Raymond Wilcox (Head of Class), Akinlabi Olawuni, Bayo Salami, Niyi Idowu, Deroju Animashaun, Segun Odukomaiya and Leke Banjo.

I must thank the Council of the University of Lagos for granting scholarships for the last two years of my undergraduate programme as well as for my Masters programme. For the same reason, I hereby express my deep gratitude to Professor Ayinla Adewunmi Abioye of blessed memory who provided the funds with which I commenced my Masters degree programme.

To my sister Laide Oyelami and my brother Yemi Ayorinde, I express heartfelt gratitude your constant assistance. Melvin Onuoha, my former student, deserves special mention for furnishing a copy of the W.T. Patton's Ph.D. thesis on "*The Backfire Bifilar Helical Antenna*" which facilitated the validation exercise of the numerical results reported in my thesis. To a colleague and close friend. Dr. Akin Fashanu, I thank you for your willingness to help always.

Mrs. A.M. Adetunji will always retain a special place in my thoughts for her genuine interest and concern in all aspects of my life; I am deeply grateful "mummy".

This section will be incomplete without the expression of my special thanks to my wife, Shereefat Adebisi Ayorinde (nee Dawodu), for her constant support and unwavering understanding in the course of my Ph.D. work. I also extend my gratitude to my father-in-law R.O. Dawodu and my mother-in-law Y.O. Dawodu, as well as my brothers-in-law and sisters-in-law, for their keen interest in me.

On a final note, I thank *ALLAH* most beneficent and most merciful for giving me the strength and perseverance to complete my Ph.D. research work in spite of numerous challenges, and several trying developments.

A.A Ayorinde, B.Sc.(Hons.), M.Sc.

The University of Lagos

December 2008.

TABLE OF CONTENTS

	Page
Title Page	i
Certification	ii
Dedication	iii
Abstract	iv
Acknowledgements	vi
Table of Contents	ix
List of Symbols	xii
List of Tables	xiv
Table of Abbreviations	xv
List of Illustrations	xvi
Chapter 1: INTRODUCTION	1
1.1 Background	1
1.2 Statement of the Research Problem	6
1.3 Solution Methodology	7
1.4 Aims and Objectives	7
1.5 Significance of the Study	8
1.6 Research Questions	9
1.7 Organization of the Thesis	10
Chapter 2: LITERATURE REVIEW	12
2.1 Cylindrical helical antennas	12
2.2 Multi-filar helical antennas	20
2.3 Arrays of helical-beam antennas	22

2.4 Non-cylindrical helical antennas 23

Chapter 3: GOVERNING EQUATIONS OF ELLIPTICAL -CYLINDRICAL HELICAL-BEAM ANTENNA 25

3.1 Integrodifferential operator equation of elliptical-cylindrical helical-beam antenna 25

3.2 Specializations of the integrodifferential operator equation to regularly-shaped thin-wire antennas 33

3.3 Electromagnetic radiation integrals of elliptical-cylindrical helical-beam antenna 37

3.4 Specializations of the radiation integrals to regularly-shaped thin-wire antennas 41

Chapter 4: METHOD OF SOLUTION AND ANTENNA DESIGN PARAMETERS 47

4.1 Method of Solution 47

4.2 Antenna Directivity 51

4.3 Side-lobe Level of Radiation Patterns 51

4.4 Input Impedance and Input Power 52

4.5 Front-to-back ratio (F/B) and Axial Ratio (AR) 52

4.6 Directive Gain and Half-Power Beam-Width (HPBW) 53

Chapter 5: COMPUTATIONAL RESULTS AND DISCUSSIONS 54

5.1 Radiation Characteristics of the Novel 'Exclusion-Mode' Helical-Beam Antenna 54

5.2 Input Parameters and Radiation Properties of Helical-Beam

Antenna mounted on a Wire-Grid Ground Plane 64

5.3 Comparison of the Numerical Results with various Published Data 76

Chapter 6: HELICAL-BEAM ANTENNAS MOUNTED ON A LARGE GROUND PLANE 87

6.1 A Helical-Beam Antenna Mounted on a Large Ground Plane: a reconsideration of Kraus' original problem 88

6.2 Planar Array of Helical-Beam Antennas Mounted on a Large Ground Plane 97

Chapter 7: CONCLUSIONS 116

7.1 Summary of Research Findings 116

7.2 Contributions to Knowledge 119

7.2 Recommendations for Future Work in this Area 119

7.3 Concluding Remarks 120

Appendix I: Some Published Papers from the Thesis

I(a): **A rigorous analysis of the radiation characteristics of helical-beam antennas** 121

I(b): **Analysis of helical-beam antennas backed by co-axial parasitic loops** 132

I(c): **Effects of centre-excitation on the radiation mechanism of helical antennas employed in communication satellites** 149

I(d) **Exclusion of ground planes in thin-wire helical antennas** 170

Appendix II: FORTRAN 77 Computer Programs for Thin-Wire Antenna Designs 187

References 233

List of Symbols

ω: angular frequency

ℓ: axial length variable

ρ: charge density

$\bar{J}$: current density

∇: del (or grad) operator

G_d: directive gain

D: directivity of the antenna

R: distance between the source point and the field point

ε: eccentricity

$\bar{E}$: electric field intensity

C_λ: electrical circumference

dv': element of volume of radiating structure

β: excitation phase

T_k: expansion (basis) functions

$\rho(\ell')$: filament of charge

$I(\ell')$: filamentary current

η_o: free-space intrinsic impedance

μ_o: free-space permeability

ε_o: free-space permittivity

k_o: free-space propagation constant

f: frequency

$[Z_{jk}]$: generalized impedance matrix

$[V_j]$: generalized voltage matrix

$\overline{E}^i$: incident electric field

P_{in}: input power

X_{in}: input reactance

R_{in}: input resistance

$\Im$: integro-differential operator

d_e: inter-element spacing (separation)

$\overline{H}$: magnetic field intensity

N: number of turns

λ: operating wavelength

$\bar{r}$: position vector to the far-field point

$\bar{r}'$: position vector to the source point

Φ: scalar electric potential

$\overline{E}^s$: scattered electric field

a: semi-major axis length

b: semi-minor axis length

α_k: superposition coefficients

δ: time-phase difference between field components

$\overline{E}^t$: total electric field

$\hat{a}$: unit vector

Hz: unit of frequency

$\overline{A}$: vector magnetic potential

W_j: weighting (testing) functions

r_w: wire radius

List of Tables

Page

Design Table I: *Computed values of directivities, half-power beamwidths and interelement separations at minimum sidelobe strengths for 2 x 2, 3 x 3 and 4 x 4 helical arrays.* 114

Design Table II: *Calculated values of directivities, half-power beamwidths and sidelobe levels of pencil beams for 2 x 2, 3 x 3 and 4 x 4 helical arrays.* 115

Design Table III: *Maximum directivities and corresponding sidelobe strengths and half-power beamwidths of radiation patterns for 2 x 2, 3 x 3 and 4 x 4 helical arrays.* 115

Table of Abbreviations

Abbreviation	Full Meaning
AF	Array Factor
AR	Axial Ratio
CWTA	Contra-Wound Toroidal Helical Antenna
DMC	Disaster Monitoring Constellation
EFIE	Electric Field Integral Equation
EMA	Exclusion Mode Antenna
F/B	Front-to-Back Ratio
FEM	Finite Element Method
GPS	Global Positioning System
HF	High Frequency
HPBW	Half-Power Beam-Width
INMARSAT	International Maritime Satellite
MoM	Method of Moments
MPIE	Mixed Potential Integral Equation
NEC	Numerical Electromagnetic Codes
SLL	Side Lobe Level
WGA	Wire Grid Antenna
QHA	Quadrifilar Helical Antenna
CWTA	Contra-Wound Toroidal Helical Antenna
NOAA	National Oceanic and Atmospheric Administration
VHF	Very High Frequency
S/N	Signal to Noise ratio
IEEE	Institute of Electrical and Electronics Engineers

List of Illustrations

Page

Figure 2.1: *Microwave traveling-wave tube with wire-helix as a guiding structure* 13

Figure 2.2: *A typical feeding arrangement for helical-beam antennas* 14

Figure 3.1: *A typical turn of the thin-wire helical antenna* 27

Figure 3.2: *(a) An elliptical helical antenna; (b) The cross-section of the elliptical helical antenna* 29

Figure 3.3a: *Specializations of elliptical helix to four regular geometries* 32

Figure 3.3b: *Specializations of elliptical helix to four other regular geometries* 32

Figure 4.1: *Typical expansion triangle functions (a) and their first derivatives (b)* 49

Figure. 5.1 : *Current distributions on the exclusion-mode helical antenna: $C_\lambda = 0.80 - 0.95$* 56

Figure 5.2: *Current distributions on the exclusion-mode helical antenna: $C_\lambda = 1.00 - 1.15$* 56

Figure 5.3a: *Normalized field patterns of the helical antenna without a ground plane: $\alpha = 10^o$ and C_λ:0.80 - 0.95.* ——— E_θ component ----- E_φ component 58

Figure 5.3b: *Normalized field patterns of the helical antenna without a ground plane: $\alpha = 10^o$ and C_λ:1.00- 1.15.* ——— E_θ component ----- E_φ component 58

Figure 5.4a: *Normalized field patterns of the helical antenna without a ground plane: $\alpha = 15^o$ and C_λ:0.80 -0.95* ——— E_θ component ----- E_φ component 59

Figure 5.4b: *Normalized field patterns of the helical antenna without a ground plane: $\alpha = 15^o$ and C_λ : 1.00 - 1.15.* ——— E_θ component ----- E_φ component 59

Figure 5.5: *Input impedance against helix electrical circumference (C_λ)* 60

Figure 5.6: *Input power versus helix electrical circumference (C_λ)* 61

Figure 5.7: *Axial ratio (dB) against helix electrical circumference (C_λ)* 62

Figure 5.8: *Front-to-back ratio (F/B) versus helix electrical circumference (C_λ)* 62

Figure 5.9: *Directive gain (dB) against C_λ* 63

Figure 5.10: *Half-power beam-width (HPBW) versus helix electrical circumference (C_λ)* 63

Figure 5.11: *Modelling of a solid ground plane by wire grids.* 65

Figure 5.12: *(a) The problem geometry of a helical antenna backed by a finite ground plane; (b) The finite ground plane modelled by wire grids* 65

Figure 5.13: *Input impedance of WGA and EMA against frequency* 69

Figure 5.14: *Input power of WGA and EMA against frequency* 69

Figure 5.15: *Front-to-back ratio (F/B) (numeric) of WGA and EMA versus Frequency* 70

Figure 5.16: *Axial ratio (dB) of WGA and EMA versus frequency* 71

Figure 5.17: *Directive gain (dB) of WGA and EMA versus frequency* 72

Figure 5.18: *Half-power beam-width (degrees) of WGA and EMA versus frequency* 73

Figure 5.19: *Current distributions on the WGA and EMA* 74

Figure 5.20: *Electric fields radiated by WGA and EMA: $\hat{\theta}$ component (a), (b): $\hat{\varphi}$ component (c), (d).* 75

Figure 5.21a: *Comparison of current magnitude of a centre-fed helical antenna at 500MHz: – – – –: Present theory (MoM); ————: Chen's theory (FS) and o o o o : Experimental results at 500MHz of Fig. 6(a), page 182, of Chen (1967)* 77

Figure 5.21b: *Comparison of current phase of a centre-fed helical antenna at 500MHz: – – – –: Present theory (MoM); ————: Chen's theory (FS) and o o o o : Experimental results at 500MHz of Fig. 6(a), page 182, of Chen (1967)* 77

Figure 5.22a: *Comparison of current magnitude of a centre-fed helical antenna at 600MHz: – – – –: Present theory (MoM); ————: Chen's theory (FS) and o o o o : Chen's Experimental results at 600MHz of Fig. 6(b), page 182, of Chen (1967)* 78

Figure 5.22b: *Comparison of current phase of a centre-fed helical antenna at 600MHz: – – – –: Present theory (MoM); ————: Chen's theory (FS) and o o o o : Chen's Experimental results at 600MHz of Fig. 6(b), page 182, of Chen (1967)* 78

Figure 5.23a: *Comparison of current magnitude of a centre-fed helical antenna at 750MHz: – – – –: Present theory (MoM); ————: Chen's theory (FS) and o o o o : Experimental results at 750MHz of Fig. 6(c), page 182, of Chen (1967)* 79

Figure 5.23b: *Comparison of current phase of a centre-fed helical antenna at 750MHz: – – – –: Present theory (MoM); ————: Chen's theory (FS) and*

o o o o o : Experimental results at 750MHz of Fig. 6(c), page 182, of Chen (1967) 79

Figure 5.24a: *$E_\theta(\theta, \varphi = 0^o)$ component: ————: computed pattern (Present MoM theory); ----------: measured pattern (Patton 1963)* 81

Figure 5.24b: *$E_\varphi(\theta, \varphi = 0^o)$ component: ———computed pattern (Present MoM theory); ---------: measured pattern (Patton 1963)* 82

Figure 5.25: *Current distribution on the helix backed by a small ground plane (pitch angle = 14°, frequency = 8.5GHz)* 83

Figure 5.26: *Current distribution on the helix backed by a small ground plane (pitch angle = 14°, frequency = 9.0GHz)* 84

Figure 5.27: *Current distribution on the helix backed by a small ground plane (pitch angle = 14°, frequency = 10.0GHz)* 84

Figure 5.28a: *Comparison of E_θ components of the radiated field of a helical antenna backed by small ground plane.; ————: Present theory; o o o o o o : radiation pattern of Nakano et al. (1988) (Fig. 5), page 1362.* 85

Figure 5.28b: *Comparison of E_φ components of the radiated field of a helical antenna backed by small ground plane.; ————: Present theory; o o o o o : radiation pattern of Nakano et al. (1988) (Fig. 5), page 1362* 86

Figure 6.1: **(a)** *The original problem of a monofilar helical antenna mounted on an infinite ground plane;* **(b)** *The equivalent problem when the image theory is invoked* 87

Figure 6.2a: *Current distributions on helical beam antenna above an infinite ground plane* 90

Figure 6.2b: *Current distributions on helical beam antenna above an infinite ground plane* 90

Figure 6.3a: *Electric fields radiated by helical beam antennas mounted on an infinite ground plane in the $\varphi=0^o$ plane. - - - - -:E_φ, ———: E_θ* 92

Figure 6.3b: *Electric fields radiated by helical beam antennas mounted on an infinite ground plane in the $\varphi=0^o$ plane. - - - - -:E_φ, ———: E_θ* 92

Figure 6.3c: *Electric fields radiated by helical beam antennas mounted on an infinite ground plane in the $\varphi=0^o$ plane. - - - - -:E_φ, ———: E_θ* 93

Figure 6.3d: *Electric fields radiated by helical beam antennas mounted on an infinite ground plane in the $\varphi=0^o$ plane. - - - - -:E_φ, ———: E_θ* 93

Figure 6.4: *Input impedance versus C_λ* 94

Figure 6.5: *Input power against C_λ* 95

Figure 6.6: *Axial ratio versus C_λ* 96

Figure 6.7: *Directive gain against C_λ* 96

Figure 6.8: *Half-power beam-width versus C_λ* 97

Figure 6.9: *Planar array of helical antennas* 99

Figure 6.10a: *Current distribution on the arm length of 8-turn, 12° helix antenna* 100

Figure 6.10b: *Radiation patterns on $\varphi = 0°$ (x - z) plane of 8-turn, 12° helix antenna - - - - - -:E_φ ————:E_θ* 101

Figure 6.11: *(a) 2 x 2 helical array; (b) 3 x 3 helical array; (c) 4 x 4 helical array* 102

Figure 6.12a: *Normalized array factors of 2 x 2, 3 x 3, and 4 x 4 helical array antennas. — — —:2 x 2; :3 x 3; ————: 4 x 4.* 103

Figure 6.12b : *Normalized array factors of 2 x 2, 3 x 3, and 4 x 4 helical array antennas. — — —:2 x 2; :3 x 3; ————: 4 x 4.* 104

Figure 6.13a: *Radiation patterns (on the x-z plane) of a 2 x 2 helical array : - - - - - -: E_φ ————:E_θ* 106

Figure 6.13b: *Radiation patterns (on the x-z plane) of a 2 x 2 helical array: - - - -: E_φ ————:E_θ* 107

Figure 6.14a: *Radiation patterns (on the x-z plane) of a 3 x 3 helical array: - - - -:E_φ ————:E_θ* 108

Figure 6.14b: *Radiation patterns (on the x-z plane) of a 3 x 3 helical array : - - - -: E_φ ————:E_θ* 109

Figure 6.15a: *Radiation patterns (on the x-z plane) of a 4 x 4 helical array: - - - -: E_φ ————:E_θ* 110

Figure 6.15b: *Radiation patterns (on the x-z plane) of a 4 x 4 helical array: - - - -: E_φ ————:E_θ* 111

Figure 6.16a: *Side-lobe levels as a function of interelement spacing (d_e)* 112

Figure 6.16b: *Half-power beam-widths versus the interelement spacing (d_e)* 113

Figure 6.16c: *Directivities against the interelement spacing (d_e)* 114

Chapter 1

INTRODUCTION

1.1 Background

It was the Scottish mathematician and physicist, James Clerk Maxwell, who in 1864, published the celebrated classical paper ***"A dynamical theory of the electromagnetic field"*** that first predicted the radiation of electromagnetic energy by conductors carrying high-frequency currents. After the successful experimental verification of Maxwell's theory, in 1887, by Heinrich Hertz, (Schrank 1986), science began the systematic exploitation of the conducting wire, as a radiator of electromagnetic energy. Hertz, in that pioneering experiment, demonstrated that high-frequency electromagnetic oscillations can be detected by an arrangement consisting of a large loop and a thin-wire element. A decade later, Pocklington (1897) published what became the first recorded analytical treatment of the electromagnetic behaviour of thin wires, in which the currents induced on arbitrarily shaped perfectly conducting wires by an incident electric field were evaluated using the Hertzian potentials.

The classical thin-wire theory thus developed by Pocklington was subsequently successfully applied to the solution of various thin-wire antenna problems, including the notable contributions of Kornhauser (1951) who addressed the circular helix problem, the planar helix problem solved by Sengupta (1958); and the multi-turn circular loop antenna problem, which Taylor and Harrison (1974), successfully addressed in 1974. Various extensions to Pocklington's theory have, over the years been developed, and these include that described by Tsandoulas (1969), for the analysis of elliptical loop antenna, Adekola's (1983) standing- and traveling-wave current distribution approach to the solution of circular-loop antenna problem, and the treatments given by Harrington (1961), on one hand, and Stutzman and Thiele (1981), on the other hand, to the respective problems of vertical and horizontal linear wires. Of those aforementioned

thin-wire antenna geometries, that of primary interest to this thesis is the helix, whose discovery as a versatile antenna did not emerge until shortly after the Second World War (1939-1945).

Prior to World War II, the practical utility in radio communication systems, of the conducting helical structure was confined to microwave tubes where it functioned not only as a waveguide but also as a conducive medium for interactions between electron beams and electromagnetic waves of reduced velocity, for the purpose of microwave amplification, (Pierce and Field 1947). However, in 1946, Kraus explored the possibility of using wire helix outside the microwave tubes, and was able to practically demonstrate that it can efficiently radiate circularly polarized electromagnetic beams in the axial direction, when its normalized circumference equals unity, at the operating frequency. These circularly polarized waves were found to be less adversely affected by variations in atmospheric/ionospheric conditions, and less susceptible to multi-path distortion in high-frequency (HF) applications, (Cooper 2001). For these reasons, the helical coil found immediate practical applications as antennas in satellite communications as well as in terrestrial transmitting/receiving systems, (Kraus 1950). More recent application areas of the helical antennas include the Global Positioning Systems (GPS) (Tranquilla and Best 1990), the Global Systems for Mobile Communications (GSM), (Rowley *et al.* 2002), and in landmines detection, (Leat 2002). It is worthy of note that the NigeriaSat-I satellite (launched in 2003) and the other micro-satellites in the Disaster Monitoring Constellation (DMC) to which it belongs, are all equipped with planar array of two quadrifilar helical antennas and two microstrip patch-antennas (Williamson 2002).

Traditionally, the helical-beam antenna as originally conceived and designed by Kraus in 1946 was excited by a feed arrangement consisting of a coaxial cable and a large ground plane, which essentially acts as a counterpoise for mounting the antenna

structure. In addition, the conducting plane served to prevent the flow of current to the outer conductor of the feeding coaxial cable (Markov 1965), and as a wave reflector.

The nature of the current distribution on the helical-beam antenna was first investigated by Kraus and Williamson (1948), who through a comprehensive analysis of the outcomes of experimental measurements, came to the conclusion that the distribution of current on the helical arm could be reasonably approximated by an equivalent uniform travelling wave, whose phase velocity is less than the free-space velocity of light. This conclusion received corroboration from Marsh (1951), who undertook extensive measurements of current distributions on a uniform circular helix, fitted to a large ground plane, and operating within the frequency band extending from 600MHz to 1700MHz.

Using Kraus' empirical current distribution as basis, Kornhauser (1951), derived rigorous formulas for the radiation fields of an axial-mode circular helix *via* the retarded vector potential approach. Kunsden (1952) followed Kornhauser's approach, and obtained expressions for the radiation fields of a square helical-beam antenna, which is particularly well-suited for practical applications in the Very High Frequency (VHF) regime. In their contribution, Wong and Loh (1959) gave an approximate analytical solution to the electromagnetic radiation problem of an elliptical helical antenna, again using the retarded vector potential method, but in this case, with Kraus' experimentally determined current distribution as basis. An extension of Kornhauser's work to include the normal-mode helical antenna has since been provided by Roy (1969).

Although the contributions of the early researchers in antenna theory as described by the representative examples of the foregoing discussions, provided tremendous insight and useful practical design equations, the problem of obtaining exact solutions by specifying the precise nature of the distribution of electric currents responsible for the radiation, remained unresolved. Measurement results were inherently

inexact because measuring instruments drew from the same currents being measured; and closed-form solutions were not available because the governing integro-differential equations did not admit analytical solutions. Attention therefore turned to finding numerical solutions to the problem, and one of the more successful quasi-numerical methods was provided by the *'reaction concept'*, which was developed by Victor Rumsey (1954). Jack Richmond (1965) extended this variational approach to what become known as the *'sinusoidal reaction integral'* method, a purely numerical method, which produced excellent results. Arguably the best computational method, the method of moments (MoM) was introduced by Roger Harrington (1967) in 1967, and it provided a means of obtaining very good numerical approximations to the distribution of current for all antenna types, including thin-wire antennas of interest to this presentation.

As a consequence of its versatility, the method of moments (MoM) (Harrington 1968), which, as earlier mentioned, makes possible the determination of approximate generalized current distribution for antenna structures, has been applied, as analytical tool, for the numerical solution of different antenna problems, including that of the helical-beam antenna. Chow *et al* (2001), for example, investigated the frequency response of a monopole antenna parasitically coupled to a normal-mode helix, while Nakano *et al* (1998) studied the radiation properties of an antenna system composed of a normal-mode helix and a monopole with the objective of enhancing the bandwidth of the monopole antenna. The first MoM analysis of the interesting problem of a spiral antenna excited through a helical wire mounted on a large ground plane is credited to Nakano *et al* (2003). And in a related development, Nakano *et al* (1988), using the MoM as the analytical tool, studied the effects of varying the ground plane (modelled by wire grids) diameter on the radiation patterns of a monofilar (single-wire) helical antenna, and successfully demonstrated that when the diameter of the ground plane is of

the same order of magnitude as the helix diameter, the helix radiates mainly in the backfire direction. Nakano and his associates did not however, consider the limiting case, in which the ground plane is excluded in the feeding scheme as well as other possible roles played by the small ground plane both of which considerations are of interest to several practical applications. All the numerical solutions provided in the publications cited in the foregoing discussions were based on the commercial version of the Numerical Electromagnetic Codes (NEC), (Miller and Burke 1992), a FORTRAN source code written from the governing integro-differential operator equation, which connects the incident electric field to the associated distribution of current induced on the antenna, through a MoM formulation and solution. Because these procedures were not readily adaptable to the rigorous analysis of the difficult elliptical-cylindrical helical-beam antenna, no NEC-based solution of that problem has been reported in the open literature. Wong and Loh (1959), however provided an approximate analytical solution, which restricted considerations to the elliptical helix of small eccentricity, that is, the essentially near-circular helix case.

The research work described in this thesis recognizes the geometry of the elliptical-cylindrical helix as representing a geometry from which other regular geometries derive. The thesis consequently proposes to solve the thin-wire elliptical-cylindrical helical-beam antenna problem, as a general case of thin-wire antenna design. In effect, the generalized solution obtained for the elliptical helix will become applicable to other regular thin-wire antenna (including non-cylindrical helical) geometries through simple specializations. Indeed, the solution, as demonstrated in Chapter 3, not only encompasses those for the problems of the thin-wire circular helix, planar helix, and multi-turn elliptical loop, but also those of horizontal and vertical thin-wires, as well as circular- and elliptical-loop thin wires. Furthermore, the systematic application of the generalized solution provides novel designs of single-element and

planar array of helical-beam antennas deployable in terrestrial and satellite communication systems.

1.2 Statement of the Research Problem

Heretofore, it has been conventional practice to analyze different thin-wire antenna geometries, either analytically, using assumed (usually harmonic) current distributions, or numerically through the use of the Method of Moments (MoM) (Harrington 1968) or Finite Element Methods (FEM) (Volakis *et al.* 1998). No attempt has been made, to the best of our knowledge, to develop a general solution (and associated source codes), for which the regular thin-wire geometries will represent special cases. This research work consequently sets out to develop such a generalized solution, using the elliptical-cylindrical helical-beam antenna as a candidate. The generalized formulation of the elliptical-cylindrical helical antenna problem developed in this thesis gives the connection between the incident electric field and the induced current on the helical arm *via* an integrodiffrential operator equation, as well as the electromagnetic radiation integrals of the antenna. After very clearly demonstrating that existing solutions for all thin-wire antennas (Kornhauser 1951, Harrington 1961, Harrington and Mautz 1968), are indeed special cases of the general solution so developed, it is further shown that the generalized formulation is particularly applicable to the hitherto unresolved problem of the '*exclusion-mode*' helical-beam antenna, through which a comparative analysis will identify all effects that may be attributable to ground-plane size in the classical structure, and hence provide more design options. The research work also considers an extension of the formulation, to considerations concerning the analysis and design of planar array of helical antennas, towards providing a radiation-pattern-shaping procedure, of interest to applications requiring specific pattern directivity performances.

1.3 Solution Methodology

Towards obtaining a generalized solution to the radiation problem of elliptical-cylindrical helical-beam antenna addressed in this thesis, the powerful analytical method of moments due to Harrington (1968) is adopted. This method provides an approximate generalized solution for the unknown current distribution featuring in the linear integrodifferential operator equation that characterizes the antenna problem. The starting point is a discretization of the wire helix, followed by a series expansion of the unknown current in terms of unknown superposition coefficients and piece-wise linear functions, each of which is defined over four consecutive segments of the wire helix. A substitution of this series representation of the current into the governing equation and the enforcement of the linearity property of the operator leads to an equation, which, upon performing an inner product operation on it with the weighting functions yields a matrix equation physically interpretable in terms of the generalized network parameters. In view of the computational benefits of the Galerkin procedure (Harrington 1968) in which the expansion and weighting functions are identically defined, this procedure is utilized in our solution methodology. The unknown current is then determined through the solution of a matrix equation in terms of generalized network parameters. Of course, with the full knowledge of the distribution of current on the wire helix, the determination of the radiation fields as well as important antenna design parameters becomes a relatively straightforward matter.

1.4 Aims and Objectives

The important outcomes expected on the completion of the research, and which consequently constitute the research objectives are itemized below, as follows.

i. Development of a more general solution to the radiation problem of thin-wire helix problem, which can be specialized for the analytical treatments of other thin-wire antennas of conventional shapes.

ii. Specialization of the general solution to the cases of some fundamental, regular wire antenna geometries such as: circular helix, planar helix, multi-turn elliptical and circular loops, single-turn elliptical and circular loops, as well as the linear dipole.

iii. Utilization of the general solution for the designs of single-element helical-beam antennas excited with different feeding mechanisms. Essentially, design curves will be generated for helical-beam antennas when excited without a ground plane, and when backed by a small ground plane modeled by wire grids, a large ground plane, and parasitic circular loops.

iv. Extension of the solution to single-element helix problem to a rectangular planar array of helical antennas invoking the pattern multiplication theorem of antenna array.

v. Compilation of computer simulation programs, using the FORTRAN 77 programming language, for the generation of antenna design profiles for the helical-beam, and other thin-wire antennas.

1.5 Significance of the Study

In the main, the thesis will for the first time, develop a rigorous solution of the thin-wire helical-beam antenna problem, using the most general geometry, that is, the elliptical cylindrical helix, which accommodates all other regular geometries in common use. When this solution is adapted for use in the analysis of planar arrays of helical antennas, such issues, of importance to several practical applications, as the determination of optimum side-lobe levels and directivities of 2 x 2, 3 x 3, and 4 x 4

arrays, will be satisfactorily addressed, also for the first time, to the best of our knowledge. Because the theory developed is of a more general nature than hitherto available, it becomes possible to systematically examine (again for the first time) the characteristic features of the single-element antenna, whose feed arrangement does not include a ground plane, and which is of important practical utility in such applications as feeds for paraboloidal dishes routinely deployed for satellite communications applications. Furthermore, the solution of the 'exclusion-mode' helix problem will evidently make additional design options available to the antenna engineer.

1.6 Research Questions

The thesis will address the following important research questions, which still remain unanswered in the open literature.

a. Is it possible to exploit the generalized nature of the elliptical cylindrical helix geometry for the development of a generalized solution to thin-wire antenna problems?

b. Can the some hitherto unknown contributions of size of ground-plane (characteristic of classical helical-beam antenna types) be identified by studying the effects of excluding a ground plane from the feeding mechanism of a monofilar helical antenna? If so, what design options do these contributions offer?

c. At what loop circumference can a parasitic array of identical loops backing a monofilar helix still be regarded as an effective reflector of backward-end-fire (backfire) radiation?

d. At what height above a wire-grid ground plane does a circular/square loop antenna resonate, and what is the corresponding input resistance at resonance?

e. What respective values of inter-element separations of (2 x 2, 3 x 3, and 4 x 4) arrays of helical antennas yield optimum side-lobe levels, directivities, and half-power beam-widths (HPBWs)?

1.7 Organization of the Thesis

This thesis comprises seven chapters with three appendices. The first Chapter describes the background to the thesis where representative research works closely related to the thrust of the thesis are discussed and unresolved problems consequently identified, thus leading to a clear statement of the research problem. Also presented in this Chapter is the solution methodology employed to solve the main research problem posed in the thesis, and its key contributions to knowledge of importance.

Previous research works, beginning from 1897, on the helical structures and of particular interest to the thesis are reviewed in Chapter 2, under four broad sub-headings, namely: cylindrical helical antennas, multi-filar helical antennas, arrays of helical-beam antennas and non-cylindrical helical antennas. The fairly comprehensive review of these literature items in that chapter enables a clear definition of those contributions to the existing body of knowledge, that the thesis proposes to make. In Chapter 3, an integrodifferential operator equation formulation of the problem of the elliptical-cylindrical helical-beam antenna is presented. After derivation of the radiation field integrals for the antenna, the expressions are specialized to thin-wire antennas of regular geometrical shapes. Chapter 4 focuses on the method of solution employed for the generalized integrodifferential operator equation, which approach is the method of moments as formalized by Harrington (1968). A discussion is also given in that chapter, on how this solution relates to the important antenna design parameters.

Numerical solutions of two important helical beam antenna problems, which serve as antenna performance metrics, concerning the radiation characteristics of the

novel exclusion-mode helical-beam antenna and the input parameters and radiation properties of helical-beam antennas mounted on a wire-grid ground plane are provided in Chapter 5. A comparison of numerical results obtained here with published numerical and experimental results in the open literature is also given in this Chapter as means of validating the formulation and associated solution. Chapter 6 presents the computational data deriving from the numerical solutions of the problem of a helical-beam antenna mounted on a large ground plane as well as that of planar array of helical-beam antennas mounted on a large ground plane. A summary of findings of the research effort is provided in Chapter 7, along with the concluding remarks.

The Appendix provided for the thesis has two sections including appendix I, where reprints of a number of publications arising from the research are presented, and Appendix II, which contains the Fortran 77 Computer Programs (source codes), with which numerical data were compiled.

Chapter 2

LITERATURE REVIEW

A comprehensive review of previous studies on the electromagnetic properties of straight wire antennas starting with the pioneering work of Pocklington (1897) and extending to other wire antenna structures over succeeding years to the present-day is presented here with the main goal of identifying some possibilities for making contributions to the body of literature materials on helical-beam antennas, in particular. This review is divided into the four sections itemized below in order to underscore the applicability of the generalized approach developed in the thesis:

(i) cylindrical helical-beam antennas,

(ii) multi-filar helical antennas,

(iii) arrays of helical-beam antennas, and

(iv) non-cylindrical helical antennas.

We now start with the first category which is the cylindrical helical-beam antenna.

2.1 Cylindrical helical-beam antennas

The formal study of the electromagnetic behaviour of helical wire structures may be said to have essentially begun in 1897, when Pocklington analytically addressed the problem of wave propagation along a circular helix, using an integro-differential equation formulated for electrical oscillations excited in perfectly conducting arbitrarily shaped thin wires. Analytical results obtained from that pioneering research work revealed that at low frequencies, the phase velocity of the traveling wave in the axial direction along a uniform circular helix is approximately equal to the free-space velocity of light; and that at high frequencies, this axially directed phase velocity is the product of the sine of the helix pitch angle and free-space velocity of light. This electromagnetic property of the circular helix informed its practical utility in the

microwave tubes, (Pierce and Field 1947), where it functioned not only as a slow-wave device, but also as a means of guiding electromagnetic waves through an electron tube for the purpose of microwave amplification, as schematically depicted in Figure 2.1 below.

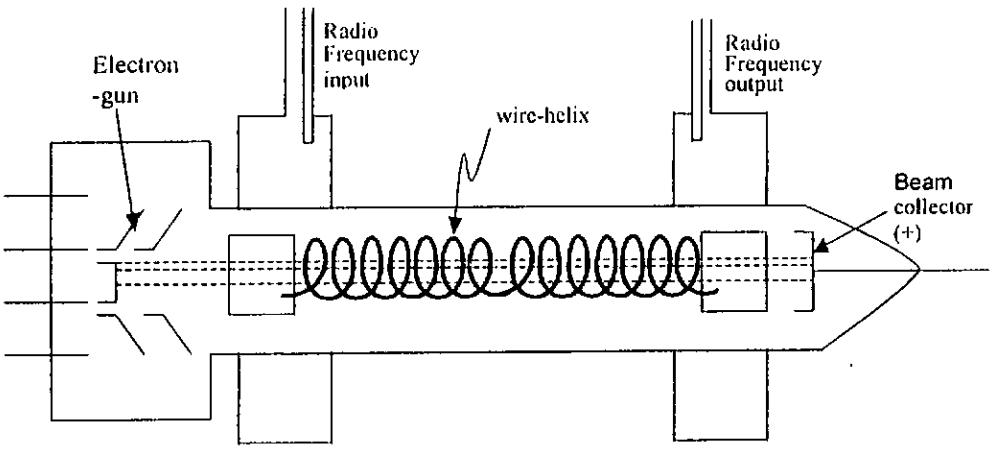

Figure 2.1: *Microwave traveling-wave tube with wire-helix as a guiding structure (Pierce and Field 1947).*

In 1946, Kraus, working at the Ohio State University, USA, demonstrated through carefully designed experiments that a circular cylindrical helix with a circumference of one wavelength (at the operating frequency) radiates predominantly and efficiently in the axial direction. Although this discovery of the helix as an electromagnetic radiator was made in 1946, the first publication on the helical antenna reported in the open literature appeared in 1947, when Kraus described the performance features of the axial-mode helix (Kraus 1947). The feeding arrangement employed by Kraus for the excitation of that axial-mode helix involved the connection of the inner conductor of a coaxial cable to the helix while the cable's outer conductor was terminated on a large ground plane (Figure 2.2).

Wheeler (1947), working independently, discovered another radiation mode of helical antenna, which came to be known as the 'normal mode', and which is

characterized by maximum radiation in a plane normal to the helix axis. The normal-mode helix, which can be adequately modelled as a superposition of electric and

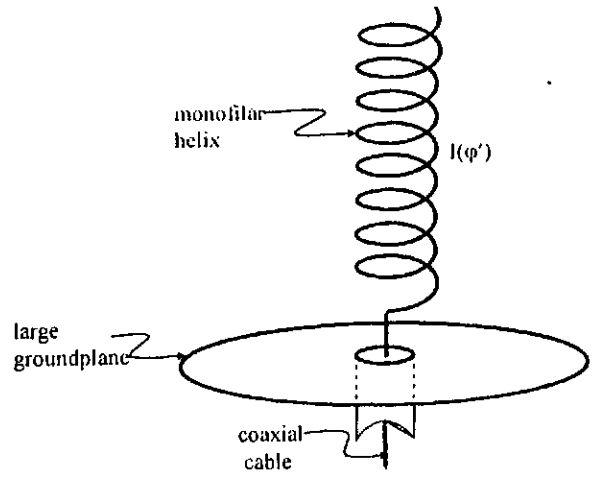

Figure 2.2: *A typical feeding arrangement for helical-beam antennas*

magnetic dipoles (Wheeler 1947), has a ratio of cross sectional area to the pitch angle that is equal to the radian-length ($\lambda/2\pi$), where the symbol λ denotes the operating wavelength. Wheeler highlighted the conditions of equal intensity and time-phase quadrature of the cross fields, as being necessary for the helix to be circularly polarised; as well as the potential use of the small helical antenna for television signal reception because of its immunity to echoes from reflecting surfaces.

Apart from the normal and axial modes of the helix antenna, there exists another mode known as the conical mode typified by a radiation pattern that resembles a cone, whose generating axis coincides with the helix axis (Kraus and Williamson 1948). Analytical and experimental results have clearly demonstrated that for the different helical antenna modes, characteristic mode radiation patterns are obtained under different conditions identified as follows, (Kraus 1988);

- <u>normal mode</u> for C less than 0.50λ;

- axial mode for C between 0.75λ and 1.3λ; and
- conical mode for C greater than 1.3λ

where the symbol C represents the electrical circumference of the helix. Of these three modes, the axial mode is the most widely used because of its stable input properties and directional characteristics over a broad frequency band (Kraus 1988). The axial-mode is also referred to as the beam-mode in the literature.

Following the discovery of the axial-mode helical antenna by Kraus, concerted efforts towards fully understanding the electromagnetic behaviour of the antenna were made by his associates at the Antenna Laboratory (later ElectroScience Laboratory) of the Ohio State University, Columbus, Ohio, USA. First, Kraus and Williamson (1948) derived approximate expressions for the far-field of the circular helix modelled as an array of loops, and using the pattern multiplication theorem to obtain the total field pattern of the array. Their investigation utilized the simplifying assumption of a travelling-wave current distribution, whose phase velocity is slightly less than the free-space velocity of light, and the approximate field expressions obtained yielded radiation patterns that compared favourably with the measured results. Second, Glasser and Kraus (1948) presented the results of an extensive experimental study of the effects of frequency, pitch angle, number of turns, diameter, and spacing, on the terminal impedances of circular helical-beam antenna mounted on a ground plane. Their results suggested that the input impedance of the helix is relatively constant over a wide frequency band in the axial mode. Third, results of further experimental work on axial-mode helix by Kraus (1948), revealed that when mounted on a ground plane, the helix performed optimally at the operating frequency of 400 MHz, when its pitch angle is 14 degrees and its number of turns equals six.

As part of his doctoral research work on long cylindrical conductors, Marsh (1951) carried out extensive measurements of the current distributions along the arm of

the uniform circular helix supported by a large ground plane, and operated in the frequency band (600 - 1700) MHz. The results of the analysis of the measurement data supported Kraus' earlier notion that for a helix operating in the axial mode, the excitation current can be adequately approximated by a single unattenuated outward travelling wave of reduced phase velocity. Adopting the vector potential approach and using Kraus' empirically determined current distribution, Kornhauser (1951) derived rigorous formulas for the radiation field of a circular helix, while Knudsen (1952) investigated the radiated fields of a square helical-beam antenna. The field patterns for the square helix obtained from Knudsen's computations were in reasonable agreement with the previous results due to Kraus and Williamson's (1948) approximate method of analysis. A number of other numerical solution techniques have been developed for the analysis of helical beam antennas, (Chen 1967, Nakano and Yamauchi 1982, Nakano *et al.* 1983), and these techniques, which avoided the use of Kraus' empirical current distribution, gave very good results and significant insight. For example, Chen (1967) developed a Fourier series solution of the integral equation describing the radiation characteristics of a centre-fed helical antenna, and obtained results that compared favorably with his own experimental measurements. On the other hand, Nakano and Yamauchi (1982) utilized the point matching technique to solve the integral equation of helical antenna tapered at the open end, which showed that the axial ratio of the radiated field is enhanced by increasing the cone angle. In a related effort, Nakano *et al* (1983) presented the numerical solution of an integral equation characterized by a simplified kernel and developed for an antenna system comprising a rectangular spiral antenna and a parasitic helix acting as a director of the radiated field. Through an application of the Mei's (1965) integral equation for thin wires, Nakano and Yamauchi (1980) determined the current distributions on a driven short helix in the presence of a parasitic helix. The

associated numerical analysis of an axial-mode helical antenna showed that the use of parasitic helix wound diametrically opposite to that of 1½ turns of the driven helix, results in an increase of the antenna gain by 1dB (Nakano *et al.* 1986). Various other thin-wire antenna problems have been solved over the years, through the use of different analytical tools, a good number of them being computer-aided tools. Representative examples include the radiation problem of a circular helix that was considered by Kornhauser (1951), the planar helix problem addressed by Sengupta (1958), and the multi-turn circular loop problem solved by Taylor and Harrison (1974). Others are the analysis of an elliptical loop antenna credited to Tsandoulas (1969), the circular loop problem comprehensively discussed by Adekola (1983), the problem of the vertical linear dipole, to which Harrington (1967) applied the method of moments, and that of the horizontal linear dipole solved by Stutzman and Thiele (1981).

One important publication of particular relevance to this thesis is that of Wong and Loh (1959), who analyzed the electromagnetic radiation problem of the elliptical helical antenna based on the assumption of a uniform traveling-wave distribution of current on the helical arm. In addition to the limitation due to the assumption of current distribution, the results obtained by Wong and Loh were restricted to those of the elliptical helix of small eccentricity which depends on the length of semi-major axis and the length of the semi-minor axis. As pointed out in the background to the research work, the elliptical helix is geometrically, a versatile shape for which the common circular helix, planar helix (zigzag shape), multi-turn elliptical and circular loops, single-turn elliptical and circular loops, as well as vertical and horizontal linear elements are all special cases. It is therefore conceivable that the solution of the problem of elliptical cylindrical helix of arbitrary eccentricity, pitch angle, and number of turns, will simultaneously provide solutions for all these other special geometrical cases. The thesis therefore sets out to develop a generalized solution to the problem of

electromagnetic radiation from the elliptical cylindrical helical antenna and hence, to these special cases, when appropriate specialization conditions are invoked. It is to be noted in that connection, that hitherto, the aforementioned antenna types have enjoyed individual analytical treatments. As examples, the radiation problem of circular helix was solved by Kornhauser (1951), that of the planar helix by Sengupta (1958), and the multi-turn circular loop by Taylor and Harrison (1974). Furthermore, the introduction of the method of moments (MoM), a versatile analytical technique for solving antenna problems, eliminated the restriction of assumed current distributions, because remarkably performing approximate generalized current distributions for virtually all antenna types and shapes became available. Successful applications of the method of moments to the solution of radiation problems include that of the problem of a short helix located on an infinite ground plane, (Nakano and Yamauchi 1980), and of a short helix backed by a conical cavity, (Nakano and Mimaki 1995). Nakano *et al.* (1988), using that analytical tool, studied the effects of ground plane size on the radiation characteristics of helical antennas. In that effort, it was established, by modeling the ground plane by wire grids, that when the diameter of the ground plane equals 0.29 wavelength, backward radiation predominates. However, the important scenario in which the ground plane is completely absent from the feed structure (equivalent to a ground plane of zero diameter, as the limiting case) was not considered. Preliminary results obtained in the research work very clearly indicate that when it can be arranged to feed a helical-beam antenna using a feed arrangement that does not include a ground plane (here designated the *'exclusion-mode helix'*) certain other design options become available (Adekola *et al.* 2001). These design options should be readily observed through a comparison of the performance characteristics of the exclusion mode helix with those of other helical antennas, whose feed structures include a ground plane. The

more prominent of these other feeding arrangements are identified in the itemized list that follows.

(i) Using a large ground plane and a coaxial cable as the feeding components (Kraus 1947), for which the helix radiates in the forward direction.

(ii) Backing the helix with a small wire-grid ground plane (Nakano *et al.* 1988), which leads to radiation in the backfire direction.

(iii) Slitting the outer conductor of the coaxial cable and using it to cover a full turn of the helix while the inner conductor is bonded to the helix (Munk and Peters 1968) to obtain a forward end-fire radiation pattern.

(iv) Using a cylindrical cavity as the backing structure (King and Wong 1980), and consequently obtaining radiation in the forward direction.

(v) Including a conical cavity as the launching structure (Carver 1967 and Nakano *et al.* 1995); which, again, gives radiation in the forward direction.

(vi) Winding the helix on a conducting cylinder (Johnson and Cotton 1984), leading to a backfire radiation pattern in the far-zone.

(vii) Terminating the outer conductor of the coaxial cable on a short conductor positioned on the helix axis and connecting the inner conductor to the helix (Patton 1963), which became another method for producing a backfire radiation pattern.

(viii) Etching the helix on a dielectric-coated cylinder and exciting the helix at its geometrical centre (Sun *et al.* 2004), with the result that the radiation pattern is multi-lobed.

(ix) Using an array of circular loops (instead of the usual ground plane) as the backing structure (Kraus 1995, Adekola *et al.* 2006), and obtaining radiation in the forward end-fire direction.

(x) Using a rectangular spiral antenna to excite a parasitic helix (Nakano *et al* 1983); this also produces a forward end-fire radiation.

(xi) Placing a normal mode helix symmetrically within a driven loop of a larger diameter (Abd-Alhameed and Excell 1999), leading to a broadside radiation pattern.

(xii) Mounting the helical antenna on a corrugated reflector (Nakano *et al* 2005), with the result that the antenna radiates in the forward end-fire direction.

Because the feeding components in these arrangements can be modeled by thin wires of regular geometrical shapes, it is apparent that the generalized formulation developed by the thesis will facilitate the generation of new design data for helical-beam antennas.

2.2 Multi-filar helical antennas

Although this review of the open literature has thus far focused attention principally on monofilar (one-wire) helical antennas, it is of interest to point out that helical antennas constructed with more than one wire have found many useful practical applications (Leach *et al.* 2000), (Letestu and Sharaiha 2006). Published analytical treatments of these (multifilar) antenna types include the inspiring experimental work of Holtum Jr. (1960), who interlaced two monofilar helices to obtain a bifilar helix, which had two separate feeds, in addition to a phasing device placed beneath a ground plane. Patton (1963), in a doctoral dissertation, formulated the governing integral equation for a bifilar helix, and utilized the Fourier transform technique for the solution of the equation. The results obtained by Patton were validated through a comparison with his measured data. Unlike the Holtum-bifilar helix, the Patton-bifilar helix radiates principally in the backward-end-fire (backfire) direction, because as pointed out by Walter (1970), the phase velocity of waves on the helical wires in the latter is directed

towards the feed point whereas the group velocity is directed away from the feed point in the former. Although the primary goal of Patton's thesis was the analytical determination of electromagnetic radiation from backfire bifilar helical antennas, a method of feeding a monofilar helix without a ground plane was described and some experimentally obtained radiation patterns were provided.

Using a numerical method, Nakano *et al.* (1983) showed that the front-to-back ratio (an important antenna design parameter) of a bifilar backfire helix can be considerably reduced by tapering only the feed end, and that the use of a bridging resistor at the terminating ends, to suppress the reflected currents, leads to an enhancement of both the front-to-back ratio and axial ratio of the bifilar helix (Nakano *et al.* 1982). A detailed study of frequency characteristics of tapered bifilar helical antenna terminated by a resistor has revealed, (Nakano *et al.* 1984), that the antenna is characterised by almost constant input impedance, a low front-to-back ratio and an improved axial ratio. On the other hand, flaring of the open end of a bifilar backfire helix (Nakano *et al.* 1993) rather than terminating the open ends with a resistor gives rise to an enhanced front-to-back ratio and approximately constant input impedance. The scanning capability of a bifilar helical antenna, having a small diameter but a large pitch angle, from the backfire direction to normal direction has been demonstrated when the phase velocity of the travelling wave on the helical structure equals the free-space velocity of light (Zimmerman 2002).

Other versions of multifilar helix, which have been deployed for use in many communication systems, include the quadrifilar (four-wire) helical antenna (QHA) invented by Kilgus (1969) and the octafilar (eight-wire) contra-wound helical antenna conceived by Gerst and Worden (1966). The QHA is a highly resonant antenna that appears well-suited for Global Positioning System (GPS), (Tranquilla and Best 1990), mobile communications, (Sharaiha and Terret 1993), GPS in the marine environment,

(Shumaker 1996), and for satellite-terrestrial mobile communications, (Letestu and Sharaiha 2006). The design and fabrication of intelligent brand of quadrifilar helix antenna for the third generation (3G) mobile handset has been published by Leach *et al* (2000). Recently, genetically optimized sleeve quadrifilar helix antenna, which comprises a normal-mode quadrifilar helix and four vertical parasitic wires all mounted on a large ground plane, characterized by a large bandwidth, has been proposed for mobile communication systems, (Rogers and Butler 2002). And the octafilar helical antenna whose design parameters (bandwidth, gain and polarization) can be independently controlled, finds applications not only in military communications, space telemetry and tracking, but also in broadcast television and frequency modulated radio communication, (Gerst and Worden 1966). It is important to note that one other contribution of this thesis is the fact that the generalized theory can be easily adapted for use in the investigation of the performance characteristics of multifilar antennas because they are usually constructed with thin wires.

2.3 Arrays of helical-beam antennas

In many applications, antennas mounted on satellite platforms are required to generate highly directive radiation patterns and possess scanning capabilities, which make the single-element helical antennas inefficient for satellite communications. The conventional solution to the problem is to deploy an array of helices arranged in a manner dictated by the requirements of the intended applications. Historically, Kraus (1948), the inventor of helical-beam antennas, was the first to empirically design a planar helical array composed of 2 x 2, 6-turn, 14° helices having an inter-element separation of 1.5 wavelengths, and uniformly fed by a simple feeding network carefully positioned under the supporting large ground plane. Although Kraus' array provided a higher gain and improved directivity over the single-element helical antenna, the design

ignored considerations for the reduction of side-lobe levels of the field-patterns, which may otherwise adversely affect the signal to noise ratio (S/N) of the system, as they become undesirably large in magnitude. Nakano *et al.* (1984) also investigated the radiation characteristics of a helical array whose elements are arranged in a linear fashion, and fed through a rectangular waveguide in conjunction with stubs for the purpose of matching the array elements to the waveguide. Using computer simulations, Phongcharoenpanich *et al* (2002), in a related work, studied the features of a circular array of four cylindrical helical antennas, which radiates conical-beam patterns, suitable for satellite mobile terminals. The design of 2 x 2 hemispherical helical antenna array having an optimum inter-element separation of 0.7 wavelength and which may be used for reliable reception of INMARSAT-M signals has been reported by Hui *et al.* (2004). The remarkably economical design of a 2 x 4 planar array of 8-turn cylindrical helical antennas for sharp reception of signals from the National Oceanic and Atmospheric Administration (NOAA) polar-orbiting satellites is credited to Gataulli *et al.* (2004). The representative research efforts described in the foregoing review clearly support the fact that as far as can be ascertained, no treatment has been given to the general problem of a planar M x N array of helical antennas. The solution of that evidently outstanding problem is yet another focus of this thesis.

2.4 Non-cylindrical helical antennas

Before closing this review, it is of interest to observe that helical antennas of the non-cylindrical geometrical variety have also received analytical treatment. The more well-known examples of these are the conical helix, for which Chattejee (1953) calculated the radiation fields of one mounted on a large ground plane with the simplifying assumption that Kraus' empirical current distribution apply. The method of moments solution of the same problem eliminates the need for an assumption of any

particular current distribution on the helical arm as demonstrated elsewhere, (Nakano *et al.* 1985). In the realm of practical applications, Dobbins and Rogers (2001) provided justification for the use of a folded conical helix as electrically small antenna. Another important example of the non-cylindrical helix antenna is the spherical helix antenna first reported in the open literature by Safaai-Jazi and Cardoso (1996). The dependence of the input impedance and gain of the spherical helix on the number of turns was investigated by Hui *et al.* (2001), while Best (2004) designed a folded spherical helix antenna suitable for application as electrically small antenna. Results of research works on the hemispherical helix, a variant of the spherical helix, are available in Chan *et al.* (2001) and Hui *et al.* (2003). Finally, a relatively new variety of the helix antenna, known as the contra-wound toroidal helical antenna (CWTA), and in which the wire helix is wound on a toroidal core, received analytical treatment (Miron 2001), whose computational results suggest that the antenna is suitable for use in several practical applications. Some other available publications on the CWTA, (Hansen and Ridgley 2001, Li *et al.* 2004, Pertl *et al.* 2005), focused attention on the antenna's radiation modes, and their conclusions are consistent with those of Miron.

Chapter 3

GOVERNING EQUATIONS OF THE ELLIPTICAL-CYLINDRICAL HELICAL-BEAM ANTENNA

3.1 Integrodifferential operator equation of elliptical-cylindrical helical-beam antenna

The theoretical framework for the solution of the helical antenna problem posed in this thesis derives from the electromagnetic potential integrals approach and the thin-wire concept, which are employed for the formulation of thin-wire antenna problems in terms of an incident electric field and the associated induced current distribution. In the potential integral formulation of electromagnetic radiation field problems, the starting point is the illumination, by a plane electromagnetic field, of a distant object, which in response to the excitation, produces a scattered field symbolized here by $\overline{E}^s$, and which admits expression as (Stutzman and Thiele 1981),

$$\overline{E}^s = -\frac{\partial \overline{A}}{\partial t} - \nabla\Phi, \tag{3.1}$$

in which the symbol ∇ denotes the del (or grad) operator, and where the vector magnetic potential denoted by $\overline{A}$ is given by

$$\overline{A} = \frac{\mu_o}{4\pi}\iiint_{v'} \overline{J}\left[\exp(-jk_o R)/R\right] dv' \ . \tag{3.2a}$$

The symbol Φ, which represents scalar electric potential, is given by Harrington (1967),

$$\Phi = \frac{1}{4\pi\varepsilon_o}\iiint_{v'} \rho\ \left[\exp(-jk_o R)/R\right] dv' \ , \tag{3.2b}$$

and in equations (3.2a) and (3.2b), $(\varepsilon_o, \mu_o, k_o)$ represent free-space permittivity, free-space permeability and free-space propagation constant, respectively; R is the separation of the source point and the field point. $(\overline{J}, \rho)$ denote current density and

charge density, respectively, and the dv' describes an element of volume of the radiating structure, whilst [exp(-jk$_o$R)/R] is the well-known free-space Green's function.

For electrically thin wire antennas, wire radius (r_w) is physically much smaller than both wire length (L) and electrically much smaller than the operating wavelength (λ), and the usual thin-wire approximations, (Harrington 1968), apply. Consequently, considerations need only be given to the axial components of the field and source quantities, and in that connection, if the symbol ℓ designates the axial variable, and if we note that an $e^{j\omega t}$ time harmonic variation has been assumed and suppressed here and henceforth, (Adekola and Okereke 1989), then, equation (3.1) passes over into the scalar expression:

$$E_\ell^s = -j\omega A_\ell - \frac{d\Phi_\ell}{d\ell} \quad , \tag{3.3}$$

where

$$A_\ell = \hat{a}_\ell \cdot \overline{A} = \frac{\mu_o}{4\pi}\int_0^L \hat{a}_\ell \cdot \hat{a}_{\ell'}\, I(\ell')\left[\exp(-jk_o R)/R\right] d\ell' , \tag{3.4a}$$

and

$$\Phi_\ell = \frac{1}{4\pi\varepsilon_o}\int_0^L \rho(\ell')\left[\exp(-jk_o R)/R\right] d\ell' \quad , \tag{3.4b}$$

provided that ω denotes angular frequency, whilst $I(\ell')$ and $\rho(\ell')$ represent the respective filamentary current and charge densities defined along the wire axis, R remain, as before, the separation of a source point on the wire axis and a field point on the wire surface, and $(\hat{a}_{\ell'}, \hat{a}_\ell)$ are unit vectors tangential to the wire axis and wire surface, respectively. Figure 3.1 depicts a typical turn of the thin-wire helix. As is customary in antenna work, source quantities are primed while field quantities are unprimed. The use of the thin-wire version of the continuity equation given as (Harrington 1968):

$$\frac{dI(\ell')}{d\ell'} = -j\omega\rho(\ell') \tag{3.5}$$

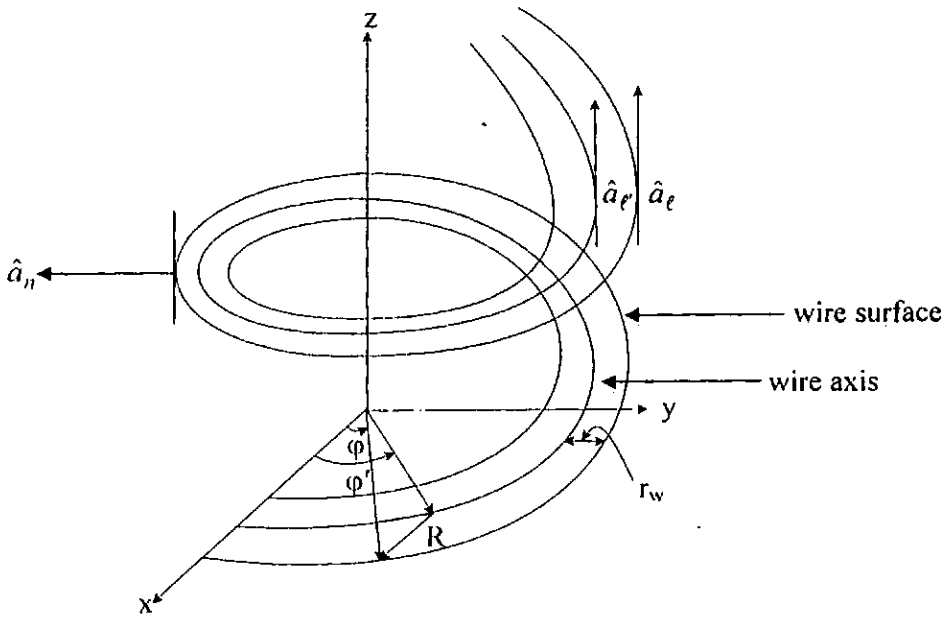

Figure 3.1: *A typical turn of the thin-wire helical antenna.*

in equation (3.4b), leads to

$$\Phi_t = \frac{-1}{j4\pi\omega\varepsilon_o}\int_0^{L}\frac{dI(\ell')}{d\ell'}\left[\exp(-jk_oR)/R\right]d\ell', \tag{3.6}$$

and when equations (3.4a) and (3.6) are substituted into equation (3.3), it is seen that the following expression emerges:

$$E_\ell^s = \frac{-j\omega\mu_o}{4\pi}\int_0^{L}\hat{a}_\ell\cdot\hat{a}_{\ell'}\,I(\ell')\left[\exp(-jk_oR)/R\right]d\ell' + \frac{-1}{j4\pi\omega\varepsilon_o}\int_0^{L}\frac{dI(\ell')}{d\ell'}\frac{d}{d\ell}\left[\exp(-jk_oR)/R\right]d\ell', \tag{3.7}$$

which is the integro-differential equation that describes the axial component of the scattered electric field E_ℓ^s in terms of the unknown wire antenna current distribution $I(\ell')$. To obtain a unique solution to any given antenna problem, the boundary conditions on the total electric field $\overline{E}^t$ existing on the antenna surface are enforced. And with the simplifying assumption that the wire antenna is perfectly conducting, the

appropriate boundary condition is that of vanishing tangential electric field on the wire surface, whose imposition here leads to the following expression:

$$\hat{a}_n \times \overline{E}^t = \hat{a}_n \times (\overline{E}^i + \overline{E}^s) = \overline{0} \quad , \tag{3.8}$$

or

$$E_\ell^i = -E_\ell^s \quad , \tag{3.8a}$$

provided that it is understood that E_ℓ^i designates the tangential component of the incident electric field $\overline{E}^i$, and $\hat{a}_n$, an outward unit vector normal to the wire surface. The introduction of equation (3.7) in equation (3.8a) results in

$$E_\ell^i = \frac{j\omega\mu_o}{4\pi}\int_0^L \hat{a}_\ell \cdot \hat{a}_{\ell'}\, I(\ell')\,[\exp(-jk_o R)/R]\,d\ell' - \frac{1}{j4\pi\omega\varepsilon_o}\int_0^L \frac{dI(\ell')}{d\ell'}\frac{d}{d\ell}[\exp(-jk_o R)/R]\,d\ell', \tag{3.9}$$

which can be succinctly recast in operator form as, (Adekola and Okereke 1989),

$$E_\ell^i = \mathcal{L}[I(\ell')] \quad , \tag{3.10}$$

in which the integro-differential operator denoted by $\mathcal{L}$ is explicitly expressed as:

$$\mathcal{L}[*] = \frac{j\omega\mu_o}{4\pi}\int_0^L \hat{a}_\ell \cdot \hat{a}_{\ell'}\,[*]\,[\exp(-jk_o R)/R]\,d\ell' - \frac{1}{j4\pi\omega\varepsilon_o}\int_0^L \frac{d[*]}{d\ell'}\frac{d}{d\ell}[\exp(-jk_o R)/R]\,d\ell'. \tag{3.10a}$$

Equation (3.10) is sometimes called the Electric Field Integral Equation (EFIE) (Wettergren and Slättman 1996) or the Mixed Potential Integral Equation (MPIE) (Wang *et al.* 2003).

Shown in Figure 3.2a is an elliptical helix whose cross-section is depicted in Figure 3.2b. In terms of the semi-major axis length a, the eccentricity ε, the pitch angle α, the differential arm length $d\ell'$ of the elliptical helix takes the form (Wong and Loh 1959):

$$d\ell' = a\sec\alpha\sqrt{1-\varepsilon^2\cos^2\varphi'}\;\; d\varphi' \quad , \tag{3.11}$$

where φ' is a parameter along the wire helix. Invoking the generalized thin-wire approximation for the distance R between a point on the wire axis defined by position vector $\bar{r}'(x', y', z')$ and a point on the wire surface specified by position vector $\bar{r}(x, y, z)$, we can write

$$R = \sqrt{r_w^2 + |\bar{r} - \bar{r}'|} \quad , \tag{3.12a}$$

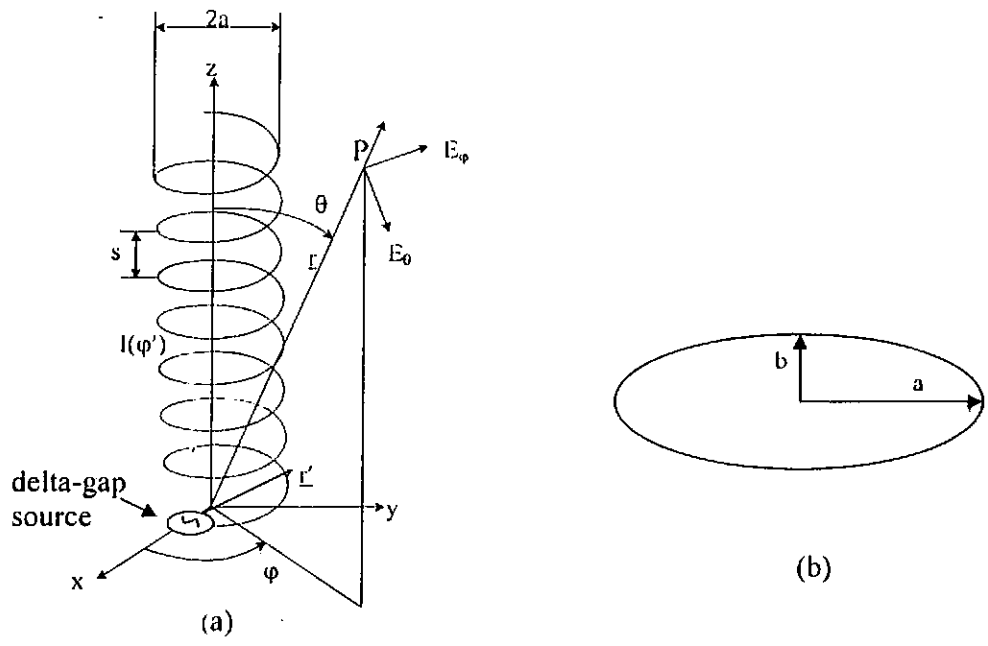

Figure 3.2: *(a) An elliptical helical antenna; (b) The cross-section of the elliptical helical antenna.*

which explicitly takes the form

$$R = \sqrt{r_w^2 + (x - x')^2 + (y - y')^2 + (z - z')^2} \quad , \tag{3.12b}$$

in the Cartesian coordinate system, provided that r_w stands for the wire radius. In the case of an elliptical-cylindrical helix which is of primary interest here: it is readily established (Wong and Loh 1959) that

$$\bar{r}' = a\cos\varphi'\,\hat{a}_x + a\sqrt{1-\varepsilon^2}\,\sin\varphi'\,\hat{a}_y + \{2/\pi\}\,a\tan\alpha\,E(\varepsilon, \pi/2)\;\varphi'\,\hat{a}_z \quad , \tag{3.12c}$$

and that

$$\bar{r} = a\cos\varphi\,\hat{a}_x + a\sqrt{1-\varepsilon^2}\,\sin\varphi\,\hat{a}_y + \{2/\pi\}\,a\tan\alpha\,E(\varepsilon, \pi/2)\;\varphi\,\hat{a}_z \quad , \tag{3.12d}$$

where $\hat{a}_x, \hat{a}_y, and\ \hat{a}_z$ are unit vectors in the x-, y- and z- directions, respectively; $E(\varepsilon, \pi/2)$ is the standard elliptical integral of the second kind (Abramowitz and Stegun 1964):

$$E(\varepsilon, \pi/2) = \int_0^{\pi/2} \sqrt{1-\varepsilon^2 \sin^2 \varphi'}\, d\varphi' \quad . \tag{3.12e}$$

Upon the substitution of equations (3.12c) and (3.12d) into equation (3.12b), and after some routine manipulations, we arrive at

$$R = a\sqrt{\left(\frac{r_w}{a}\right)^2 + 4\sin^2\left(\frac{\varphi-\varphi'}{2}\right) - \varepsilon^2(\sin^2\varphi - 2\sin\varphi\sin\varphi' + \sin^2\varphi') + \frac{4\tan^2\alpha}{\pi^2}E^2(\varepsilon,\frac{\pi}{2})(\varphi-\varphi')^2}\,. \tag{3.12f}$$

The unit vectors $\hat{a}_{\ell'}$ and $\hat{a}_\ell$ are obtainable from the standard formula

$$\hat{a}_{\ell'} \triangleq \frac{d\bar{r}'}{d\varphi'} \Big/ \left|\frac{d\bar{r}'}{d\varphi'}\right| , \tag{3.12g}$$

which with the use of equations (3.11c) and (3.11d) is readily seen to yield the following expressions:

$$\hat{a}_{\ell'} = \frac{-\sin\varphi'\hat{a}_x + \sqrt{1-\varepsilon^2}\cos\varphi'\hat{a}_y + \{2/\pi\}\tan\alpha E(\varepsilon,\pi/2)\hat{a}_z}{\sqrt{1-\varepsilon^2\cos^2\varphi' + \{4/\pi^2\}\tan^2\alpha E^2(\varepsilon,\pi/2)}} \quad , \tag{3.13a}$$

and

$$\hat{a}_\ell = \frac{-\sin\varphi\,\hat{a}_x + \sqrt{1-\varepsilon^2}\cos\varphi\,\hat{a}_y + \{2/\pi\}\tan\alpha E(\varepsilon,\pi/2)\,\hat{a}_z}{\sqrt{1-\varepsilon^2\cos^2\varphi + \{4/\pi^2\}\tan^2\alpha E^2(\varepsilon,\pi/2)}} \quad . \tag{3.13b}$$

By substituting equations (3.13a), (3.13b), and (3.11a) into equation (3.9) and noting that the helical arm extends from $\varphi' = 0$ to $\varphi' = 2\pi N$, (where N designates the number of helix turns) we find that

$$E_{\varphi}^{i} = \int_{0}^{2\pi N} \left\{ \left[\frac{\sin\varphi \sin\varphi' + (1-\varepsilon^2)\cos\varphi\cos\varphi' + \{4/\pi^2\}\tan^2\alpha E^2(\varepsilon,\pi/2)}{\sqrt{1-\varepsilon^2\cos^2\varphi + \{4/\pi^2\}\tan^2\alpha E^2(\varepsilon,\pi/2)}\sqrt{1-\varepsilon^2\cos^2\varphi' + \{4/\pi^2\}\tan^2\alpha E^2(\varepsilon,\pi/2)}} \right] \right.$$

$$\left. \times \left[\frac{j\omega\mu_o}{4\pi} \right] I(\varphi') a \sec\alpha \sqrt{1-\varepsilon^2\cos^2\varphi'} - \left[\frac{1}{j4\pi\omega\varepsilon_o a \sec\alpha \sqrt{1-\varepsilon^2\cos^2\varphi}} \right] \frac{dI(\varphi')}{d\varphi'} \frac{d}{d\varphi} \right\} \frac{e^{-jk_o R}}{R} d\varphi' , \tag{3.14}$$

which can readily be expressed in operator form as

$$E_{\varphi}^{i} = \Im[I(\varphi')] \quad , \tag{3.15}$$

provided that the operator $\Im[*]$ assumes the form:

$$\Im[*] = \int_{0}^{2\pi N} \left\{ \left[\frac{\sin\varphi \sin\varphi' + (1-\varepsilon^2)\cos\varphi\cos\varphi' + \{4/\pi^2\}\tan^2\alpha E^2(\varepsilon,\pi/2)}{\sqrt{1-\varepsilon^2\cos^2\varphi + \{4/\pi^2\}\tan^2\alpha E^2(\varepsilon,\pi/2)}\sqrt{1-\varepsilon^2\cos^2\varphi' \{4/\pi^2\}\tan^2\alpha E^2(\varepsilon,\pi/2)}} \right] \right.$$

$$\left. \times \left[\frac{j\omega\mu_o}{4\pi} \right] [*] a \sec\alpha \sqrt{1-\varepsilon^2\cos^2\varphi'} - \left[\frac{1}{j4\pi\omega\varepsilon_o a \sec\alpha \sqrt{1-\varepsilon^2\cos^2\varphi'}} \right] \frac{d[*]}{d\varphi'} \frac{d}{d\varphi} \right\} \frac{e^{-jk_o R}}{R} d\varphi' . \tag{3.15a}$$

Equation (3.15) is the integro-differential operator equation for the electric field due to the thin-wire elliptical-cylindrical helical antenna, and as will be shown in what follows, this equation represents a general expression for which different other thin-wire antennas of regular geometrical shapes are special cases, as suggested by the illustrations of Figures 3.3a and 3.3b. In other words, the linear operators for **eight conventional thin-wire antennas derivable from the elliptical helix are deducible from equation (3.15).**

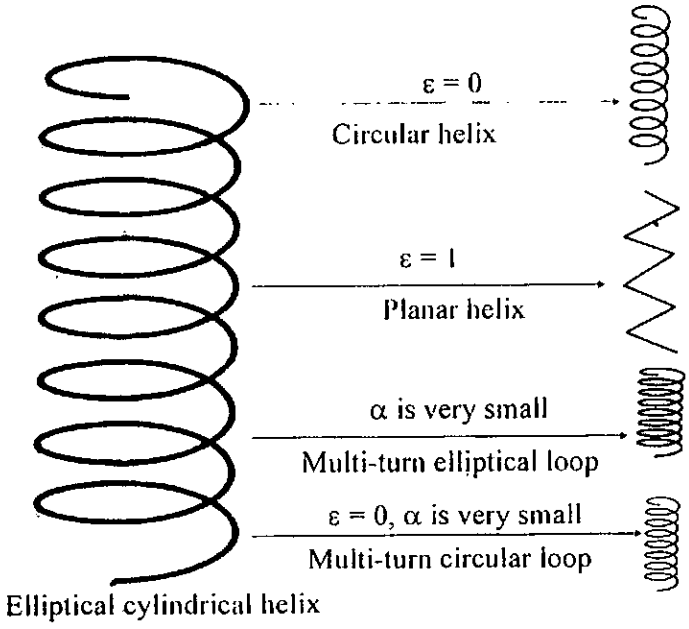

Figure 3.3a: *Specializations of elliptical helix to four regular geometries.*

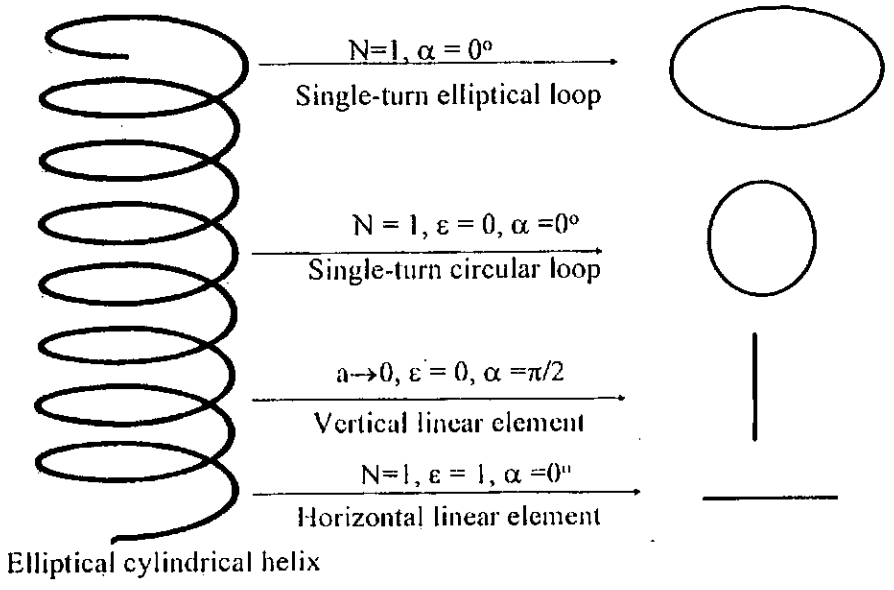

Figure 3.3b: *Specializations of elliptical helix to four other regular geometries.*

3.2 Specializations of the integrodifferential operator equation to eight regularly-shaped thin-wire antennas

Having formulated the generalized integrodifferential operator for an elliptical helical antenna by virtue of equation (3.15), we are now in a position to discuss the specializations of the operator for basic thin-wire antennas of regular shapes, starting with the traditional circular helix.

3.2.1 Linear operator for a circular helix

Upon setting the eccentricity ε to zero in equation (3.15), and noting that E(0,π/2) = π/2, the linear operator for a circular helix emerges as:

$$L[*] = \int_0^{2\pi N} \left\{ [\cos\alpha\cos(\varphi-\varphi') + \tan\alpha\sin\alpha] \left[\frac{j\omega\mu_o a}{4\pi}\right][*] - \frac{1}{j4\pi\omega\varepsilon_o a\sec\alpha}\frac{d[*]}{d\varphi'}\frac{d}{d\varphi}\right\}\frac{e^{-jk_o R}}{R}d\varphi', \tag{3.16}$$

where

$$R = a\sqrt{\left(\frac{r_w}{a}\right)^2 + 4\sin^2\left(\frac{\varphi-\varphi'}{2}\right) + \tan^2\alpha(\varphi-\varphi')^2} \tag{3.16a}$$

3.2.2 Linear operator for a planar helix

When the eccentricity ε equals unity, the elliptical helix transforms to a planar helix. Since E(1, π/2) = 1, the linear operator for a planar helix based on equation (3.15) assumes the form:

$$L[*] = \int_0^{2\pi N} \left\{ \left[\frac{\sin\varphi\sin\varphi' + \{4/\pi^2\}\tan^2\alpha}{\sqrt{1-\cos^2\varphi + \{4/\pi^2\}\tan^2\alpha}\sqrt{1-\cos^2\varphi' + \{4/\pi^2\}\tan^2\alpha}}\right] \times \left[\frac{j\omega\mu_o}{4\pi}\right][*]a\sec\alpha\sqrt{1-\varepsilon^2\cos^2\varphi'} - \left[\frac{1}{j4\pi\omega\varepsilon_o a\sec\alpha\sqrt{1-\cos^2\varphi}}\right]\frac{d[*]}{d\varphi'}\frac{d}{d\varphi}\right\}\frac{e^{-jk_o R}}{R}d\varphi', \tag{3.17}$$

where

$$R = a\sqrt{\left(\frac{r_w}{a}\right)^2 + 4\sin^2\left(\frac{\varphi-\varphi'}{2}\right) - (\sin^2\varphi - 2\sin\varphi\sin\varphi' + \sin^2\varphi') + \frac{4\tan^2\alpha}{\pi^2}(\varphi-\varphi')^2}\,. \tag{3.17a}$$

3.2.3 Linear operator for a multi-turn elliptical loop

A multi-turn elliptical loop is realized from the elliptical helix when the pitch angle α is so small that the approximations $\tan\alpha \approx \alpha$, $\sin\alpha \approx \alpha$ and $\sec\alpha \approx 1$ become valid. Invoking these approximations on equation (3.15), we obtain the linear operator for the multi-turn elliptical loop as follows:

$$L[*] = \int_0^{2\pi N}\left\{\left[\frac{\sin\varphi\sin\varphi' + (1-\varepsilon^2)\cos\varphi\cos\varphi' + \{4/\pi^2\}\alpha^2 E^2(\varepsilon,\pi/2)}{\sqrt{1-\varepsilon^2\cos^2\varphi + \{4/\pi^2\}\alpha^2 E^2(\varepsilon,\pi/2)}\sqrt{1-\varepsilon^2\cos^2\varphi' + \{4/\pi^2\}\alpha^2 E^2(\varepsilon,\pi/2)}}\right]\right.$$
$$\left.\times\left[\frac{j\omega\mu_o a}{4\pi}\right][*]\sqrt{1-\varepsilon^2\cos^2\varphi'} - \left[\frac{1}{j4\pi\omega\varepsilon_o a\sqrt{1-\varepsilon^2\cos^2\varphi}}\right]\frac{d[*]}{d\varphi'}\frac{d}{d\varphi}\right\}\frac{e^{-jk_oR}}{R}d\varphi'\,, \tag{3.18}$$

where

$$R = a\sqrt{\left(\frac{r_w}{a}\right)^2 + 4\sin^2\left(\frac{\varphi-\varphi'}{2}\right) - \varepsilon^2(\sin^2\varphi - 2\sin\varphi\sin\varphi' + \sin^2\varphi') + \left(\frac{4\alpha^2}{\pi^2}\right)E^2(\varepsilon,\frac{\pi}{2})(\varphi-\varphi')^2}\,. \tag{3.18a}$$

3.2.4 Linear operator for a multi-turn circular loop

The linear operator for a multi-turn circular loop is obtained from equation (3.15) when the following substitutions are made: $\varepsilon = 0$, $E(0,\pi/2) = \pi/2$, $\tan\alpha \approx \alpha$, $\sin\alpha \approx \alpha$ and $\sec\alpha \approx 1$:

$$L[*] = \int_0^{2\pi N}\left\{[\cos(\varphi-\varphi') + \alpha^2]\left[\frac{j\omega\mu_o a}{4\pi}\right][*] - \frac{1}{j4\pi\omega\varepsilon_o a}\frac{d[*]}{d\varphi'}\frac{d}{d\varphi}\right\}\frac{e^{-jk_oR}}{R}d\varphi'\,, \tag{3.19}$$

where

$$R = a\sqrt{\left(\frac{r_w}{a}\right)^2 + 4\sin^2\left(\frac{\varphi-\varphi'}{2}\right) + \alpha^2(\varphi-\varphi')^2} \quad . \tag{3.19a}$$

3.2.5 Linear operator for a single-turn elliptical loop

To deduce the linear operator for a single-turn elliptical loop from equation (3.15), we merely equate the pitch angle α to zero and the number of turns N to unity in equation (3.15), to arrive at:

$$L[*] = \int_0^{2\pi}\left\{\left[\frac{\sin\varphi\sin\varphi' + (1-\varepsilon^2)\cos\varphi\cos\varphi'}{\sqrt{(1-\varepsilon^2\cos^2\varphi)(1-\varepsilon^2\cos^2\varphi')}}\right]\left[\frac{j\omega\mu_o}{4\pi}\right][*]a\sqrt{1-\varepsilon^2\cos^2\varphi'} - \left[\frac{1}{j4\pi\omega\varepsilon_o a\sqrt{1-\varepsilon^2\cos^2\varphi}}\right]\frac{d[*]}{d\varphi'}\frac{d}{d\varphi}\right\}\frac{e^{-jk_oR}}{R}d\varphi' , \tag{3.20}$$

where

$$R = a\sqrt{\left(\frac{r_w}{a}\right)^2 + 4\sin^2\left(\frac{\varphi-\varphi'}{2}\right) - \varepsilon^2(\sin^2\varphi - 2\sin\varphi\sin\varphi' + \sin^2\varphi')} \quad . \tag{3.20a}$$

3.2.6 Linear operator for a single-turn circular loop

By equating both the pitch angle α and the eccentricity ε to zero, and the number of turns N to unity in equation (3.15), the linear operator for a circular loop emerges as:

$$L[*] = \int_0^{2\pi}\left\{\frac{j\omega\mu_o a}{4\pi}[\cos(\varphi-\varphi')][*] - \frac{1}{j4\pi\omega\varepsilon_o a}\frac{d[*]}{d\varphi'}\frac{d}{d\varphi}\right\}\frac{e^{-jk_oR}}{R}d\varphi' \quad , \tag{3.21}$$

provided

$$R = a\sqrt{\left(\frac{r_w}{a}\right)^2 + 4\sin^2\left(\frac{\varphi-\varphi'}{2}\right)} \quad , \tag{3.21a}$$

and where both equations (3.21) and (3.21a) are consistent with the published results of Harrington and Mautz (1968).

3.2.7 Linear operator for a linear element along the z-axis

By equating the eccentricity ε to zero and effecting the following transformations:

$$\left.\begin{array}{ll} a = 0 & \\ \alpha = \dfrac{\pi}{2} & \\ a\tan\alpha\,\varphi' \to z', & a\tan\alpha\,\varphi \to z \\ a\tan\alpha\,d\varphi' \to dz', & a\tan\alpha\,d\varphi \to dz \end{array}\right\}, \tag{3.22}$$

in equation (3.15), we readily obtain the expression for the linear operator applicable to a linear antenna of length L, positioned along the z-axis as follows:

$$L[*] = \int_0^L \left\{ j\omega\mu_o[*] - \frac{1}{j\omega\varepsilon_o}\frac{d[*]}{dz'}\frac{d}{dz} \right\} \frac{e^{-jk_oR}}{4\pi R}\,dz', \tag{3.23}$$

where

$$R = \sqrt{r_w^2 + (z - z')^2} \quad . \tag{3.23a}$$

Equation (3.23) is identical to the linear operator formulated for a linear antenna by Stutzman and Thiele (1981).

3.2.8 Linear operator for horizontal linear antenna on the x-axis

The elliptical helix degenerates to a linear element on the x-axis when the pitch angle α is zero and both the number of turns and the eccentricity ε are equal to unity. Consequently, upon effecting the substitutions:

$$\left.\begin{array}{l} N = 1 \\ \alpha = 0 \\ \varepsilon = 1 \\ E(1, \pi/2) = 1 \end{array}\right\} \tag{3.24}$$

in equation (3.15), we obtain the expression for the linear operator as:

$$L[*] = -\int_{-a}^{a} \left\{ j\omega\mu_o[*] - \frac{1}{j\omega\varepsilon_o}\frac{d[*]}{dx'}\frac{d}{dx} \right\} \frac{e^{-jk_oR}}{4\pi R}\,dx' \quad , \tag{3.25}$$

where

$$R = \sqrt{r_w^2 + (x - x')^2} \quad . \tag{3.25a}$$

This completes the formal specializations of the generalized integrodifferential operator of the elliptical helix to the cases of eight basic antenna geometries. In the next chapter, the generalized solution of the integrodifferential operator equation will be presented through an application of the versatile method of moments. Before then, the next section addresses the development of the general integral expressions for the radiated fields due to the elliptical helix using the vector potential approach.

3.3 Electromagnetic radiation integrals of elliptical-cylindrical helical-beam antenna

In view of the fact that the elliptical-cylindrical helical-beam antenna of interest here is electrically thin, we employ the thin-wire version of equation (3.2a) which admits a representation given as follows:

$$\overline{A}(\overline{r}) = \frac{\mu_o}{4\pi} \int_0^L \hat{a}_{\ell'} \, I(\ell') \left[\exp(-jk_o R)/R\right] d\ell' , \tag{3.26}$$

where the differential element of arm length represented by $d\ell'$ is given by Wong and Loh (1959) as

$$d\ell' = a \sec\alpha \sqrt{1 - \varepsilon^2 \cos^2 \varphi'} \, d\varphi' \quad , \tag{3.27a}$$

in which ε denotes the eccentricity of the cross-sectional ellipse expressible in terms of the semi-major axis length a and semi-minor axis length b as

$$\varepsilon = \sqrt{1 - (b/a)^2} \quad . \tag{3.27b}$$

Since $\overline{r}'$, which denotes the position vector from the origin of the coordinate system to any point on the helical structure is already evaluated in equation (3.12c) and is given by

$$\bar{r}' = a\cos\varphi'\,\hat{a}_x + a\sqrt{1-\varepsilon^2}\,\sin\varphi'\,\hat{a}_y + \{2/\pi\}\,a\tan\alpha\,E(\varepsilon,\pi/2)\;\varphi'\,\hat{a}_z \tag{3.28a}$$

provided that α denotes the helix pitch angle and that $E(\varepsilon,\pi/2)$ is the elliptic integral of the second kind (Abramowitz and Stegun 1964), where

$$E(\varepsilon,\pi/2) = \int_0^{\frac{\pi}{2}} \sqrt{1-\varepsilon^2\sin^2\varphi'}\;d\varphi' \quad . \tag{3.28b}$$

it therefore, follows that $\hat{a}_{\ell'}$ which by definition is

$$\hat{a}_{\ell'} \equiv \frac{d\bar{r}'}{d\varphi'} \Big/ \left|\frac{d\bar{r}'}{d\varphi'}\right|, \tag{3.29a}$$

is readily evaluated (in terms of antenna geometrical parameters) from equation (3.28a) as

$$\hat{a}_{\ell'} = \frac{-\sin\varphi'\hat{a}_x + \sqrt{1-\varepsilon^2}\,\cos\varphi'\hat{a}_y + \{2/\pi\}\tan\alpha\,E(\varepsilon,\pi/2)\hat{a}_z}{\sqrt{1-\varepsilon^2\cos^2\varphi' + \{4/\pi^2\}\tan^2\alpha\,E^2(\varepsilon,\pi/2)}}. \tag{3.29b}$$

The substitution of equations (3.27a) and (3.29b) in equation (3.26) gives

$$\bar{A}(\bar{r}) = \frac{\mu_o}{4\pi}\int_0^{2\pi N}\left[\frac{-\sin\varphi'\hat{a}_x + \sqrt{1-\varepsilon^2}\,\cos\varphi'\hat{a}_y + \{2/\pi\}\tan\alpha\,E(\varepsilon,\pi/2)\hat{a}_z}{\sqrt{1-\varepsilon^2\cos^2\varphi' + \{4/\pi^2\}\tan^2\alpha\,E^2(\varepsilon,\pi/2)}}\right]$$
$$\times\, I(\varphi')\frac{\exp(-jk_o\,|\bar{r}-\bar{r}'|)}{|\bar{r}-\bar{r}'|}\,a\sec\alpha\sqrt{1-\varepsilon^2\cos^2\varphi'}\;d\varphi' \quad , \tag{3.30}$$

where R has been replaced by $|\bar{r}-\bar{r}'|$, where $\bar{r}$ represents the position vector from the origin of the coordinate system to a far-field point, and N stands for the number of helix turns, whilst φ' is the running variable along the axis of helix. Far away from the elliptical helix, the quantity $|\bar{r}-\bar{r}'|$ appearing in the denominator of equation (3.30) simply becomes r ("magnitude approximation") whilst a similar quantity in the exponent has been shown, (Stutzman and Thiele 1981), to be given in the far zone by:

$$|\bar{r}-\bar{r}'| \approx r - \hat{a}_r\cdot\bar{r}', \tag{3.31a}$$

provided that $\hat{a}_r$ is a unit vector in the radial direction of spherical coordinate system, and whose Cartesian components are identified below:

$$\hat{a}_r = \sin\theta\cos\varphi\,\hat{a}_x + \sin\theta\sin\varphi\,\hat{a}_y + \cos\theta\,\hat{a}_z . \tag{3.31b}$$

The introduction of equations (3.28a) and (3.31b) in equation (3.31a) yields

$$|\bar{r}-\bar{r}'| \approx r - a\sin\theta[\cos\varphi\cos\varphi' + \sqrt{1-\varepsilon^2}\,\sin\varphi\sin\varphi' + \{2/\pi\}\tan\alpha\cot\theta E(\varepsilon,\pi/2)\varphi'], \tag{3.31c}$$

which readily assumes the compact form:

$$|\bar{r}-\bar{r}'| \approx r - a\zeta\sin\theta , \tag{3.31d}$$

where

$$\zeta \equiv \cos\varphi\cos\varphi' + \sqrt{1-\varepsilon^2}\,\sin\varphi\sin\varphi' + \{2/\pi\}\tan\alpha\cot\theta E(\varepsilon,\pi/2)\varphi' . \tag{3.31e}$$

When equation (3.31d) is inserted into equation (3.30), and after some rearrangements, the three Cartesian components of the magnetic vector potential, that is, A_x, A_y, and A_z, emerge as follows:

$$A_x = \frac{-\mu_o a\sec\alpha\, e^{-jk_o r}}{4\pi r}\int_0^{2\pi N}\frac{\sin\varphi'\sqrt{1-\varepsilon^2\cos^2\varphi'}}{\sqrt{1-\varepsilon^2\cos^2\varphi'+\{4/\pi^2\}\tan^2\alpha E^2(\varepsilon,\pi/2)}}I(\varphi')e^{jk_o a\zeta\sin\theta}\,d\varphi' , \tag{3.32a}$$

$$A_y = \frac{\mu_o a\sqrt{1-\varepsilon^2}\sec\alpha\, e^{-jk_o r}}{4\pi r}\int_0^{2\pi N}\frac{\cos\varphi'\sqrt{1-\varepsilon^2\cos^2\varphi'}}{\sqrt{1-\varepsilon^2\cos^2\varphi'+\{4/\pi^2\}\tan^2\alpha E^2(\varepsilon,\pi/2)}}I(\varphi')e^{jk_o a\zeta\sin\theta}\,d\varphi', \tag{3.32b}$$

and

$$A_z = \frac{\mu_o a\tan\alpha\sec\alpha\, E(\varepsilon,\frac{\pi}{2})e^{-jk_o r}}{2\pi^2 r}\int_0^{2\pi N}\frac{\sqrt{1-\varepsilon^2\cos^2\varphi'}}{\sqrt{1-\varepsilon^2\cos^2\varphi'+\{4/\pi^2\}\tan^2\alpha E^2(\varepsilon,\pi/2)}}I(\varphi')e^{jk_o a\zeta\sin\theta}\,d\varphi'. \tag{3.32c}$$

Noting that the corresponding far-zone spherical components of $\overline{A}$, namely, A_θ and A_φ, are expressible in terms of the Cartesian components, A_x, A_y, and A_z, through the equations given as (Hayt 1988):

$$\left.\begin{aligned} A_\theta &= \cos\theta\cos\varphi\, A_x + \cos\theta\sin\varphi\, A_y - \sin\varphi\, A_z \\ A_\varphi &= -\sin\varphi\, A_x + \cos\varphi\, A_y \end{aligned}\right\} \quad , \tag{3.33}$$

it becomes easy to see that

$$A_\theta = \frac{\mu_o a \sec\alpha\, e^{-jk_o r}}{4\pi r} \int_0^{2\pi N} \left\{ \frac{\sqrt{1-\varepsilon^2\cos^2\varphi'}}{\sqrt{1-\varepsilon^2\cos^2\varphi' + \{4/\pi^2\}\tan^2\alpha\, E^2(\varepsilon,\pi/2)}} \right\} I(\varphi')\,[-\cos\theta\cos\varphi\sin\varphi'$$
$$+ \sqrt{1-\varepsilon^2}\cos\theta\sin\varphi\cos\varphi' - \{2/\pi\}\sin\theta\tan\alpha\, E(\varepsilon,\pi/2)]\, e^{jk_o a\zeta\sin\theta}\, d\varphi' , \tag{3.34a}$$

and

$$A_\varphi = \frac{\mu_o a \sec\alpha\, e^{-jk_o r}}{4\pi r} \int_0^{2\pi N} \left\{ \frac{\sqrt{1-\varepsilon^2\cos^2\varphi'}}{\sqrt{1-\varepsilon^2\cos^2\varphi' + \{4/\pi^2\}\tan^2\alpha\, E^2(\varepsilon,\pi/2)}} \right\} I(\varphi')\,[\sin\varphi\sin\varphi'$$
$$+ \sqrt{1-\varepsilon^2}\cos\theta\cos\varphi']\, e^{jk_o a\zeta\sin\theta}\, d\varphi' , \tag{3.34b}$$

It is well-known, (Harrington 1961), that for time-harmonic electromagnetic fields, the far-zone electric field $\overline{E}$ is simply related to the magnetic vector potential $\overline{A}$ in the following manner:

$$\overline{E} = \hat{a}_\theta\, E_\theta + \hat{a}_\varphi\, E_\varphi = -j\omega\left(\hat{a}_\theta\, A_\theta + \hat{a}_\varphi\, A_\varphi\right) \tag{3.35}$$

thus, the $\hat{\theta}$ - component of the radiated electric field E_θ is obtained as

$$E_\theta = \frac{-j\omega\mu_o a \sec\alpha\, e^{-jk_o r}}{4\pi r} \int_0^{2\pi N} \left\{ \frac{\sqrt{1-\varepsilon^2\cos^2\varphi'}}{\sqrt{1-\varepsilon^2\cos^2\varphi' + \{4/\pi^2\}\tan^2\alpha\, E^2(\varepsilon,\pi/2)}} \right\} I(\varphi')$$
$$\times [-\cos\theta\cos\varphi\sin\varphi' + \sqrt{1-\varepsilon^2}\cos\theta\sin\varphi\cos\varphi' - \{2/\pi\}\sin\theta\tan\alpha\, E(\varepsilon,\pi/2)]\, e^{jk_o a\zeta\sin\theta}\, d\varphi' , \tag{3.36a}$$

while the $\hat{\varphi}$ - component of the radiated electric field E_φ is given by

$$E_{\varphi} = \frac{-j\omega\mu_o a \sec\alpha\, e^{-jk_o r}}{4\pi r} \int_0^{2\pi N} \left\{ \frac{\sqrt{1-\varepsilon^2\cos^2\varphi'}}{\sqrt{1-\varepsilon^2\cos^2\varphi' + \{4/\pi^2\}\tan^2\alpha\, E^2(\varepsilon,\pi/2)}} \right\} I(\varphi')\,[\sin\varphi\sin\varphi' + \sqrt{1-\varepsilon^2}\cos\theta\cos\varphi']\, e^{jk_o a\zeta\sin\theta}\, d\varphi' . \tag{3.36b}$$

The associated magnetic field components H_θ and H_φ at the far-field region are related to E_θ and E_φ by the following simple equations (Jordan and Balmain 1968):

$$H_{\varphi} = \frac{E_{\theta}}{\eta_o} \quad and \quad H_{\theta} = -\frac{E_{\varphi}}{\eta_o} \quad , \tag{3.37}$$

where η_o (=377Ω) is the intrinsic impedance of free space. ***Equations (3.36a) and (3.36b) represent the generalized electric field integral expressions, from which, as explained in section 3.2, corresponding results for thin-wire antennas of regular geometrical shapes derive.*** We now apply the generalized solution expressed by equations (3.36a) and (3.36b) to fundamental thin-wire antenna problems.

3.4 Specializations of the generalized radiation integrals to regularly-shaped thin-wire antennas

Following the procedures adopted in section 3.2, the corresponding radiation integrals of eight thin-wire antennas of regular geometries will now be deduced from the generalized radiation integrals of equations (3.36a) and (3.36b), beginning with the common circular helix.

3.4.1 Radiated fields of a circular helix

Because an ellipse transforms to a circle when its eccentricity ε is zero, we simply set ε to zero in equations (3.36a) and (3.36b), and thence, taking cognizance of the fact that E(0,π/2) equals one, we arrive at the radiated fields of a circular helix as follows:

$$E_\theta = \frac{-j\omega\mu_o a\, e^{-jk_o r}}{4\pi r} \int_0^{2\pi N} I(\varphi')\, [\cos\theta \sin(\varphi - \varphi') - \sin\theta \tan\alpha]\, e^{jk_o a\zeta \sin\theta}\, d\varphi' , \tag{3.37a}$$

and

$$E_\varphi = \frac{-j\omega\mu_o a\, e^{-jk_o r}}{4\pi r} \int_0^{2\pi N} I(\varphi')[\cos(\varphi - \varphi')]\, e^{jk_o a\zeta \sin\theta}\, d\varphi' , \tag{3.37b}$$

where

$$\zeta = \cos(\varphi - \varphi') + (\tan\alpha \cot\theta)\varphi' , \tag{3.37c}$$

which expressions are consistent with those for the far-field expressions derived by Kornhauser (1951) who directly specialized the radiation field formula for thin wire as developed by King (1945).

3.4.2 Radiated fields of a planar helix

It is well known that an elliptical helix degenerates to a planar helix (commonly referred to as the zigzag structure) when the eccentricity ε assumes a value of unity; also, $E(1,\pi/2)$ equals unity. Therefore, upon making the substitution $\varepsilon = 1$ in equations (3.36a) and (3.36b) for the elliptical helix, we obtain the following expressions for the planar helix:

$$E_\theta = \frac{-j\omega\mu_o a \sec\alpha\, e^{-jk_o r}}{4\pi r} \int_0^{2\pi N} \left\{ \frac{\sqrt{1-\varepsilon^2\cos^2\varphi'}}{\sqrt{1-\cos^2\varphi' + \{4/\pi^2\}\tan^2\alpha}} \right\} I(\varphi')\, [-\cos\theta\cos\varphi\sin\varphi' - \{2/\pi\}\sin\theta\tan\alpha]\, e^{jk_o a\zeta\sin\theta}\, d\varphi' , \tag{3.38a}$$

$$E_\varphi = \frac{-j\omega\mu_o a \sec\alpha\, e^{-jk_o r}}{4\pi r} \int_0^{2\pi N} \left\{ \frac{\sqrt{1-\cos^2\varphi'}}{\sqrt{1-\cos^2\varphi' + \{4/\pi^2\}\tan^2\alpha}} \right\} I(\varphi') \times [\sin\varphi\sin\varphi'\, e^{jk_o a\zeta\sin\theta}\, d\varphi' , \tag{3.39b}$$

provided that

$$\zeta = \cos\varphi\cos\varphi' + (2/\pi)(\tan\alpha\cot\theta)\varphi' . \tag{3.39c}$$

3.4.3 Radiated fields of a multi-turn elliptical loop

To obtain the radiated field expressions for a multi-turn elliptical loop, we simply allow the pitch angle α to assume a small value such that $\tan\alpha$ is approximated by α and $\sec\alpha$ by 1. Thus, effecting these approximations in equations (3.36a) and (3.36b), the following results emerge:

$$E_\theta = \frac{-j\omega\mu_o a e^{-jk_o r}}{4\pi r} \int_0^{2\pi N} \left\{ \frac{\sqrt{1-\varepsilon^2\cos^2\varphi'}}{\sqrt{1-\varepsilon^2\cos^2\varphi' + \{4/\pi^2\}\alpha^2 E^2(\varepsilon,\pi/2)}} \right\} I(\varphi')\,[-\cos\theta\cos\varphi\sin\varphi'$$
$$+\sqrt{1-\varepsilon^2}\cos\theta\sin\varphi\cos\varphi' - \{2/\pi\}\alpha\sin\theta E(\varepsilon,\pi/2)]\, e^{jk_o a\zeta\sin\theta}\, d\varphi' \quad , \qquad (3.40a)$$

$$E_\varphi = \frac{-j\omega\mu_o a e^{-jk_o r}}{4\pi r} \int_0^{2\pi N} \left\{ \frac{\sqrt{1-\varepsilon^2\cos^2\varphi'}}{\sqrt{1-\varepsilon^2\cos^2\varphi' + \{4/\pi^2\}\alpha^2 E^2(\varepsilon,\pi/2)}} \right\} I(\varphi')\,[\sin\varphi\sin\varphi'$$
$$+\sqrt{1-\varepsilon^2}\cos\theta\cos\varphi']\, e^{jk_o a\zeta\sin\theta}\, d\varphi' , \qquad (3.40b)$$

where

$$\zeta = \cos\varphi\cos\varphi' + \sqrt{1-\varepsilon^2}\sin\varphi\sin\varphi' + \{2/\pi\}\alpha\cot\theta E(\varepsilon,\pi/2)\varphi' \quad . \qquad (3.40c)$$

3.4.4 Radiated fields of a single-turn elliptical loop

Towards deriving the field expressions of a single-turn elliptical loop from those of the elliptical helix, we set the number of turns N to unity and the pitch angle α to zero in equations (3.36a) and (3.36b) accordingly, and arrive at:

$$E_\theta = \frac{-j\omega\mu_o a\cos\theta\, e^{-jk_o r}}{4\pi r} \int_0^{2\pi N} I(\varphi')\,[-\cos\varphi\sin\varphi' + \sqrt{1-\varepsilon^2}\sin\varphi\cos\varphi']\, e^{jk_o a\zeta\sin\theta}\, d\varphi' , \qquad (3.41a)$$

and

$$E_\varphi = \frac{-j\omega\mu_o a e^{-jk_o r}}{4\pi r} \int_0^{2\pi N} I(\varphi')\,[\sin\varphi\sin\varphi' + \sqrt{1-\varepsilon^2}\cos\theta\cos\varphi']\, e^{jk_o a\zeta\sin\theta}\, d\varphi' , \qquad (3.41b)$$

in which

$$\zeta = \cos\varphi\cos\varphi' + \sqrt{1-\varepsilon^2}\sin\varphi\sin\varphi' \quad . \qquad (3.41c)$$

3.4.5 Radiated fields of a multi-turn circular loop

The analytical expressions for the radiated fields of a multi-turn circular loop are readily deducible from equations (3.36a) and (3.36b) for the elliptical helix by setting the pitch angle α to a small value such that $\tan\alpha \approx \alpha$, $\sec\alpha \approx 1$. The choice of eccentricity ε equals zero is also made, so that the field equations modify to

$$E_\theta = \frac{-j\omega\mu_o a\cos\theta\, e^{-jk_o r}}{4\pi r}\int_0^{2\pi N} I(\varphi')\,[\sin(\varphi-\varphi') - \alpha\tan\theta]\, e^{jk_o a\sin\theta[\cos(\varphi-\varphi')+\alpha\cot\theta\varphi']}\, d\varphi', \qquad (3.42a)$$

and

$$E_\varphi = \frac{-j\omega\mu_o a\, e^{-jk_o r}}{4\pi r}\int_0^{2\pi N} I(\varphi')\,[\cos(\varphi-\varphi')]\, e^{jk_o a\sin\theta[\cos(\varphi-\varphi')-\alpha\cot\theta\varphi']}\, d\varphi' \quad , \qquad (3.42b)$$

for a multi-turn circular-loop thin-wire antenna.

3.4.6 Radiated fields of a single-turn circular loop

When the substitutions N =1, $\alpha = 0^o$, $\varepsilon = 0$, and $E(0,\pi/2) = \pi/2$ are made in equations (3.36a) and (3.36b), we arrive at the radiation field formulas for a single-turn circular loop positioned on the z = 0 plane:

$$E_\theta = \frac{-j\omega\mu_o a\cos\theta\, e^{-jk_o r}}{4\pi r}\int_0^{2\pi N} I(\varphi')\,[\sin(\varphi-\varphi')]\, e^{jk_o a\sin\theta\cos(\varphi-\varphi')}\, d\varphi' \quad , \qquad (3.43a)$$

and

$$E_\varphi = \frac{-j\omega\mu_o a\, e^{-jk_o r}}{4\pi r}\int_0^{2\pi N} I(\varphi')\,[\cos(\varphi-\varphi')]\, e^{jk_o a\sin\theta\cos(\varphi-\varphi')}\, d\varphi' \quad , \qquad (3.43b)$$

which are in agreement with the exact field expressions formulated for a circular loop antenna by Adekola (1983).

3.4.7 Radiated fields of a linear antenna along the z-axis

When in equations (3.36a) and (3.36b), the substitutions identified as

$$\left.\begin{aligned} &\varepsilon = 0 \\ &E(0, \pi/2) = \pi/2 \end{aligned}\right\} \tag{3.44a}$$

and the limiting values

$$\left.\begin{aligned} &a \to 0 \\ &\alpha \to \pi/2 \\ &a \tan\alpha\, \varphi' \to z' \\ &a \tan\alpha\, d\varphi' \to dz' \end{aligned}\right\} \tag{3.44b}$$

are made, the radiated fields of a linear antenna of length L lying along the z-axis will admit description according to the expressions:

$$E_\theta = \frac{j\omega\mu_o \sin\theta\, e^{-jk_o r}}{4\pi r} \int_0^L I(z')\, e^{jk_o z' \cos\theta}\, dz' \quad , \tag{3.45a}$$

and

$$E_\varphi = 0 \quad . \tag{3.45b}$$

Equations (3.45a) and (3.45b) are consistent with the results reported by Harrington (1961) for a linear antenna positioned on the z-axis.

3.4.8. Radiated fields of a linear antenna on the x-axis

In this case, specialization is defined by the values given, for the relevant antenna parameters, as:

$$\left.\begin{aligned} &\varepsilon = 1 \\ &N = 1 \\ &E(1, \pi/2) = 1 \\ &\alpha = 0 \\ &x' = a\cos\varphi' \\ &dx' = -a\sin\varphi'\, d\varphi' \end{aligned}\right\} \quad , \tag{3.46}$$

And when these specialization values are substituted into equations (3.36a) and (3.36b), we find that for a linear horizontal antenna lying on the x-axis,

$$E_\theta = \frac{-j\omega\mu_o \cos\theta\, e^{-jk_o r}}{4\pi r} \int_{-a}^{a} I(x') \cos\varphi\, e^{jk_o x' \cos\varphi \sin\theta}\, dx' \quad , \tag{3.47a}$$

and

$$E_{\varphi} = \frac{j\omega\mu_o\, e^{-jk_o r}}{4\pi r} \int_{-a}^{a} I(x') \sin\varphi\, e^{jk_o x' \cos\varphi \sin\theta}\, dx' \quad . \tag{3.47b}$$

This concludes the specializations of the generalized radiation integrals to the special cases of **eight basic thin-wire antennas**. In the next chapter, the method adopted for the solution of the generalized integrodifferential operator equation, as well as the definitions of antenna design parameters of interest in this thesis will be presented.

Chapter 4

METHOD OF SOLUTION AND ANTENNA DESIGN PARAMETERS

4.1 Method of Solution

Having formulated the integrodifferential operator equation governing the electromagnetic response of an elliptical-cylindrical helical beam antenna to excitation by incident plane electromagnetic field in Section 3.2, this section focuses attention on the solution of the aforesaid equation. The said solution essentially concerns the determination of the current distribution on the helical arm, which quantity remains the only unknown in the governing equation. In this thesis, the solution for this unknown is effected through the method of moments, which has been established [Harrington 1967, 1968] as a versatile technique for determining the distribution of current on virtually all antenna types.

The operator equation governing the elliptical-helical antenna problem has been deduced in §3.2 as

$$E_{\varphi}^{i} = \Im[I(\varphi')] \quad , \tag{4.1}$$

in which the unknown quantity I(φ') represents the current distribution, E_{φ}^{i} incident electric field, whilst the integrodifferential operator $\Im[*]$ takes the form:

$$\Im[*] = \int_{0}^{2\pi N} \left\{ \left[\frac{\sin\varphi\sin\varphi' + (1-\varepsilon^2)\cos\varphi\cos\varphi' + \{4/\pi^2\}\tan^2\alpha E^2(\varepsilon,\pi/2)}{\sqrt{1-\varepsilon^2\cos^2\varphi + \{4/\pi^2\}\tan^2\alpha E^2(\varepsilon,\pi/2)}\sqrt{1-\varepsilon^2\cos^2\varphi' + \{4/\pi^2\}\tan^2\alpha E^2(\varepsilon,\pi/2)}} \right] \right.$$
$$\left. \times \left[\frac{j\omega\mu_o}{4\pi} \right] [*] a\sec\alpha\sqrt{1-\varepsilon^2\cos^2\varphi'} - \left[\frac{1}{j4\pi\omega\varepsilon_o a\sec\alpha\sqrt{1-\varepsilon^2\cos^2\varphi}} \right] \frac{d[*]}{d\varphi'}\frac{d}{d\varphi} \right\} \frac{e^{-jk_o R}}{R} d\varphi' \tag{4.1a}$$

where

$$R = a\sqrt{\left(\frac{r_w}{a}\right)^2 + 4\sin^2\left(\frac{\varphi-\varphi'}{2}\right) - \varepsilon^2(\sin^2\varphi - 2\sin\varphi\sin\varphi' + \sin^2\varphi') + \frac{4\tan^2\alpha}{\pi^2}E^2(\varepsilon,\frac{\pi}{2})(\varphi-\varphi')^2} \tag{4.1b}$$

with all symbols retaining their previous definitions. The starting point in the solution for this unknown is the discretization of the wire helix into small segments, followed by the series expansion of the unknown current $I(\varphi')$ in terms of the expansion (or basis) functions symbolized here by $T_k(\varphi')$ and unknown superposition coefficients α_k in the following manner:

$$I(\varphi') = \sum_{k=1}^{K} \alpha_k T_k(\varphi') \quad . \tag{4.2}$$

In this work, the expansion functions $T_k(\varphi')$ are piecewise linear functions (triangles) of unit height, defined over four consecutive wire segments, in which each segment length is greater than five times the wire radius (Kuo and Strait 1972); that is:

$$T_k(\varphi') = \begin{cases} \dfrac{\varphi' - \varphi'_{2k-1}}{\varphi'_{2k+1} - \varphi'_{2k-1}} & \varphi'_{2k-1} \le \varphi' \le \varphi'_{2k+1} \\ \dfrac{\varphi'_{2k+3} - \varphi'}{\varphi'_{2k+3} - \varphi'_{2k+1}} & \varphi'_{2k+1} \le \varphi' \le \varphi'_{2k+3} \\ 0 & elsewhere \end{cases} \quad . \tag{4.2a}$$

Typical triangle expansion functions are depicted in Figure 4.1a. It is clear from equation (4.1a) that there is a need for the first derivative of the triangular expansion function which, analytically, is expressible as:

$$\frac{dT_k(\varphi')}{d\varphi'} = \begin{cases} \dfrac{1}{\varphi'_{2k+1} - \varphi'_{2k-1}} & \varphi'_{2k-1} \le \varphi' \le \varphi'_{2k+1} \\ \dfrac{-1}{\varphi'_{2k+3} - \varphi'_{2k+1}} & \varphi'_{2k+1} \le \varphi' \le \varphi'_{2k+3} \\ 0 & elsewhere \end{cases} \quad , \tag{4.3}$$

and whose diagrammatic representation is provided in Figure 4.1b.

Upon substituting equation (4.2) in equation (4.1), and invoking the intrinsic linearity property of the operator $\Im[*]$, we arrive at the expression given as

$$E'_{\varphi} = \sum_{k=1}^{K} \alpha_k \, \Im[T_k(\varphi')] \quad , \tag{4.4}$$

which, contains K unknown constants. Next, we define an inner product for two vectors $\langle \overline{A}, \overline{B} \rangle$, and then take the inner product of both sides of equation (4.4) with the weighting (testing) functions $W_j(\varphi)$ defined on the wire surface resulting in

$$\langle W_j(\varphi), E'_{\varphi} \rangle = \sum_{k=1}^{K} \alpha_k \langle W_j(\varphi), \Im[T_k(\varphi')] \rangle \tag{4.5}$$

provided that the notation $\langle \bullet, \bullet \rangle$ represents the inner product operation.

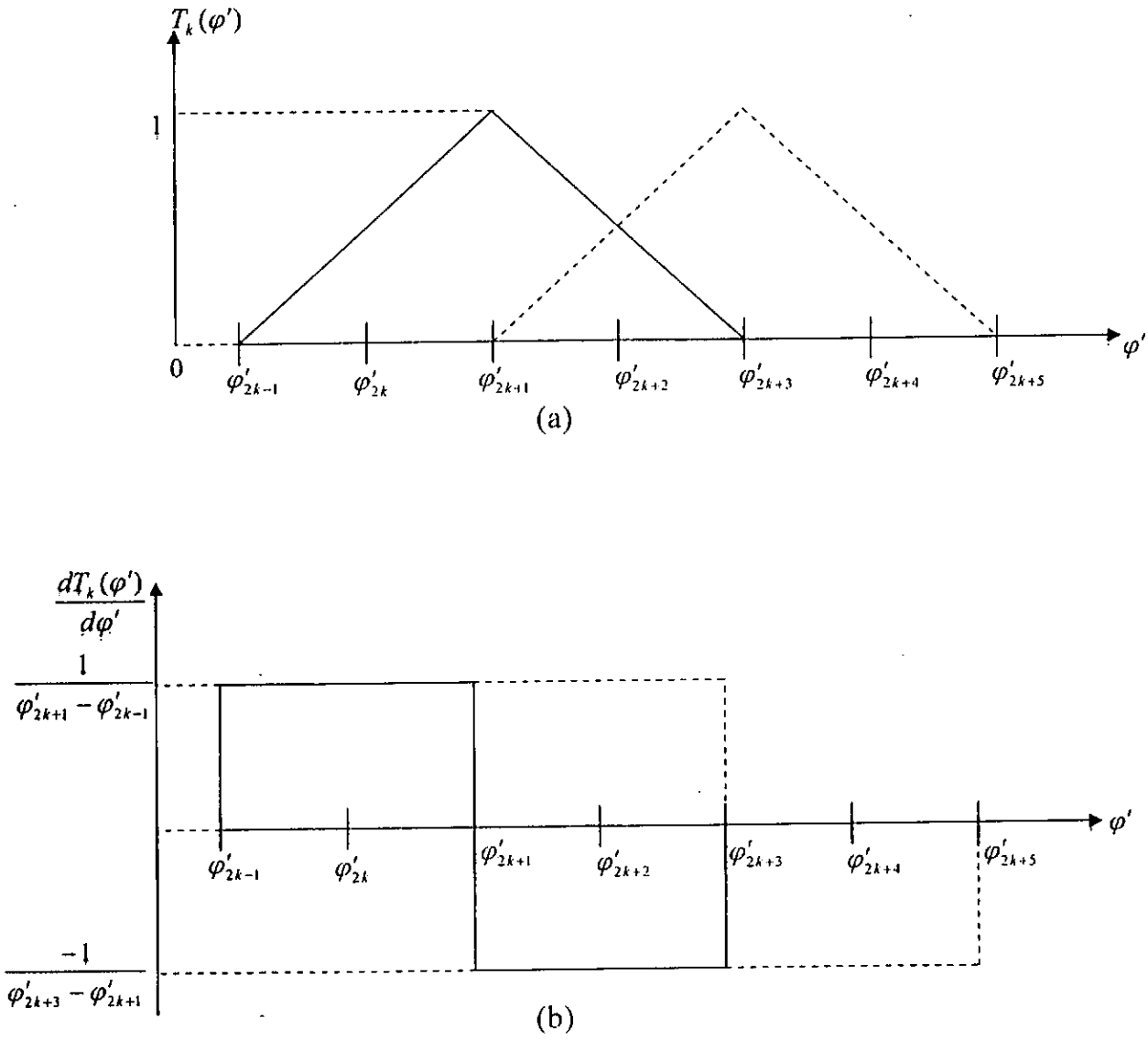

Figure 4.1: Typical expansion triangle functions **(a)** and their first derivatives **(b)**.

On account of the computational merits of the Galerkin scheme in which the expansion and weighting functions are identically defined, we adopt this scheme by defining the weighting functions as follows:

$$W_j(\varphi) = \begin{cases} \dfrac{\varphi - \varphi_{2j-1}}{\varphi_{2j+1} - \varphi_{2j-1}} & \varphi_{2j-1} \le \varphi \le \varphi_{2j+1} \\ \dfrac{\varphi_{2j+3} - \varphi}{\varphi_{2j+3} - \varphi_{2j+1}} & \varphi_{2j+1} \le \varphi \le \varphi_{2j+3} \\ 0 & elsewhere \end{cases} \tag{4.6}$$

which is structurally akin to $T_k(\varphi')$ of equation (4.2a). Following Harrington (1968), we recast equation (4.5) in matrix form in terms of the generalized network parameters:

$$[V_j] = [Z_{jk}][I_k] \tag{4.7}$$

where

$$\left.\begin{aligned} [V_j] &= \langle W_j(\varphi), E^i_\varphi \rangle \\ [Z_{jk}] &= \langle W_j(\varphi), \Im[T_k(\varphi')] \rangle \\ [I_k] &= [\alpha_k] \end{aligned}\right\} \tag{4.7a}$$

and $[V_j]$ stands for generalized voltage matrix, $[Z_{jk}]$ for generalized impedance matrix, and $[I_k]$ for generalized current matrix. Thus, equation (4.7) is generally referred to as the generalized Ohm's law equation (Harrington 1967). Through matrix operations of inversion and multiplication, the desired superposition coefficients emerge as

$$[I_k] = [\alpha_k] = [Z_{jk}]^{-1}[V_j] \tag{4.8}$$

where $[*]^{-1}$ denotes matrix inversion. This completes the formal determination of generalized current distribution on the elliptical helical antenna consequent upon which the calculation of the radiated fields of the antenna as well as certain important antenna design parameters becomes a relatively straightforward matter. In the ensuing section,

analytical expressions for the conventional antenna parameters are developed, in terms of the fields associated with $I(\varphi')$.

4.2 Antenna Directivity

The directivity of an antenna, symbolized by $D(\theta,\varphi)$, may be defined as the ratio of the far-zone power density to the total radiated power (Stutzman and Thiele 1981) given mathematically, in the following manner:

$$D(\theta,\varphi) = 4\pi \frac{P(\theta,\varphi)}{P_{total}} \quad , \tag{4.9}$$

where

$$P(\theta,\varphi) = \frac{1}{2\eta_o}\left[\left|E_\theta(\theta,\varphi)\right|^2 + \left|E_\varphi(\theta,\varphi)\right|^2\right] \quad , \tag{4.10}$$

and η_o ($=377\Omega$) is the intrinsic impedance of free space. The field components E_θ and E_φ featuring in equation (4.10) are calculated from equations (3.36a) and (3.36b), respectively, using the current distribution $I(\varphi')$ given by equation (4.8). When the antenna is supported by a ground plane of infinite extent, no field will be radiated to the lower half-space. Bearing this fact in mind, the total power radiated assumes a form given as

$$P_{total} = \int_0^{2\pi}\int_0^{\frac{\pi}{2}} P(\theta,\varphi) r^2 \sin\theta \quad d\theta\, d\varphi \quad , \tag{4.11}$$

which can be readily evaluated numerically.

4.3 Side lobe level of radiation patterns

As contained in the IEEE Definitions of Terms for Antennas (1983), the side-lobe level (*SLL*) of a radiation pattern is the ratio of the radiation intensity of a side lobe in the direction of its maximum value to that of the intended lobe, and is usually expressed in decibels. According to Stutzman and Thiele (1981), this definition admits expression as

$$SLL = 20\log\left[\frac{|F(SLL)|}{|F(\max)|}\right] \quad (dB) \quad , \tag{4.12}$$

in which |F(SLL)| denotes the pattern value of the highest side lobe magnitude, and |F(max)| stands for the maximum value of the pattern magnitude which is unity for a normalized pattern.

4.4 Input impedance and input power

Input impedance Z_{in} of the antenna is given by the ratio of the applied voltage V_{in} to the current I_{in} at the feed-point. That is to say,

$$Z_{in} = \frac{V_{in}}{I_{in}} = R_{in} + jX_{in} = |Z_{in}|\angle\theta_{in} \quad , \tag{4.13}$$

where $|Z_{in}|$ and θ_{in} are, respectively, the magnitude and phase of the input impedance, and R_{in} and X_{in} stand for the input resistance and input reactance, respectively. On the other hand, the input power P_{in} to the antenna at the feed-point is calculated using the usual power formula:

$$P_{in} = \tfrac{1}{2}|I_{in}|^2\,\Re e(Z_{in}) \quad , \tag{4.14}$$

where $\Re e(Z_{in})$ represents the real part of the input impedance and | * | means the absolute value.

4.5 Front-to-back ratio and axial ratio

The front-to-back ratio (F/B) of an antenna's radiation intensity at the far-zone may be determined using the expression (Adekola and Okereke 1997):

$$F/B(dB) = 10\log_{10}\left[\frac{|E_\theta(\theta_f,\varphi_f)|^2 + |E_\varphi(\theta_f,\varphi_f)|^2}{|E_\theta(\theta_b,\varphi_b)|^2 + |E_\varphi(\theta_b,\varphi_b)|^2}\right], \tag{4.15}$$

where (θ_f, φ_f) and (θ_b, φ_b) assume the respective values (0°, 0°) and (180°, 0°). The calculation of the axial ratio AR(dB) of the radiated fields (E_θ, E_φ) along the helix axis ($\theta = 0°$, $\varphi = 0°$) which describes the **degree of circular polarization** of the radiated

field is performed without assuming time-phase quadrature between E_θ and E_φ components (Balanis 1982); this quantity is given by

$$AR(dB) = 10\log_{10}\left[\frac{|E_\theta|^2 + |E_\varphi|^2 + [|E_\theta|^4 + |E_\varphi|^4 + 2|E_\theta|^2|E_\varphi|^2\cos(2\delta)]^{1/2}}{|E_\theta|^2 + |E_\varphi|^2 - [|E_\theta|^4 + |E_\varphi|^4 + 2|E_\theta|^2|E_\varphi|^2\cos(2\delta)]^{1/2}}\right], \quad (4.16)$$

where δ denotes the time-phase difference between the field components.

4.6 Directive gain and half-power beam-width

The directive gain of an antenna symbolized by G_d is evaluated in terms of the far-zone radiation field components by the expression (Stutzman and Thiele 1981):

$$G_d(\theta,\varphi)(dB) = 10\log_{10}\left[\frac{[|E_\theta(\theta,\varphi)|^2 + |E_\varphi(\theta,\varphi)|^2]r^2}{60P_{in}}\right], \quad (4.17)$$

where $(\theta, \varphi) = (0^\circ, 0^\circ)$, P_{in} input power given by equation (4.14), and r is the distance from the origin to the field point. The half-power beam-width (HPBW) of the radiated field patterns is taken as **the average of the HPBWs of the E_θ and E_φ patterns in the vertical plane defined by $\varphi = 0^\circ$.**

Chapter 5

COMPUTATIONAL RESULTS AND DISCUSSIONS

Numerical results obtained for two helical-beam antenna configurations, through the use in computations, of the general analytical results developed by the thesis, are presented and discussed in this chapter. These results concern the two cases itemized below:

(i) helical antenna excited without a ground plane, or the *exclusion-mode helix*,

(ii) helical antenna backed by a small ground plane modelled by a wire grid.

The solution of the exclusion-mode helix problem not only fills the existing gap in the open literature, but also facilitates a comparative study directed at eliciting new design options. On the other hand, the solution of the problem described in case (ii) validates the applicability of the generalized theory of the thesis, and also elucidates the contributions to antenna performance features attributable to the small ground plane. Computed results are compared with published experimental and theoretical results of other authors, and this exercise validates the correctness of the results reported in this thesis.

5.1 Electromagnetic characteristics of the exclusion-mode helical antenna

The candidate, exclusion-mode helix, is excited by a delta-gap feed point generator, and has the following physical parameters: number of turns (N) = 7; the electrical circumference (C_λ): 0.8λ - 1.15λ, pitch angle (α): 10^0 and 15^0, which have been shown to be characteristic of the axial/beam-mode of helical antenna radiation (Lee and Wong 1984, Kraus 1988). A centre frequency of 2GHz, which is the intermediate frequency between L and S bands commonly utilized for satellite communications, is selected. The discussion of the numerical results obtained begins with the current distributions on the helical arm.

5.1.1 Current distributions on the helical arm

In order to investigate the dependence of the current distributions on the helix pitch angle, numerical data for the magnitude of current is displayed as a function of normalized helical arm, in Figures 5.1 and 5.2. It is evident from Figures 5.1 and 5.2 that the current profiles of the exclusion-mode helix when the parameter C_λ is within the range specified by $0.8 \leq C_\lambda \leq 1.15$, are exponentially decaying in character, with the maximum value of magnitude of current at the feed-point. It is also to be seen from the same illustrations that for values of C_λ greater than 1.05, the surface wave component of the current profiles becomes more noticeable, evidently, due to the significant increase in reflection from the open end and also increase in the total electrical arm length of the helix. With exception of the region close to the feed-point, the current profiles for the 10° helix and the 15° helix are distinct from one another. This contrasts with the current distribution on a monofilar helix backed by a small ground plane, whose magnitude is virtually independent of the pitch angle (Nakano *et al.* 1988).

It is clearly observed from both figures that the magnitude of current at the feed-point increases as the C_λ increases, and that the location of first minimum point shifts towards the feed-point as C_λ increases. The curves indicate that current distribution is characterized by a standing wave component at the open end (due to reflections at that end), and that the magnitude of this component assumes higher values as the operating frequency increases. One important conclusion arising from the foregoing observations is **that any desirable current distribution along the arm of an exclusion-mode helix may be realized through an informed choice of a combination of pitch angle and the operating frequency.**

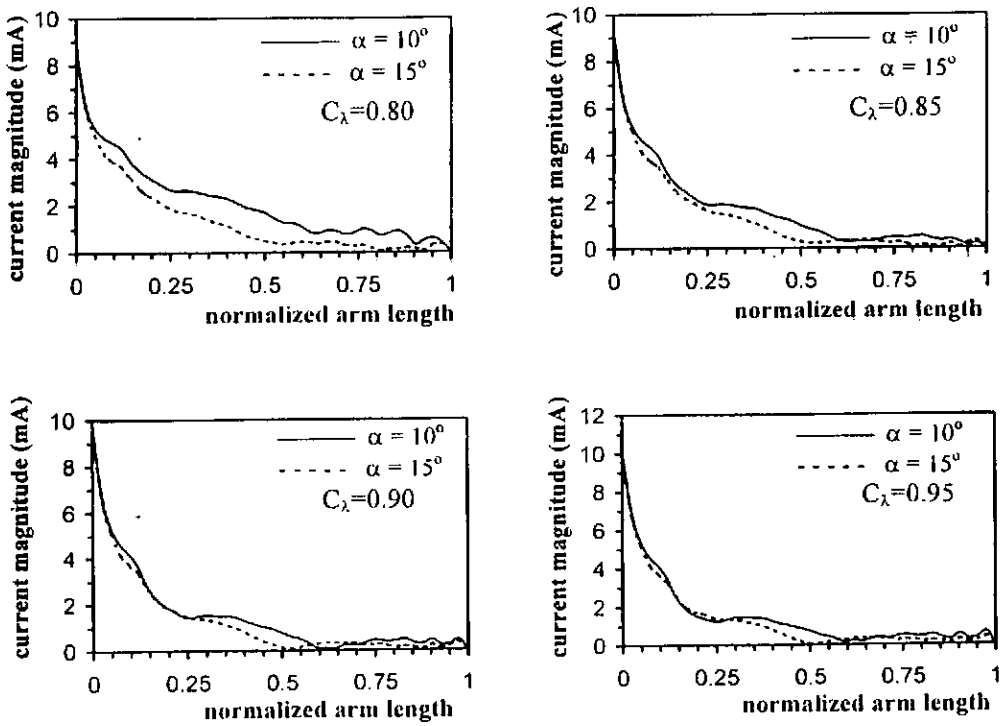

Figure. 5.1 : *Current distributions on the exclusion-mode helical antenna:*
C_λ = 0.80 - 0.95

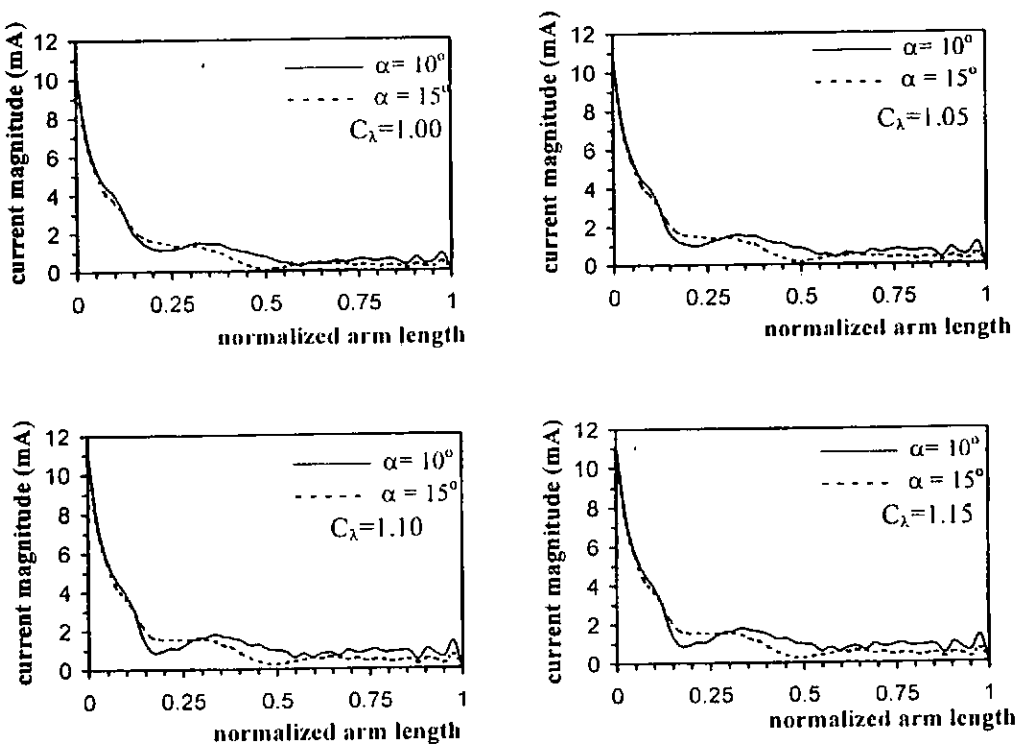

Figure 5.2: *Current distributions on the exclusion-mode helical antenna:*
C_λ = 1.00 - 1.15

5.1.2 Far-zone electric fields

The far-zone electric field patterns on the vertical plane (x-z plane, defined by $\varphi = 0^{o}$) generated by the corresponding current distributions described by Figures 5.1 and 5.2 and computed from equations (3.37a) and (3.37b), are displayed in Figures 5.3 and 5.4 for $\alpha = 10^{o}$ and 15°, respectively. In the aforementioned illustrations, the dashed curves represent the $\hat{\varphi}$-component of the electric field (E_{φ}) while the solid curves depict the $\hat{\theta}$-component of the electric field (E_{θ}). It is evident from Figures 5.3 and 5.4 that the main lobes of the radiation patterns are virtually in the backward direction ($\theta = 180^{o}$), which reveals that the radiated electromagnetic energy is concentrated in the backfire direction. According to the dictates of electromagnetic theory and practice (Walter 1970), these features suggest that the phase velocity of the current wave is directed towards the feed-point while the group velocity is directed away from the feed-point. We may conclude therefore that, an *exclusion-mode helix* may be categorized as a backfire antenna, the type utilized in practice as feed for the paraboloidal reflector. The radiation patterns also reveal that directivity decreases as the helix circumference increases; in other words, as the frequency increases, the half-power beam-width also increases. This phenomenon is contrary to a general observation in antenna work, (Kraus 1950), that the half-power beam-width decreases as the frequency increases. One other noteworthy observation is that as C_{λ} increases, radiation in the axial forward direction also increases, without doubt, due to the marked increase in the surface wave component of the current distributions of the exclusion-mode helix. Finally, it can be seen that for the value of pitch angle $\alpha = 15^{o}$, the radiation patterns are generally broader than when $\alpha = 10^{o}$, and this observation leads to the important conclusion that the far-zone field patterns of an exclusion-mode helix can readily be controlled, as may be desired, by a judicious selection of both the pitch angle and the helix circumference.

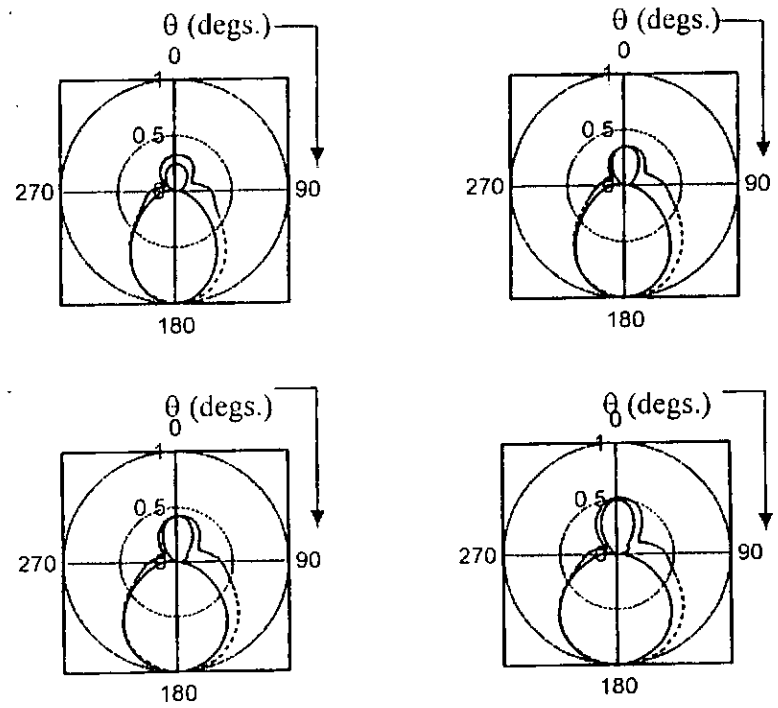

Figure 5.3a: *Normalized field patterns of the helical antenna without a ground plane: $\alpha = 10^o$ and C_λ:0.80 - 0.95.* ——— E_θ component ----- E_φ component

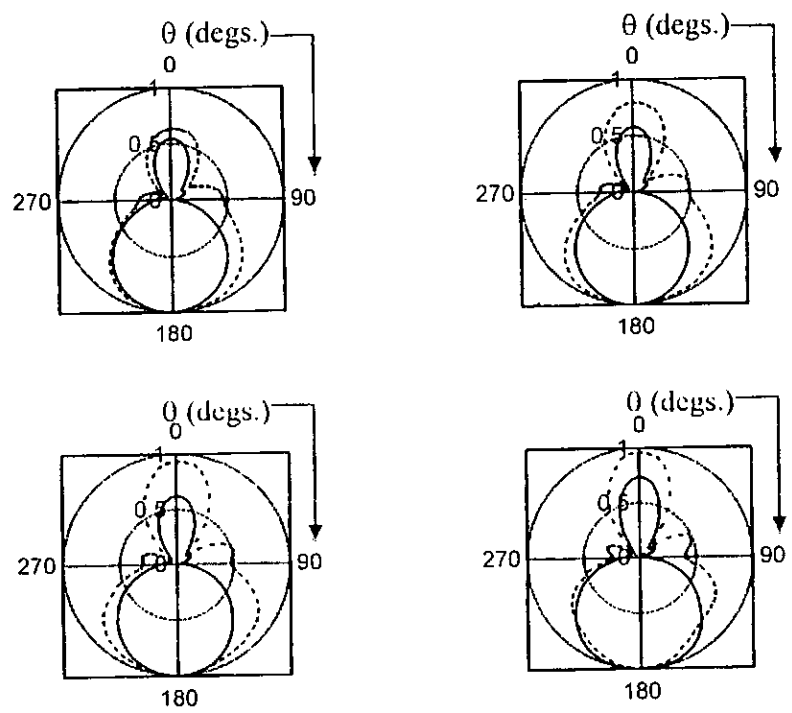

Figure 5.3b: *Normalized field patterns of the helical antenna without a ground plane: $\alpha = 10^o$ and C_λ:1.00- 1.15.* ——— E_θ component ----- E_φ component

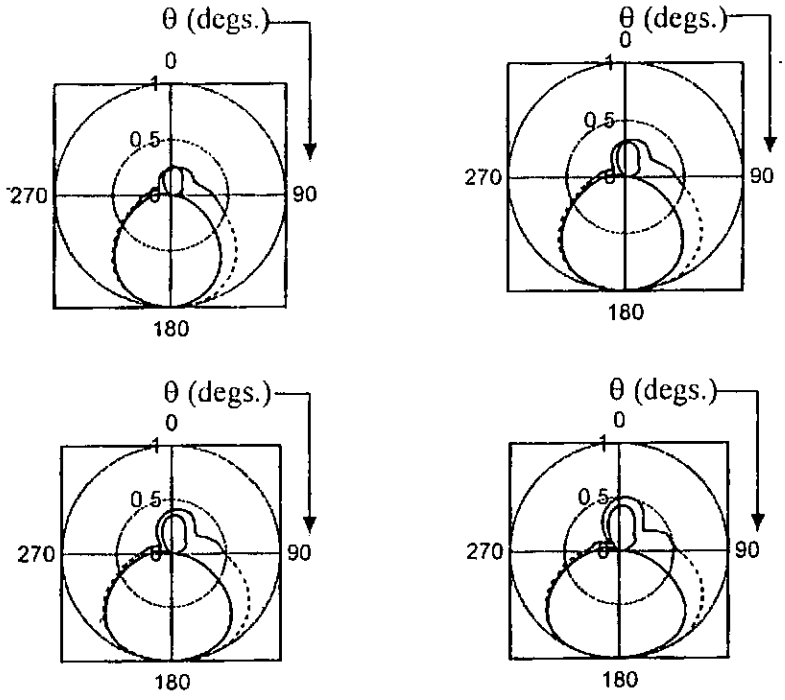

Figure 5.4a: *Normalized field patterns of the helical antenna without a ground plane: α =15° and C_λ:0.80 -0.95* ——— E_θ component - - - - - E_φ component

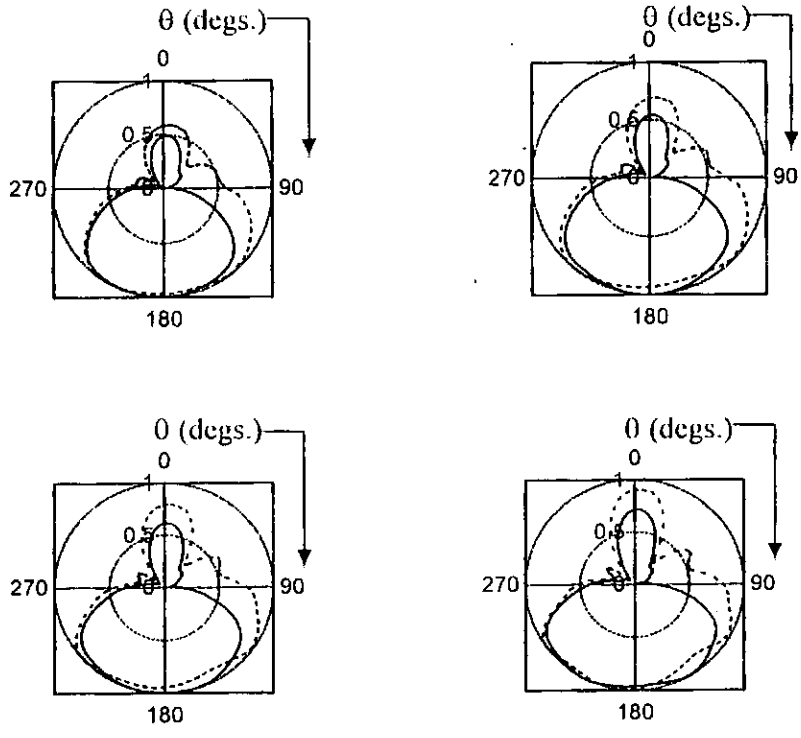

Figure 5.4b: *Normalized field patterns of the helical antenna without a ground plane: α =15° and C_λ : 1.00 - 1.15.* ——— E_θ component - - - - - E_φ component

5.1.3 Input impedance

Computed values of input impedance of the antenna are displayed as a function of C_λ in Figure 5.5. It is clear from that figure that the resistive part of the input impedance denoted by R_{in} has a nearly flat profile, indicating that the input resistance does not generally depend on frequency. Nonetheless, we find that R_{in} assumes lower values when $\alpha = 10^\circ$ compared with its values for $\alpha = 15^\circ$. An average value of R_{in} over the frequency range investigated when $\alpha = 10^\circ$ is about 75Ω while an average value of about 80Ω is recorded for the case $\alpha = 15^\circ$.

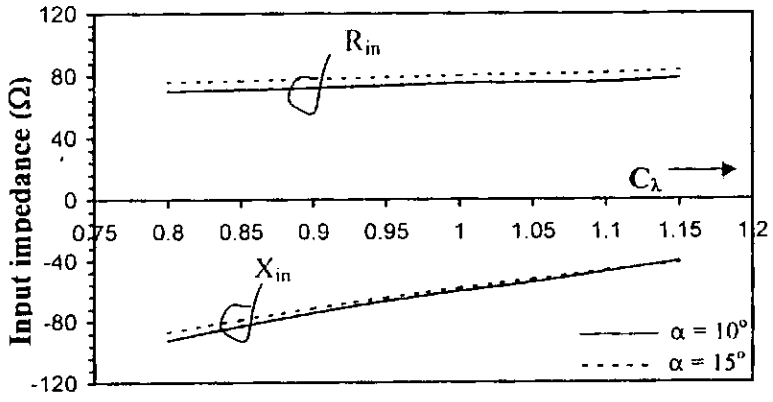

Figure 5.5: *Input impedance against helix electrical circumference (C_λ)*

Except at lower values of C_λ, the input reactance (X_{in}) is almost the same for the two values of pitch angles (10° and 15°) considered. X_{in} varies linearly with frequency, with a positive slope for both α=10° and 15°. In other words, the input reactance increases as C_λ increases or as the frequency increases. And for the range of C_λ investigated, the input reactance is predominantly capacitive regardless of the values of C_λ and α. *Because the magnitude of X_{in} ranges uniformly between 41Ω and 92Ω, it is apparent that the design of an impedance matching network for the exclusion-mode helical antenna is feasible, especially if the desire is for a broadband antenna.*

5.1.4 Input power

The input power symbolized by P_{in} is defined as the active power available to the antenna at its input terminals. The variations of P_{in} as a function of C_λ for both α =10° and 15° are depicted in Figure 5.6. It can be seen from the figure that P_{in} increases linearly with C_λ, with moderate differences for α =10° and 15°; but for C_λ =1.05, a value of 4.33mW is recorded for both α =10° and 15°. *The P_{in} profile suggests that the input power increases as the arm length of the exclusion-mode helix increases.*

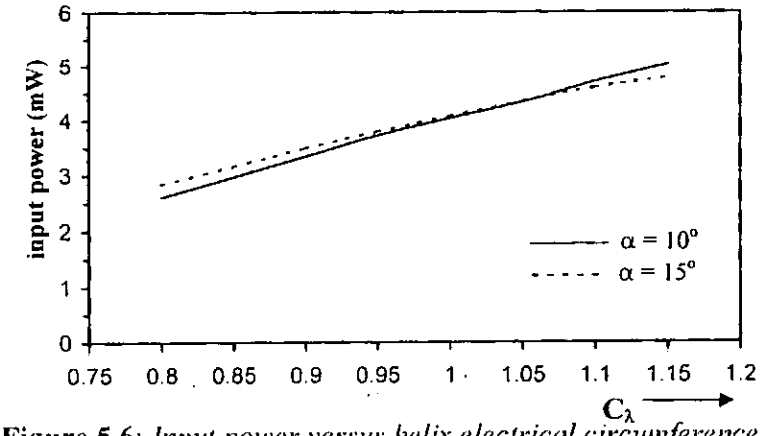

Figure 5.6: *Input power versus helix electrical circumference (C_λ)*

5.1.5 Axial Ratio and Front-to-Back Ratio

The axial ratio is a measure of the degree of circular polarization attained by the radiated fields, and is usually specified to be less than 3dB for circularly polarized antennas (Nakano and Mimaki 1997). For the computation of the axial ratio, the time-phase difference between the $\hat{\theta}$ and $\hat{\varphi}$ components of the fields is usually taken into consideration. As can be seen from Figure 5.7, the axial ratio curve has a wavy character in relation to C_λ , and for the range of C_λ studied, the axial ratio is less than 3dB for the two cases identified by α =10° and 15°. *It is a matter of interest to note that the minimum value of the axial ratio occurred for values of α = 10°, and C_λ =1, the*

latter having been identified by Kraus (1988), as the optimum circumference for the axial-mode operation of helical antennas.

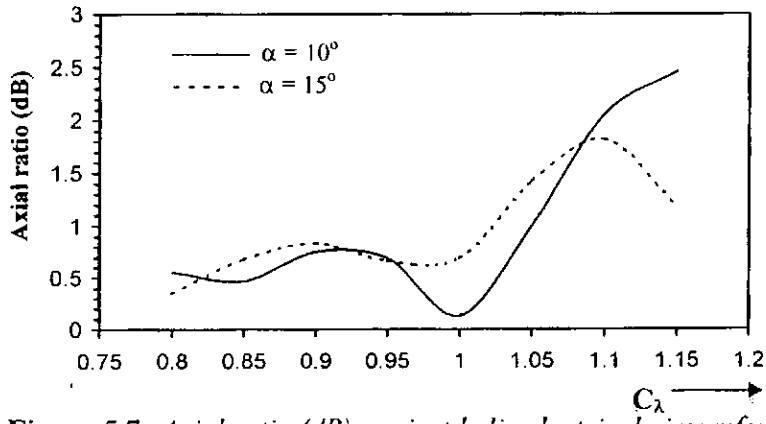

Figure 5.7: *Axial ratio (dB) against helix electrical circumference (C_λ)*

The variation of the front-to-back ratio (F/B) of the radiated field intensity of the exclusion-mode helix with C_λ is illustrated in Figure 5.8. Because the F/B is less than unity for the values of C_λ considered, and for the cases $\alpha = 10^\circ$ and 15°, *the exclusion-mode helical antenna radiates predominantly in the backfire direction, which is consistent with the prediction of Kraus (1950), that when the ground plane is removed from the feeding system of a monofilar helix, it radiates naturally in the backfire direction. This result and associated deduction, it should be remarked, is apparently the first time that Kraus' prediction is being verified through analysis and computational data, to the best of our knowledge.*

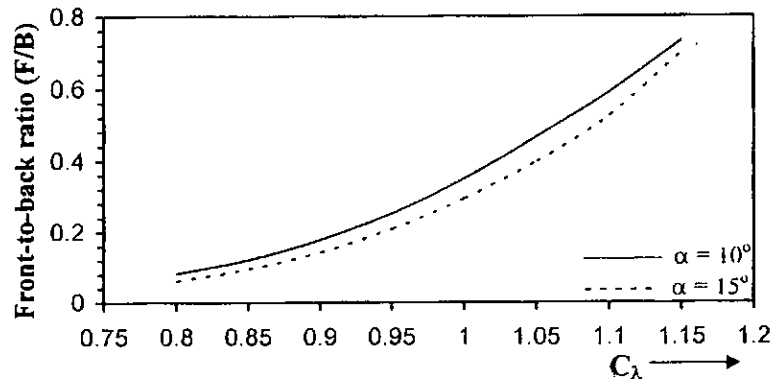

Figure 5.8: *Front-to-back ratio (F/B) versus helix electrical circumference (C_λ).*

5.1.6 Directive gain and half-power beam-width (HPBW)

The variations of the directive gain of the exclusion-mode helix with antenna electrical circumference (C_λ) are portrayed in Figure 5.9, from which it is seen that the directive gain decreases linearly as C_λ increases. It is also to be observed from the curves that for the values of C_λ considered, the antenna has a higher directive gain for a value of $\alpha = 10^\circ$ than for $\alpha = 15^\circ$. Furthermore, we find that the directive gain attains its maximum values for the two cases $\alpha = 10^\circ$ and 15° when $C_\lambda = 0.8$, which suggests that the 10° helix radiates more power in the backward direction than the 15° helix.

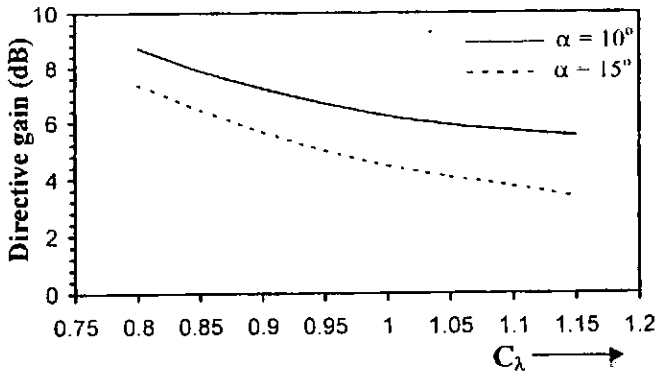

Figure 5.9: *Directive gain (dB) against C_λ*

The half-power beam-width (HPBW) of the radiation pattern produced by the exclusion-mode helix is a performance measurement index for its directional characteristics, and the results describing its variation are displayed in Figure 5.10, for

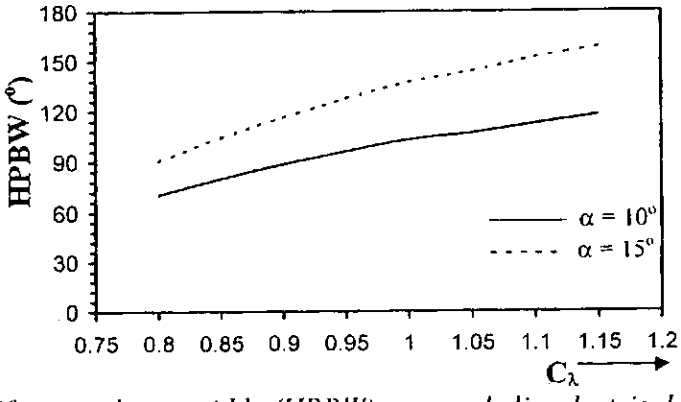

Figure 5.10: *Half-power beam-width (HPBW) versus helix electrical circumference (C_λ)*

values of C_λ ranging between 0.8 and 1.15 and for pitch angles $\alpha = 10^0$ and 15^0 .These profiles of the HPBW reveal that *the HPBW increases as C_λ increases an indication that the HPBW increases as the operating frequency increases.* This is in contrast with a general observation in antenna work that the HPBW decreases as the frequency increases; though this characteristic feature has been reported for the backfire bifilar helical antennas by Nakano and his associates (Nakano *et al.* 1984). The problem of helical-beam antenna backed by a small ground plane is addressed in what follows.

5.2 Input and radiation characteristics of helical-beam antenna backed by wire-grid ground plane

A useful physical approximation valid for conducting surfaces of finite size is provided by the wire-grid originally proposed by Richmond (1966) for the study of scattering of electromagnetic fields by conducting bodies. The model has since been successfully employed by Lin and Richmond (1975), for the electromagnetic characterization of the aircraft body at low frequencies. Nakano *et al* (1988), also utilized the approach for the modeling of the small ground plane supporting a monofilar helix; and Nakano and Nakayama (1999), for a conducting cylinder backing a curved spiral antenna, to mention a few. Apart from their use for modeling conducting bodies, wire-grid screens are commonly utilized for electromagnetic shielding because they are much more cost-effective and lighter in weight than the conventional metal shields, (Hill and Wait 1977). When this model is applied for analysis in the MoM environment, the generalized thin-wire integro-differential equation formulated naturally accommodates the mutual electromagnetic interactions of the wires, as well as the Kirchhoff's current law applicable at the wire junctions, (Kuo and Strait 1972). This thesis is particularly interested in the wire-grid modeling of ground planes of circular cross-sections, which typically feature in the feed mechanism of helical-beam antennas,

and as informed by the results obtained by Jones (1974), who gave a comprehensive analysis of the factors that govern choice of wire-grid dimensions, in practical applications. For ground plane dimensions of interest to the research work reported here, excellent results are obtained, when four circular wires and twelve radial wires form the wire-grid model for the solid plane, as depicted in Figure 5.11 below.

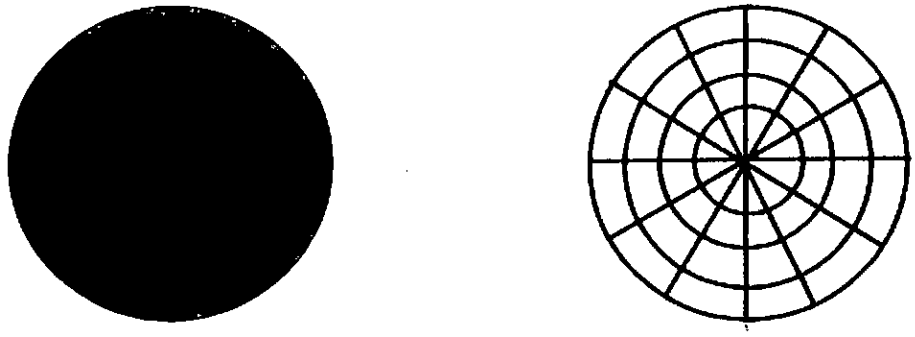

(a) Solid ground plane (b) Wire-grid model of the ground plane

Figure 5.11: *Modelling of a solid ground plane by wire grids.*

For the solution of the design problem of the helical antenna backed by a ground plane of finite extent, (depicted in Figure 5.12a) the attached small ground plane is modelled by wire grids formed by four circular and twelve radial wires (Figure 5.12b), for reasons earlier advanced. Essentially, the problem reduces to that of an exclusion-mode helix operating above a small wire-grid ground plane, and the electromagnetic

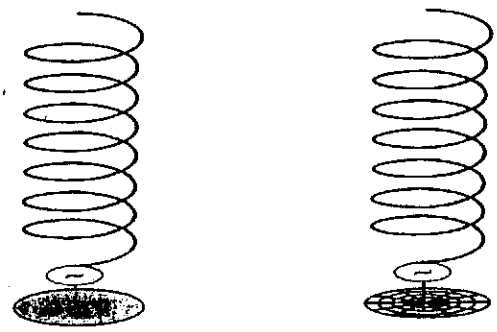

Figure 5.12: *(a) The problem geometry of a helical antenna backed by a finite ground plane; (b) The finite ground plane modeled by wire grids.*

interactions between the exclusion-mode helix and wire grids are completely accounted for by the inclusion of mutual impedance submatrices in the generalized Ohm's law equation formulated for the antenna problem:

$$\begin{bmatrix} Z_{pq}^{11} & Z_{pn}^{11} & Z_{pn}^{12} & Z_{pn}^{13} & Z_{pn}^{14} & Z_{pl}^{11} & Z_{pl}^{12} & Z_{pl}^{13} & Z_{pl}^{14} & Z_{pl}^{15} & Z_{pl}^{16} \\ Z_{mq}^{11} & Z_{mn}^{11} & Z_{mn}^{12} & Z_{mn}^{13} & Z_{mn}^{14} & Z_{ml}^{11} & Z_{ml}^{12} & Z_{ml}^{13} & Z_{ml}^{14} & Z_{ml}^{15} & Z_{ml}^{16} \\ Z_{mq}^{21} & Z_{mn}^{21} & Z_{mn}^{22} & Z_{mn}^{23} & Z_{mn}^{24} & Z_{ml}^{21} & Z_{ml}^{22} & Z_{ml}^{23} & Z_{ml}^{24} & Z_{ml}^{25} & Z_{ml}^{26} \\ Z_{mq}^{31} & Z_{mn}^{31} & Z_{mn}^{32} & Z_{mn}^{33} & Z_{mn}^{34} & Z_{ml}^{31} & Z_{ml}^{32} & Z_{ml}^{33} & Z_{ml}^{34} & Z_{ml}^{35} & Z_{ml}^{36} \\ Z_{mq}^{41} & Z_{mn}^{41} & Z_{mn}^{42} & Z_{mn}^{43} & Z_{mn}^{44} & Z_{ml}^{41} & Z_{ml}^{42} & Z_{ml}^{43} & Z_{ml}^{44} & Z_{ml}^{45} & Z_{ml}^{46} \\ Z_{kq}^{11} & Z_{kn}^{11} & Z_{kn}^{12} & Z_{kn}^{13} & Z_{kn}^{14} & Z_{kl}^{11} & Z_{kl}^{12} & Z_{kl}^{13} & Z_{kl}^{14} & Z_{kl}^{15} & Z_{kl}^{16} \\ Z_{kq}^{21} & Z_{kn}^{21} & Z_{kn}^{22} & Z_{kn}^{23} & Z_{kn}^{24} & Z_{kl}^{21} & Z_{kl}^{22} & Z_{kl}^{23} & Z_{kl}^{24} & Z_{kl}^{25} & Z_{kl}^{26} \\ Z_{kq}^{31} & Z_{kn}^{31} & Z_{kn}^{32} & Z_{kn}^{33} & Z_{kn}^{34} & Z_{kl}^{31} & Z_{kl}^{32} & Z_{kl}^{33} & Z_{kl}^{34} & Z_{kl}^{35} & Z_{kl}^{36} \\ Z_{kq}^{41} & Z_{kn}^{41} & Z_{kn}^{42} & Z_{kn}^{43} & Z_{kn}^{44} & Z_{kl}^{41} & Z_{kl}^{42} & Z_{kl}^{43} & Z_{kl}^{44} & Z_{kl}^{45} & Z_{kl}^{46} \\ Z_{kq}^{51} & Z_{kn}^{51} & Z_{kn}^{52} & Z_{kn}^{53} & Z_{kn}^{54} & Z_{kl}^{51} & Z_{kl}^{52} & Z_{kl}^{53} & Z_{kl}^{54} & Z_{kl}^{55} & Z_{kl}^{56} \\ Z_{kq}^{61} & Z_{kn}^{61} & Z_{kn}^{62} & Z_{kn}^{63} & Z_{kn}^{64} & Z_{kl}^{61} & Z_{kl}^{62} & Z_{kl}^{63} & Z_{kl}^{64} & Z_{kl}^{65} & Z_{kl}^{66} \end{bmatrix} \begin{bmatrix} I_q^1 \\ I_n^1 \\ I_n^2 \\ I_n^3 \\ I_n^4 \\ I_l^1 \\ I_l^2 \\ I_l^3 \\ I_l^4 \\ I_l^5 \\ I_l^6 \end{bmatrix} = \begin{bmatrix} V_p^1 \\ V_m^1 \\ V_m^2 \\ V_m^3 \\ V_m^4 \\ V_k^1 \\ V_k^2 \\ V_k^3 \\ V_k^4 \\ V_k^5 \\ V_k^6 \end{bmatrix} \tag{5.1}$$

In equation (5.1) the subscripts p and q are used for the weighting functions and expansion functions of the helix, the subscripts m and n, the circular-loop element quantities, and the subscripts k and l, the radial element quantities; such that p=1,2,• • • •, M; q=1,2,• • • •, M; i=1,2,• • • •,N; j=1,2,• • • •, N; k=1,2,• • • •, Q; and l=1,2,• • • •, Q. A compact form of equation (5.1) is obtained when the new superscripts α, β, and γ are introduced such that: α = 1; β=1,2,.,4; and γ=1,2,....6; while any combination of two of the superscripts gives the order and number of the sub-matrices:

$$\begin{bmatrix} Z_{pq}^{\alpha\alpha} & Z_{pn}^{\alpha\beta} & Z_{pl}^{\alpha\gamma} \\ Z_{mq}^{\beta\alpha} & Z_{mn}^{\beta\beta} & Z_{ml}^{\beta\gamma} \\ Z_{kq}^{\gamma\alpha} & Z_{kn}^{\gamma\beta} & Z_{kl}^{\gamma\gamma} \end{bmatrix} \begin{bmatrix} I_q^{\alpha} \\ I_n^{\beta} \\ I_l^{\gamma} \end{bmatrix} = \begin{bmatrix} V_p^{\alpha} \\ V_m^{\beta} \\ V_k^{\gamma} \end{bmatrix} \tag{5.2}$$

In physical terms, $Z_{pq}^{\alpha\alpha}$ is the impedance sub-matrix of an isolated exclusion-mode helix; $Z_{pn}^{\alpha\beta}$ is a mutual impedance sub-matrix, which models the electromagnetic interactions between the helix and the indicated circular-loop elements; $Z_{pl}^{\alpha\gamma}$ is another

mutual impedance sub-matrix, and in this case, it models interactions between the helix and the indicated radial elements; the sub-matrix $Z_{mq}^{\beta\alpha}$ models the mutual coupling between circular-loop elements and the helix, whilst $Z_{mn}^{\beta\beta}$ is the corresponding impedance sub-matrix for an isolated circular element; the other impedance sub-matrices appearing in the equation can be physically interpreted in the same manner. I_q^α is the column vector containing the unknown current expansion coefficients for the monofilar helix; and I_n^β the corresponding column vector for the respective circular elements, and I_l^γ that for the respective radial elements. V_p^α is the voltage excitation submatrix of the monofilar helix; V_m^β is the voltage excitation submatrix of the respective circular elements; and V_k^γ is the voltage excitation submatrix of the respective radial elements. Taking cognizance of the fact that only the monofilar helix is excited by a delta-function generator of 1V, all the entries of the sub-matrices V_m^β and V_k^γ are zero accordingly. It can readily be verified that the compact and well-structured impedance matrix of equation (5.2) is actually an (11x11) matrix as clearly shown in equation (5.1). It is now a simple matter to obtain the desired complete solution of the current distributions for the radiating elements of the antenna system as follows:

$$\begin{bmatrix} I_q^\alpha \\ I_n^\beta \\ I_l^\gamma \end{bmatrix} = \begin{bmatrix} Z_{pq}^{\alpha\alpha} & Z_{pn}^{\alpha\beta} & Z_{pl}^{\alpha\gamma} \\ Z_{mq}^{\beta\alpha} & Z_{mn}^{\beta\beta} & Z_{ml}^{\beta\gamma} \\ Z_{kq}^{\gamma\alpha} & Z_{kn}^{\gamma\beta} & Z_{kl}^{\gamma\gamma} \end{bmatrix}^{-1} \begin{bmatrix} V_p^\alpha \\ V_m^\beta \\ V_k^\gamma \end{bmatrix} \tag{5.3}$$

Without much difficulty, equation (5.2) can be readily perturbed to address the design problem of a monofilar helix backed by an array of parasitic loops, whose solution has been reported in a paper contained in Appendix Ia.

One way of determining the effects of the small ground plane that typically features in the feed arrangement of helical-beam antennas is to compare the

performance characteristics of the antenna with a small ground plane modelled by wire grids which is designated as **Wire-Grid Antenna (WGA)**, with those of the **Exclusion-Mode Antenna (EMA)**. Computational results generated for the WGA and EMA were based on the following geometrical parameters: *the number of helix turns = 7, wire radius = 0.043mm, helix radius = 4mm, pitch angle (α) = 10° and 15°, small ground plane radius = 0.8 of the helix radius.* The operating frequency lies between 9GHz and 14GHz, so that the helix circumference (in units of wavelength) varies from 0.75λ to 1.17λ. This frequency range is chosen to facilitate the comparisons of the computational results with those of Nakano *et al* (1988). Both the WGA and EMA are excited by a 1V delta-gap generator, and the results are discussed in the next section.

5.2.1 Input impedance and input power

The magnitude and phase profiles of the input impedance for both the WGA and EMA are displayed in figures 5.13a and 5.13b for α = 10° and 15°, respectively. It can be seen from the figures that within the frequency band 9.0GHz - 14.0GHz, the magnitude of the input impedance for EMA is higher than that for WGA for both α = 10° and 15°. Whereas the $|Z_{in}|$ for the EMA decreases somewhat uniformly as the frequency increases, that of WGA varies significantly at the lower end of the frequency regime but displays a linear variation with a small negative slope at the upper stratum of the frequency band. This behaviour of $|Z_{in}|$ for the WGA is akin to that of a monopole antenna mounted on a finite ground plane (Awadalla and Maclean 1978). It is also observed that there is a moderate reduction in the values of $|Z_{in}|$ for both WGA and EMA when the pitch angle α assumes a value of 15°.

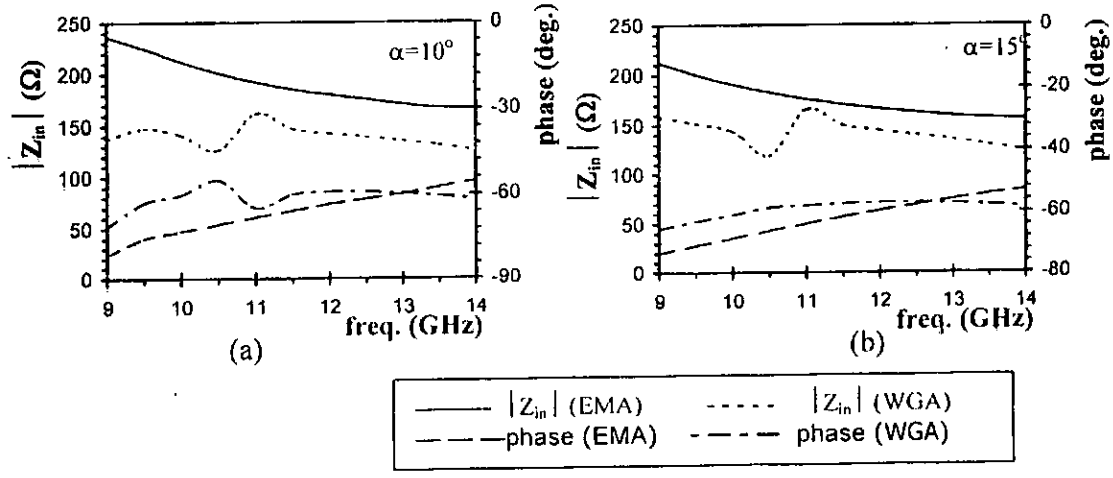

Figure 5.13: *Input impedance of WGA and EMA against frequency*

The phase profiles of both EMA and WGA show that the input impedance is capacitive over the entire frequency band stated above for both $\alpha = 10^{\circ}$ and 15°. Based on this comparative analysis of $|Z_{in}|$ profiles of WGA and EMA, we can infer ***that the presence of a small ground plane in the feeding scheme of WGA results in an appreciable reduction in the magnitude of the input impedance of the monofilar helix.***

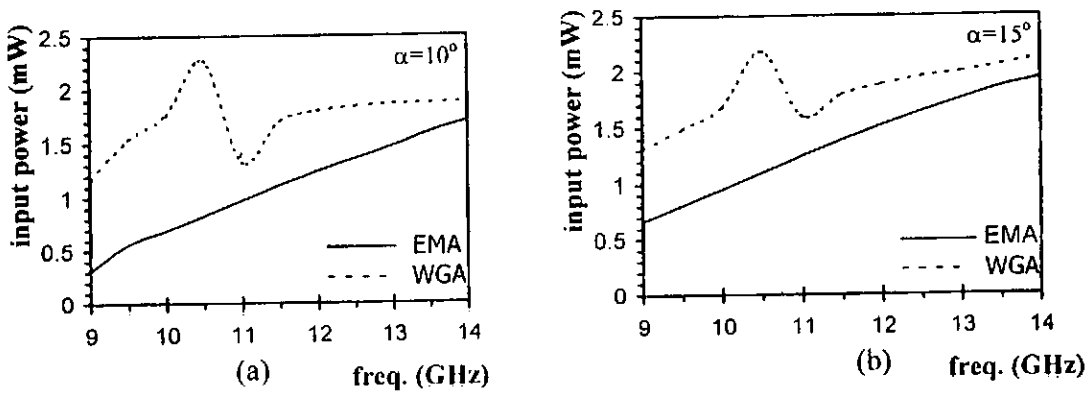

Figure 5.14: *Input power of WGA and EMA against frequency*

Figures 5.14a and 5.14b describe the nature of the frequency dependence of input power for both WGA and EMA when $\alpha = 10^{\circ}$ and 15°, respectively. A close

examination of Figures 5.14a and 5.14b shows that input power values for the WGA are generally higher than that for the EMA in the frequency range considered and for both cases of $\alpha = 10^{\circ}$ and 15°, indicating **that the WGA extracts more power from the feeding system.** We further find from the input power profiles of EMA that the input power increases steadily as the frequency increases, while corresponding profiles for the WGA exhibit a non-linear variation at the lower end of the frequency band and a linear variation at frequencies at the upper end of the frequency regime.

5.2.2 Front-to-back ratio and axial ratio

In order to examine the nature of the directional properties of the EMA and WGA, the front-to-back ratio (F/B) and the axial ratio of their radiation field patterns were computed without the imposition of the assumption of a time-phase quadrature between the field components, as is usually supposed, (Kraus 1950). The variations of F/B with frequency are depicted in Figures 5.15a and 5.15b for $\alpha = 10^{\circ}$ and 15°, respectively. From the aforementioned figures, we find that the numeric values of F/B for both EMA and WGA are less than unity within the frequency band (9GHz - 14GHz)

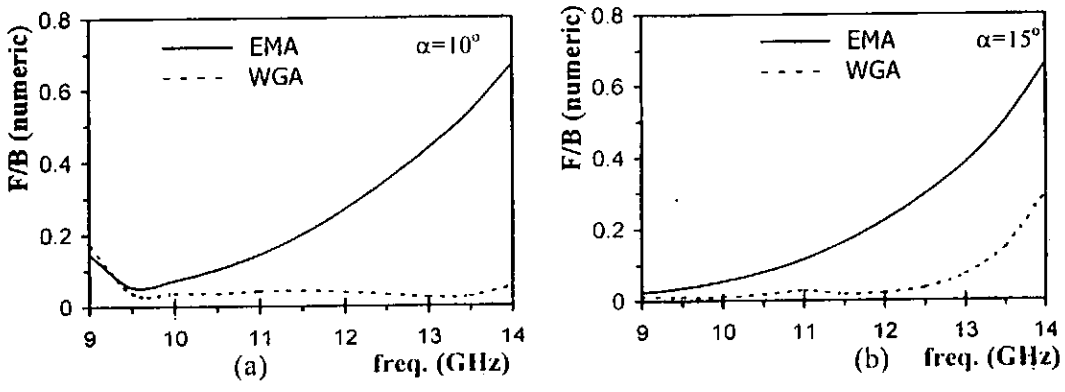

Figure 5.15: *Front-to-back ratio (F/B) (numeric) of WGA and EMA versus frequency*

which means that both EMA and WGA radiate primarily in the backfire direction. It is also observed from Figures 5.15a and 5.15b that WGA radiates more power in the backfire direction than the EMA, and for $\alpha = 10^{\circ}$, the F/B of WGA is almost independent of frequency when compared with the case when $\alpha = 15^{\circ}$. However, for both $\alpha = 10^{\circ}$ and 15°, the EMA has almost identical F/B profiles. The foregoing observations highlight some of the crucial roles played by the small wire-grid ground plane in the radiation mechanism of the WGA.

The extent to which the radiated fields in the backfire direction are circularly polarized is examined by computing the axial ratio of the fields. For most practical applications, it is desirable to limit the axial ratio to values below 3dB (Nakano and Mimaki 1997). Indeed, the 3dB criterion is commonly used to define the operating bandwidth of circularly polarized antennas such as helical antennas. Figures 5.16a and 5.16b , which describe the variations of axial ratio with frequency for $\alpha = 10^{\circ}$ and 15°, respectively, show that the EMA has an axial ratio which is less than 3dB in the entire frequency band considered, whereas for the WGA, the axial ratio overshoots the 3dB limit at 11GHz for 10° helix and at 14GHz for 15° helix. This means that the WGA will not perform satisfactorily as circularly polarized antenna at the aforestated frequencies.

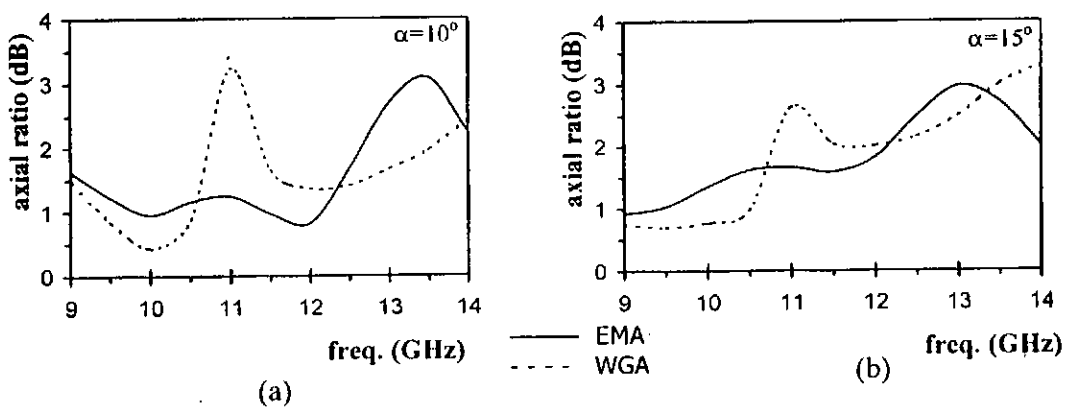

Figure 5.16: *Axial ratio (dB) of WGA and EMA versus frequency*

5.2.3 Directive gain and half-power beam-width

To give further insight into the directional performance of EMA and WGA, the directive gain and the half-power beam-width (HPBW) of their radiated fields are calculated in the backfire direction, since both the EMA and WGA radiate predominantly in the backward direction. The values calculated for the directive gain and HPBW as a function of frequency are plotted in Figures 5.17 and 5.18, respectively. Clearly, Figures 5.17a and 5.17b suggest that the WGA has more directive gain than EMA in the entire frequency band of interest here. In addition, the directive gains of both EMA and WGA are higher at $\alpha = 10^\circ$ than at $\alpha = 15^\circ$. Variations of HPBW with frequency are shown in Figures 5.18a and 5.18b for values of $\alpha = 10^\circ$ and 15°, respectively.

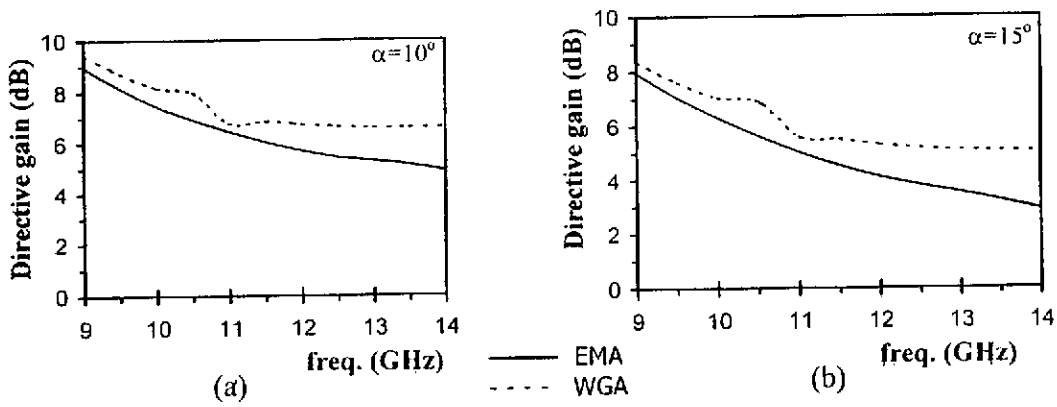

Figure 5.17: *Directive gain (dB) of WGA and EMA versus frequency*

The curves indicate that the radiation patterns of WGA are more directive than those of EMA. It is to be observed that the HPBWs when $\alpha = 10^\circ$ are lower than when $\alpha = 15^\circ$ for both WGA and EMA. This implies that the main beams of the 10° helix are more directive than those of the 15° helix.

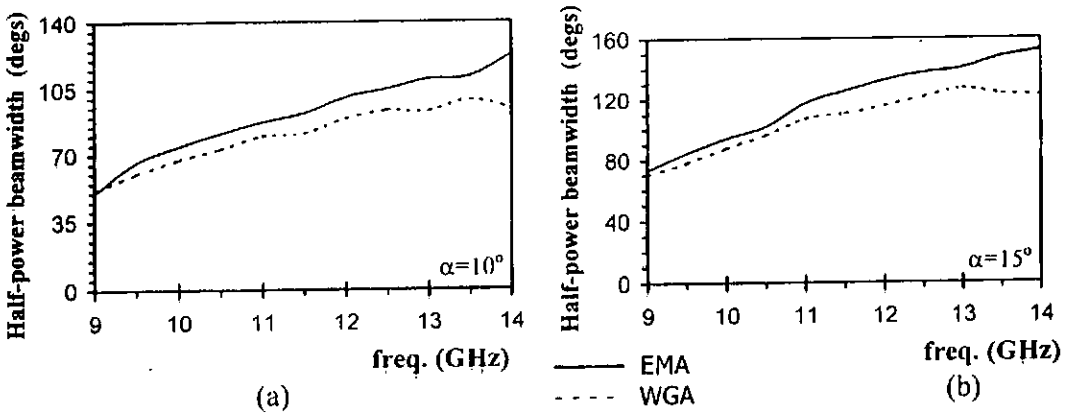

Figure 5.18: *Half-power beam-width (degrees) of WGA and EMA versus frequency*

5.2.4 Current distributions and radiated fields

The results for directive gain and half-power beam-width (HPBW) discussed above, reveal that both WGA and EMA exhibit the best directivity measures in the lower frequency end of the frequency regime considered. In view of this observation the ensuing discussions on the current distributions on the helical arm and the associated radiated fields will be restricted to the two specific cases defined as follows:

Case I: $\alpha = 10^{\circ}$, frequency = 10GHz , $C_{\lambda} = 0.83\lambda$.

Case II: $\alpha = 15^{\circ}$, frequency = 9GHz , $C_{\lambda} = 0.75\lambda$.

First, the current distributions that are shown in Figures 5.19a and 5.19b for the above-mentioned two cases will be discussed. It is seen from Figures 5.19a and 5.19b that the current distributions for both EMA and WGA are essentially decaying exponential curves with maximum values at the location of the feed-point, as expected. Also, the profiles of magnitude of current for EMA and WGA depicted in Figure 5.19a indicate that the reflected current component from the open end of the helix is insignificant, even though the helix is not tapered at that end. Figure 5.19b, which illustrates the profiles of current distribution along the helical arm for case II, reveals that the current distribution also varies exponentially along the helical conductor for

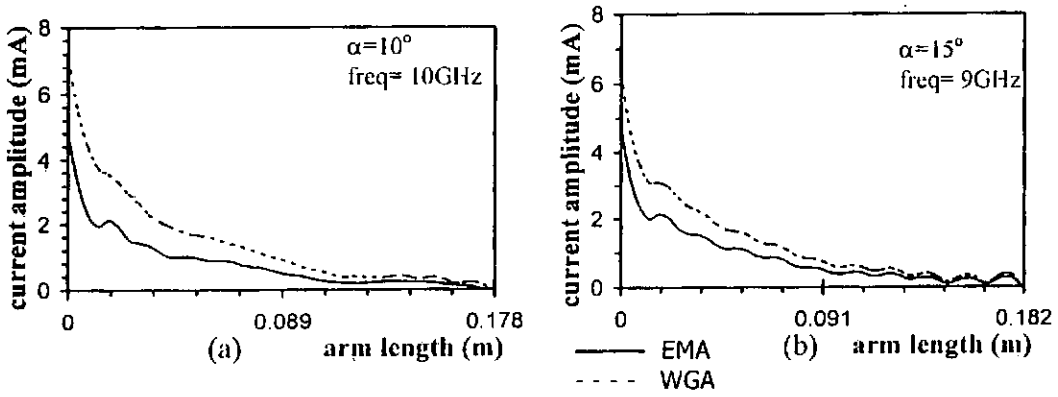

Figure 5.19: *Current distributions on the WGA and EMA*

both EMA and WGA but with a noticeable wavelike variation at the open end which is an indication of considerable reflection from the open end (Yamauchi and Nakano 1981). **It is conceivable that the appreciable reflections from the open end is due to the smaller arm length of the latter, when compared with the former case.** It is also to be observed that for the entire helical arm, values for the magnitude of current for the WGA are higher than those for EMA. More importantly, **the current profiles of WGA are identical to those reported by Nakano *et al.* (1988), for a monofilar helix backed by a small ground plane.**

Displayed in Figures 5.20 (a-d) are the radiated fields associated with the current distributions discussed in the foregoing. To ascertain the contributions of the small ground plane of WGA, the $\hat{\theta}$ components of the radiated fields of EMA and WGA are superimposed on one another, and likewise the $\hat{\varphi}$ components. All the radiation patterns of EMA and WGA show that both antenna types radiate principally in the backfire direction, but with some certain subtle differences, which will now be highlighted. Figures 5.20a and 5.20b reveal that the $\hat{\theta}$- components of the radiated fields of EMA and WGA for case I (with α = 10° and frequency =10GHz) and for case

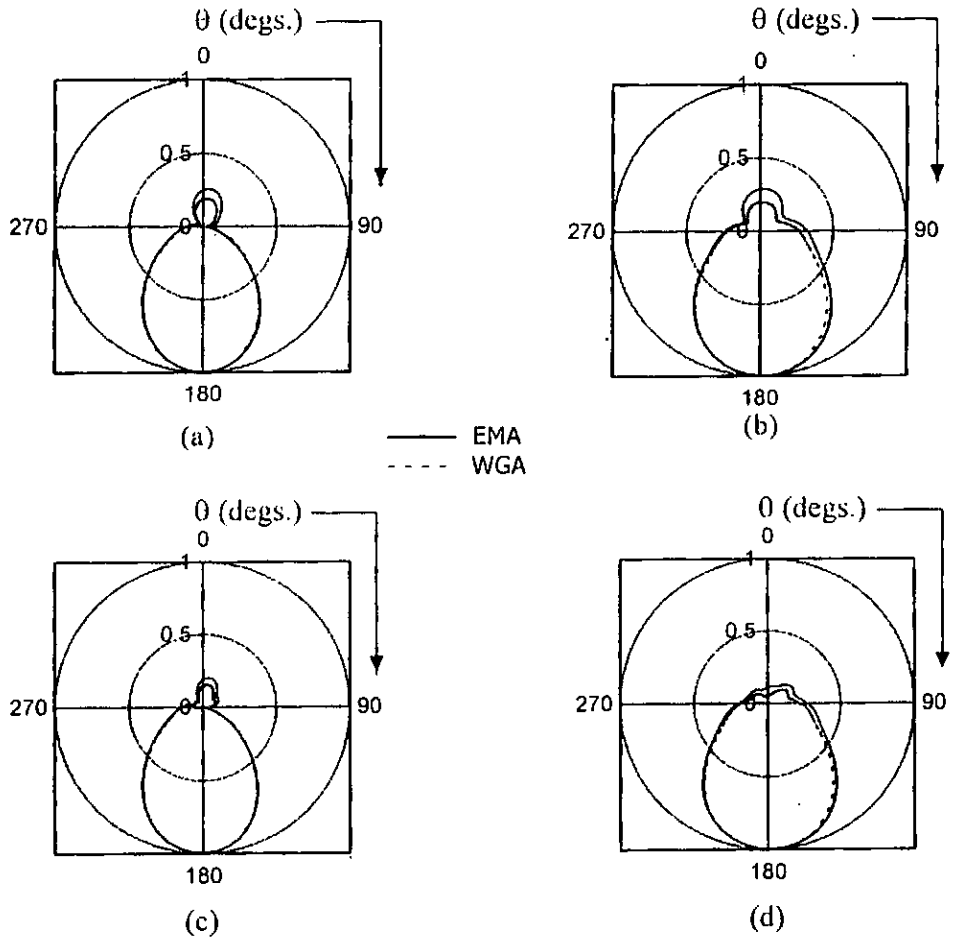

Figure 5.20: *Electric fields radiated by WGA and EMA: $\hat{\theta}$ component (a), (b): $\hat{\varphi}$ component (c), (d).*

II (for α = 15° and frequency = 9GHz) are identical in the backward direction. However, in the forward direction, the magnitude of the radiation field for the WGA is lower than that of EMA. Regarding the $\hat{\varphi}$ - components of the radiated field patterns displayed Figures 5.20c and 5.20d, some notable differences are readily observed in both the forward and backward directions, for both WGA and EMA. Indeed, in this case the beamwidth of the WGA is slightly less as observed in Figure 5.20(d) which is consistent with the reduced HPBW for WGA as already illustrated in Figures 5.18a and 5.18b.

5.3 Comparison of numerical results with published experimental and computed data

5.3.1 Balanced (centre-fed) helical antenna

Chen (1967) provided a Fourier Series (FS) solution of the problem of thin-wire helical antenna excited at its geometrical centre, which was validated by comparison with computed and measured experimental data. Towards the validation of the numerical results obtained in this work, the general Fortran program is specialized to the case of a balanced (centre-fed) helical antenna, and the numerical results then obtained are compared with the published experimental and computed results of Chen. Specifically, we examine both the magnitude and phase of current distribution on the helical arm length, when the balanced helix is characterized by the following physical dimensions (Chen 1967):

(i) helix-wire radius: 0.3175cm

(ii) helix radius: 7.62cm

(iii) pitch angle: 18.5^{o}

(iv) pitch: 16.02cm

(v) number of turns: 6

(v) length of one-turn at 500MHz operating frequency: 0.844λ ($\lambda = 0.6$m)

(vi) length of one-turn at 600MHz operating frequency: 1.01λ ($\lambda = 0.5$m)

(vii) length of one-turn at 750MHz operating frequency: 1.27λ ($\lambda = 0.4$m)

For ease of comparison of our MoM results with those of Chen, we superimpose the magnitude and phase of the current distribution obtained on similar profiles earlier reported by Chen, as depicted in Figures 5.21-5.23. Concerning the current magnitude, there are reasonable agreements between the current profiles and those reported by Chen as evident in the aforementioned Figures. Indeed, the computed values for current

phase profiles agree excellently with the current phase curves in Chen's paper. The foregoing comparison exercise clearly validates the MoM solution to the balanced helical antenna problem.

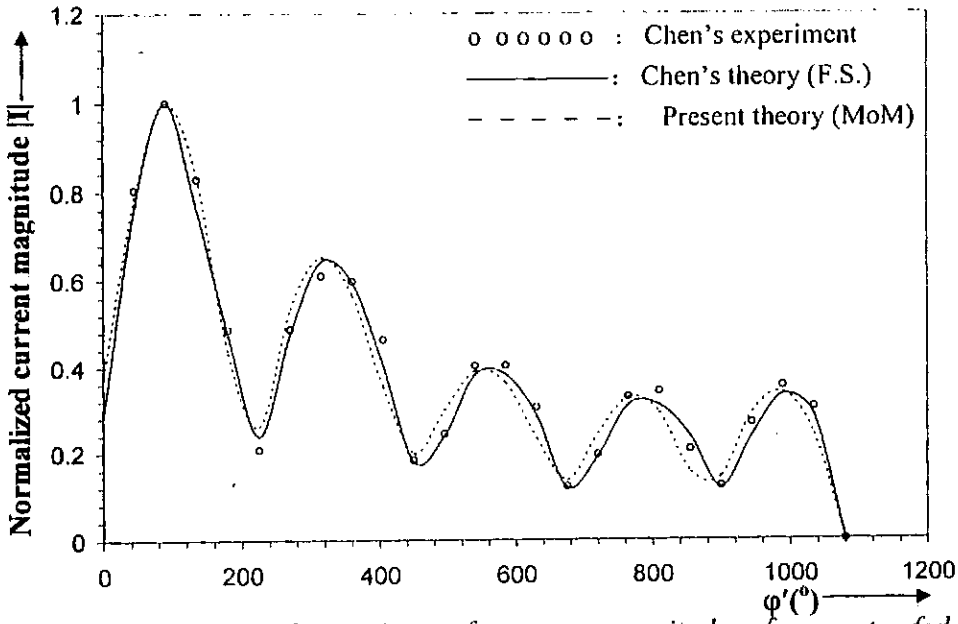

Figure 5.21a: *Comparison of current magnitude of a centre-fed helical antenna at 500MHz: – – – –: Present theory; ————: Chen's theory and o o o o : Experimental results at 500MHz of Fig. 6(a), page 182, of Chen (1967)*

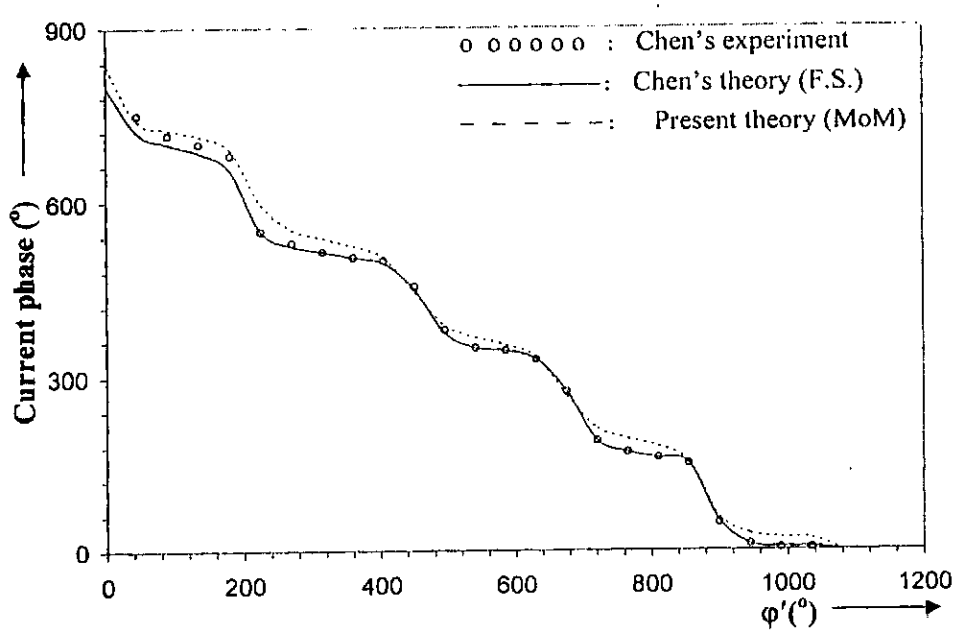

Figure 5.21b: *Comparison of current phase of a centre-fed helical antenna at 500MHz: – – – –: Present theory; ————: Chen's theory and o o o o : Experimental results at 500MHz of Fig. 6(a), page 182, of Chen (1967)*

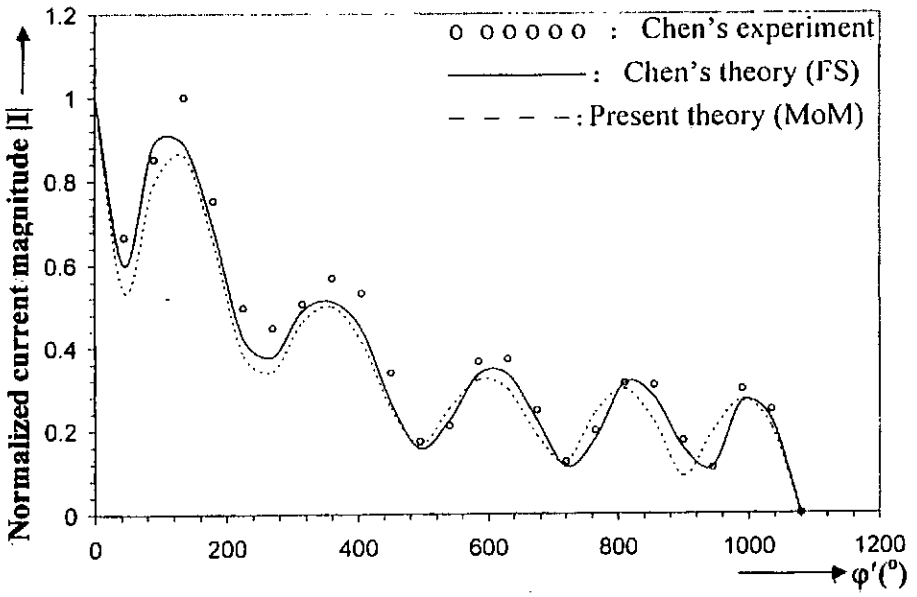

Figure 5.22a: *Comparison of current magnitude of a centre-fed helical antenna at 600MHz: – – – –: Present theory (MoM); ————: Chen's theory (FS) and o o o o : Chen's Experimental results at 600MHz of Fig. 6(b), page 182, of Chen (1967)*

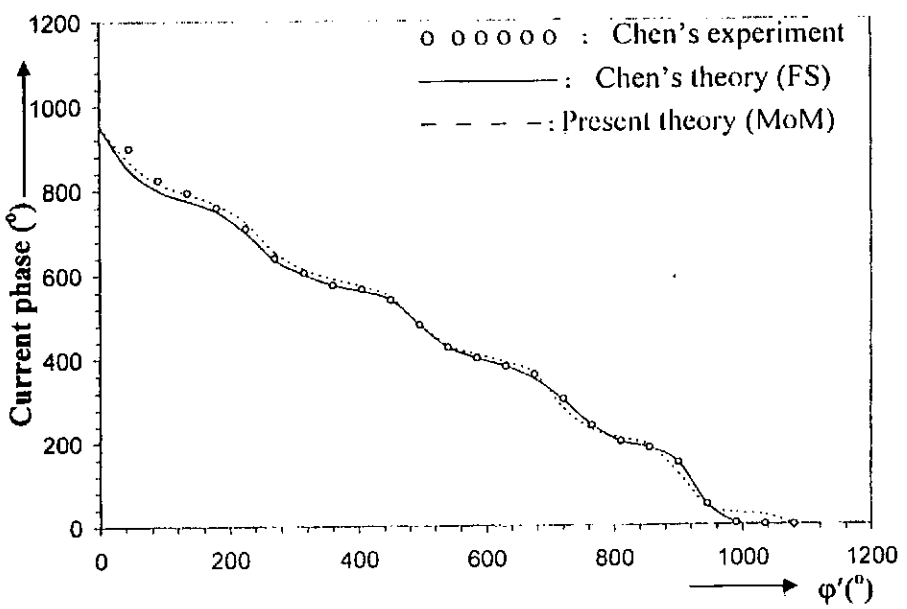

Figure 5.22b: *Comparison of current phase of a centre-fed helical antenna at 600MHz: – – – –: Present theory (MoM); ————: Chen's theory (FS) and o o o o : Chen's Experimental results at 600MHz of Fig. 6(b), page 182, of Chen (1967)*

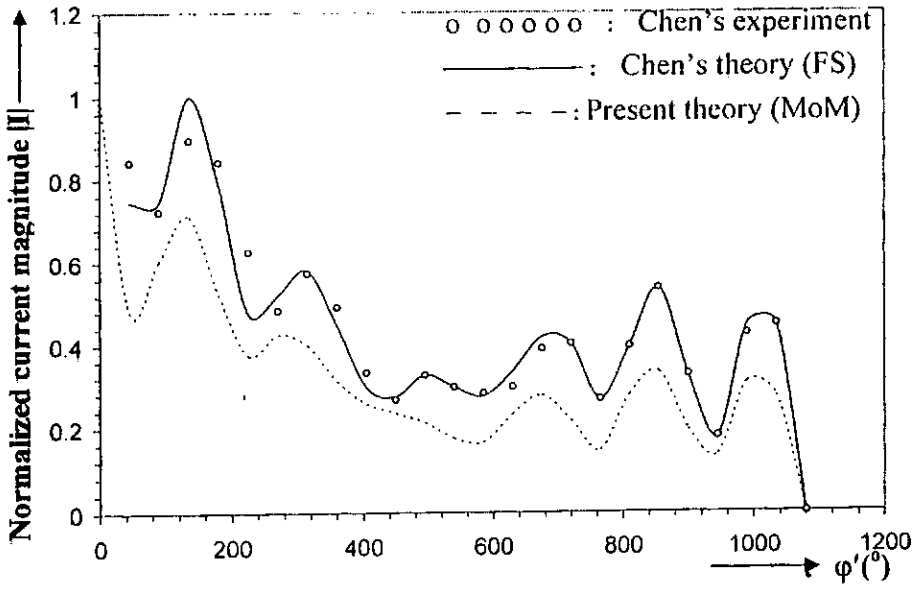

Figure 5.23a: *Comparison of current magnitude of a centre-fed helical antenna at 750MHz: – – – –: Present theory (MoM); ————: Chen's theory (FS) and o o o o: Experimental results at 750MHz of Fig. 6(c), page 182, of Chen (1967)*

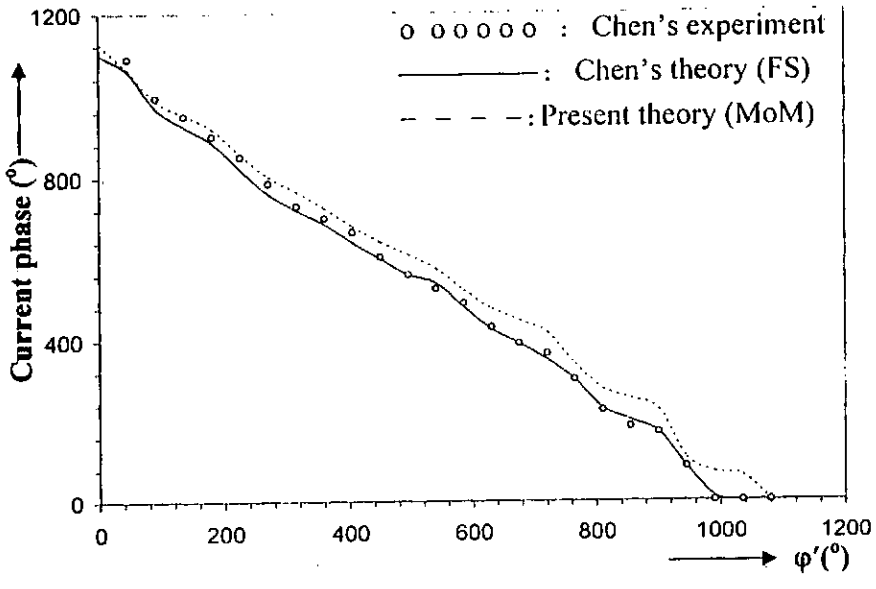

Figure 5.23b: *Comparison of current phase of a centre-fed helical antenna at 750MHz: – – – –: Present theory (MoM); ————: Chen's theory (FS) and o o o o: Experimental results at 750MHz of Fig. 6(c), page 182, of Chen (1967)*

5.3.2 Exclusion-mode helical-beam antenna: comparisons of theory (MoM) and experiment

For the verification of our Method of Moments (MoM) solution to the exclusion-mode helical antenna problem, we compute the radiation field patterns of a monofilar helix excited without a ground plane, previously experimentally investigated by Patton (1963). The geometrical dimensions of the monofilar (one-wire) helix specified by Patton are:

(i)	helix-wire radius :	0.644mm
(ii)	helix radius:	2.663cm
(iii)	pitch angle:	10.18^{o}
(iv)	pitch:	3cm

which are utilized in our computer codes for the solution of the exclusion-mode helix problem. Because Patton only stated that the helix should be reasonably long, a choice of number of helix turns equals 7 was made, while the operating frequency range from 1400MHz to 1700MHz was selected. It should be remarked that in Patton's experiment, the feed point was located at the upper end of the helical structure. The computed E_θ and E_φ patterns along with the corresponding patterns measured by Patton are displayed in Figures 5.24a and 5.24b, respectively, for the sake of comparisons.

We find, from Figures 5.24a and 5.24b that, there is a fair conformity between the measured patterns of Patton and our computed patterns because the major radiation lobes of the patterns are predominantly in the backfire direction, as one would expect. In the frequency range examined (1400MHz – 1700MHz), the radiation in the forward direction is, in general, less than half of the radiation in the backfire direction except the measured E_θ component of the pattern obtained at 1700MHz. It is worthy of note that the E_θ component of the calculated pattern when the antenna is operating at 1400MHz,

closely resembles that of the measured pattern, while at operating frequency of 1500MHz, the E_φ component of the computed pattern reasonably approximates the corresponding measured pattern. It is not unlikely that the measured patterns may not be exact since they are susceptible to both experimental and measurement errors. In conclusion, Figures 5.24a and 5.24b, to a large extent, support the correctness of the MoM solution to the exclusion-mode helical antenna problem, which clearly reveals that when the helix is fed without a backing structure, it radiates principally in the backfire direction.

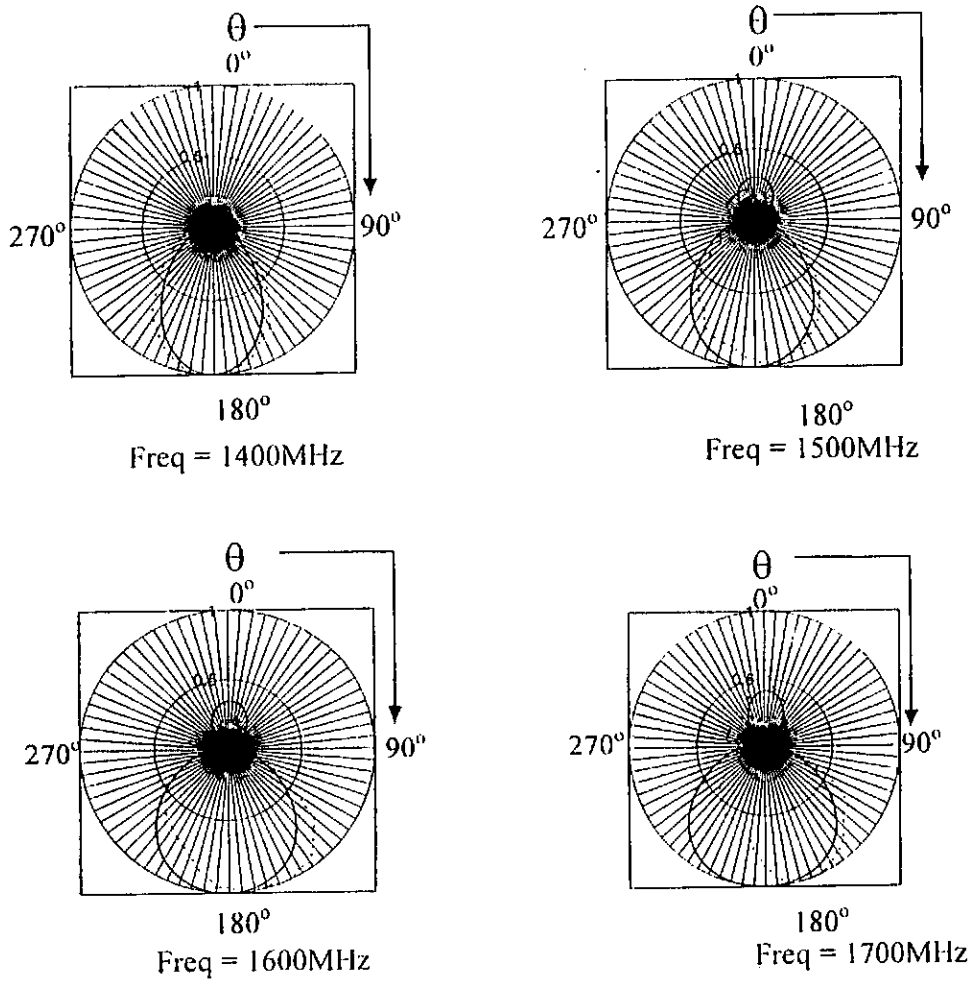

Figure 5.24a: *$E_\theta(\theta, \varphi = 0^\circ)$ component:* ————: *computed pattern;* ----------: *measured pattern (Patton 1963)*

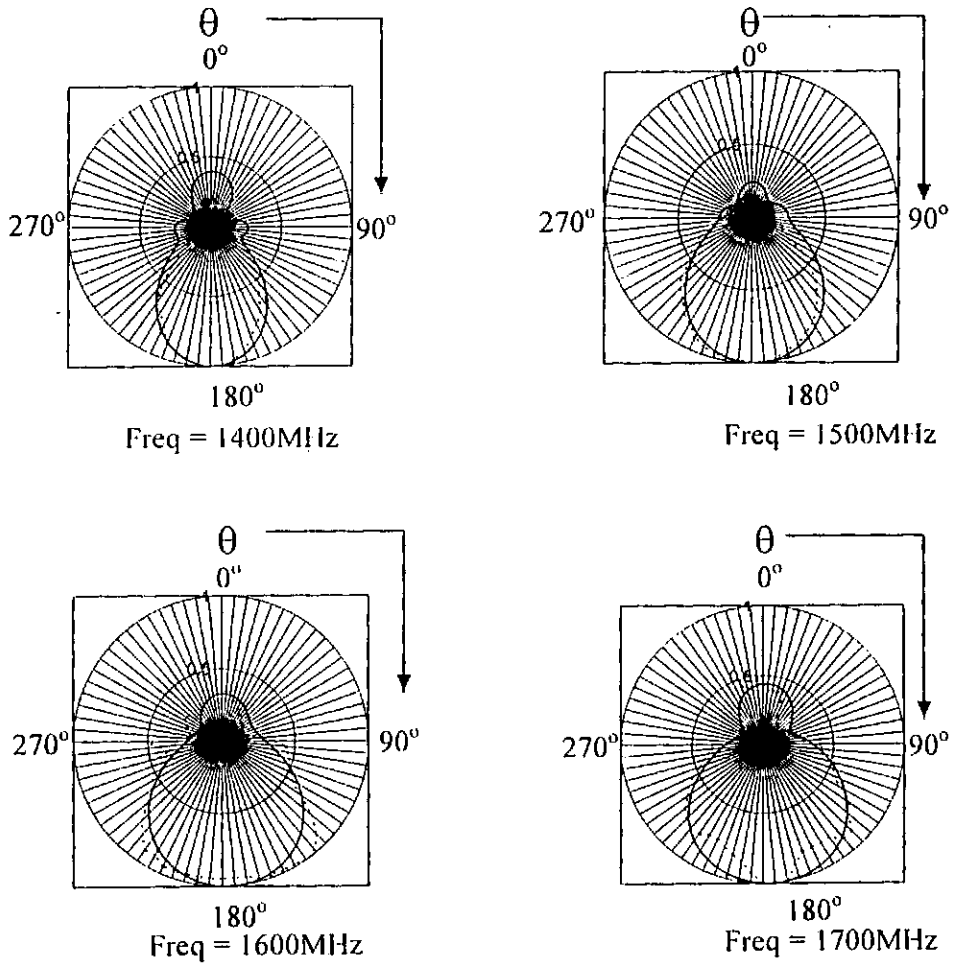

Figure 5.24b: *$E_\varphi(\theta, \varphi = 0^o)$ component: ———computed pattern; ---------: measured pattern (Patton 1963)*

5.3.3 Helical-beam antenna backed by a small wire-grid ground plane: validation of the numerical solution

In an attempt to check the validity of the numerical solution developed in the thesis, for the problem of a helical antenna backed by a small ground plane modelled by wire grids, the computational results obtained are compared with those of Nakano *et al* (1988) who addressed a similar problem. The data utilized for this comparative analysis were extracted from Nakano *et al* (1988), and they are as follows:

(i)	number of turns:	7
(ii)	helix circumference:	2.5cm
(iii)	ground plane diameter:	7.2mm
(iv)	wire radius:	0.3mm
(v)	pitch angle:	14°
(vi)	excitation voltage:	1.0V
(vii)	frequency band:	8.5GHz – 10.0GHz.

It is of interest to note that, whereas Nakano and his associates modelled the small ground plane by using **2 circular wires and 8 radial wires; the model utilized here consists of 4 circular wires and 12 radial wires**. The results of the comparison effort are graphically presented in Figures 5.25-5.28, of which Figure 5.28 depicts the radiation pattern of the antenna when the helix pitch angle is 14° and the operating frequency is 10.0GHz.

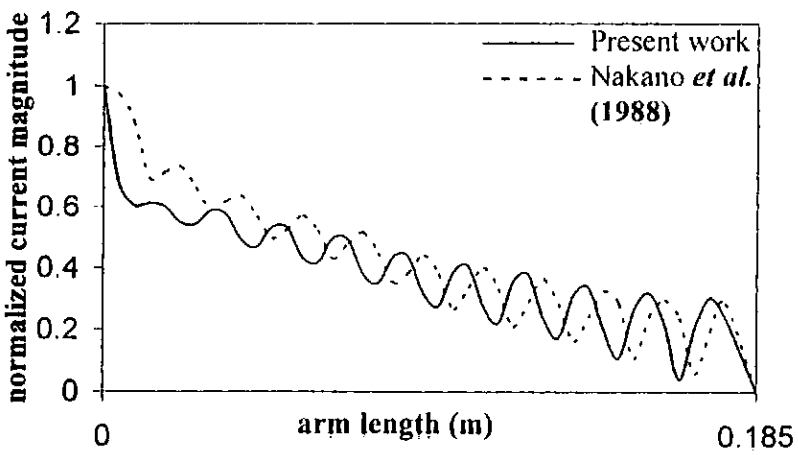

Figure 5.25: *Current distribution on the helix backed by a small ground plane (pitch angle = 14°, frequency = 8.5GHz)*

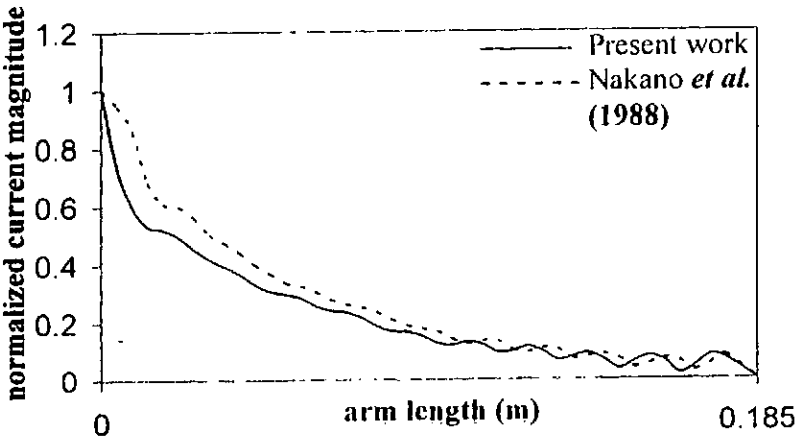

Figure 5.26: *Current distribution on the helix backed by a small ground plane (pitch angle = 14°, frequency = 9.0GHz)*

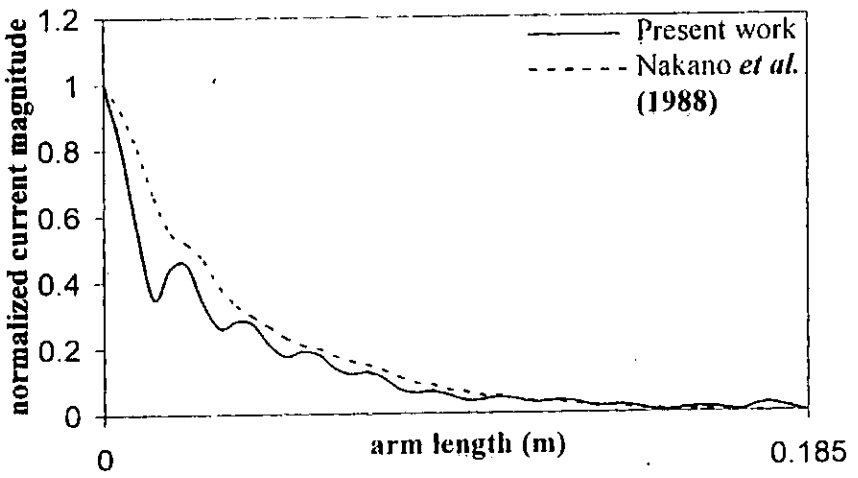

Figure 5.27: *Current distribution on the helix backed by a small ground plane (pitch angle = 14°, frequency = 10.0GHz)*

The current waveforms shown in Figure 5.25, for operating frequency of 8.5GHz and helix circumference in wavelength (λ) of 0.71λ, are somewhat identical except in the vicinity of the feed point where there exists moderate difference in the two current profiles. An examination of Figures 5.26 and 5.27 shows that our results are consistent with the published results of Nakano *et al* (1988), and the slight difference in

current magnitudes may probably be attributable to the higher number of wire elements employed in the wire-grid model utilized here for the ground plane. The associated radiation pattern of the antenna when the helix pitch angle is 14° and the operating frequency is 10.0GHz shown in Figures 5.28 (a-b) are almost the same as the patterns reported in Figure 5 of Nakano *et al* (1988) for an identical antenna. In view of the similarities between our results and those of Nakano *et al* (1988), the validity of our solution to the problem of helical antenna backed by a small ground plane consisting of wire grids is fairly ascertained.

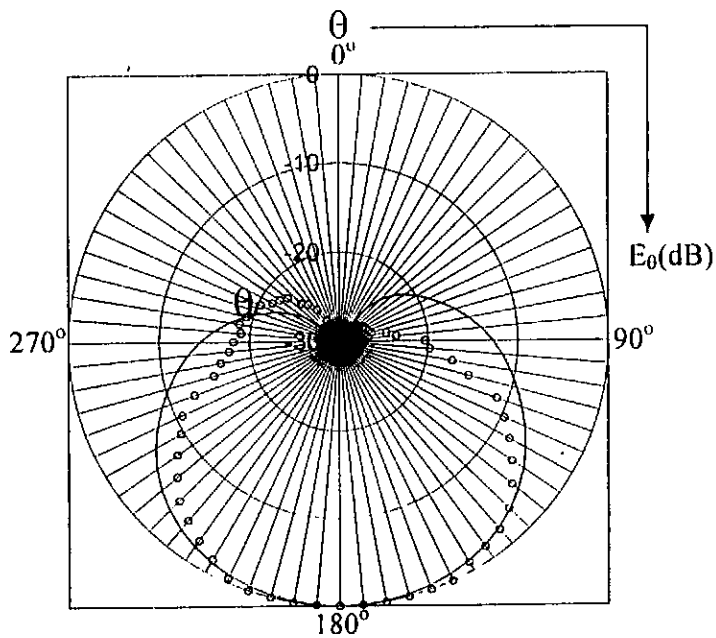

Figure 5.28a: *Comparison of E_θ components of the radiated field of a helical antenna backed by small ground plane.; ———: Present theory; o o o o o o : computed radiation pattern reported by Nakano et al. (1988) (Fig. 5), page 1362.*

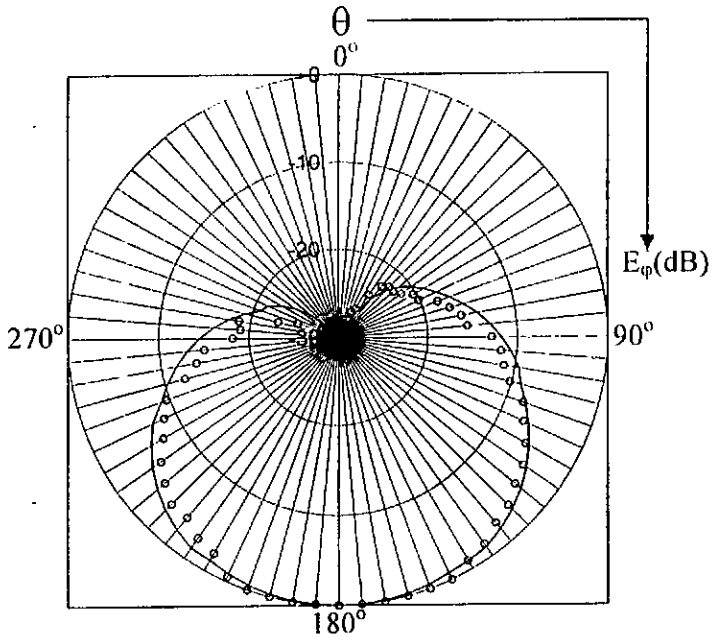

Figure 5.28b: *Comparison of E_φ components of the radiated field of a helical antenna backed by small ground plane.; ————: Present theory; o o o o o : computed radiation pattern reported by Nakano et al. (1988) (Fig. 5), page 1362.*

Chapter 6

HELICAL-BEAM ANTENNAS MOUNTED ON A LARGE GROUND PLANE

One important feature of the classical feeding arrangement for helical-beam antennas is the ground plane whose functions have been earlier highlighted in Chapter 2. By convention, the ground plane is said to be electrically large in size when its physical dimensions are large compared with those of the wire helix dimensions. For such electrically large ground planes, it becomes possible to invoke certain simplifying assumptions in the classical analysis methods, (Stutzman and Thiele 1981, Nakano and Mimaki 1997), by assuming that the ground plane is perfectly conducting and that it is of negligible thickness. The consequent analysis of the helical antenna mounted on a large ground plane, is then informed by a model that considers the ground plane as

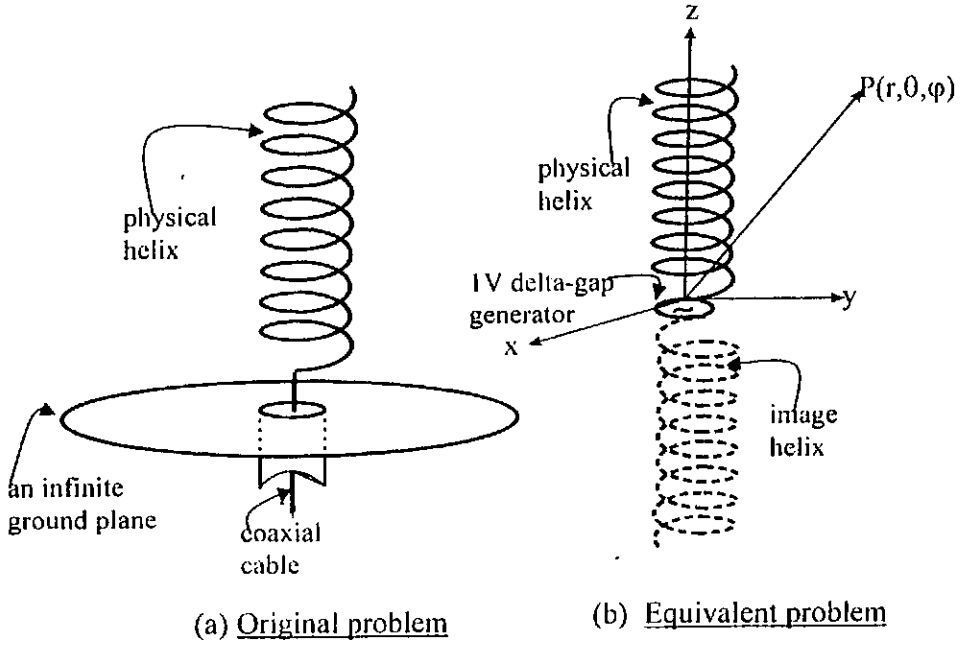

Figure 6.1: (a) *The original problem of a monofilar helical antenna mounted on an infinite ground plane;* **(b)** *The equivalent problem where the image theory is invoked.*

being essentially infinite in extent, which makes the image theory applicable, and significantly reduces the analytical efforts required for the solution of the problem. Two important practical problems are of interest here:

(i) a helical-beam antenna mounted on a large ground plane, which was first experimentally investigated by Kraus (1947), the inventor of helical-beam antennas,

(ii) arrays of helical-beam antennas arranged on a large ground plane, commonly found on the satellite platforms.

Essentially, the application of the image theory to the problem of helical antenna mounted above an infinite ground plane leads to the equivalent problem of physical helix and image helix without the ground plane. It should be remarked that while the physical helix is right-handed, the (mirror) image helix is left-handed.

6.1 A helical-beam antenna mounted on a large ground plane: a reconsideration of Kraus' original problem

In order to apply the generalized formulation and solution to the design problem of a helical antenna mounted on an infinite ground plane as portrayed in Figure 6.1a, the application of the method of images, (Maxwell 1873), is invoked, leading to the equivalent problem consisting of the physical helix and an image helix (replacing the ground plane) as depicted in Figure 6.1b. Accordingly, the generalized Ohm's law equation for the equivalent problem admits the form:

$$\begin{bmatrix} [Z_{mn}^{pp}] & [Z_{mn}^{pk}] \\ [Z_{mn}^{kp}] & [Z_{mn}^{kk}] \end{bmatrix} \begin{bmatrix} [I_n^p] \\ [I_n^k] \end{bmatrix} = \begin{bmatrix} [V_m^p] \\ [V_m^k] \end{bmatrix} , \tag{6.1}$$

where the mutual electromagnetic coupling between the physical helix and image helix is fully accounted for by entries to the sub-matrices $[Z_{mn}^{pk}]$ *and* $[Z_{mn}^{kp}]$, the subscripts m = 1,2,• • • •, K and n = 1,2,• • • •, K, while the superscripts p and k refer to the physical helix and the image helix, respectively. The distribution of current for the physical helix defined by entries into $[I_n^p]$, and that for the image helix by entries into $[I_n^k]$, are readily obtained from equation (6.1) via matrix operations of inversion followed by matrix multiplication.

Numerical results from the computer simulations of helical antenna situated over an infinite ground plane were obtained for a circular helix characterized by the following geometrical parameters:

Number of turns: 8

Pitch angle (α): 12° and 14°

Circumference in wavelengths (C_{λ}): in the range 0.8 - 1.2

Centre frequency: 2GHz

The discussion of the numerical results, which are presented in graphical formats, begins with the current distributions, in what follows.

6.1.1 Current distributions

The current distributions on the helix when $\alpha = 12^{\circ}$ and 14° and for C_{λ} varying from 0.8 to 1.2 as functions of the normalized helical arm length are shown in Figures 6.2a and 6.2b. As it is readily observed, the current profiles of the 12° helix and 14° helix are superimposed on one another as a means of demonstrating the effects of the pitch angle on the current distributions. A close examination of the aforementioned figures shows that for all values of C_{λ} considered, **the current distributions are typified by two distinct regions, namely, an exponentially decaying region and a surface wave profile**. This is consistent with the published results of Nakano *et al.* (1986). The difference between the magnitudes of the current distributions at the feed-point for the 12° helix and 14° helix is insignificant as evident from Figures 6.2a and 6.2b. It may also be observed that apart from the case for $C_{\lambda} = 0.8$, **the exponentially decaying region exists between the feed-point and about a quarter of the total length of the helix down the arm length**. This feature clearly supports one conclusion

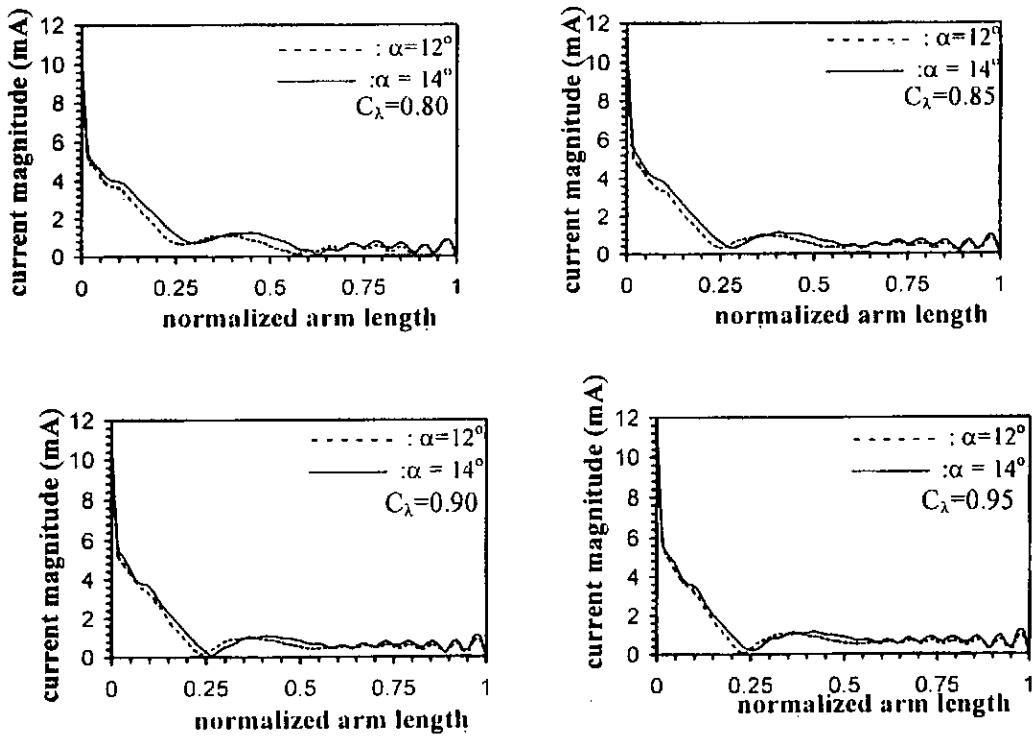

Figure 6.2a: *Current distributions on helical beam antenna above an infinite ground plane*

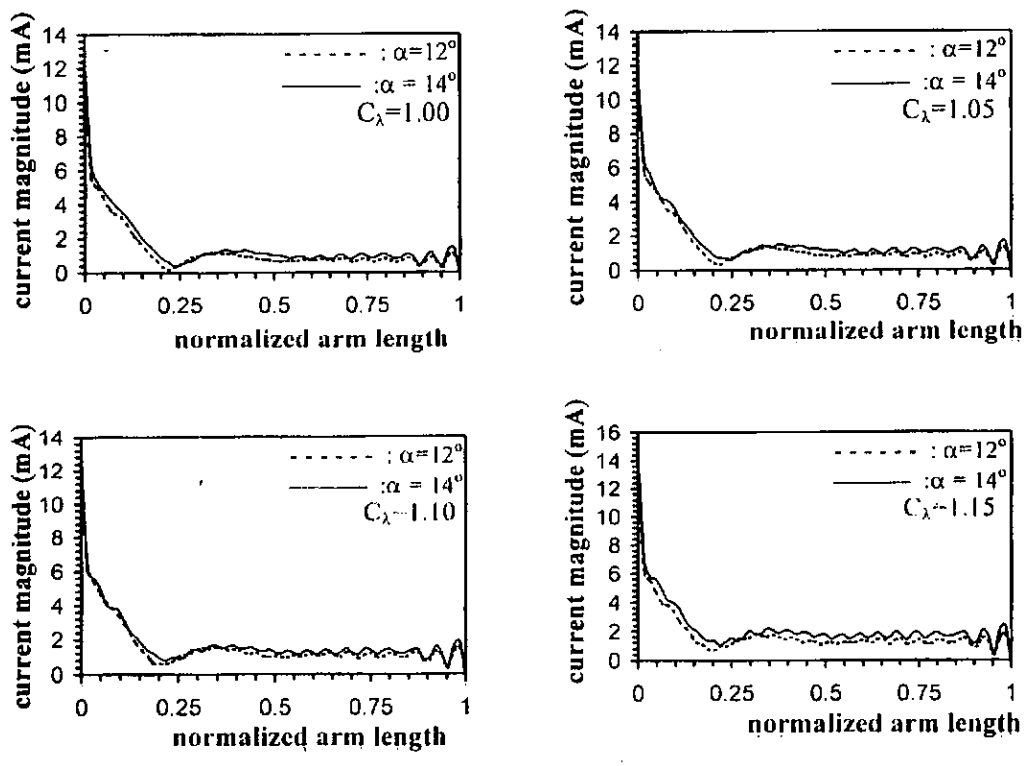

Figure 6.2b: *Current distributions on helical beam antenna above an infinite ground plane*

from Kraus and Williamson (1948) that the current on a circular helix backed by a large ground plane can be adequately approximated by a single uniform travelling wave. The ripples appearing on the surface wave region of the current distribution **may be interpreted as being attributable to multiple reflections from the open end of the helix**. It is noted that as C_λ increases, that is, as the helical arm length increases, the current magnitude at the feed-point also increases. Although the current profiles for both 12° helix and 14° helix are almost identical, the current magnitudes are higher for the14° helix. We may conclude therefore, that as α and C_λ increase, the magnitude of the reflected current also increases. The radiated fields associated with the current distributions of Figures 6.2a and 6.2b will now be described.

6.1.2 Radiated fields

The fields radiated on the vertical plane $\varphi = 0°$ and due to the current distributions of Figures 6.2a and 6.2b are depicted in Figures 6.3 (a – d), where the solid curves are used for the E_θ components while the dashed curves are employed for the E_φ components. For comparison, the radiation patterns of the 12° helix are placed adjacent to those of the 14° helix for every value of C_λ considered. A general property of the radiated patterns is that of a null field below the large ground plane, which is in agreement with the physics of the problem. This is because the ground plane attenuates the field at the reverse side, consequently serving as a reflecting mirror. For the values of C_λ investigated, the radiation is concentrated in the forward endfire direction with reasonable side-lobe levels. It is observed that as C_λ increases, or as the frequency increases, the radiation patterns become more directive, but the number and levels of the side-lobes assume higher values. This observation conforms with the general behaviour of antennas, in that, as the directivity improves there is a payoff of increased level of sidelobes. Furthermore, an examination of Figures 6.3a – 6.3d reveals that the fields

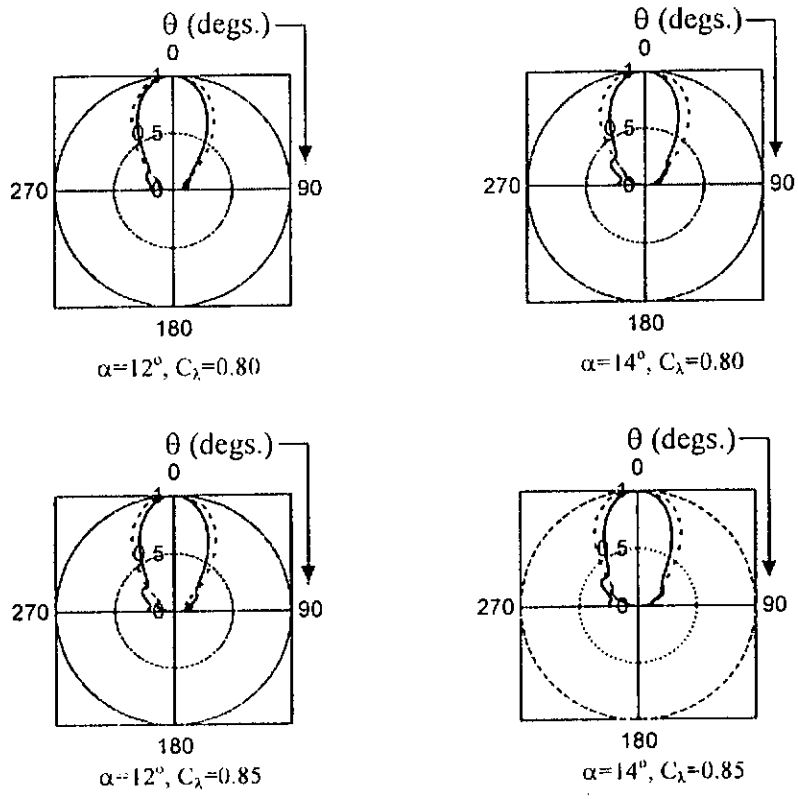

Figure 6.3a: *Electric fields radiated by helical beam antennas mounted on an infinite ground plane in the $\varphi=0^o$ plane. - - - - -:E_φ,———: E_θ*

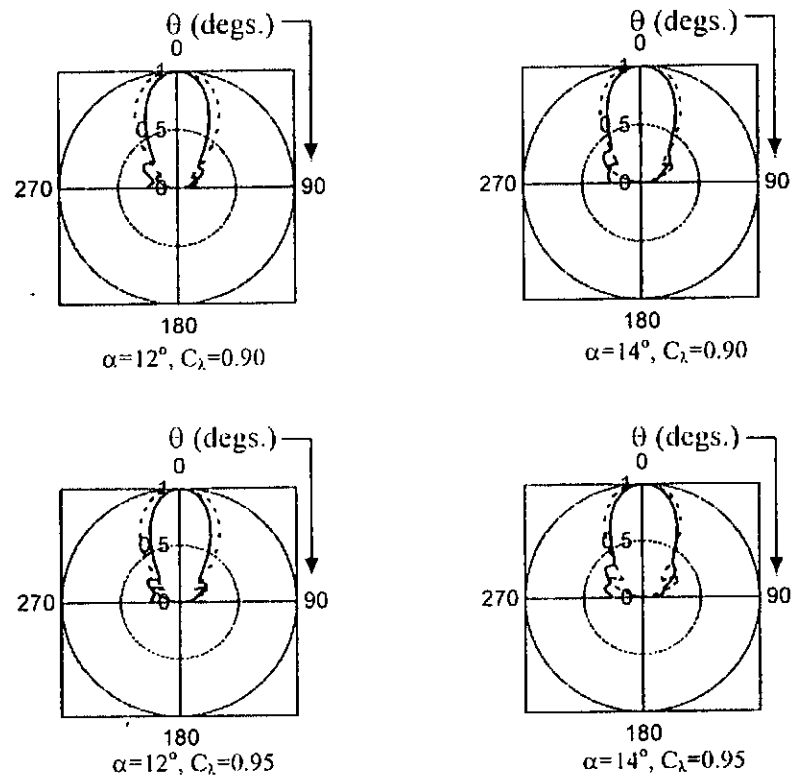

Figure 6.3b: *Electric fields radiated by helical beam antennas mounted on an infinite ground plane in the $\varphi=0^o$ plane. - - - - -:E_φ,———: E_θ*

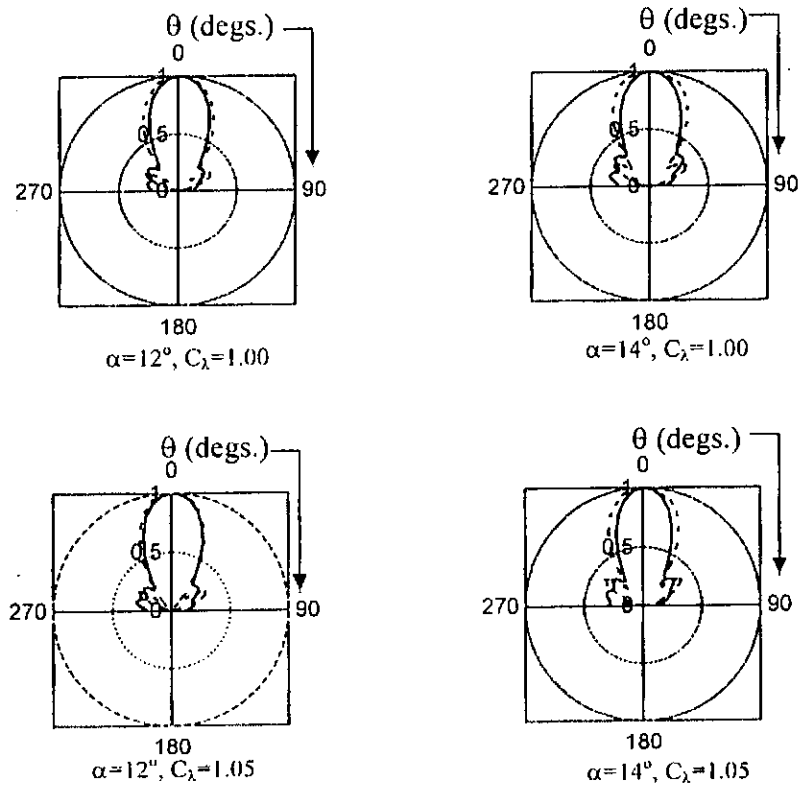

Figure 6.3c: *Electric fields radiated by helical beam antennas mounted on an infinite ground plane in the $\varphi=0^o$ plane.* - - - - -: E_φ, ———: E_θ

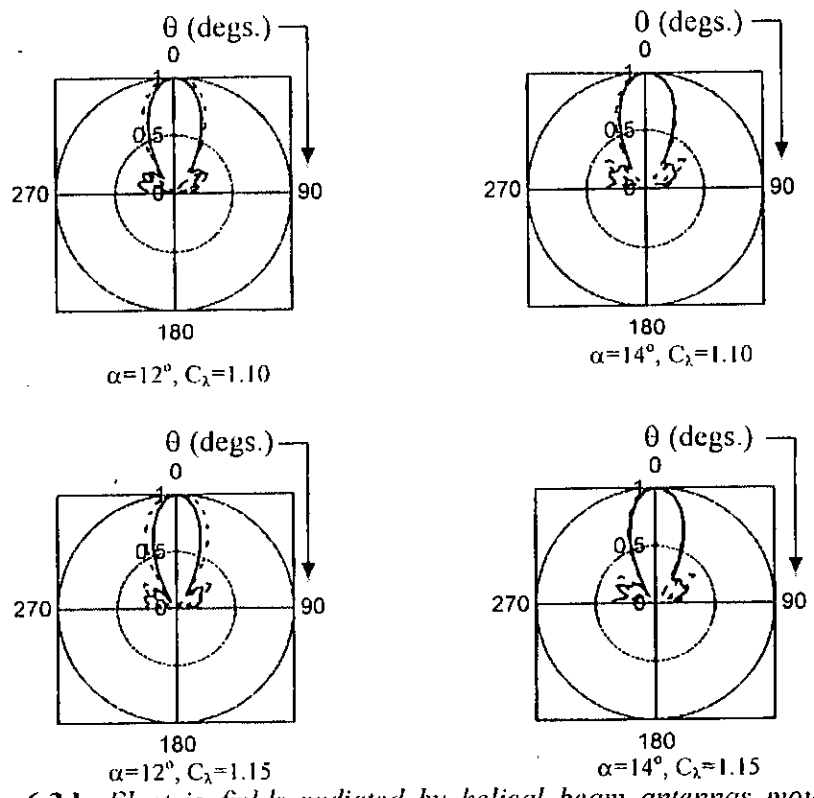

Figure 6.3d: *Electric fields radiated by helical beam antennas mounted on an infinite ground plane in the $\varphi=0^o$ plane.* - - - - -: E_φ, ———: E_θ

radiated are somewhat independent of the pitch angle, and the E_θ patterns are more directive than the E_φ patterns. This suggests that with a reasonable number of helix turns, an optimum axial-mode operation of the helix may be achieved by a careful selection of its circumference probably regardless of the value of the pitch angle, within certain limits. Because, as earlier demonstrated, the exclusion-mode helix radiates predominantly in the backfire direction, it may be concluded that the large ground plane in the feeding mechanism of the axial-mode helix accounts for its forward endfire radiation. In other words, the ground plane serves as a reflecting mirror of the fields radiated in the backward direction.

6.1.3 Input impedance

Figure 6.4 displays the input resistance R_{in} and the input reactance X_{in} of a helical antenna backed by a large ground plane. The input resistance profiles show that the 14° helix has higher R_{in} than the 12° helix for all the values of C_λ, except at C_λ =1.2. Numerically, R_{in} lies between 66.59Ω and 52Ω for the 12° helix and between 78.78Ω and 48.76Ω for the 14° helix. In other words, the R_{in} decreases as the frequency increases. Regarding the input reactance X_{in}, it is capacitive for both the 12° helix and 14° helix.

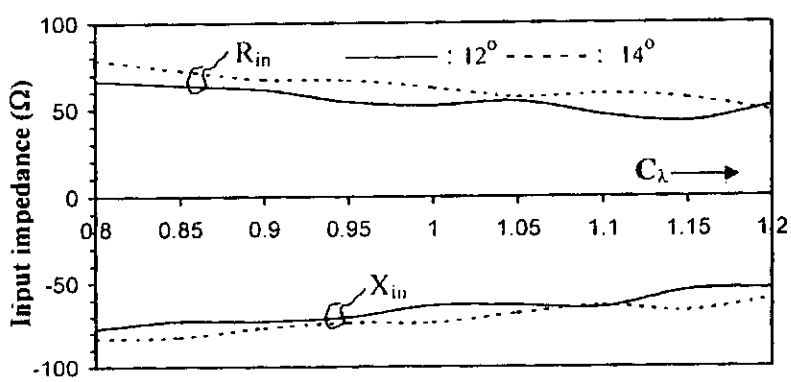

Figure 6.4: *Input impedance versus C_λ*

For the 12° helix, X_{in} ranges between -77.46Ω and -53.24Ω, while for the 14° helix, X_{in} varies from -83.24Ω and -59.84Ω as C_λ ranges from 0.8 to 1.2. That is to say, X_{in} increases as the frequency increases. It can also be seen from Figure 6.4 that the input reactance of the 12° helix is higher than that of 14° helix. **Because the variations in R_{in} and X_{in} over a wide frequency band are not pronounced, an impedance matching network can readily be designed to realise a broadband helical beam antenna.**

6.1.4 Input power

The active power available to the helical antenna backed by a large ground plane at the feed-point plotted against the circumference in wavelengths (C_λ) is shown in Figure 6.5. For $0.8 \leq C_\lambda \leq 1.05$, the input power increases somewhat moderately as the C_λ increases, however, beyond C_λ =1.05, the input power is characterised by an unsteady variation for both 12° helix and 14° helix. The input power profiles suggest that more power is available to the 12° helix than to the14° helix except in the neighbourhood of, where a value of 3.70mW is recorded at exactly C_λ =1.1 for the 12° helix as against a value of 3.93mW for the 14° helix at the same C_λ =1.1.

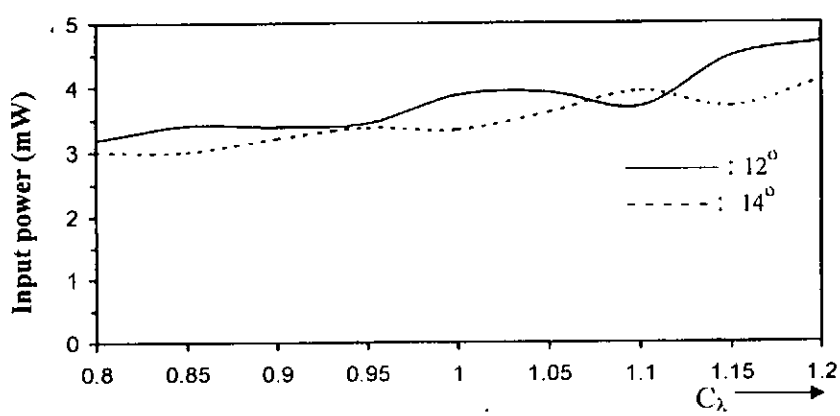

Figure 6.5: *Input power against C_λ*

6.1.5 Axial ratio, directive gain and half-power beam-width (HPBW)

The axial ratio of the radiated fields, (which is a measure of the degree of circular polarization of the helical beam antenna) as a function of C_λ is depicted in Figure 6.6. For both 12° helix and 14° helix, the axial ratio profiles are characterized by somewhat rapid oscillations at $C_\lambda < 1$, while for $C_\lambda > 1$ region, the oscillations are less rapid with amplitude values that are less than 2dB. This is satisfactory because, for most practical applications, the axial ratio of the fields radiated must be less than 3dB (Nakano and Mimaki 1997).

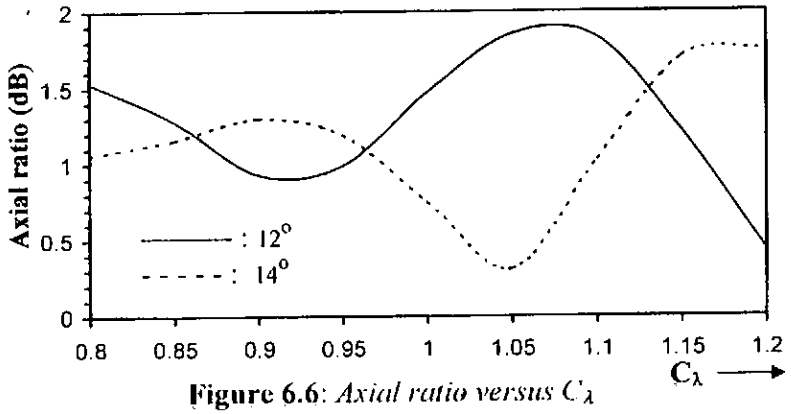

Figure 6.6: *Axial ratio versus* C_λ

Figure 6.7 portrays the manner in which the directive gain varies with the circumference in wavelengths (C_λ) for the pitch angles 12° and 14°. The illustration shows that the directive gain of the axial-mode helical antenna increases as C_λ increases.

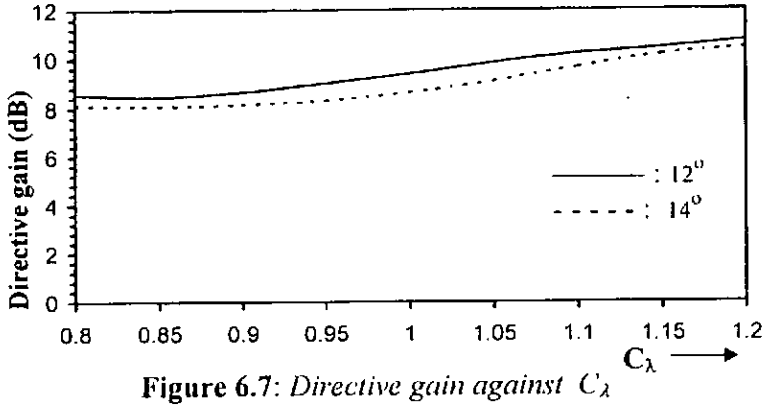

Figure 6.7: *Directive gain against* C_λ

The directive gain profiles for 12° helix and 14° helix are somewhat linear with positive slope. **For all C_λ, the 12° helix has a higher directive gain than the 14° helix.** The half-power beam-width (HPBW) of the radiated fields against the C_λ is shown in Figure 6.8. It is clear from the figure that the HPBW is almost the same for both 12° helix and 14° helix at various values of C_λ studied. In addition, the characteristics reveal that the HPBW diminishes as the frequency increases which is

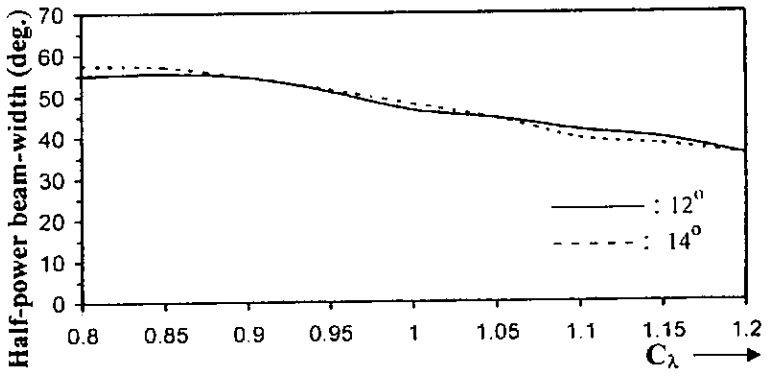

Figure 6.8: *Half-power beam-width versus C_λ*

consistent with expectation. That is to say, the helical beam antenna becomes more directive as the frequency increases.

Having investigated a single-element helical-beam antenna on a large ground plane in this section, it is logical to examine the consequences of mounting several helical elements on a ground plane, and this is the subject matter of the following section.

6.2 Planar array of helical-beam antennas mounted on a large ground plane

Practical applications involving satellite communications, invariably demand the utilization of arrays of helical antennas for the radiation and reception of electromagnetic signals (Hui *et al.* 2004, Gataulin 2004). In view of this observation, the generalized theory of single-element helical antenna developed in this thesis is

extended to the analysis of planar arrays of helical antennas, of which the common broadside and end-fire linear arrays are special cases. According to the principle of pattern multiplication of antenna arrays, (Balanis 1982), the resultant electromagnetic field at the far-zone of a planar array of helical antennas shown in Figure 6.9 may be expressed as the product of the radiation field of a single element positioned at the origin of the coordinate system and the so-called array factors of the two constituent linear arrays, located, in the case of the Cartesian system, along the x- and y- axes. Suppose then, that the planar array has N_x elements and N_y elements uniformly excited and equally spaced in the x- and y- directions, respectively, with the corresponding inter-element separations denoted by d_x and d_y. If the excitation phase progressions along the x- and y- directions are represented by β_x and β_y, respectively, and assuming that the mutual coupling between the elements is negligible, as is usually the case, (King and Wong 1975), then the total electric field E_t at the far-zone may be simply expressed in the following manner:

$$E_t = E_e \, (AF)_x \, (AF)_y \quad , \tag{6.2}$$

where E_e is the field due to a single-element helical antenna positioned at the origin, and (Balanis 1982):

$$(AF)_x = \frac{\sin\left(\frac{N_x \Psi_x}{2}\right)}{\sin\left(\frac{\Psi_x}{2}\right)}, \qquad (AF)_y = \frac{\sin\left(\frac{N_y \Psi_y}{2}\right)}{\sin\left(\frac{\psi_y}{2}\right)}, \tag{6.3}$$

provided that

$$\begin{aligned} \Psi_x &= kd_x \sin\theta \cos\varphi + \beta_x \\ \Psi_y &= kd_y \sin\theta \sin\varphi + \beta_y \end{aligned} \tag{6.4}$$

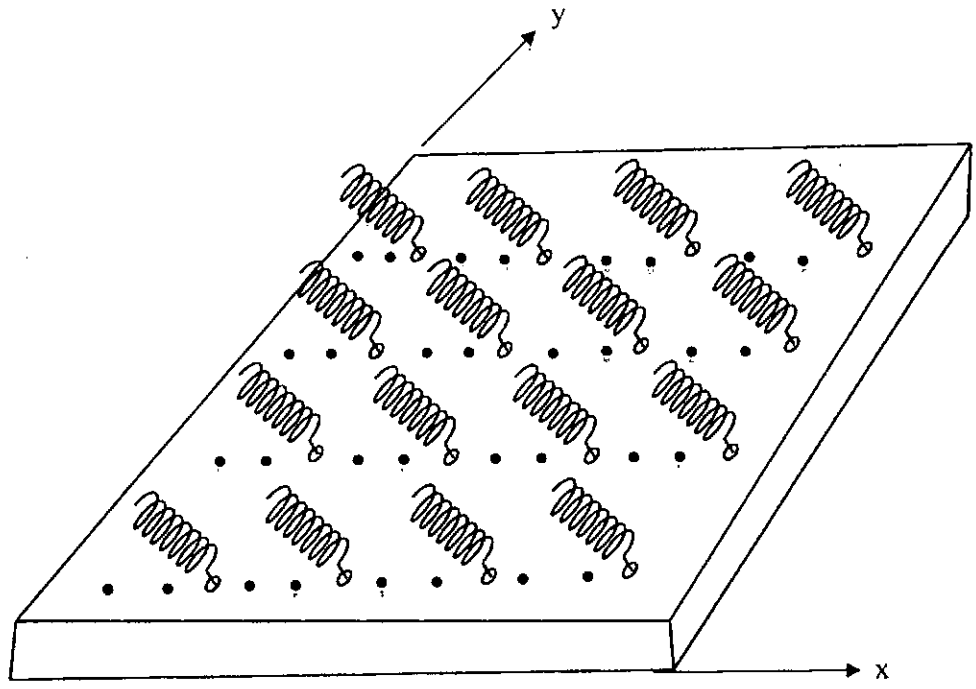

Figure 6.9: *Planar array of helical antennas.*

When it is noted that the maximum value of the function $\frac{\sin(nx)}{\sin(x)}$ is n, it is easy to see that normalized (to maximum value) version of equation (6.2) has the form given as

$$E_{tn} = E_{en}\,(AF)_{xn}\,(AF)_{yn} \quad , \tag{6.5}$$

where

$$(AF)_{xn} = \frac{\sin\left(\frac{N_x \Psi_x}{2}\right)}{N_x \sin\left(\frac{\Psi_x}{2}\right)} \quad and \quad (AF)_{yn} = \frac{\sin\left(\frac{N_y \Psi_y}{2}\right)}{N_y \sin\left(\frac{\Psi_y}{2}\right)} \quad , \tag{6.6}$$

and E_{en} denotes the normalized field of a single element with respect to the maximum field value.

6.2.1 Radiation characteristics of a single-element helical-beam antenna

First, we compute the field of a single element before considering the pattern multiplication rule to obtain the field of a planar array. In this regard, use is made of a 1V delta-gap generator as the excitation of the single element. The single element is

mounted on an infinite ground plane. Specifications of the other parameters of the helical antenna are taken as follows: number of turns: 8, pitch angle: 12°, circumference of one turn of the helix = 1λ, and a microwave frequency of 2GHz (L/S Bands) has been adopted for the ensuing numerical experiments.

Using the method of moments, we compute the current distribution and the field pattern of a single-element helical-beam antenna, in a manner earlier elucidated in this thesis. Figure 6.10a shows the distribution of current on the helical arm, while Figure

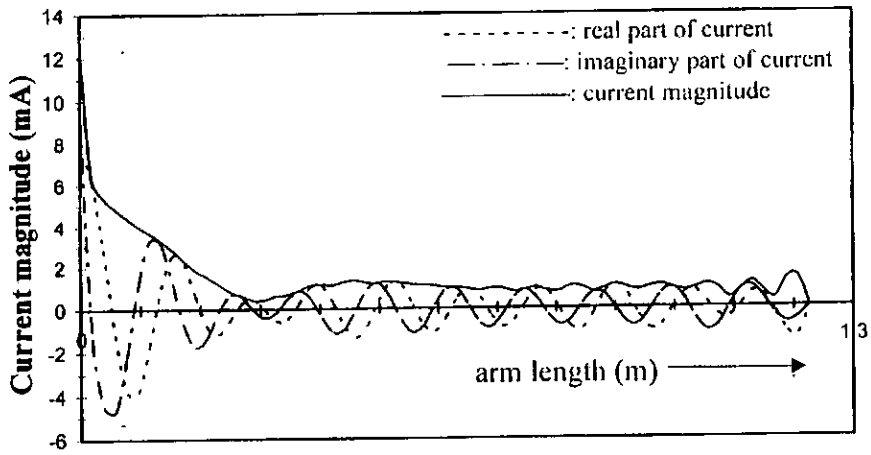

Figure 6.10a: *Current distribution on the arm length of 8-turn, 12° helix antenna*

6.10b depicts the corresponding radiation field components (E_θ and E_φ) of the helix. It is evident from Figure 6.10a that the current distribution consists of two regimes, namely, an exponentially decaying regime which starts from the feed-point to about one quarter of the arm length, and a surface wave domain which covers the remaining part of the helical arm. Current ripples noticeable near the open end are attributable to the multiple reflections from that end. The current peak of 12.07mA occurs at the feed-point. On the other hand, an observation of Figure 6.10b clearly reveals that the helical antenna radiates principally in the forward endfire direction ($\theta = 0^o$) with a null field in the backward direction as a consequence of the infinite ground plane on which the

antenna is mounted. The field pattern radiated has a maximum side-lobe level of -10.0dB, an axial ratio of 1.47dB, and the half-power beamwidths of E_θ and E_φ patterns are 56° and 65°, respectively. In the ensuing discussion, the behaviour of the array factor when the interelement spacing, d_e, is varied will be examined.

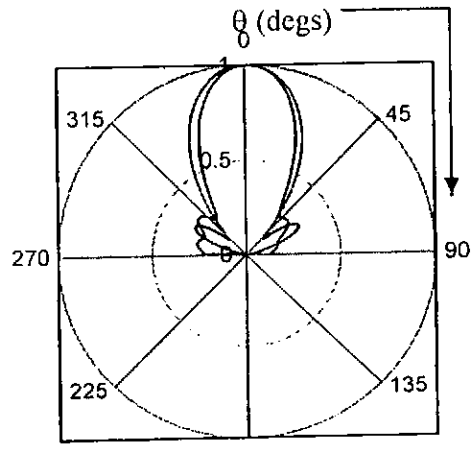

Figure 6.10b: *Radiation patterns on $\varphi = 0°$ (x - z) plane of 8-turn, 12° helix antenna* - - - - -:E_φ, _____:E_θ

6.2.2 Array Factor Profiles

By virtue of equation (6.5), the resultant field of the array antenna is the product of the single element field and the array factor, thus it is instructive to examine first, how the array factor (AF) behaves at different values of the interelement separation. To this end, the variations of the normalized array factor $(AF)_n$ with the interelement separation (d_e) for an N x N square array were computed when the excitation phase progressions, β_x and β_y, are set to zero by means of equation (6.4), in order to evaluate the effects of the spatial arrangement of the elements on the overall radiation patterns of the array.

Three practical square array configurations, namely, 2 x 2, 3 x 3, and 4 x 4 shown in Figures 6.11(a-c) are simulated on the computer when the interelement spacing varies from 0.25λ to 2.0λ, and the numerical results obtained are graphically illustrated in Figures 6.12a and 6.12b.

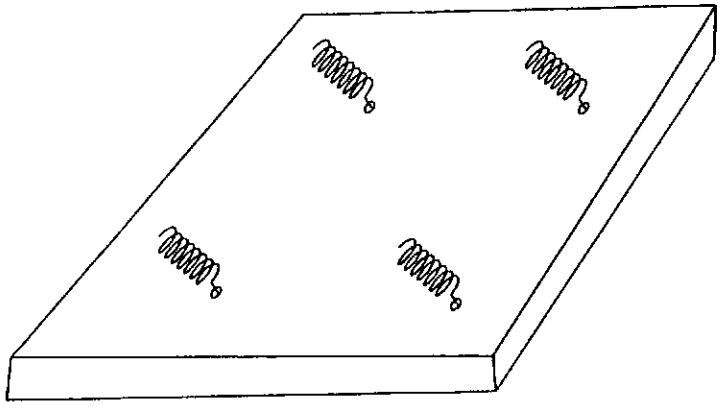

(a) *2 x 2 helical array*

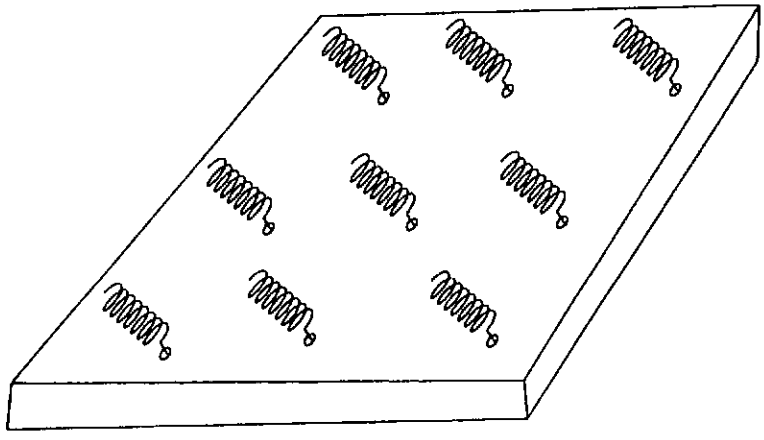

(b) *3 x 3 helical array*

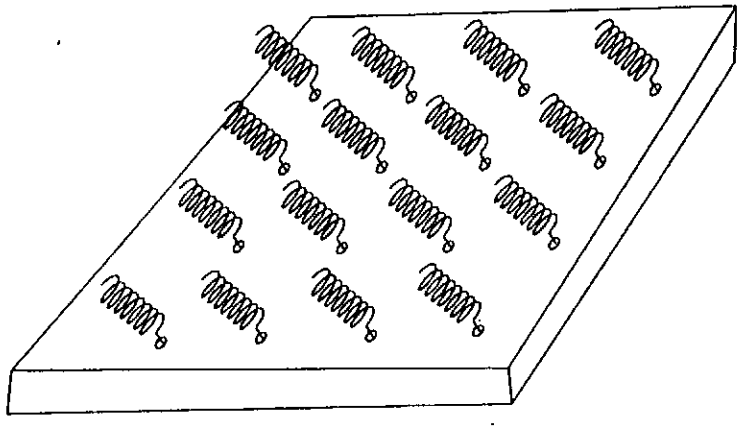

(c) *4 x 4 helical array*

Figure 6.11: *(a) 2 x 2 helical array; (b) 3 x 3 helical array; (c) 4 x 4 helical array.*

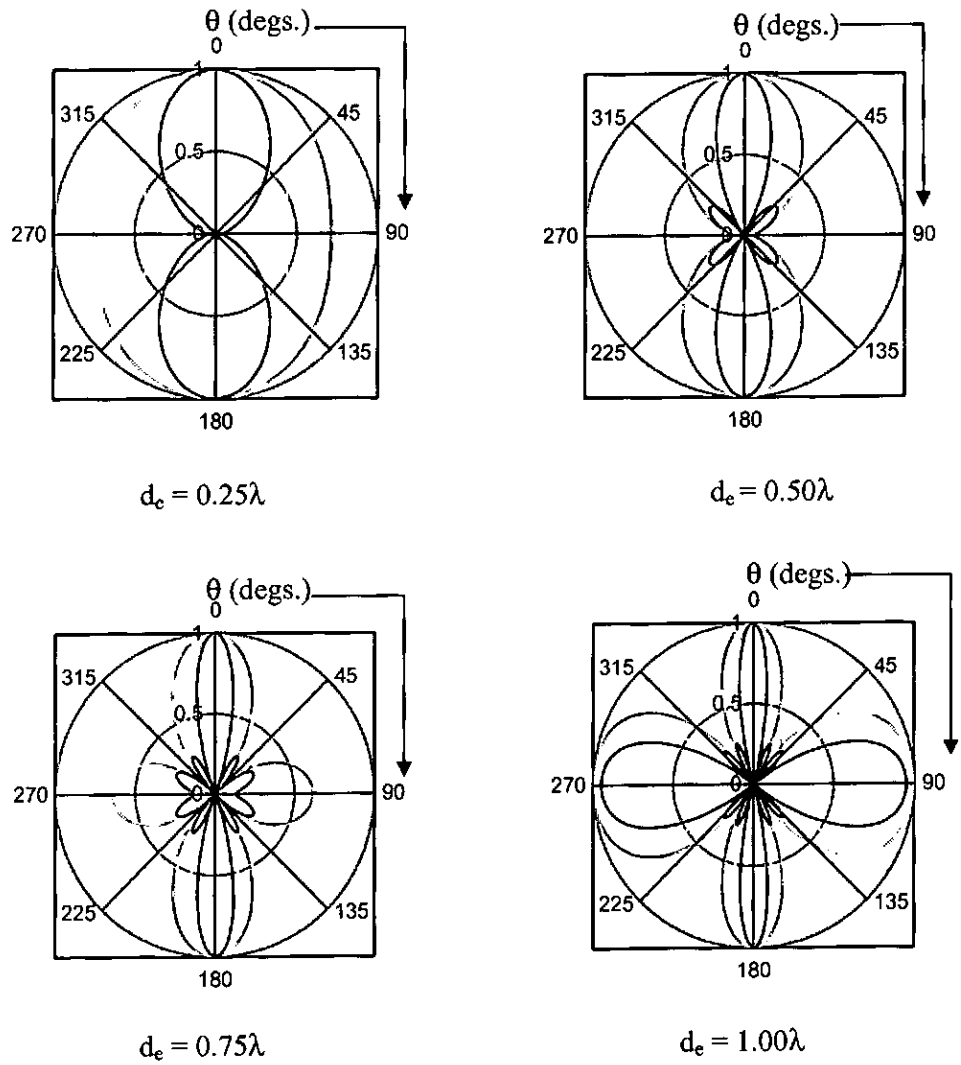

Figure 6.12a: *Normalized array factors of 2 x 2, 3 x 3, and 4 x 4 helical array antennas.* — ---:*2 x 2;* :*3 x 3;* ————: *4 x 4.*

We find from Figure 6.12a, that at an interelement spacing of 0.25λ, only the 4 x 4 array-factor profile has two well-defined major lobes in the two directions $\theta = 0^\circ$ and 180°, whereas the other arrays are characterized by oval-shaped patterns, with the 3 x 3 array having noticeable dips at $\theta = 90^\circ$ and 270°. It is noteworthy that at $d_e = 0.5\lambda$, only the array-factor pattern of the 2 x 2 array has only two major lobes without any minor lobes, while the 3 x 3 and 4 x 4 array-factor patterns consist of two sharp beams along $\theta = 0^\circ$ and 180° but with some side lobes.

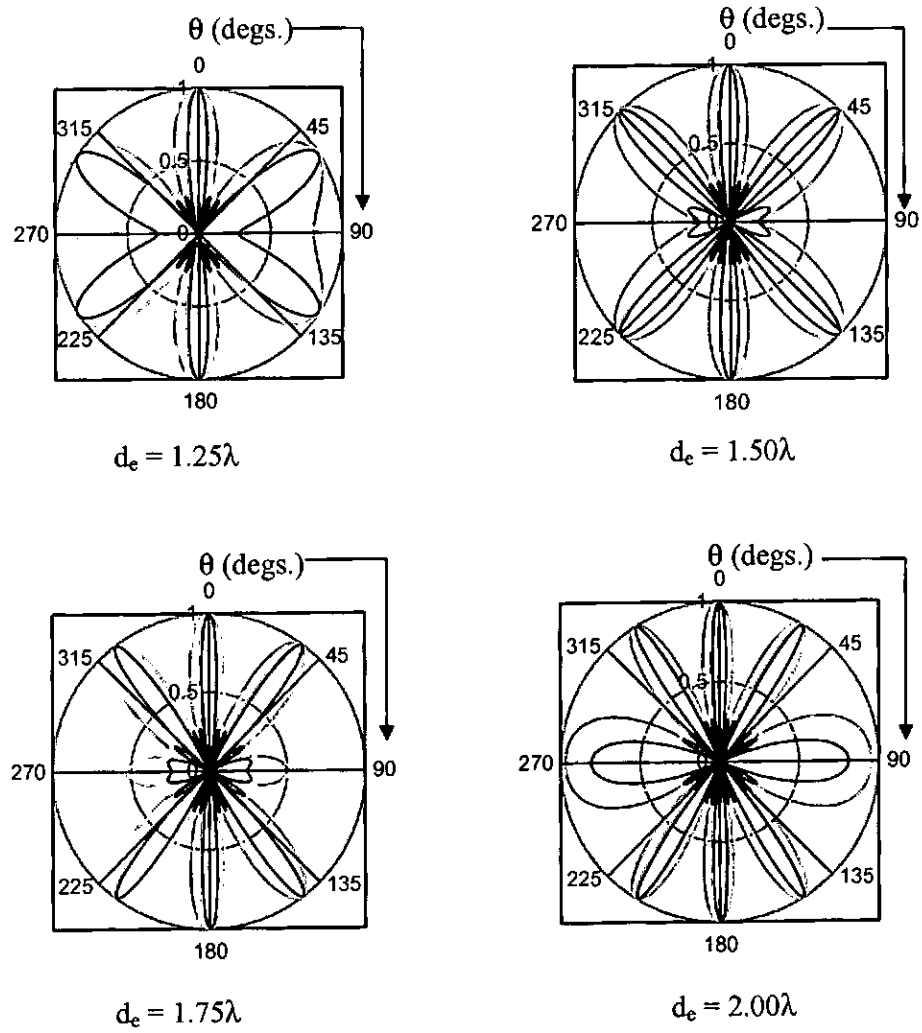

Figure 6.12a: *Normalized array factors of 2 x 2, 3 x 3, and 4 x 4 helical array antennas.* - - -·- -: *2 x 2;* : *3 x 3;* ———: *4 x 4.*

It should be pointed out that the 4 x 4 array main beams are more directive than those of the 3 x 3 array, because of higher number of array elements. When d_e equals 0.75λ, the array factor patterns of the three arrays are characterized by two main lobes with minor lobes of considerable strengths, although the minor lobes of the 2 x 2 array which occur at $\theta = 90^\circ$ and $\theta = 270^\circ$ are most pronounced. Interestingly, at a 1.0λ interelement separation, all the array factor patterns possess four major lobes, with two of the lobes in the $\theta = 0^\circ$ and $\theta = 180^\circ$ directions being the more directive. The major

lobes along $\theta = 90^o$ and $\theta = 270^o$ are commonly referred to as the *grating lobes* (Balanis 1982). This observation is consistent with the proposition of Balanis (1982) that the interelement spacing in a planar array must be less than one wavelength to avoid the occurrence of the grating lobes, which are undesirable in practical applications. It is noticed from Figure 6.12b that beyond an interelement separation of 1.0λ, more grating lobes are generated by the array factors of all the aforementioned arrays. It is noteworthy that at $d_e = 2.0\lambda$, all the array factor patterns have six grating lobes which are diametrically located, apart from the two main lobes in the $\theta = 0^o$ and $\theta = 180^o$ directions.

This preliminary study has reasonably demonstrated how the array factor depends on the interelement separation of planar array elements. It is seen that the interelement spacing should be less than 1.0λ to avoid the generation of grating lobes which may degrade the overall pattern of the array.

6.2.3 Radiation patterns of the 2 x2 array of helical antennas

Normalized radiation patterns (E_θ, E_φ) for the 2 x 2 helical array for different values of inter-element spacing are computed based on equation (6.5). The numerical results in graphical formats, are displayed Figures 6.13a and 6.13b, where the inter-element separation is allowed to vary between 0.1λ and 2.0λ. Although not all the patterns in the specified range of d_e are displayed, their characteristic features such as the half-power beam width (HPBW), side-lobe level (SLL) and directivity, are summarized in the representative profiles of Figures 6.16(a-c).

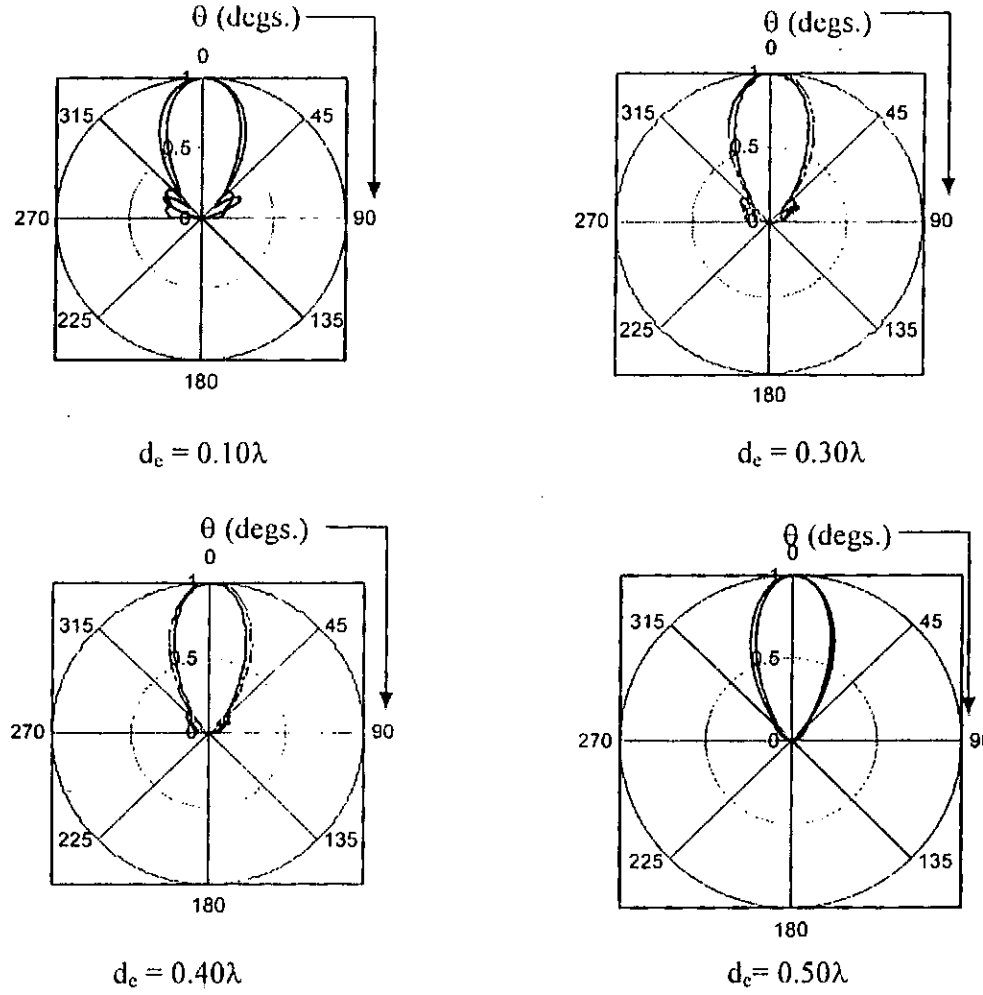

Figure 6.13a: *Radiation patterns (on the x-z plane) of a 2 x 2 helical array : - - - -: E_φ ———:E_θ*

It is observed from Figure 6.13a that when the inter-element spacing is 0.1λ, the patterns of the array have significant side lobes which are comparable to the side lobes of the patterns of a single helix. This result can be attributed to the close proximity of the array elements as well as the small size of the array. However, as the inter-element separation increases, the main beams of the patterns become more directive with reduction in the side-lobe strengths. It is important to observe that for $d_e = 0.6\lambda$, the side lobes are almost totally suppressed, leaving only the main lobes of the E_θ and E_φ patterns.

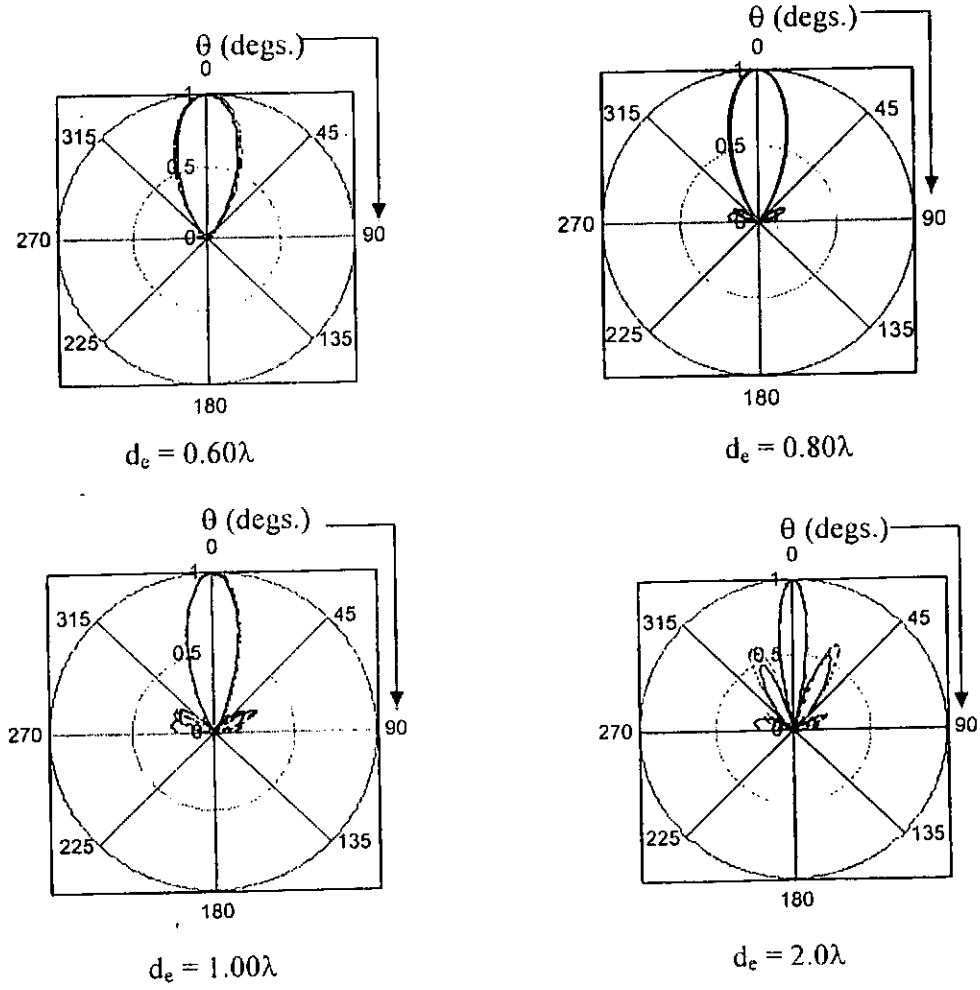

Figure 6.13b: *Radiation patterns (on the x-z plane) of a 2 x 2 helical array:* - - - -: E_φ ———: E_θ

However, beyond a value of 0.6λ for inter-element spacing, the side lobe levels begin, again, to appear with appreciation in magnitude, although the main beams become sharper. The number and levels of the side lobes when d_e is greater than or equal to one wavelength undergoes appreciable growth, due to the generation of grating lobes owing to the large spatial distribution of the array elements. If the design objective is to minimize the side-lobe level of the radiation patterns, then it is apparent that the value of d_e equals 0.6λ represents the optimum inter-element spacing of the 2 x 2 cylindrical helical array. This conclusion is consistent with that reached by Hui *et al* (2004), who

reported an optimum inter-element separation of 0.7λ for 2 x 2 *hemispherical helical array* based on circular polarization property of the radiated fields.

6.2.4 Radiation patterns of the 3 x 3 array of helical antennas

Displayed in Figures 6.14 (a-b) are the radiation patterns of the 3 x 3 helical array for different values of inter-element spacing (d_e) ranging between 0.1λ and 2.0λ.

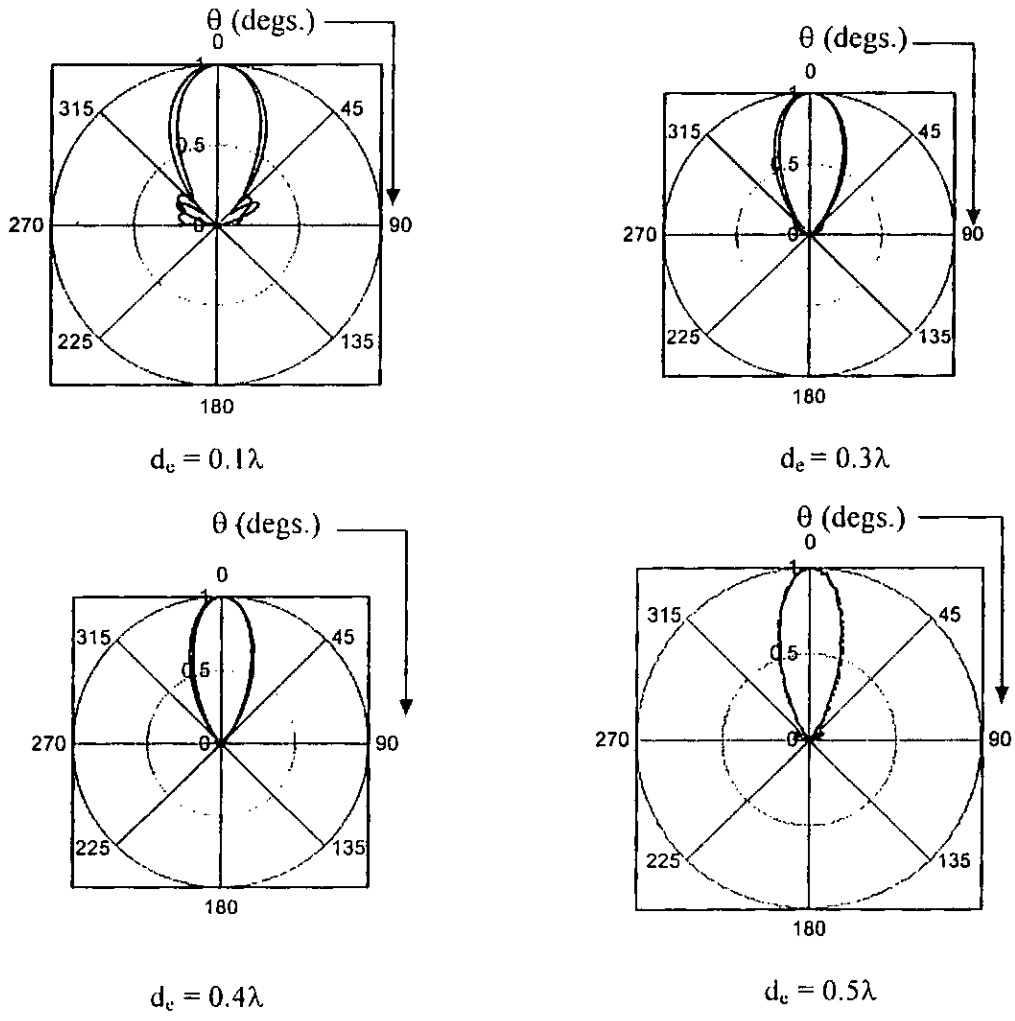

Figure 6.14a: *Radiation patterns (on the x-z plane) of a 3 x 3 helical array: - - - -:E_φ ———:E_θ*

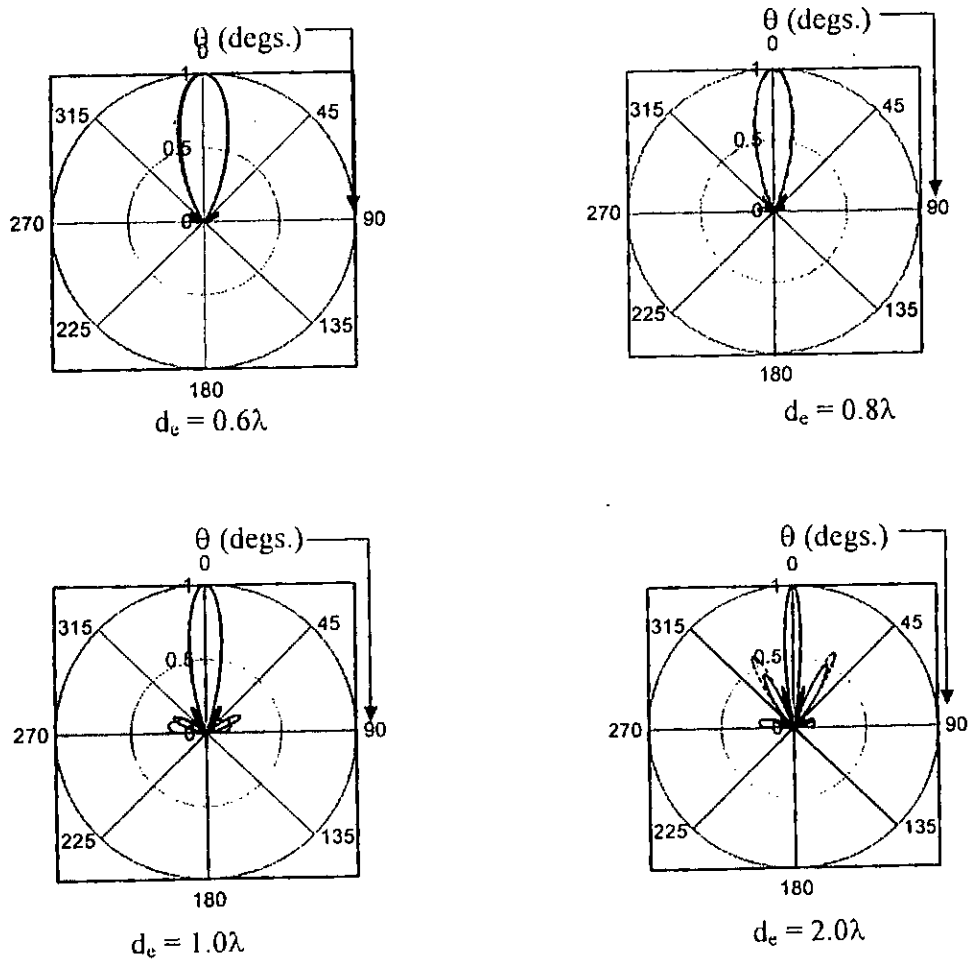

Figure 6.14b: *Radiation patterns (on the x-z plane) of a 3 x 3 helical array : - - - -: E_φ ———:E_θ*

When d_e equals 0.1λ, the E_θ and E_φ patterns are characterized by some side lobes with the main beams in the broadside ($\theta = 0^o$) direction. Further increases in the inter-element spacing result in noticeable decreases in strength of side-lobe levels , whilst the principal beams of the patterns become more directive. Remarkably, at $d_e = 0.4\lambda$, the side lobes are nearly completely suppressed with an attendant enhancement in the directivities of the E_θ and E_φ patterns. On the other hand, beyond the 0.4λ inter-element separation, the side lobe strengths appear to increase slightly, though within acceptable limits insofar as d_e is less than one wavelength. For values of d_e equal to or greater than 1.0λ, the radiation patterns are typified by several side lobes as anticipated. In particular, at $d_e = 2.0\lambda$, the number and strengths of the side lobes are considerably high

as a consequence of the *grating lobes* associated with the corresponding array-factor pattern (Balanis 1982). We can infer from these results that the right inter-element spacing of the 3 x 3 array is 0.4λ if the design goal is the reduction of the side lobe strength to the barest minimum.

6.2.4 Radiation patterns of the 4 x 4 array of helical antennas

Figures 6.15(a-b) depict the radiation patterns of the 4 x 4 helical array for various inter-element spacing ranging between 0.1λ and 2.0λ. The radiation patterns

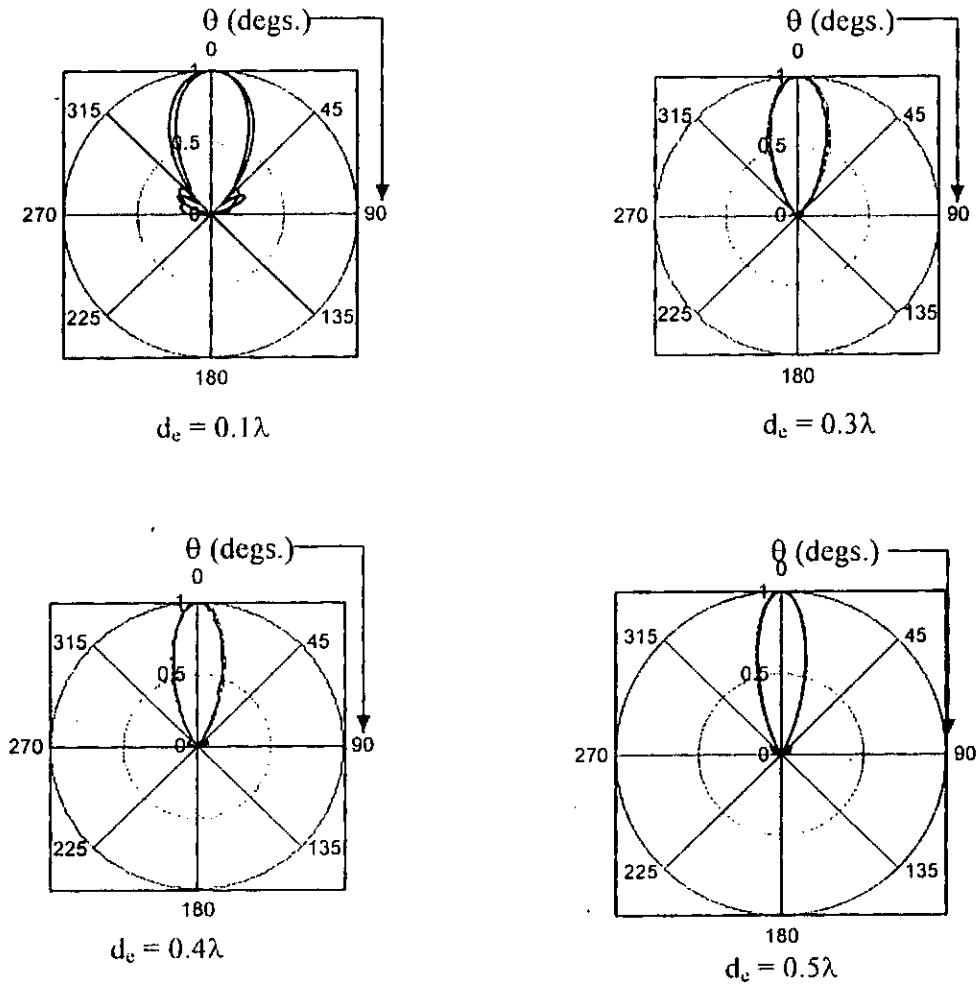

Figure 6.15a: *Radiation patterns (on the x-z plane) of a 4 x 4 helical array: - - - -: E_φ ———:E_θ*

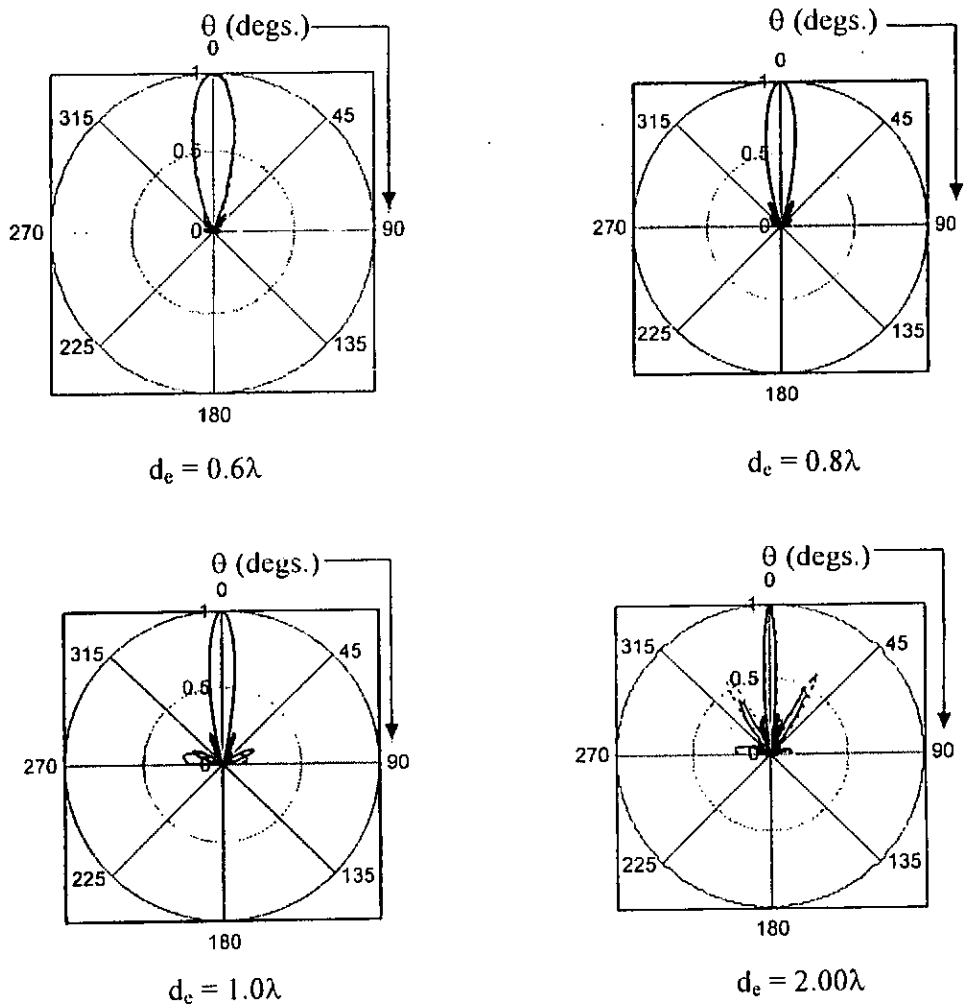

Figure 6.15b: *Radiation patterns (on the x-z plane) of a 4 x 4 helical array: - - - -: E_φ ———: E_θ*

(E_θ, E_φ) for the case $d_e = 0.1\lambda$ have many side lobes with the main beams aligned along the broadside ($\theta = 0^\circ$) direction. These side lobes are almost nonexistent when $d_e = 0.3\lambda$, and the directivities of the main beams of the E_θ and E_φ patterns are significantly enhanced. Above 0.3λ inter-element spacing, the side lobes steadily build up, though within the acceptable level. When d_e assumes the values of 1.0λ and 2.0λ, the number and levels of the side lobes are large, and this is in conformity with the array-factor profiles of the 4 x 4 helical array when d_e equal to or greater than one wavelength. In view of the above results, an inter-element spacing of 0.3λ may be regarded as the

optimum inter-element spacing for the 4 x 4 array, if the design objective is to minimize the side lobe strengths.

6.2.6 Side Lobe Level, Half-Power Beam-Width and Directivity

Variations of the important antenna design parameters such as the side-lobe level, (SLL), half-power beam-width (HPBW) and the directivity of the helical arrays with interelement spacing (which ranges from 0.1λ to 2.0λ) are evaluated, and displayed in Figures 6.16a, 6.16b and 6.16c. It can be seen from the SLL profiles for the 2 x 2, 3 x 3and 4 x 4 helical arrays depicted in Figure 6.16a that the SLLs initially slope downwards and after reaching different minima, begin to rise gradually. Specifically, the minimum SLLs are recorded at the interelement spacings of 0.6λ, 0.4λ and 0.3λ for the 2 x 2, 3 x 3 and 4 x 4 arrays, respectively. These results show that as the number of array elements is increased, the interelement spacing required to achieve minimum SLL of the radiation patterns is reduced.

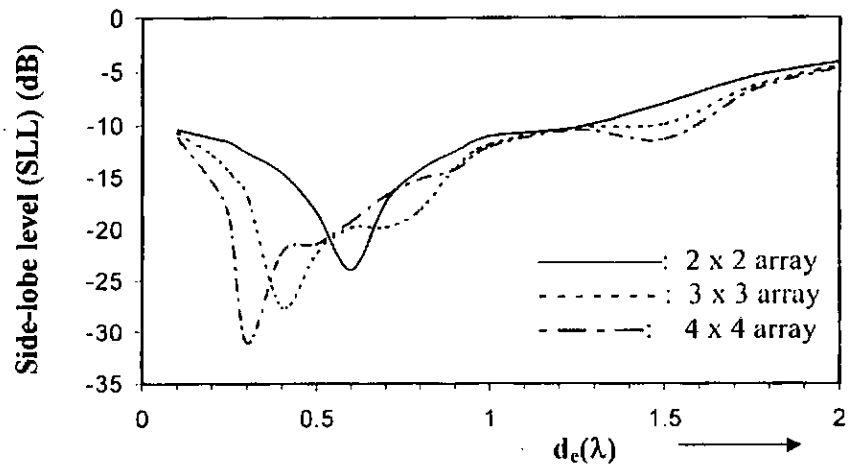

Figure 6.16a: *Side-lobe levels as a function of interelement spacing (d_e)*

Figure 6.16b reveals that the half-power beam-width of the radiation patterns decreases almost monotonically as the interelement spacing is increased. Furthermore,

it is apparent that as the number of array elements is increased, there is a significant reduction in the HPBWs. Since the pattern directivity is inversely related to the pattern HPBW, it follows that there is an improvement in the array pattern directivity when the number of array elements is increased.

The directivity curves of the 2 x 2, 3 x 3, and 4 x 4 helical arrays when the interelement separation (d_e) varies from 0.1λ to 2.0λ, are illustrated in Figure 6.16c. These curves show that the directivity increases as the interelement spacing increases provided that d_e is less than 1.0λ, and attains peak values when d_e equals 0.9λ.

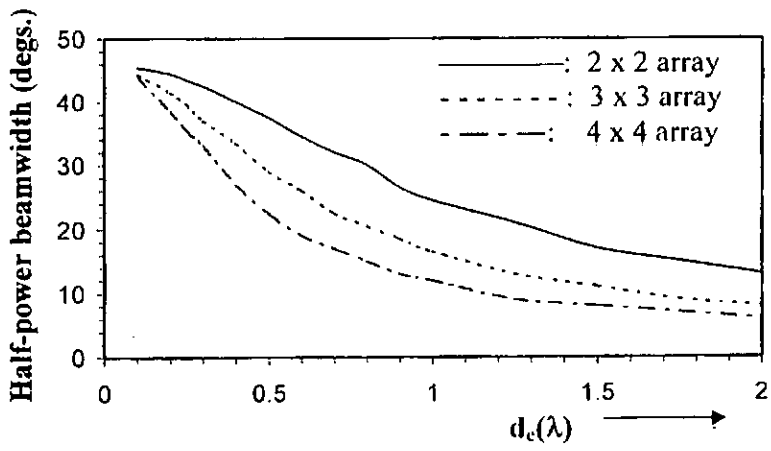

Figure 6.16b: *Half-power beam-widths versus the interelement spacing (d_e)*

Beyond a 0.9λ interelement spacing, the directivity has an unsteady profile for the 3 x 3 and 4 x 4 arrays, while the directivity of the 2 x 2 array reduces slowly in a somewhat linear manner. The directivity profiles reported here resemble the earlier directivity curves of King and Wong (1975) for uniformly fed N x N array of directive elements, of which helical antenna is a typical example.

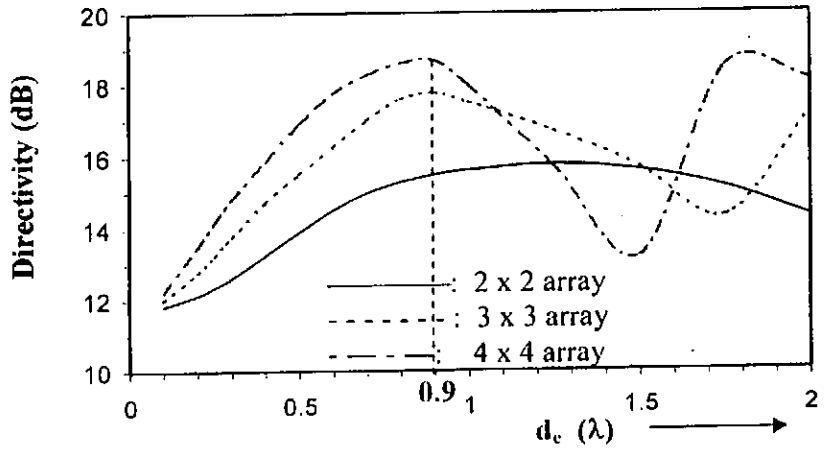

Figure 6.16c: *Directivities against the interelement spacing (d_e)*

A summary of the aforementioned antenna design parameters is presented in the following three Design Tables.

Design Table I

Computed values of directivity, half-power beamwidth and interelement separation at minimum sidelobe strength for 2 x 2, 3 x 3 and 4 x 4 helical arrays.

Array Type	Interelement separation (d_e)	Minimum side-lobe strength	Half-Power Beam-Width	Directivity of the main beams
2 x 2	0.6λ	-23.94dB	48°	14.5dB
3 x 3	0.4λ	-27.54dB	46.5°	14.73dB
4 x 4	0.3λ	-31.06dB	45.5°	14.81dB

Design Table II

Calculated values of directivity, half-power beamwidth and sidelobe level of pencil beams of 2 x 2, 3 x 3 and 4 x 4 helical arrays.

Array Type	Interelement separation (d_e)	Side-lobe strength	Half-Power Beam-Width	Directivity of the pencil beam
2 x 2	2.0λ	-4.124dB	13°	14.29dB
3 x 3	2.0λ	-4.470dB	8°	17.17dB
4 x 4	2.0λ	-4.690dB	6°	18.1dB

Design Table III

Maximum directivities and corresponding sidelobe strengths and half-power beamwidths of radiation patterns of 2 x 2, 3 x 3 and 4 x 4 helical arrays

Array Type	Interelement separation (d_e)	Side-lobe strength	Half-Power Beam-Width	Directivity
2 x 2	1.25λ	-10.20dB	21°	15.77dB
3 x 3	0.90λ	-14.02dB	18.5°	17.17dB
4 x 4	0.90λ	-14.24dB	13°	18.67dB

Chapter 7

CONCLUSIONS

7.1 Summary of findings

The research problem of systematically developing a generalized solution to the analytical problem of thin-wire antenna design has been successfully addressed by this thesis. By applying the generalized procedure to the analysis of a number of helical antenna problems and comparing computational results with published data obtained through the use of other analytical tools, it has been firmly established that the procedure reported here is both valid and accurate in formulation and solution. The main research findings, including contributions to knowledge of importance in the area of antenna theory and practice, are summarized in this chapter.

7.1.1 Novel design of helical-beam antenna without a ground plane (exclusion problem)

It has been demonstrated that for this antenna design problem,

- the distribution of current on the exclusion-mode helix antenna, when its electrical circumference lies between 0.8λ and 1.15λ, is characterized by an exponentially decaying curve, whose maximum value occurs at the feed point. Except at the region close to the feed point, the current profiles for $\alpha = 10^{\circ}$ and $\alpha = 15^{\circ}$ are distinct from one another, which consequently offer α as a viable design parameter.
- the main lobes of the radiation patterns of the exclusion-mode helix are essentially in the backfire direction ($\theta = 180^{\circ}$), which means that the radiated electromagnetic energy from the exclusion-mode helix is concentrated in the backfire direction, and that the antenna is suitable as feed for dish antennas.

- the input resistance of exclusion-mode helix is virtually independent of the normalized circumference (C_λ), whereas the input reactance, which is dominantly capacitive, has a linear variation with a positive slope as a function of the normalized circumference; these are important considerations for the design of impedance matching, in practical applications.
- although the directive gain of the exclusion-mode helix decreases linearly as C_λ increases, the 10° helix possesses higher directive gain when compared with that of 15° helix.

7.1.2 Design of helical-beam antenna backed by a small ground plane

- Through a comparative analysis of exclusion-mode helix and the helix backed by a small ground plane (modeled by a wire-grid), it is revealed that the presence of the small ground plane in the feeding arrangement of the helix is responsible for the substantial reduction in the input impedance of the monofilar helix.
- Whereas helical antennas, with or without small ground planes, radiate in the backfire direction, the helix with a small ground plane radiates more power in the backfire direction than the exclusion-mode helix.
- Higher values of directive gain are obtainable from the helix with a small ground plane than from the exclusion-mode helix; in addition, the half-power beam-width profiles show that the radiation patterns of the former helix are more directional than those of the exclusion-mode helix.

7.1.3 Design of helical-beam antenna mounted on a large ground plane

- Current distribution on the arm length of helical antenna above a large ground plane (modelled as infinite in size) is characterized by two distinct regimes;

namely an exponentially decaying domain and a surface-wave region. The former component exists from the feed point to about a quarter of the arm length, while the latter part extends over the rest of helical arm. It is observed that as the pitch angle and normalized circumference increase, the magnitude of the reflected current from the open end also increases.

- The helical antenna radiates mainly in the forward end-fire direction with a null field in the backward direction. Consequently, the large ground plane serves as a perfect reflector for the backward radiation.
- It is noted that as C_λ increases, or as frequency increases, the radiation patterns of the helical-beam antenna become more directive, but the number and levels of the sidelobes assume higher values.
- An optimum axial-mode operation of the helix above a large ground plane may be achieved by a judicious selection of its circumference in wavelengths with less consideration being given to the pitch angle.

7.1.4 Planar array of helical-beam antennas

- The minimum side-lobe levels are recorded at the inter-element separations of 0.6λ, 0.4λ and 0.3λ for the 2 x 2, 3 x 3, and 4 x 4 arrays of helical-beam antennas, respectively. This suggests that as the number of array elements is increased, the inter-element spacing required to achieve minimum side-lobe level of the radiation patterns is reduced.
- The maximum directivities of the 2 x 2, 3 x 3 and 4 x 4 arrays of helical-beam antennas which are 15.77dB, 17.17dB and 18.67dB, respectively, occurred at the respective inter-element spacing of 1.25λ, 0.9λ and 0.9λ, where λ represents the wavelength.

7.2 Contributions to Knowledge

Apart from research findings listed in the foregoing, the thesis, has in addition, contributed to knowledge of importance as follows:

- ◊ In the main, the thesis has undertaken a novel formulation of the thin-wire antenna design problem, in a manner general enough to simultaneously accommodate such regular thin-wire geometries as circular helix, planar helix, multi-turn elliptical and circular loops, elliptical and circular loops, and linear elements, as special cases of the general elliptical cylindrical helix geometry.
- ◊ The resolution of the important roles played by the ground plane conventionally included in the feeding schemes for helical antennas; analytical and computational results clearly reveal that in addition to its traditional roles, the size and orientation of the plane significantly affect input and radiation characteristics of the antenna.
- ◊ A rigorous evaluation, for the first time, of the electromagnetic response of the 'exclusion-mode' helical antenna as a design alternative to traditional helical-beam antenna design for which feeding mechanisms are obliged to incorporate a ground plane.
- ◊ A systematic investigation, using the generalized approach developed in the thesis, of radiation characteristics of 2 x 2, 3 x 3, and 4 x 4 planar arrays of helical antennas commonly deployed on satellite platforms.

7.3 Recommendations for future work in this area

Having provided a generalized solution to thin-wire antenna problem in this thesis, a natural extension, of course, is the development of a generalized theory of (2M+1) by (2N+1) planar array of thin-wire helical-beam antennas, accounting for the mutual interaction/coupling between the helical elements, from which the basic array

types, namely, linear broadside, linear endfire, circular, square, rectangular and triangular arrays would be readily realizable. In the case of the single-element helical antenna, the application of genetic algorithm for optimization of its various design parameters constitutes one of the directions for future work towards adding to the body of knowledge. Another potential research problem concerns the analysis and characterization of thin-wire antennas when radiating in medium other than the free space adopted in this thesis, the result of which will find practical applications in the design of deep-space, underground and submarine communication systems. Finally, the most general problem concerning arbitrary configurations of thin-wire geometries should naturally develop from the formulation given in this thesis.

7.4 Concluding Remarks

A novel generalized formulation and solution of the thin-wire antenna problem, employing the elliptical-cylindrical helix as the radiating structure, enunciated in this thesis has brought under one coverage, the solutions of eight fundamental thin-wire antennas that have profound practical applications. Additionally, a systematic application of the generalized solution furnishes the performance characteristics of helical-beam antennas excited without a ground plane, with a small ground plane modelled by wire grids, and when backed by an array of parasitic loops. An extension of the generalized solution to the radiation problem of planar arrays of helical antennas, routinely deployed on the satellite platforms, is also provided in the dissertation. Finally, it is readily conceivable that the generalized solution reported here will substantially facilitate the investigations of linear end-fire and broadside arrays of thin-wire antennas of regular geometries, as well as the electromagnetic response of wire antennas operating in the presence of wire-grid ground plane.

APPENDIX I(a):

A RIGOROUS ANALYSIS OF THE RADIATION CHARACTERISTICS OF HELICAL-BEAM ANTENNAS

European Journal of Scientific Research
ISSN 1450-216X Vol.16 No.2 (2007), pp.317-326
© EuroJournals Publishing, Inc. 2007
http://www.eurojournals.com/ejsr.htm

A Rigorous Analysis of the Radiation Characteristics of Helical-Beam Antennas

Adekola, S. Adeniyi
Department of Electrical and Electronics Engineering
University of Lagos, Akoka, Lagos

Mowete, Ike
Department of Electrical and Electronics Engineering
University of Lagos, Akoka, Lagos
Email: mowete@hotmail.com
Tel: +234-8033057776

Ayorinde, A Ayotunde
Department of Electrical and Electronics Engineering
University of Lagos, Akoka, Lagos

Abstract

A rigorous analysis of the radiation characteristics of helical-beam antennas commonly employed for terrestrial and satellite communications is presented in this paper. Use is made, in that connection, of a formulation for the elliptical helical antenna, whose geometry represents a general case for several wire antennas of regular geometrical shapes. After the deriving the governing integro-differential equation by connecting an incident electric field and the distribution of current excited by its incidence, a solution to the problem so defined is obtained through the use of the method of moments with a Galerkin procedure. As a demonstration of the utility of the formulation, the paper then addresses the problem of a circular helical antenna excited without the conventional ground plane. The computational results obtained are consistent with those available in the open literature, and clearly reveal that the antenna structure may find useful application as feed for a dish antenna of the type utilized for radio communications at the satellite frequencies.

1. Introduction

The accurate determination of the input characteristics and radiation properties of an antenna is inextricably tied to the exact prediction of the nature of the current distribution associated with the antenna structure. Because of the difficulties associated obtaining accurate experimental measurements of the current distributions, pioneers of antenna theory typically worked with assumptions of uniform current, standing-wave current and travelling-wave current distributions, [2], [3]. With the advent of high-speed, high-capacity digital computers came a number of numerical methods, including the method of moments formalized by Harrington [1], through which excellent approximations to the current waveform on any antenna structures may be determined. The method of moments may be described as an adaptation of the least-squares approximation technique, and involves the series expansion of the unknown current in terms of finite set of basis functions and

unknown coefficients, which are determined by essentially imposing boundary conditions appropriate to the problem, and hence reduce an integro-differential equation to a matrix equation.

Of particular interest to this presentation is the early work on the radiation characteristics of a circular helix by Kraus and Williamson [2], who modelled the circular helix as a square helix of equivalent circumference, and assumed that the current distribution may be approximated by a travelling wave of constant amplitude, defined along the linear segments. With this formulation, the authors were able to obtain analytical and numerical results for the electromagnetic fields radiated by the one-turn "square" helix; and thereafter, invoked the pattern multiplication theorem for an array of isotropic sources, to determine the total field of the helix. Using the same current approximation, Kornaushcr, [3] , developed radiation integrals for circular helix having integral and non-integral number of turns, while Kunsden , [4], evaluated the radiation fields from a square helix operating in the Very High Frequency (VHF) band. Nakano *et al*, [5] , using the Numerical Electromagnetic Codes (NEC), which is essentially based on the method of moments, computed numerical results for the directive gain of an axial-mode helical antenna in the presence of a parasitic helix. Certain other aspects of the circular helical antenna problem have been addressed by Nakano et al [6], [7], also using the NEC, and who also described a number of important practical applications of this antenna type. To the best of our knowledge, no treatment has been reported in the literature, of circular helical antenna as a special case of the elliptical helical antenna.

In this paper, we systematically develop a formulation for the problem of determining the current distribution and associated far-zone electromagnetic fields of the elliptical helical antenna, which formulation is then specialized to the case of the circular helical antenna.. The helical wire is modelled as a perfectly conducting, electrically thin wire, and it is shown that the formulation readily facilitates the determination of current along the helical arm through the use of the method of moments. Computational results are obtained for the circular helix fed without a conventional supporting ground plane, and these results for current distributions and the far-field patterns clearly show that in this form, the circular helix operates as a backfire antenna. A practical application of how to use the helix without a ground plane as feed for a parabolic-dish antenna is presented, as an example of the utility of that antenna configuration.

2. Formulation

In terms of the retarded electromagnetic potentials, an electric field represented by $\overline{E}^i$, which impinges on a conducting body in free space , excites a scattered electric field denoted by $\overline{E}^s$, and which admits description in the from:

$$\overline{E}^s = -j\omega\mu_o\overline{A} - \nabla\phi, \tag{1}$$

where $\overline{A}$ stands for the vector magnetic potential, ϕ scalar electric potential, μ_o free-space peameability, ∇ , the (del) gradient operator, $j=\sqrt{-1}$,and ω angular frequency in radians per second. For thin-wire structures in which only the axial quantities are significant, eqn. (1) simply reduces to the one-dimensional equation given [1], as:

$$E_\lambda^s = -j\omega\mu_o A_\lambda - \frac{d\phi}{d\lambda} \tag{2}$$

in which A_λ and ϕ , and for which

$$A_\lambda = \frac{1}{4\pi}\int_{c'} \hat{a}_{\lambda'}\cdot\hat{a}_\lambda I(\lambda')[\exp(-jk_o R)/R]d\lambda' \tag{2a}$$

$$\phi = \frac{1}{4\pi\varepsilon_o}\int_{c'} q(\lambda')[\exp(-jk_o R)/R]d\lambda'; \tag{2b}$$

$$R = a\sqrt{\left(\frac{r_w}{a}\right)^2 + 4\sin^2\left(\frac{\varphi-\varphi'}{2}\right) + \tan^2\alpha(\varphi-\varphi')^2} \tag{14a}$$

In the next section, a generalized solution to the operator equation (13) through the use of the method of moments [1], [10], is presented.

3. Method of Moments Solution

Having reduced the elliptical helix antenna problem, as specialized for a circular helical antenna, to an integro-differential equation as described by the $I(\varphi')$ operator form of eqn. (13), the method of moments technique becomes readily applicable to the solution for the unknown current $I(\varphi')$. In this regard, we first divide the thin-wire helical structure into a finite number of equal linear short segments, and then define piece-wise (triangular) expansion (or basis) functions along the wire axis in which each function spans over four consecutive linear segments. In terms of these basis functions, the unknown axial current is analytically given by:

$$I(\varphi') = \sum_n \gamma_n T_n(\varphi') \tag{15}$$

where γ_n's are the unknown complex expansion coefficients to be determined and the set $\{T_n(\varphi')\}$represents a finite set of known triangular expansion functions. On substituting eqn. (15) into eqn. (13) and using the linearity property of the integro-differential operator $L[*]$, we arrive at the expression given as

$$E_\varphi^i = \sum_n \gamma_n L[T_n(\varphi')] \tag{16}$$

An integro-differential equation, whose solution is effected by taking the weighted inner product of both sides of the equation with the weighting functions denoted by $W_m(\varphi)$, and defined on the wire surface. This process yields:

$$\langle W_m(\varphi), E_\varphi^i\rangle = \sum_n \gamma_n \langle W_m(\varphi), L[T_n(\varphi')]\rangle \tag{17}$$

In this paper, the Galerkin's procedure is adopted in which the weighting functions are identical to the expansion functions in all respects. As described elsewhere, [8], eqn. (17) may be recast as the generalized Ohm's law equation:

$$[V_m] = [Z_{mn}][I_n] \tag{18}$$

where $[V_m] = \langle W_m(\varphi), E_\varphi^i\rangle$ is a generalized voltage matrix, $[Z_{mn}] = \langle W_m(\varphi), L[T_n(\varphi')]\rangle$, a generalized impedance matrix, and $[I_n] \doteq [\gamma_n]$, a generalized current matrix whose entries are the unknown current expansion coefficients.

Evidently, the matrix operations of inversion and multiplication will provide numerical values for the unknown current matrix elements.

4. A Numerical Example: The Circular Helix Excited Without a Ground Plane Structure

As an example of the application of the foregoing analysis, we now consider the radiation problem of a circular helix excited without the usual ground plane structure. For the sake of brevity, only the current distributions on the helical arm and the associated radiated fields are presented and discussed. The feed model adopted for use is the delta-gap model, with an excitation voltage of 1 volt, and

operated at 2GHz. Numerical results obtained and displayed in graphical formats are discussed in what follows.

Figure 4.1 suggests that the current profiles of the helical antenna when $0.8 \leq C_\lambda \leq 0.95$, (where C_λ is the electrical circumference of the helix) are exponentially decaying in character, with the maximum value for magnitude of current recorded at the feed-point. Away from the region near the feed-point, the current waveforms, for $\alpha = 10°$ and $\alpha = 15°$ are distinct from one another, unlike what obtains with the current distribution for a circular helix backed by a small ground plane, which has been reported to be independent of the pitch angle (α) [9]. We also find that the magnitude of current at the feed point, increases as the C_λ increases, while the first minimum point shifts towards the feed point as C_λ increases.

Figure 4.1: *Current distributions on a circular helix fed without a ground plane: C_λ = 0.80 - 0.95*
The numerical values for the far-zone electric fields, in the vertical plane (x-z plane) defined by $\varphi = 0°$, associated with the current distributions discussed above and computed with the use of the fields equations derived in the text are shown in figures 4.2 and 4.3 for $\alpha = 10°$ and $\alpha = 15°$, respectively. In the those figures, the continuous curves represent the $\hat{\theta}$ component of the electric field (E_φ) while the discontinuous curves depict the $\hat{\varphi}$ component of the electric field (E_φ). We find from the said figures that the main lobes of the radiation patterns are virtually in the backward direction ($\theta = 180°$), which reveals that the radiated electromagnetic energy is concentrated in the backfire direction. As previously explained by Walter [11], these feature indicates that the phase velocity of the current wave is directed towards the feed-point while

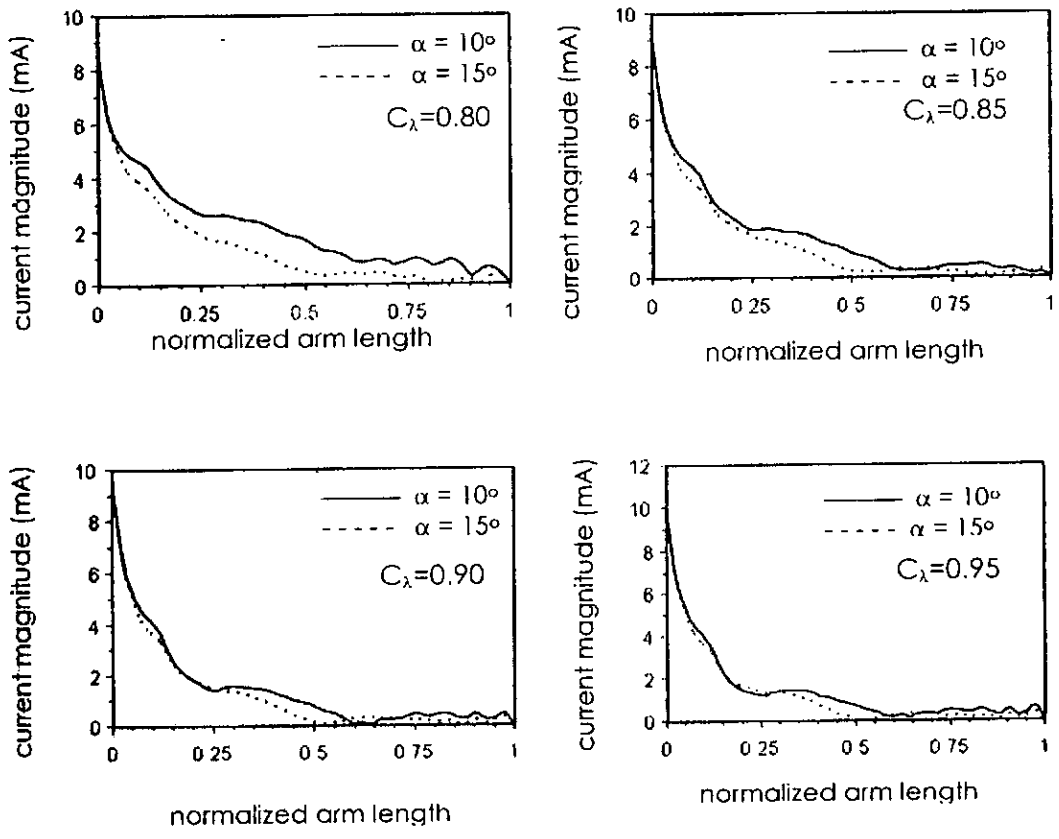

Figure 4.2: *Normalized field patterns of a circular helix fed without a ground plane* $\alpha = 10^o$ *and* C_λ *: 0.80 and 0.95* ——— E_θ *component* - - - - - E_φ *component*

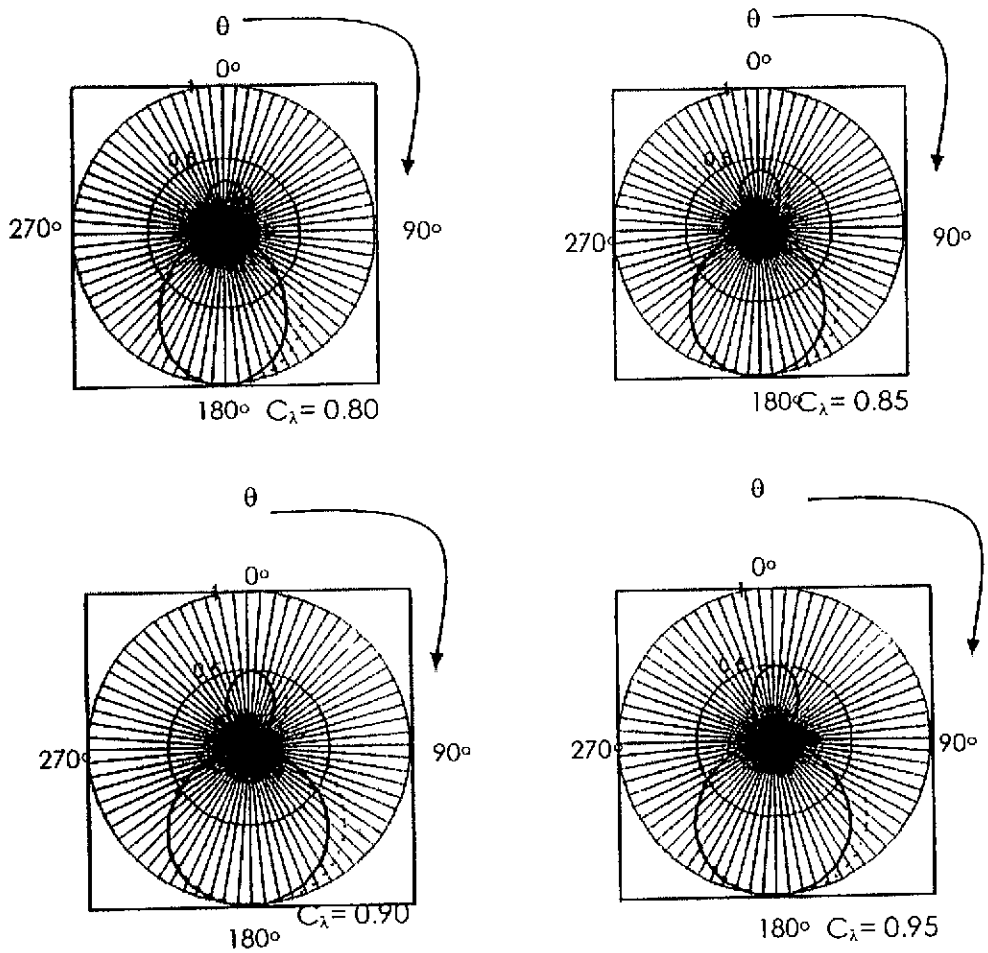

the group velocity is directed away from the feed-point. In other words, we may conclude that the circular helix fed without a ground plane structure belongs to the class of backfire antennas; and may thus, find practical applications as a feed for the paraboloidal dish used in satellite communications [12]. This scenario is schematically illustrated in figure 5.

Figure 4.3: *Normalized field patterns of a circular helix fed without a ground plane $\alpha = 15°$ and C_λ : 0.80 - 0.95*
——— E_θ component - - - - - E_φ component

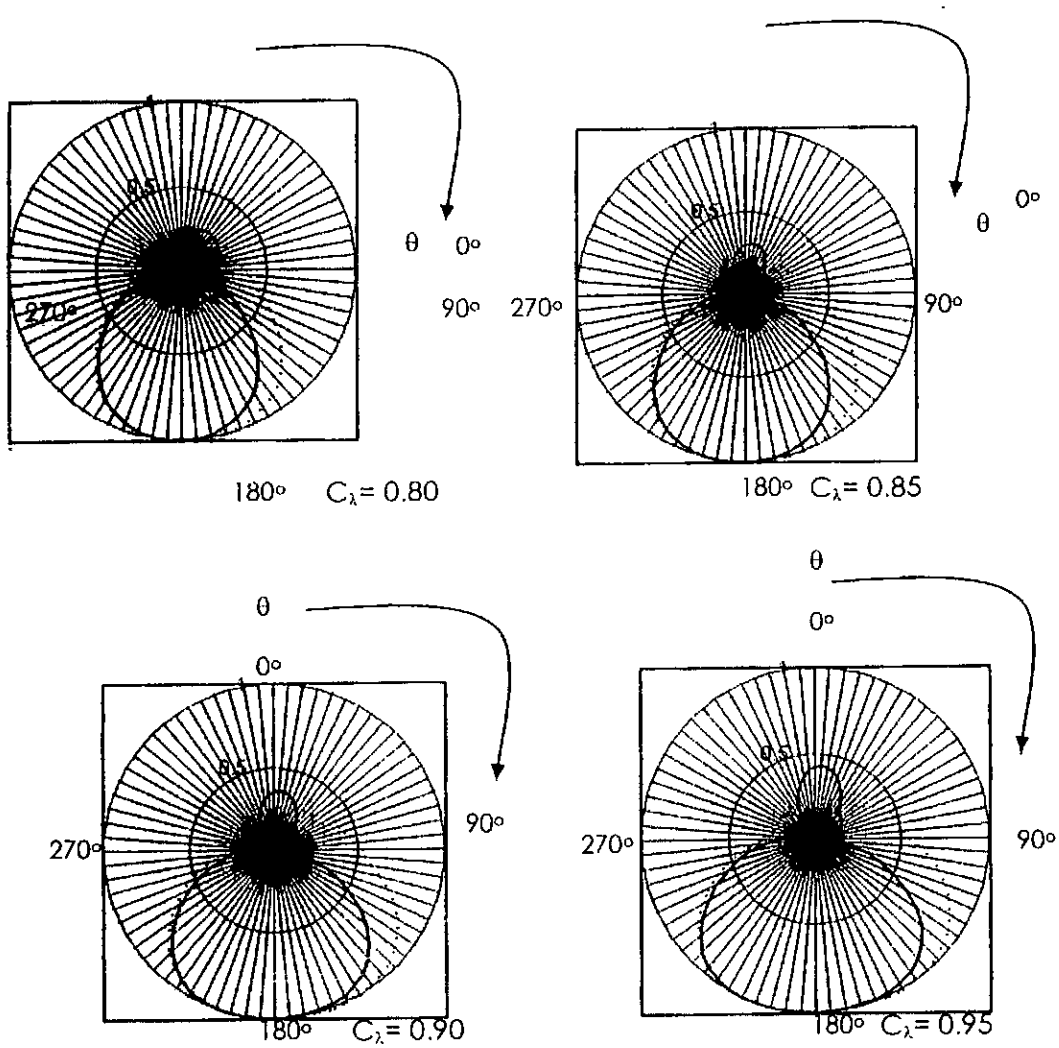

Figure 5: *A circular helix without a ground plane as a feed-element for a satellite dish.*

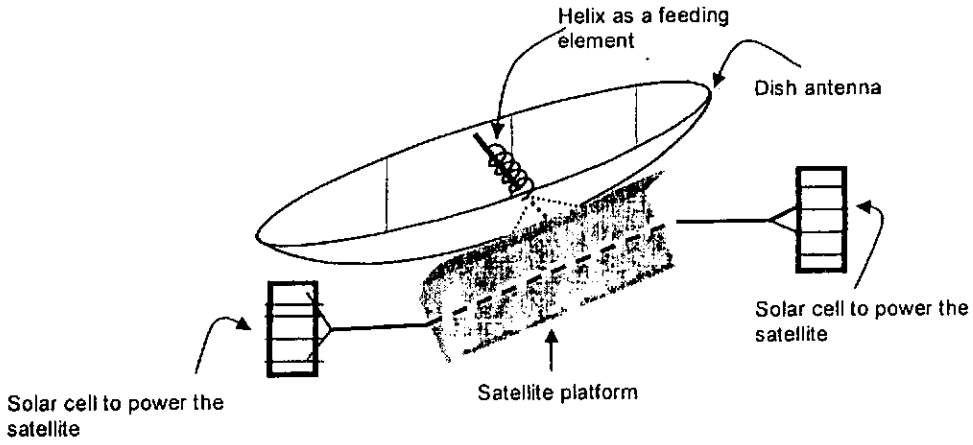

5. Concluding Remarks

A systematic derivation of the integro-differential equation as model for the electromagnetic behaviour of an elliptical helix antenna has been presented in this paper. After specializing the general analytical results to the case of the circular helix, a solution to the problem thus formulated was obtained through the use of the method of moments procedure. Representative numerical results for an approximate generalized current distribution along the helical arm as well as the associated far-zone electromagnetic fields were displayed in graphical formats, with important highlights identified and briefly discussed. As an illustrative example of the application of the derivation, the radiation characteristics of a circular helix excited without the conventional ground plane was investigated, and the results obtained indicate the possible use of the antenna as a feed for paraboloidal-dish.

References

[1] Harrington, R.F., **(1968)**: "*Field computation by moment methods*," The Macmillian Book Company, New York, 125pp.

[2] Kraus, J.D., and Williamson, J.C.,**(1948)**: "*Characteristics of helical antenna radiating in the axial mode*," Jour. Appl. Phys., Jan., vol. 19, pp. 87 - 96.

[3] Kornhauser, E.T. **(1951)**: "*Radiation field of helical antennas with sinusoidal current*," Jour. Appl. Phys., Jul., vol.22, No.7, pp. 887-891.

[4] Knudsen, H.L. **(1952)**: "*Radiation field of a square, helical beam antenna*," Jour. App. Phys., Apr., vol. 23, No.4, pp. 483-491.

[5] Nakano, H., Samada, Y., and Yamauchi, J. **(1986)**: "*Axial mode helical antennas*," IEEE Trans. Ant. & Prop., vol. 34, No.9, pp. 1143-1148.

[6] Nakano, H., Yamane, T., and Yamauchi, J., **(1983)**: "*Directive properties of parasitic helix and its application to circularly polarized antenna*," IEE Proc. Microw. Ant. & Prop., vol.130, No. 6, pp. 391-396.

[7] Nakano, H., and Yamauchi, J. **(1982)**: "*Characteristics of modified spiral and helical antennas*," IEE Proc. Microw. Ant. & Prop., vol.129, No. 5, pp. 232-237.

[8] Harrington, R.F. **(1967)**: "*Matrix methods for field problems*," Proc. IEEE, vol. 55, pp.136-149.

[9] Nakano, H., Yamauchi, J., and Mimaki, H. **(1988)**: "*Backfire radiation from a monofilar helix with a small ground plane*," IEEE Trans. Ant. & Prop., vol.36, No.10, pp. 1359-1364.

[10] Adekola, S.A., Mowete, A.I., and Ayorinde, A.A., **(2001)**: "*Exclusion of ground planes in thin-wire helical antennas*," JER, vol. 9, Nos. 3&4, pp. 13-28.

[11] Walter, C.H., **(1970)**: "*Traveling wave antennas*," Dover, New York, pp. 331-333.

[12] King, H.E., and Wong., J.L., **(1977)**: "*240-400 MHz antenna system for the Fleet-SatCom satellites*," IEEE Int'l Symposium on Antennas and Propagation, Stanford University, Stanford, California, U.S.A., June 20 - 22, AP-S Session 12, 1000, Tuesday June 21, 1977, pp. 349-352.

[13] Abramowitz, Milton, and Stegun, Irene, A. Eds.**(1970)**: " *Hand book of mathematical functions*", National Bureau of Standards, Washington, USA. November, 1970.

APPENDIX I(b):

ANALYSIS OF HELICAL-BEAM ANTENNAS BACKED BY CO-AXIAL PARASITIC LOOPS

Analysis of Helical-Beam Antennas Backed by Co-axial Parasitic Loops

S.A. Adekola, A.I. Mowete and A.A. Ayorinde
Communications Group
Department of Electrical and Electronics Engineering
University of Lagos, Akoka, Lagos.

Abstract

This paper investigates the radiation characteristics of helical-beam antennas backed by an array of three, co-axial parasitic circular loops – the implementation of which is of dire importance when such helical antennas are not made of copper but of high-temperature super-conducting materials which may be impractical to mount on a conventional ground plane serving as a counterpoise. Numerical modeling adopted is through the rigorous method of moments. Feeding at the lower end of the helix is achieved using 1-volt delta-gap generator. It is shown that the current distributions on the helical antenna consist of two distinct regimes - an exponentially decaying domain followed by a surface wave region. Ripples appearing in the surface wave region are attributable to multiple reflections from the open end of the helix. Fields radiated are circularly polarized with an axial ratio of less than 3dB. It is, therefore, established that co-axial parasitic loops constitute effective reflectors for monofilar helix.

1. Introduction

Helical-beam antennas, commonly employed for satellite communications because they radiate circularly polarized waves which are less adversely affected by variations in atmospheric conditions, are traditionally excited by a combination of a coaxial cable and a large groundplane as first demonstrated by Kraus [1]. Apart from serving as a counterpoise for the antenna, the groundplane also reflects the electromagnetic radiation in the backfire direction, and prevents the flow of current to the outer conductor of the coaxial cable feeding the antenna [2]. Other backing structures that have been utilized with acceptable degree of success in the feeding arrangements of axial-mode helical antennas include the conical cavity [3] and uniform cavity [4]. Modelling the conical cavity by wire grids, Nakano and Minaki [5] numerically determined the radiation characteristics of a short monofilar helix placed inside the cavity.

The cumbersome nature of the large groundplane and other supporting structures motivated Kraus [6] to propose their replacements by parasitic circular loops, thereby promoting pole-mounting applications of the antenna. As a demonstration of the satisfactory performance of the loops-backed helix,

Kraus [6] reported an experimentally measured radiation pattern of a 10-turn monofilar helix with three coaxial loops in its feeding mechanism. It is worth remarking that an axial-mode helical antenna backed by one circular loop which has been successfully deployed for the Mars Observer Experiment, has been reported in the literature [7]. Theoretically, Abd-Alhameed and Excell [8], via the method of moments approach, comprehensively studied a parasitic normal-mode helix coaxially positioned inside a circular loop antenna, which can be readily physically realized with high-temperature super-conducting materials.

Motivated by the important practical applications of helical antennas radiating in the presence of circular loops and the recognition that high-temperature super-conductor helical antennas are preferably backed by circular loops rather than by conventional groundplanes, this paper investigates both the current distributions and radiation properties of an axial-mode helical antenna excited by an array of three parasitically coupled circular loops. Also addressed is the determination of the electrical circumference of the loops when considered as effective reflectors for the antenna. The method of moments technique is adopted, as usual, for the numerical solution of the loops-backed helix problem, in which a 1-volt delta-gap source is connected to the lower end of the helix. Remarkably, the generalized matrix equation formulated for the problem fully accounts for the electromagnetic interactions between the helix and the loops. The numerical results generated here show that the current distribution on the loops-backed helix consists of an exponentially decaying part and a surface wave component, and the electromagnetic fields radiated are circularly polarized with an axial ratio of less than 3dB in the frequency band 1.6GHz – 2.7GHz considered.

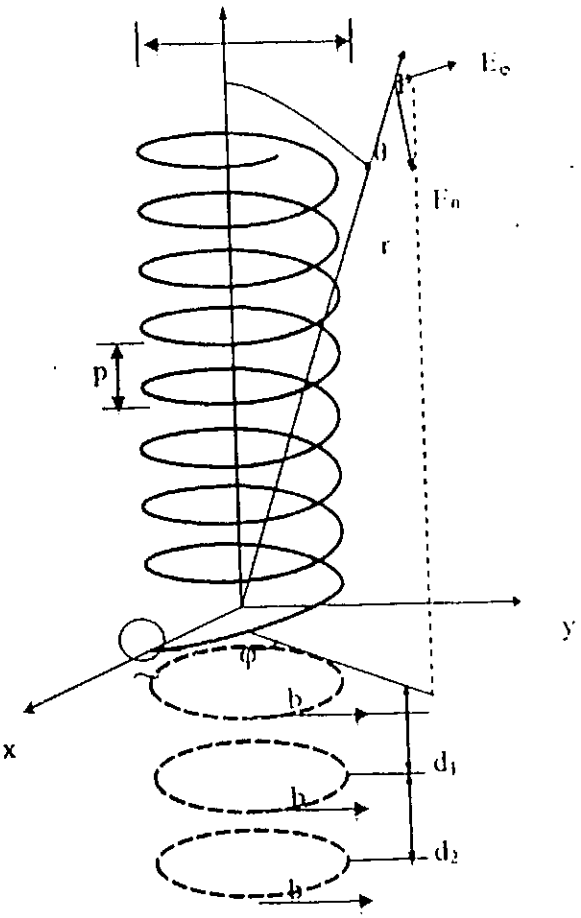

Figure 1: Geometry of a monofilar helix backed by three parasitic circular loops.

2. Generalized Matrix Equations

Figure 1 depicts the geometry of the radiation problem of a monofilar helix backed by an array of three parasitic circular loops, where the symbol a denotes the helix radius, b loop radius, p ($= 2\pi a \tan\alpha$) turn-to-turn distance, α pitch angle, d_1 the separation between the first and the second loops, and d_2 the separation between the second loop and the third loop. It is assumed, *ab initio*, that the helix and the loops are constructed with electrically thin and perfectly conducting wires. Employing the method of moments procedure for the determination of currents on the helix and the loops, we first define the linear integrodifferential operators for the helix and the loops connecting the tangential component of the incident electric field and the resulting axial current. And subsequently we account for the mutual electromagnetic interactions between the

helix and the loops, and between the loops in the generalized impedance matrix of the loops-backed helix through the mutual impedance sub-matrices. Starting with the helix, its governing operator equation may be expressed as Adekola *et al.* [14]:

$$E'_{\varphi} = L^{h}[I_{\varphi}] \qquad (1a)$$

where the linear operator L[*] admits the representation:

$$L^{h}[*] = \int_{0}^{2\pi N}\left\{ j\omega\mu_{o}a[\cos\alpha\cos(\varphi-\varphi') + \tan\alpha\sin\alpha][*] - \frac{1}{j\omega\varepsilon_{o}a\sec\alpha}\frac{d[*]}{d\varphi'}\frac{d}{d\varphi}\right\}\frac{\exp(-jk_{o}R)}{4\pi R}d\varphi'$$

provided R, which is the distance between a point on the wire axis and a point on the wire surface, mathematically takes the form

$$R = a\sqrt{\left(\frac{\rho}{a}\right)^{2} + 4\sin^{2}\left(\frac{\varphi-\varphi'}{2}\right) + \tan^{2}\alpha(\varphi-\varphi')} \qquad (1c)$$

In equations (1a) - (1c), E'_{φ} stands for the tangential component of the incident electric field, I_{φ} the induced axial current on the helical wire, (ε_o, μ_o, k_o) stand for free-space permittivity, free-space permeability, and free-space phase constant, respectively, N the number of helix turns, $j=\sqrt{-1}$, and ρ represents the wire radius. As usual, source quantities are primed entities, while field quantities are unprimed. Of course, the relevant linear operator for the circular loop, L^{c}, may be deduced from eqn. (1b) by setting α to zero and N to 1, which leads to

$$L^{c}[*] = \int_{0}^{2\pi}\left\{ j\omega\mu_{o}a\cos(\varphi-\varphi')[*] - \frac{1}{j\omega\varepsilon_{o}a}\frac{d[*]}{d\varphi'}\frac{d}{d\varphi}\right\}\frac{\exp(-jk_{o}R)}{4\pi R}d\varphi' \qquad (2a)$$

provided R is now given by

$$R = a\sqrt{\left(\frac{\rho}{a}\right)^{2} + 4\sin^{2}\left(\frac{\varphi-\varphi'}{2}\right)} \qquad (2b)$$

upon substituting $\alpha = 0$ and N = 1 in eqn. (1c). For the veracity of the present formulation, it is worth pointing out that eqns. (2a) and (2b) are in full agreement with previous results of Harrington [9]. Next, we discretize the helix and loop wires, and define the current expansion (or basis) functions T along the wire centreline, and the weighting (or testing) functions W along the wire surface. Here, both expansion and weighting functions are triangles defined over four consecutive segments of each wire. When the subscripts (m,n) are used for the monofilar helix quantities, (p, q) the first loop, (i, j) the second loop, and (u, v)

the third loop, where m, n=1, ...L, and p, q, i, j, u, v=1, ...K, the generalized matrix equation for the loops backed helix geometry may be written as:

$$\begin{bmatrix} <W_m, E_\varphi^i> \\ <W_p, E_\varphi^i> \\ <W_i, E_\varphi^i> \\ <W_u, E_\varphi^i> \end{bmatrix} = \begin{bmatrix} <W_m, L^h[T_n]> & <W_m, L^l[T_q]> & <W_m, L^l[T_j]> & <W_m, L^l[T_v]> \\ <W_p, L^h[T_n]> & <W_p, L^l[T_q]> & <W_p, L^l[T_j]> & <W_p, L^l[T_v]> \\ <W_i, L^h[T_n]> & <W_i, L^l[T_q]> & <W_i, L^l[T_j]> & <W_i, L^l[T_v]> \\ <W_u, L^h[T_n]> & <W_u, L^l[T_q]> & <W_u, L^l[T_j]> & <W_u, L^l[T_v]> \end{bmatrix} \begin{bmatrix} \alpha_n \\ \alpha_q \\ \alpha_j \\ \alpha_v \end{bmatrix} \quad (3)$$

provided the quantity <*, *> is the inner product of two tangential vectors, and α's are the unknown current superposition coefficients. Exploiting the generalized network parameters [10], equation (3) may be recast in a compact form:

$$\begin{bmatrix} [V_m] \\ [V_p] \\ [V_i] \\ [V_u] \end{bmatrix} = \begin{bmatrix} [Z_{mn}] & [Z_{mq}] & [Z_{mj}] & [Z_{mv}] \\ [Z_{pn}] & [Z_{pq}] & [Z_{pj}] & [Z_{pv}] \\ [Z_{in}] & [Z_{iq}] & [Z_{ij}] & [Z_{iv}] \\ [Z_{un}] & [Z_{uq}] & [Z_{uj}] & [Z_{uv}] \end{bmatrix} \begin{bmatrix} [I_n] \\ [I_q] \\ [I_j] \\ [I_v] \end{bmatrix} \quad (4)$$

where V's are the generalized voltages, Z's generalized impedances and I's generalized currents. The impedance submatrices of eqn. (4) may be physically interpreted as follows: $[Z_{nn}]$ is the self-impedance submatrix of an isolated monofilar helix; $[Z_{pq}]$ is the self-impedance submatrix of the first loop; $[Z_{ij}]$the self impedance submatrix of the second loop; and $[Z_{uv}]$ the self-impedance submatrix of the third loop. Moreover, $[Z_{mq}]$ denotes the mutual impedance submatrix of the helix and the first loop; $[Z_{mj}]$ the mutual impedance submatrix of the helix and the second loop; $[Z_{mv}]$ the mutual impedance submatrix of the helix and the third loop; $[Z_{pq}]$ the mutual impedance submatrix of the first loop and the second loop; $[Z_{pv}]$ the mutual impedance submatrix of the second loop and the third loop. Other impedance submatrices can be explained in the same manner. On the other hand, the current submatrices $[I_n]$, $[I_q]$, $[I_j]$ and $[I_v]$ represent the unknown current expansion coefficients of the helix, first, second, and third loops, respectively. Because the loops are parasitic, it follows that the entries of the voltage submatrices $[V_p]$, $[V_i]$, and $[V_u]$ are identically zero, and $[V_m]$ is the excitation voltage submatrix of the monofilar helix fed by a 1-volt delta-gap source at its lower end. Through the process of matrix inversion and multiplication on eqn. (4), the desired currents on the elements of the antenna system are obtained. In what follows, the expressions of the electric fields radiated by the loops-backed helical antenna are presented.

3. Electric Fields

Essentially, the total electric field radiated by the loops-backed helix is the superposition of the fields from the monofilar helix as well as all the three loops. Using the currents calculated from eqn. (4), the $E_\theta(\theta,\varphi)$ and $E_\varphi(\theta,\varphi)$ components of the electric field are given by Adekola [11] and Adekola *et al* [14]:

$$
\begin{aligned}
E_\theta(\theta,\varphi) = {} & \frac{-j\omega\mu_o a e^{-jk_o r}\cos\theta}{4\pi r}\int_0^{2\pi N}[\sin(\varphi-\varphi') - \tan\theta\tan\alpha]I_n(\varphi')e^{jk_o a(\sin\theta\cos(\varphi-\varphi')+(\tan\alpha\cos\theta)\varphi')}d\varphi' \\
& \frac{-j\omega\mu_o b e^{-jk_o r}\cos\theta}{4\pi r}\int_0^{2\pi}[\sin(\varphi-\varphi')][I_q(\varphi')]e^{jk_o b\sin\theta\cos(\varphi-\varphi')}d\varphi' \\
& \frac{-j\omega\mu_o b e^{-jk_o r}\cos\theta}{4\pi r}\int_0^{2\pi}[\sin(\varphi-\varphi')][I_l(\varphi')e^{jk_o(b\sin\theta\cos(\varphi-\varphi')+d_1\cos\theta)}d\varphi' \\
& \frac{-j\omega\mu_o b e^{-jk_o r}\cos\theta}{4\pi r}\int_0^{2\pi}[\sin(\varphi-\varphi')][I_s(\varphi')]e^{jk_o(b\sin\theta\cos(\varphi-\varphi')+(d_1+d_2)\cos\theta)}d\varphi'
\end{aligned}
\tag{5a}
$$

and

$$
\begin{aligned}
E_\varphi(\theta,\varphi) = {} & \frac{-j\omega\mu_o a e^{-jk_o r}}{4\pi r}\int_0^{2\pi N}[\cos(\varphi-\varphi')]I_n(\varphi')e^{jk_o a(\sin\theta\cos(\varphi-\varphi')+(\tan\alpha\cos\theta)\varphi')}d\varphi' \\
& \frac{-j\omega\mu_o b e^{-jk_o r}}{4\pi r}\int_0^{2\pi}[\cos(\varphi-\varphi')][I_q(\varphi')]e^{jk_o b\sin\theta\cos(\varphi-\varphi')}d\varphi' \\
& \frac{-j\omega\mu_o b e^{-jk_o r}}{4\pi r}\int_0^{2\pi}[\cos(\varphi-\varphi')][I_l(\varphi')e^{jk_o(b\sin\theta\cos(\varphi-\varphi')+d_1\cos\theta)}d\varphi' \\
& \frac{-j\omega\mu_o b e^{-jk_o r}}{4\pi r}\int_0^{2\pi}[\cos(\varphi-\varphi')][I_s(\varphi')]e^{jk_o(b\sin\theta\cos(\varphi-\varphi')+(d_1+d_2)\cos\theta)}d\varphi'
\end{aligned}
\tag{5b}
$$

where the symbol N again designates the number of helix turns. On the recognition that the helix and loop wires have been discretized, the integrals featuring in eqns. (5a) and (5b) are changed to summations accordingly. Thus, the discretized versions of eqns. (5a) and (5b) are:

$$
\begin{aligned}
E_\theta(\theta,\varphi) = {} & \frac{-j\omega\mu_o a e^{-jk_o r}\cos\theta}{4\pi r}\sum_{n=1}^{L}[\sin(\varphi-\varphi'_n)-\tan\theta\tan\alpha][I_n(\varphi'_n)]e^{j\,[illegible]}\Delta\varphi'_n \\
& \frac{-j\omega\mu_o b e^{-jk_o r}\cos\theta}{4\pi r}\sum_{q=1}^{K}[\sin(\varphi-\varphi'_q)][I_q(\varphi'_q)]e^{j\,[illegible]}\Delta\varphi'_q \\
& \frac{-j\omega\mu_o b e^{-jk_o r}\cos\theta}{4\pi r}\sum_{i=1}^{K}[\sin(\varphi-\varphi'_i)][I_i(\varphi'_i)]e^{j\,[illegible]}\Delta\varphi' \\
& \frac{-j\omega\mu_o b e^{-jk_o r}\cos\theta}{4\pi r}\sum_{v=1}^{K}[\sin(\varphi-\varphi'_v)][I_v(\varphi')]e^{j\,(b\sin\theta\cos\varphi\,e^{-j(d_1+d_2)\cos\theta})}\Delta\varphi'
\end{aligned}
\tag{6a}
$$

and

$$
\begin{aligned}
E_\varphi(\theta,\varphi) = {} & \frac{-j\omega\mu_o a e^{-jk_o r}}{4\pi r}\sum_{n=1}^{L}[\cos(\varphi-\varphi'_n)][I_n(\varphi'_n)]e^{j\,[illegible]}\Delta\varphi'_n \\
& \frac{-j\omega\mu_o b e^{-jk_o r}}{4\pi r}\sum_{q=1}^{K}[\cos(\varphi-\varphi'_q)][I_q(\varphi'_q)]e^{j\,(b\sin\theta\cos\varphi\,e^{-j\,[illegible]})}\Delta\varphi'_q \\
& \frac{-j\omega\mu_o b e^{-jk_o r}}{4\pi r}\sum_{i=1}^{K}[\cos(\varphi-\varphi'_i)][I_i(\varphi'_i)]e^{j\,(b\sin\theta\cos\varphi\,e^{-j(d_1\cos\theta)})}\Delta\varphi'_i \\
& \frac{-j\omega\mu_o b e^{-jk_o r}}{4\pi r}\sum_{v=1}^{K}[\cos(\varphi-\varphi'_v)][I_v(\varphi'_v)]e^{j\,(b\sin\theta\cos\varphi\,e^{-j(d_1+d_2)\cos\theta})}\Delta\varphi'_v
\end{aligned}
\tag{6b}
$$

In the ensuing section, numerical results of current distributions obtained from the solution of eqn. (4) and the electric fields computed from eqns. (6a) and (6b) are graphically presented and discussed.

4. Discussion of Numerical Results

In the computer simulations of the loops-backed helix problem, we utilize the following geometrical parameters in the FORTRAN 77 Program developed for the problem:

Number of helix turns: 8

Number of parasitic loops: 3

Helix pitch angle (α): 12°

Separation between first loop and second loop (d_1): 0.5λ (λ: wavelength)

Separation between second loop and third loop (d_2): 0.5λ

Helix radius = loop radius: $.127\lambda$, 0.215λ

Helix circumference: 0.8λ - 1.35λ.

The centre frequency of operation is fixed at 2GHz (λ = 0.15m), and the monofilar helix is excited at the lower end by a 1-volt delta-gap generator as explained earlier. We start with the discussion of current distributions on the helical arm.

4.1 Current Distributions

Although the solution of equation (4) yields the current distributions on the monofilar helix as well as on the parasitic loops, only the currents on the helical arm, which are of primary interest here, are given consideration. These currents computed here, are graphically illustrated in Figures 2a-2c. It is noted that when the electrical circumference of the helix denoted by C_λ, ranges between 0.80 and 0.90, the current distributions on the helical arm are essentially an exponential decaying waves with moderate reflections from the open end as a result of small ripples visible at that end

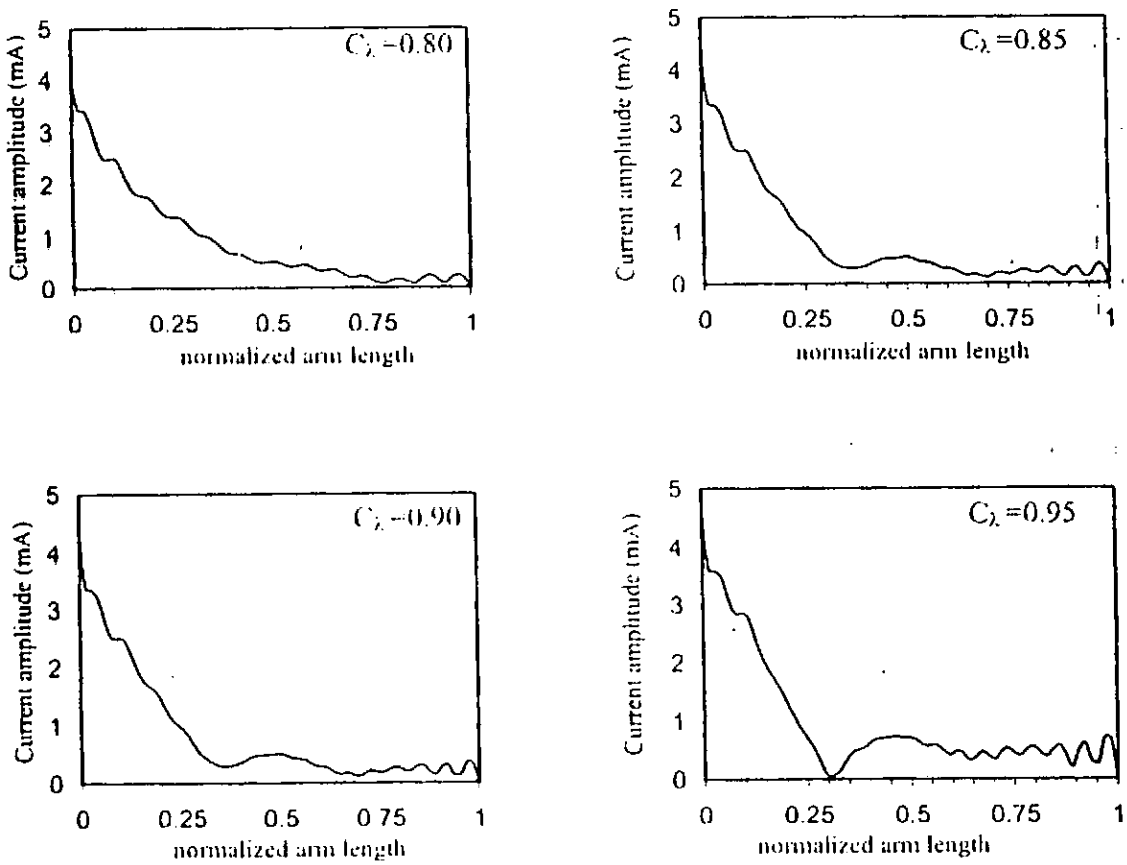

Figure 2a: Current distributions on the helical arm when C_λ ranges from 0.80 -- 0.95 and $\alpha = 12^o$.

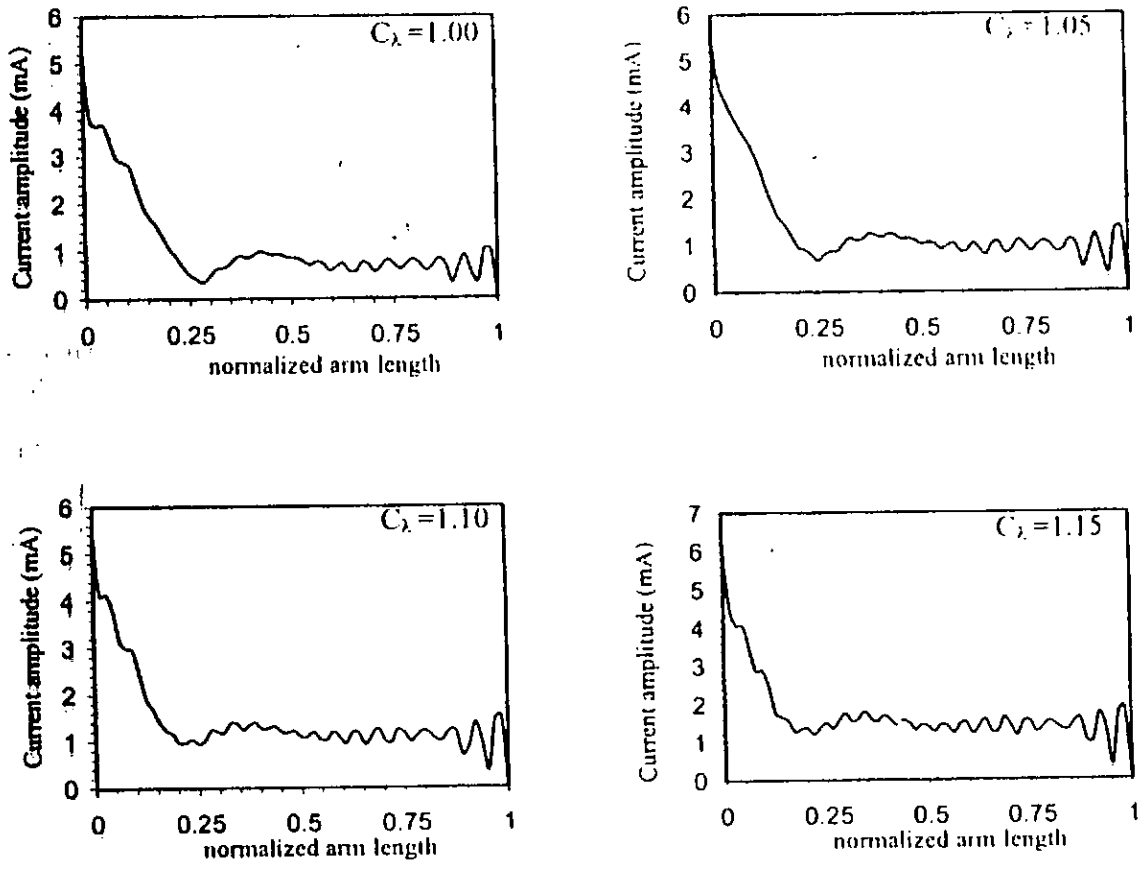

Figure 2b: Current distributions on the helical arm when C_λ ranges from 1.00 – 1.15 and $\alpha = 12^o$.

Within the aforementioned range of C_λ, the current magnitude at the feedpoint remains almost constant. Beyond $C_\lambda = 0.90$, the current distributions on the helix are typified by two distinct components, viz., an exponentially decaying regime and a surface wave region. Initially, the former regime exists from the feedpoint to about a quarter of the arm length, but as C_λ increases, the region reduces in length. Conversely, the latter component extends over three quarters of the helical arm for the band identified as $0.95 \leq C_\lambda \leq 1.00$, and shifts towards the feed point as C_λ assumes higher values. It is noteworthy that as C_λ increases, the current magnitude at the feedpoint also increases, but with an attendant multiple reflections from the open end as evidenced by appreciable ripples superimposed on the current waveforms.

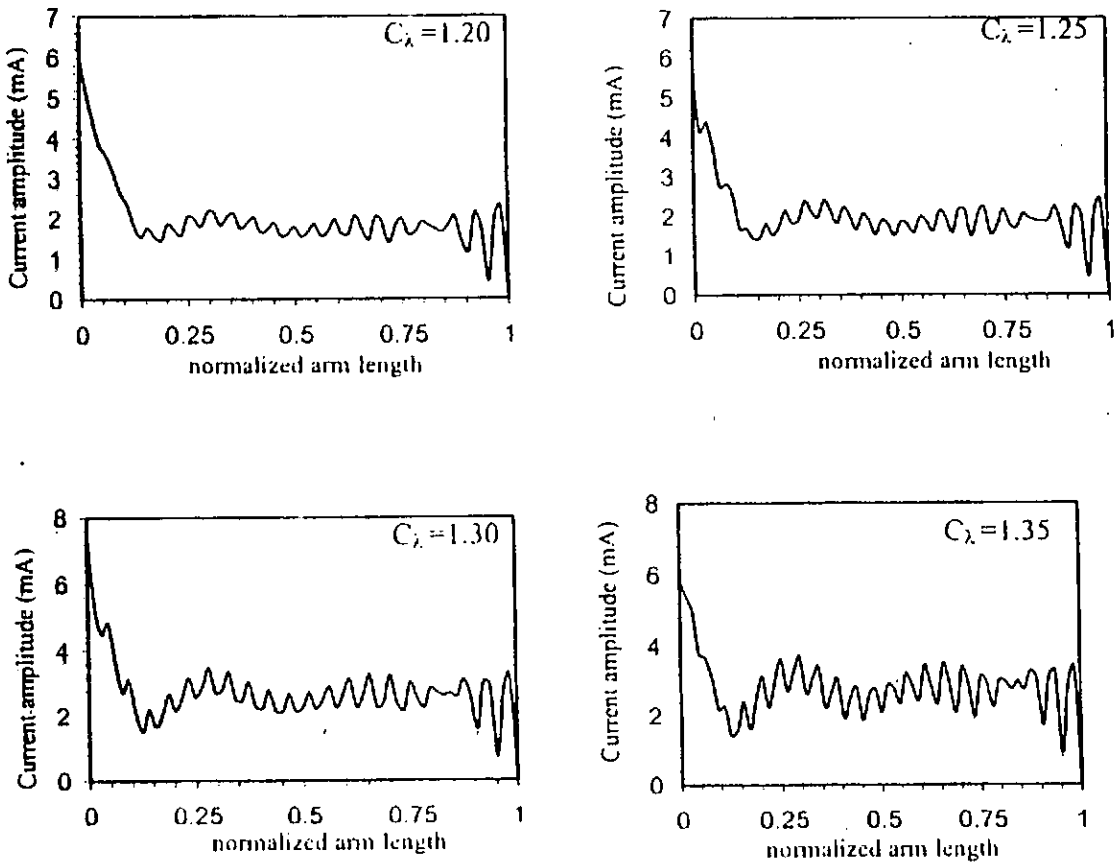

Figure 2c: Current distributions on the helical arm when C_λ ranges from 1.20 – 1.35 and $\alpha = 12°$.

It should be pointed out that when C_λ = 1.35, the surface wave part of the corresponding current is significantly distorted. Remarkably, the current distributions on the loops-backed helix for C_λ greater than 0.9 are analogous to those on the helix backed by an infinite groundplane [12].

4.2 Electric Fields

Portrayed in Figures 3a-3c are the radiated field patterns of the loops-backed helix in the $\varphi = 0°$ plane computed from equations (6a) and (6b) using the current distributions of Figures 2a- 2c, respectively. Solid lines are used for the E_θ component while dashed lines are employed for the E_φ component. An examination of the field patterns reveals the following interesting features. First,

when C_λ assumes numerical values of 0.8, 0.85 and 0.9, the maximum radiation occurs in the backfire direction, i.e. $\theta = 180^0$, as a consequence of the exponential form of the corresponding current distributions [13]. In effect, at the aforestated values of C_λ, the array of parasitic loops cannot be regarded as an effective reflector for the monofilar helix, and the loops-backed helix behaves identically as a helix fed without any backing structures (or counterpoise). Second, when C_λ is greater than 0.9, the radiation from the antenna is concentrated in the axial forward direction ($\theta = 0^0$), except at $C_\lambda = 0.95$ in which the backward radiation appears comparable to the forward radiation. This observation may be attributed to the well-defined exponentially decaying part of the helix current when $C_\lambda = 0.95$ as apparent from Figure 2a. Furthermore, this observation points to the fact that when C_λ is greater than 0.95, the array of parasitic loops constitutes effective reflector for the monofilar helical antenna. The actual cutoff value of C_λ when the loop array acts as an effective reflector, will be determined from the front-to-back ratio profile presented in the next section. Third, although E_θ and E_φ patterns resemble one another, the main lobes of the E_θ patterns are more directive than those of E_φ patterns. Fourth, the principal lobes of both E_θ and E_φ patterns are symmetrical about $\theta = 0^0$ which coincides with the axis of the helix. Fifth, as C_λ increases, the directivity of the radiated field patterns is enhanced but with substantial growth in the sidelobe strengths of the patterns.

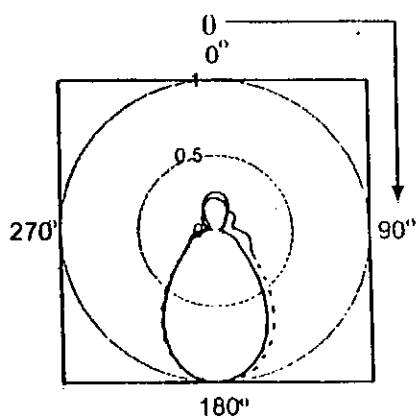

(a) $C_\lambda = 0.80$

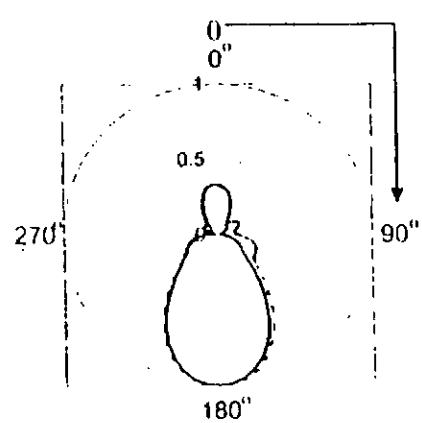

(b) $C_\lambda = 0.85$

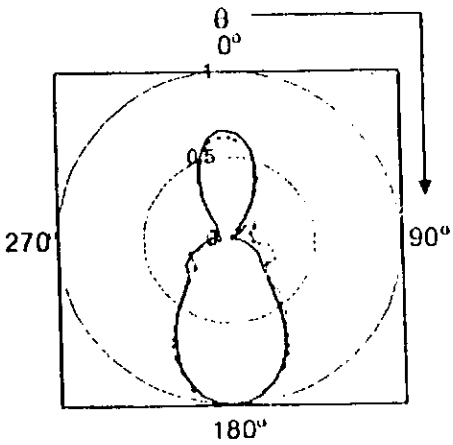

(c) C_λ =0.90

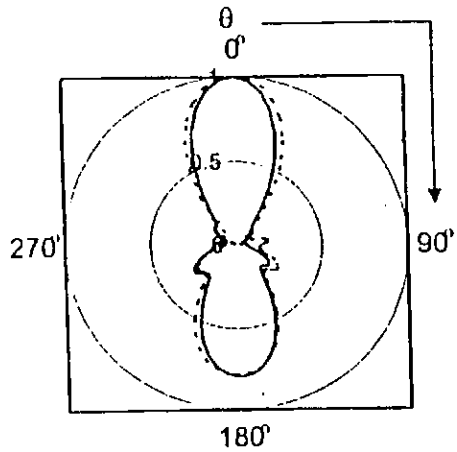

(d) C_λ =0.95

Figure 3a: Electric field components (E_θ and E_φ) on the $\varphi = 0°$ plane when the helix pitch angle (α) is 12°. _____ : E_θ - - - - - - - - - E_φ

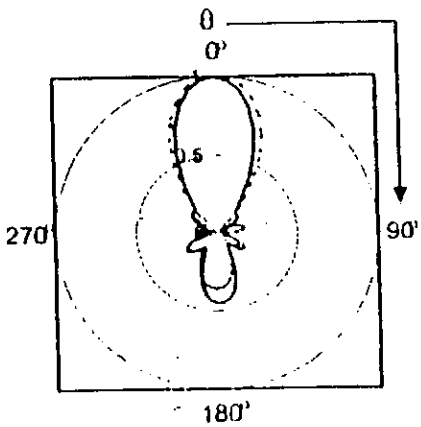

(e) C_λ =1.00

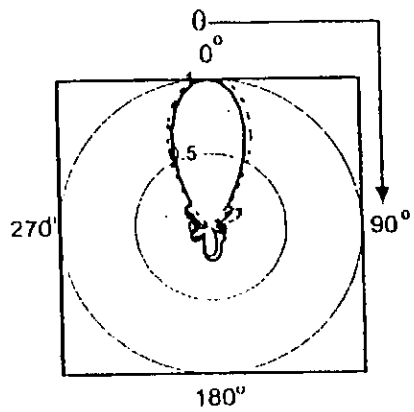

(f) C_λ =1.05

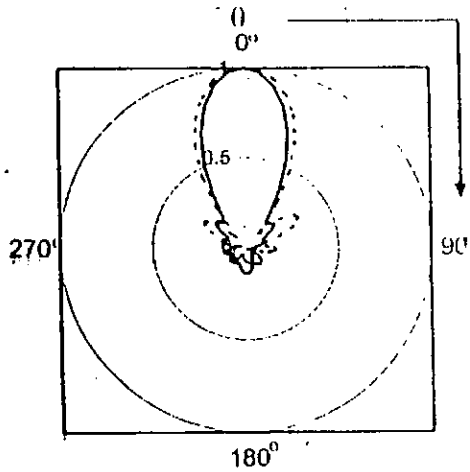

(g) $C_\lambda = 1.10$

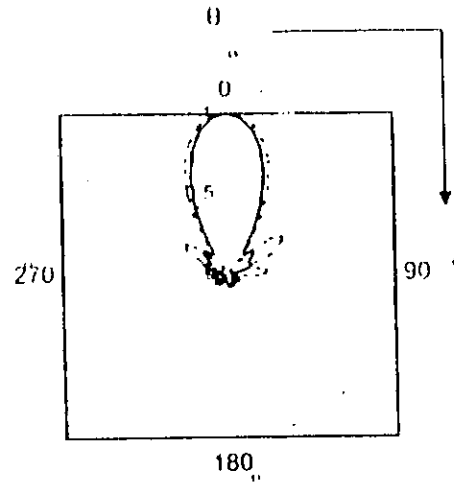

(h) $C_\lambda = 1.15$

Figure 3b: Electric field components (E_θ and E_φ) on the $\varphi = 0°$ plane when the helix pitch angle (α) is 12°. _____ : E_θ ..... E_φ

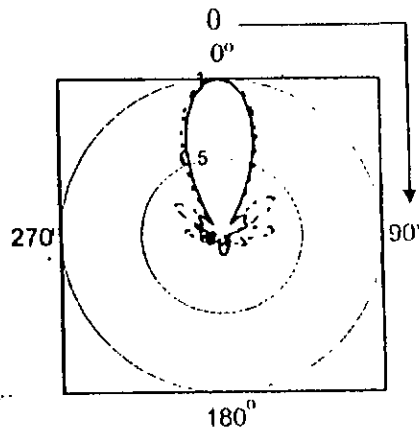

(i) $C_\lambda = 1.20$

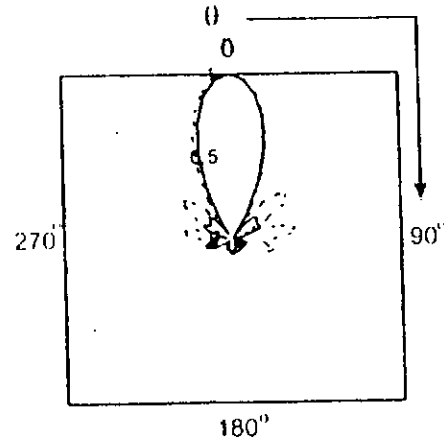

(j) $C_\lambda = 1.25$

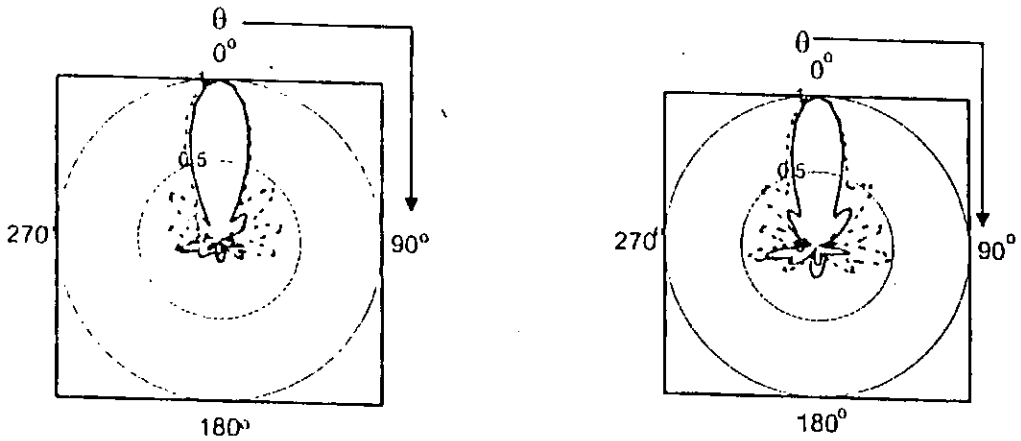

(k) C_λ =1.30 (l) C_λ =1.35

Figure 3c: Electric field components (E_θ and E_φ) on the $\varphi = 0°$ plane when the helix pitch angle (α) is 12°. ————: E_θ ---------- E_φ

4.3 Front-to-back ratio and axial ratio

The front-to-back ratio (F/B), commonly expressed in dB, is a pointer as to whether or not the radiation intensity from an antenna is concentrated in either forward or backward directions. The F/B of the loops-backed helix against C_λ is plotted in Figure 4a. It is seen from the Figure that the F/B has both positive and negative values with a zero value at C_λ = 0.95. The physical meaning of this result is that when C_λ is less than 0.95, the radiation is predominantly in the backward direction, while above 0.95, the radiation is directed principally in the forward direction. It is logical, therefore, to designate C_λ = 0.95 as the cutoff value of the electrical circumference of the helix and the loops at which equal radiation is observed in both forward and backward directions. For design purposes, therefore, the C_λ of the loops must be greater than 0.95 for the loop array to act as an effective reflector which will ensure that the helix radiates in the forward endfire direction. There is a steady increase in the F/B from Figure 4a until C_λ equals 1.15, after which the F/B begins to fall gradually.

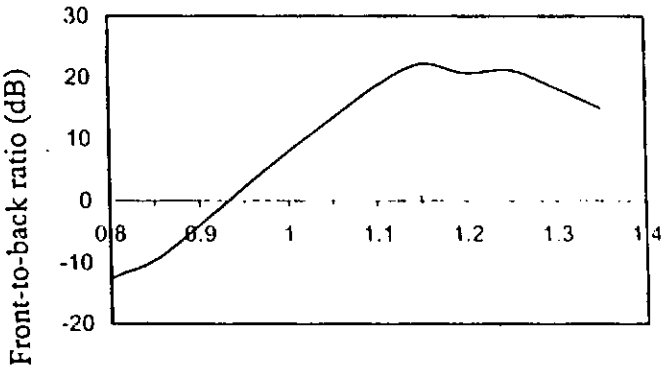

Figure 4a: Front-to-back ratio (dB) versus C_λ

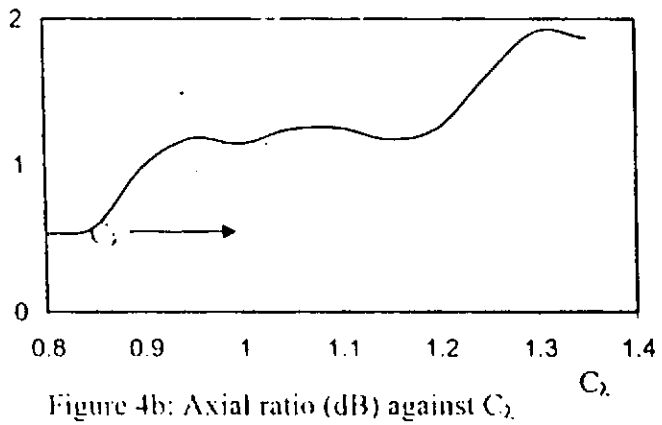

Figure 4b: Axial ratio (dB) against C_λ

Axial ratio (AR) of the radiated fields is a measure of the degree of circular polarization of the fields, and for circularly polarized antennas, the AR must be less than 3dB. Figure 4b shows the axial ratio of the fields from loops-backed helix against C_λ. Generally, the AR is less than 3dB for $0.8 \leq C_\lambda \leq 1.35$ for the 12" helix, suggesting that the helix may find practical applications as circularly polarized antennas.

5. Concluding remarks

This paper has focused attention on the formulation and numerical solution of electromagnetic radiation problem of an axial-mode helical antenna backed by an array of three parasitic loops rather than by the usual groundplane counterpoise. The generalized matrix equation formulated for the loops-backed helix takes into full consideration important mutual electromagnetic interactions of the radiating elements, and the monofilar helix is fed at its lower end by 1-volt delta-gap source. It is demonstrated that the radiation properties of the loops-backed helix are comparable to the helix mounted on a large ground plane, when the electrical circumference of the helix and loops is greater than 0.95 wavelength. In effect, the loop array acts as effective reflector for the monofilar helix when the electrical circumference of the loops is above 0.95 wavelength.

References

1. Kraus, J.D., 1947, "Helical beam antenna," Electronics, Apr., pp. 109-111

2. Markov, G., 1965, "Antennas," Progress Publishers, Moscow, 1st Edition, pp 355-360.

3. Carver, K.R., 1967, "The helicone - a circularly polarized antenna with low sidelobe level." Proc. IEEE, April, p. 559.

4. King, H.E., and Wong, J.L., 1980, "Characteristics of 1 to 8 wavelength uniform helical antennas," IEEE Trans. Ant. & Prop., vol.28, No.2, pp. 291-296.

5. Nakano, H., and Mimaki, H., 1995, "Radiation from a short helical antenna backed by a cavity," Electronics Letters, vol.31, No. 8, pp.602-604.

6. Kraus, J.D, 1995, "A helical-beam antenna without a ground plane," IEEE Ant. & Prop. Magazine, vol.37, No.2, p. 45.

7. www.a new helix antenna design for the mars observer experiment.ht

8. Abd-Alhameed, R.A., and Excell, P.S., 1999, "Analysis of a normal-mode helical antenna including non-uniform wire surface current effects," IEE Proc.-Microw. Ant. & Prop., vol.146, No.1, pp. 1-5.

9. Harrington, R.F., and Mautz, M.S., 1968, "Electromagnetic behaviour of circular wire loops with arbitrary excitation and loading," Proc. IEE, Vol. 115, No.1, pp. 68-77.

10. Harrington, R.F., 1968, "Field computation by moment methods," The Macmillian Book Company, New York, pp. 1-125.

11. Adekola, S.A., 1983, "On the excitation of a circular loop antenna by travelling- and standing-wave current distributions," Int'l Jour. Electronics, U.K., 54, pp. 705-732.

12. Nakano, H., Yamane, T., and Yamauchi, J., 1983, "Directive properties of parasitic helix and its application to circularly polarized antenna," IEE Proc. Microw. Ant. & Prop., vol.130, No. 6, pp. 391-396.

13. Nakano, H., Yamauchi, J., and Mimaki, H., 1988, "Backfire radiation from a monofilar helix with a small ground plane," IEEE Trans. Ant. & Prop., vol.36, No.10, pp. 1359-1364.

14. Adekola, S.A., Mowete, A.I., and Ayorinde, A.A., 2001, "Exclusion of ground planes in thin-wire helical antennas," JER, vol. 9, Nos. 3&4, pp. 13-28.

APPENDIX I(c):

EFFECTS OF CENTRE-EXCITATION ON THE RADIATION MECHANISM OF HELICAL ANTENNAS EMPLOYED IN COMMUNICATION SATELLITES

JER - 8, No. 1 & 2, 1-20 May 2001

Effects of Centre-Excitation on the Radiation Mechanism of Helical Antennas Employed in Communication Satellites

S. Adeniyi Adekola and A. Ayotunde Ayorinde
Department of Electrical & Electronics Engineering
University of Lagos, Akoka - Yaba, Lagos, Nigeria

ABSTRACT

The main objective of this paper is to determine the electrical properties of the helical antenna when excited at its geometrical centre. Results presented suggest that the antenna behaves like a Chireix-coil, 4-lobed-made helix when the helical circumference C_λ in wavelengths and the pitch angle α in degrees, (C_λ, α), assume the respective numerical values of (1.94, 35°) and (2.15, 40°). Also presented, is the interesting profile of the input impedance, which provides an insight into how the electrical properties of the helical antenna behave with change of frequency. The formulation is pivoted on the use of the moment method, with a delta-gap feed, and Galerkin's procedure is utilized for the numerical solution for the unknown approximate generalized current distribution. The results reveal that the current is symmetrically distributed about the feed-point which is consistent with expectations. Computed current distribution re-drafted and displayed in rectangular formats, shows distinct similarities with published data obtained via another analytical technique.

1. INTRODUCTION

Before World War II, the wire helix was only known to be of invaluable engineering utility in travelling-wave tubes where it played the role of a guiding structure for amplifying microwave signals travelling down the tube in a manner depicted in Figure 1. In that configuration, the helix acts as a wave-propagating structure, and makes possible a continuous interaction of a longitudinal electron beam and a radio-frequency wave travelling along it, which enables the amplification of the radio wave [Howard W. Sams & Co., Ref. (14), p. 16-20]. At that time, Engineers and research Scientists never envisaged, that the helix could be of great engineering significance in other applications. Barely two years after the war, precisely in 1947, Kraus [9] fortuitously brought the

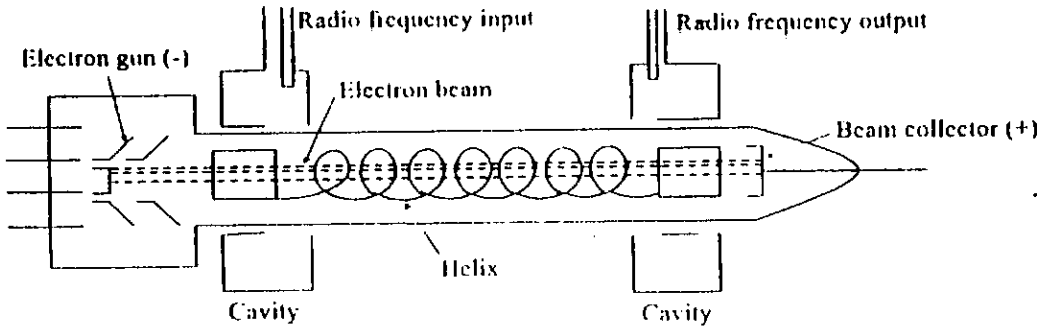

Figure 1: *Travelling-wave tube with helix as a guiding structure* ***(Ref 13, pp. 16-20)***

helix out of the travelling-wave tube to test its applicability as a radiating element in free-space. This led to his invention christened the helical beam antenna. His discovery revolutionized the use of the helix as a radiating element in free space culminating in such practical applications as communication satellites where the helix is mounted in two modes as clearly portrayed in the published works of Kraus (Ref. (4), p.270) and those of King and Wong (Ref. (14), p.351). In the aforementioned references, the helix is employed not only as a versatile transceiver of satellite signals but also as a feeding element for a parabolic dish antenna, on a satellite platform, powered by solar cells.

Extensive use of wireless communication in present-day services associated with reliability, speed and quality of voice-video-data signals, has generated renewed impetus in the study of radiation mechanism of helical antennas. Investigative efforts have focused on applications involving exploratory works on mars and the moon, data-relay satellites as well as global positioning satellites. Indeed, this antenna has found applications in the more recent advent of cellular telephony [Lazzi and Gandhi 1998].

In the aforementioned antenna works, the feeding arrangements and the antenna characteristics emanating therefrom are of particular interest. Whereas linear dipole antennas excited at the centre have enjoyed numerous experimental and analytical investigations reported in the open literature and their radiation characteristics are well documented in standard antenna textbooks, literature on centre-fed helical antennas appears to be very scanty. This dearth of literature on the latter antenna type may be attributed to the fact that the first monofilar helix studied by Kraus (1947), was fed at one of its ends by a coaxial cable in conjunction with a flat ground plane, as the counterpoise. This feeding arrangement has been found suitable for most practical applications, and to a large extent, subsequent research works on helix have been restricted to this mode of feeding. It may be remarked that other feeding arrangements have been devised over the years. As examples, Nakano (1995) reported a helical antenna backed by a cavity, Kraus (1995) proposed loops-backed helical antennas,

while Munk and Peters Jnr. (1968) suggested a feeding arrangement excluding the usual ground plane, for the beam-mode operation of the helical antennas. Other relevant contributions include those of Lee *et al.* (1982) and Nakano *et al* (1980).

Perhaps, the only notable work on a finite balanced helical wire antenna, that is to say, a continuous helical wire excited at the centre, as being proposed in this paper, was by Chen (1967), who employed the Fourier series method to show that the current distribution on a centre-fed helical antenna decays exponentially toward the open end with marked dips at certain points along the helical structure. However, Chen limited his investigations to a restricted current excitation.

Apart from Chen's pioneering work on a finite centre-fed helical antenna, no significant research, either theoretical or experimental, has been reported, to the best of our knowledge, in the open literature. Adopting Chen's choice of dimensions, we investigate, in this paper a centre-fed, 8-turn helical antenna, whose circumference in free-space wavelengths C_λ, and pitch angle α in degrees, are within the ranges $1.1 \le C_\lambda \le 2.15$ and $5^\circ \le \alpha \le 40^\circ$, respectively. This choice of dimensions will facilitate an examination of similarities or dissimilarities of our computed data with those of Chen [2]. In the procedure adopted here, an integro-differential equation for the current distribution along the helical structure is transformed to a straightforward matrix equation using the method of moments, the solution of which is obtained via computer programming. To fill the existing gap in the literature, we then compute the far-fields generated by the current distributions obtained. Other antenna parameters determined here include the input resistance and reactance as well as the total power radiated by the antenna. An excitation voltage of 1 volt is employed for all numerical computations. As a means of checking the validity of our formulation, our computed data are redrafted and displayed in rectangular formats consistent with what obtains in the existing literature [2].

2. GOVERNING EQUATIONS

Figure 2(a) depicts the problem geometry of an 8-turn thin-wire helical antenna excited at the centre by a delta function generator of 1 V, while Figure 2(b) shows the enlarged version of a typical turn of the helix. In the aforementioned figures, the symbols a, b and s represent the helix radius with reference to the helix centreline, wire radius and the pitch of the helix, respectively. It is well-known from basic electromagnetic field theory, that the scattered electric field by any perfectly conducting body in free-space is explicitly determinable from the following equation:

$$E^s = j\omega A - \nabla\phi \tag{1}$$

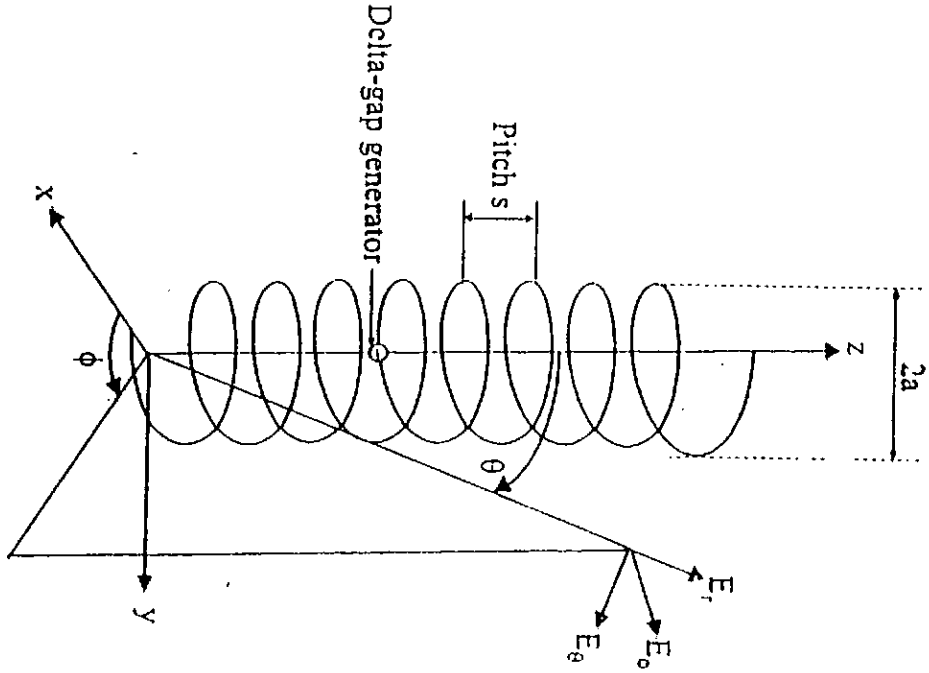

Figure 2(a): *8-turn balanced thin-wire helical antenna*

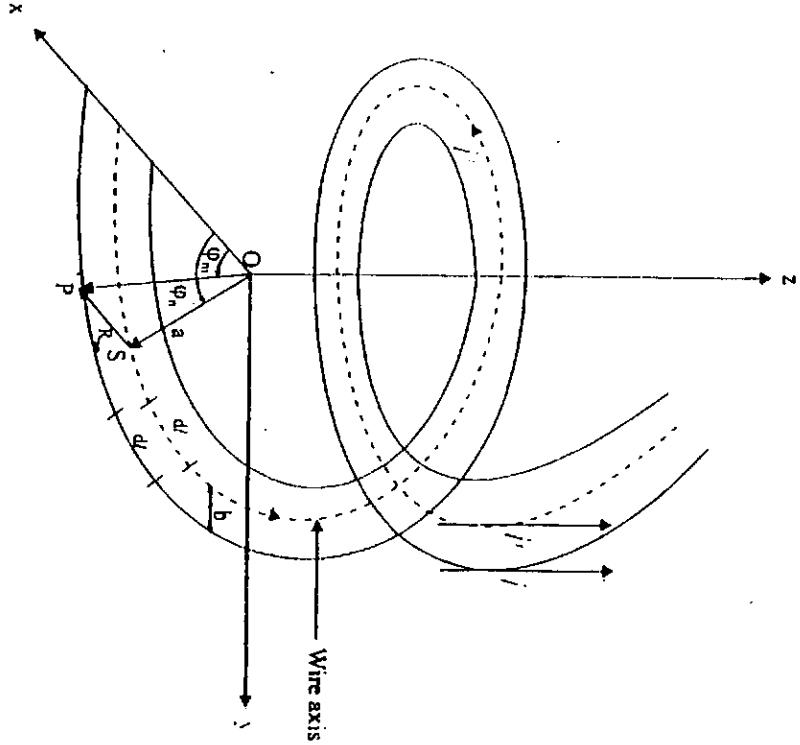

Figure2(b): *A typical turn of the helix depicting the source point* $S(a, \varphi_n, z')$ *observation point* $P(\rho = a + b, \varphi_m, z)$ *and the unit vectors along the helical surface and centreline, respectively*

in which $\underline{E}^s$ represents the scattered field, $\underline{A}$ magnetic vector potential, Φ electric scalar potential, ω the angular frequency, μ_o permeability of free space, $j = \sqrt{-1}$ and ∇ the usual del operator. When use is made of the Lorentz's condition expressed mathematically as

$$\Phi = \frac{-1}{j\omega\varepsilon_0\mu_0}\nabla\cdot\underline{A} \tag{2}$$

equation (1) passes over to

$$\underline{E}^s = -j\omega\underline{A} + \frac{1}{j\omega\varepsilon_0\mu_0}\nabla(\nabla\cdot\underline{A}) \tag{3}$$

where ε_o denotes the permittivity of free-space, and the magnetic vector potential $\underline{A}$ assumes the integral representation:

$$\underline{A} = \frac{\mu_0}{4\pi}\int_{V'} \underline{J}'\frac{\exp(-j\beta_o R)}{R}\,dV' \tag{4}$$

In equation (4), R is the distance from the source point to the field point, $\underline{J}'$ represents the current distribution density, $\beta_o = \sqrt{\mu_o\varepsilon_o}$ stands for the free-space propagation constant.

3. FORMULATION

Because the helix which is of primary interest here is electrically thin, it is legitimate to restrict the total filamentary current $I(\ell')$ to the antenna length. Thus, the thin-wire version of equation (3) can be written explicitly as [Harrington 1968 and Adekola *et al.* 1989]:

$$E_\ell^s = -\int_{\substack{\text{antenna}\\ \text{length}}}\left[j\omega\mu_o I(\ell') - \frac{1}{j\omega\varepsilon_o}\frac{dI(\ell')}{d\ell'}\frac{d}{d\ell}\right]\frac{\exp(-j\beta_o R_{mn})}{4\pi R_{mn}}\,d\ell' \tag{5}$$

where ℓ denotes antenna length variable, $d\ell$ and $d\ell'$ are clearly described in Figure 2(b) and the required integration is carried out along the helix length as indicated. The symbol R_{mn} which appears in equation (5) represents the separation between the source point on the helix centre-line and the observation point on the antenna surface (m: match point index and n: source point index) and is analytically given by:

$$\begin{aligned} R_{mn} &= [b^2 + (\ell_m - \ell_n')^2]^{1/2} \\ &= \left\{b^2 + 4a^2\sin^2\left(\frac{\varphi_m - \varphi_n'}{2}\right) + a^2(\varphi_m - \varphi_n')^2\tan^2\alpha\right\}^{1/2} \end{aligned} \tag{6(a)}$$

where α, the pitch angle, is expressible as

$$\alpha = \tan^{-1}\left(\frac{s}{2\pi a}\right). \qquad (6(b))$$

When the assumption is made that the helix wire is perfectly conducting, the conventional boundary condition on the electric field for wires of infinite conductivity can be imposed, that is,

$$\hat{n} \times (\underline{E}^i_\ell + \underline{E}^s_\ell) = 0 \qquad (7)$$

where $\hat{n}$ is a unit vector normal to the antenna surface and $\underline{E}^i_\ell$ represents the impressed electric field. Introducing equation (5) in equation (7), the following equation readily emerges

$$E^i_\ell = \int_{\substack{\text{antenna}\\ \text{length}}} \left[j\omega\mu_o I(\ell') - \frac{1}{j\omega\varepsilon_o}\frac{dI(\ell')}{d\ell'}\frac{d}{d\ell}\right] \frac{\exp(-j\beta_o R_{mn})}{4\pi R_{mn}}\, d\ell' \qquad (8)$$

which has $I(\ell')$, the current distribution, as the only unknown quantity. This integro-differential equation for the approximate generalized current distribution will now be solved by the method of moments.

As it is customary with the method of moments procedure, the helix structure is first subdivided into short segments and the filamentary current $I(\ell')$ flowing along the wire axis, is then expanded using the triangle functions symbolized by T_n's, which are linearly independent, as follows:

$$I(\ell') = \sum c_n T_n(\ell') \qquad (9)$$

where c_n's are the unknown complex coefficients to be determined. In this formulation, each triangle function is defined over four short segments of the helix in the following manner:

$$T_n(\ell') = \begin{cases} \dfrac{\ell' - \ell'_{2n-1}}{\ell'_{2n+1} - \ell'_{2n-1}} & , \ell'_{2n-1} \le \ell' \le \ell'_{2n+1} \\[2ex] \dfrac{\ell'_{2n+3} - \ell'}{\ell'_{2n+3} - \ell'_{2n+1}} & , \ell'_{2n+1} \le \ell' \le \ell'_{2n+3} \\[2ex] 0 & , \text{elsewhere} \end{cases} \qquad (10)$$

Because of the inherent computational efficiency associated with the Galerkin approach, we adopt it here, and therefore construct the weighting functions $G_m(\ell)$, defined on a contour on the wire surface parallel to the axis of the helix wire, and identical to the expansion functions. In this connection, $G_m(\ell)$ admits the representation

$$G_m(\ell) = \begin{cases} \dfrac{\ell - \ell_{2m-1}}{\ell_{2m+1} - \ell_{2m-1}} & , \ell_{2m-1} \le \ell \le \ell_{2m+1} \\ \dfrac{\ell_{2m+3} - \ell}{\ell_{2m+3} - \ell_{2m+1}} & , \ell_{2m+1} \le \ell \le \ell_{2m+3} \\ 0 & , \text{elsewhere} \end{cases} \tag{11}$$

Substituting equation (9) in equation (8) and taking the inner product of the resulting expression with the weighting function $G_m(\ell)$, the integro-differential equation readily reduces to

$$\int_m G_m(\ell) E_t^i d\ell = \sum_n \alpha_n \iint_{m\,n} \left[j\omega\mu_o G_m(\ell) T_n(\ell') - \frac{1}{j\omega\varepsilon_o} \frac{dT_n(\ell')}{d\ell'} \times \frac{dG_m(\ell)}{d\ell} \right] \frac{\exp(-j\beta_o R_{mn})}{4\pi R_{mn}} d\ell' d\ell. \tag{12}$$

When we compare equation (12) with the generalized network equation given as

$$[V_m] = [Z_{mn}] [I_n] \tag{13}$$

which connects the generalised voltage matrix $[V_m]$ with the product of the generalized impedance matrix $[Z_{mn}]$ and the generalized current matrix $[I_n]$, and if $[\bullet]^{-1}$ stands for the matrix inversion notation, then we have

$$[I_n] = [Z_{mn}]^{-1} [V_m] \tag{14}$$

where

$$
\left.
\begin{aligned}
[V_m] &= \int_m G_m(\ell)\, E_\ell^i \, d\ell, \\
[I_n] &= [\alpha_n], \\
[Z_{mn}] &= \iint_{m\,n} \left[j\omega\mu_o \Omega_{mn}(\ell,\ell') - \frac{1}{j\omega\varepsilon_o}\Theta_{mn}(\ell,\ell') \right] \times \frac{\exp(-j\beta_o R_{mn})}{4\pi R_{mn}}\, d\ell' d\ell \\
\Omega_{mn}(\ell,\ell') &= G_m(\ell)\, \Gamma_n(\ell'), \\
\Theta_{mn}(\ell,\ell') &= \frac{dG_m(\ell)}{d\ell}\,\frac{d\Gamma_n(\ell')}{d\ell'}, \\
R_{mn}(\ell,\ell') &= [(\ell-\ell')^2 + b^2]^{1/2}.
\end{aligned}
\right\} \qquad (15)
$$

It may be remarked that since the helix is fed at the centre, all the elements of the voltage matrix are zero except the middle element, which equals the voltage of the delta function generator, employed at the feed-point. Physically, the helix structure has been reduced essentially to approximate an array of short current elements connected in series. With the explicit determination of the approximate generalized current distribution on the antenna by virtue of equation(14), the electric far-field radiated by the helical antenna can now be determined in a classical manner in terms of the vector magnetic potential.

3.1 Electric Far-Fields

It is well-known that far away from any antenna, the dominant components of the electric field intensity are the $\hat{\theta}$ and $\hat{\varphi}$ components, which can be computed from

$$E_\theta = j\omega A_\theta \quad \text{and} \quad E_\varphi = j\omega A_\varphi \qquad (16)$$

based on the vector potential concept. For the helical antenna, which is of primary interest here, we have,

$$A_\theta = \frac{\mu_o a \sec\alpha}{4\pi} \int_{\pi N}^{\pi N} [\sin\alpha \sin\theta - \cos\alpha \cos\theta \sin(\varphi - \varphi')]\, I(\varphi') \frac{\exp(-j\beta_o R)}{R}\, d\varphi' \qquad (17(a))$$

and

$$A_\varphi = \frac{\mu_o a}{4\pi} \int_{\pi N}^{\pi N} [\cos(\varphi - \varphi')]\, I(\varphi') \frac{\exp(-j\beta_o R)}{R}\, d\varphi' \qquad (17(b))$$

The symbol R appearing in the phase exponential terms of equations (17(a)) and (17(b)) is given by [Kornhauser (1951)] as

$$R = r - a\varphi' \tan\alpha \cos\theta - a\sin\theta\cos(\varphi - \varphi') \tag{18}$$

based on the usual far-field phase approximation, and N denotes the number of helix turns, which is 8 in this case, while $d\varphi'$ is related to $d\ell'$ by:

$$d\ell' = a\sec\alpha\, d\varphi' \tag{19}$$

Because the helical structure has been modelled as a series of short current elements, the integrals of equations (17(a)) and (17(b)) can be replaced by summations accordingly. Thus, the expressions of equation (16) for E_θ and E_φ become [1]

$$E_\theta(\theta, \varphi) = \frac{j\omega\mu_o a}{4\pi r}\sum_n [-\tan\alpha\sin\theta - \cos\theta\sin(\varphi - \varphi_n)][I_n]\exp(-j\beta_o R_n) \tag{20(a)}$$

and

$$E_\varphi(\theta, \varphi) = \frac{j\omega\mu_o a}{4\pi r}\sum_n [\cos(\varphi - \varphi_n)][I_n]\exp(-j\beta_o R_n) \tag{20(b)}$$

in which

$$R_n = r - a\varphi_n \tan\alpha\cos\theta - a\sin\theta\cos(\varphi - \varphi_n) \tag{22}$$

and, in accord with the far-field magnitude approximation, the R featuring in the denominator of equations (17(a)) and (17(b)) has been replaced by r.

3.2 Input Impedance (Z_{in}) and Total Power Radiated (P_r)

With the determination of the antenna current distributions and the far-zone electric fields, it is a fairly straightforward matter to evaluate the input impedance Z_{in} of, and the total power, P_r, radiated by the helical antenna. Typically, the input impedance consists of two parts namely, the input resistance R_{in} and the input reactance X_{in} computable from

$$Z_{in} = \frac{V_{in}}{I_{in}} = R_{in} + jX_{in} \tag{23}$$

where V_{in} and I_{in} are the voltage and current, respectively, at the feed point. Numerically, we can easily calculate the total power, P_r, radiated [Adekola *et al.* 1989] from

$$P_r = \frac{r^2}{2\eta_o}\sum_{i=1}^{n}\sum_{j=1}^{n/2}[|E_\theta(j\Delta\theta, i\Delta\varphi)|^2 + |E_\varphi(j\Delta\theta, i\Delta\varphi)|^2]\sin(j\Delta\theta)\Delta\theta\Delta\varphi \tag{24}$$

here $E_\theta(\bullet,\bullet)$ and $E_\varphi(\bullet,\bullet)$ are the electric field components at the far-zone given by equations (20a) and (20b), respectively, and $\eta_o = 120\pi$, the free-space characteristic impedance. In the ensuing section, the results of the computer simulations of the above equations will be discussed.

4. DISCUSSION OF RESULTS

The equations formulated in the preceding section are solved with the aid of a digital computer using Fortran 77 software, and the discussion of the results obtained constitutes the subject of this section.

4.1 Current Distributions

The current distributions computed from equation(14) for a centre-fed 8-turn helical antenna whose circumference in free-space wavelengths symbolized by C_λ and pitch angle denoted by α are within the ranges $1.1 \le C_\lambda \le 2.15$ and $5^\circ \le \alpha \le 40^\circ$, respectively are graphically illustrated in Figs. 3a and 3b. For all the numerical computations, an

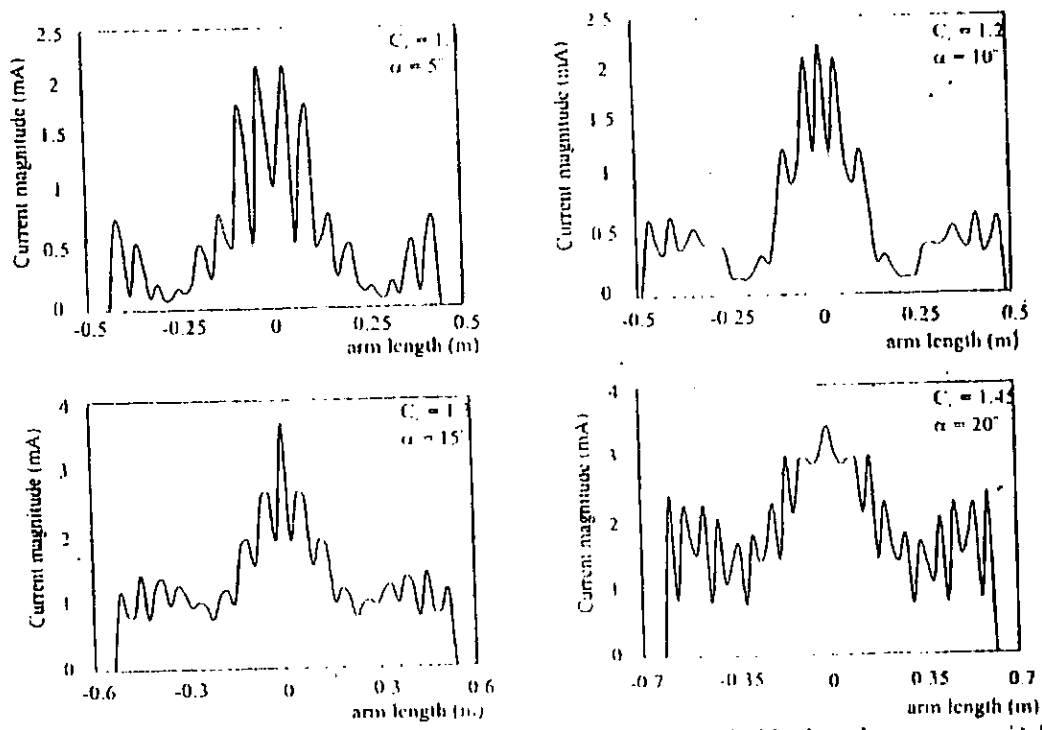

Figure 3(a): *Current distribution on a centrally fed helical antenna with pitch angle (α) ranging from 5° to 20°*

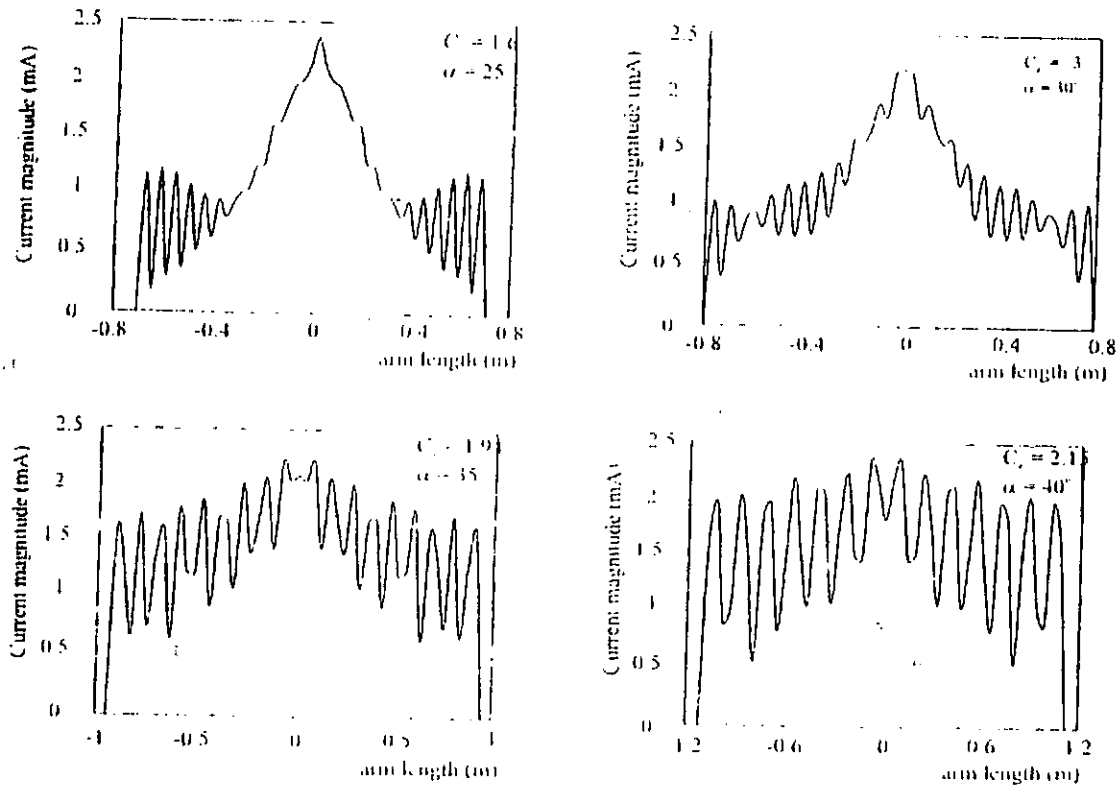

Figure 3(b): *Current distribution on a centrally fed helical antenna with pitch angle (α) ranging from 25° to 40°*

excitation voltage of 1V is utilized. The helix circumference C_λ and spacing in free-space wavelengths, S_λ, of the centre-fed helical antenna considered here are approximately related by $C_\lambda = [2S_\lambda + 1]^{1/2}$.

A close examination of Figures 3(a) and 3(b) shows that, regardless of the helical antenna dimensions, the current distribution is completely symmetrical about the feed-point. This is consistent with expectations. In addition, the current distribution profiles are characterized by significant dips at certain points along the helical structure. This observation conforms with Chen's results (validated by experimental measurements) who studied a centre-fed helical antenna using a less versatile Fourier series approach. Apart from the helical antenna with the dimensions $C_\lambda = 1.3$ and $\alpha = 15°$ whose current peak is 3.68 mA, all other helical antennas studied here, have their current peaks in the neighbourhood of 2.5 mA. Between $1.1 \le C_\lambda \le 1.73$ and $5° \le \alpha \le 30°$, the exponential nature of the current profile is fairly well-defined, whereas beyond the latter dimensions, the current distribution behaves nearly like a pure standing wave.

On the other hand, for a helix antenna fed via an infinite ground plane [Nakano *et al.* 1980] the current distribution has two distinct regions viz., a decaying exponential region and a nearly uniform region. This suggests that Nakano's balanced helical antenna is characteristically different from a continuous centre-fed helical antenna whose current distribution has no uniform region.

4.2 Analogy with Published Data

Chen (1967) previously reported the results of current distributions of a centre-fed helical antenna. His approach is based on a Fourier series approximation in contrast with the more generalised and versatile moment method adopted in this paper. The parameters used in Chen's work are

No. of turns:	6
Operating frequency:	600MHz
C_λ :	1.01λ
Excitation:	centre-fed.

We made use of the above parameters in our present work to compute the magnitude and phase of the current distribution.

For ease of analogy, the results obtained here for both the current magnitude and phase distributions are re-drafted and portrayed in rectangular formats consistent with what was reported by Chen [2]. Furthermore, Chen has validated his own results by experimentation. Our own results displayed in Figures 3(c) and 3(d) have reasonable agreements with those reported by Chen in Ref. (2). This justifies the validity of the present formulation.

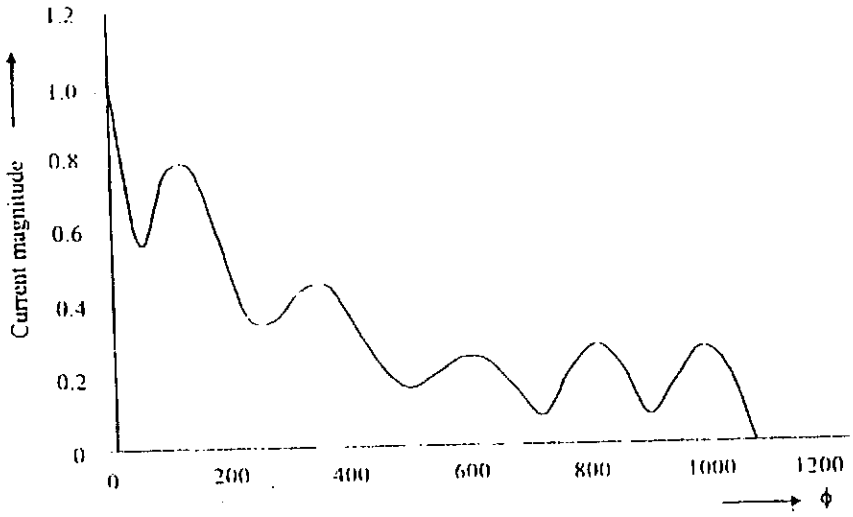

Figure 3(c): *Current magnitude of a centre-fed helical antenna at 600 MHz*

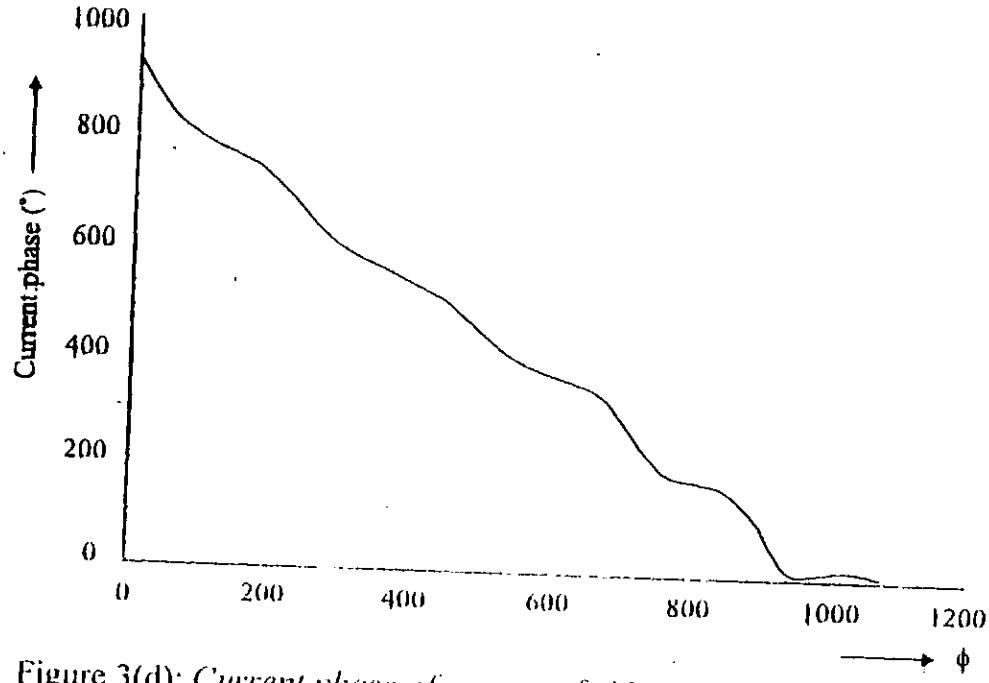

Figure 3(d): *Current phase of a centre-fed helical antenna at 600 MHz*

4.3 Electric Far- Fields

It is conventional practice to examine the radiation characteristics of the helical antenna once the current distribution has been determined. Consequently, in this section, we present the far-fields generated in free-space, by the generalised approximate current distributions displayed in Figures 3(a) and 3(b).

4.3.1 Horizontal Plane

At the horizontal $\theta=90°$ plane, Figure 4(a) shows the (E_θ , E_φ) fields generated by the current distribution of the helix, which is depicted in Figure 3(a) where the parameters (C_λ, α) vary from (1.1, 5°) to (1.45, 20°). It is shown in that figure that when (C_λ, α) change from (1.1, 5°) to (1.45, 20°), E_θ reverses its maximum from $\varphi = 180°$ to $\varphi = 0°$ while E_φ changes its maximum from $\varphi = 0°$ to $\varphi = 180°$.

Evolution into a 4-lobed Chireix mode

Figure 4(b) shows how the field radiated by the helix when (C_λ, α) vary within (1.6, 25°) and (2.15, 40°). The figure describes the evolution of the (E_θ , E_φ) fields into the Chireix coil, 4-lobed patterns when (C_λ, α) assume values given as (1.94, 35°) and (2.15, 40°), respectively. It is worth pointing out that, for this 4-lobed mode, the peak of the patterns are normal to the helix axis since they are on the horizontal plane orthogonal to the helix axis as evident from the geometrical configuration depicted in Figure 2(a).

It should also be noted that the current distributions producing those 4-lobed patterns, behave like pure standing waves symmetrical about the feed-point, as portrayed in Figure 3(b).

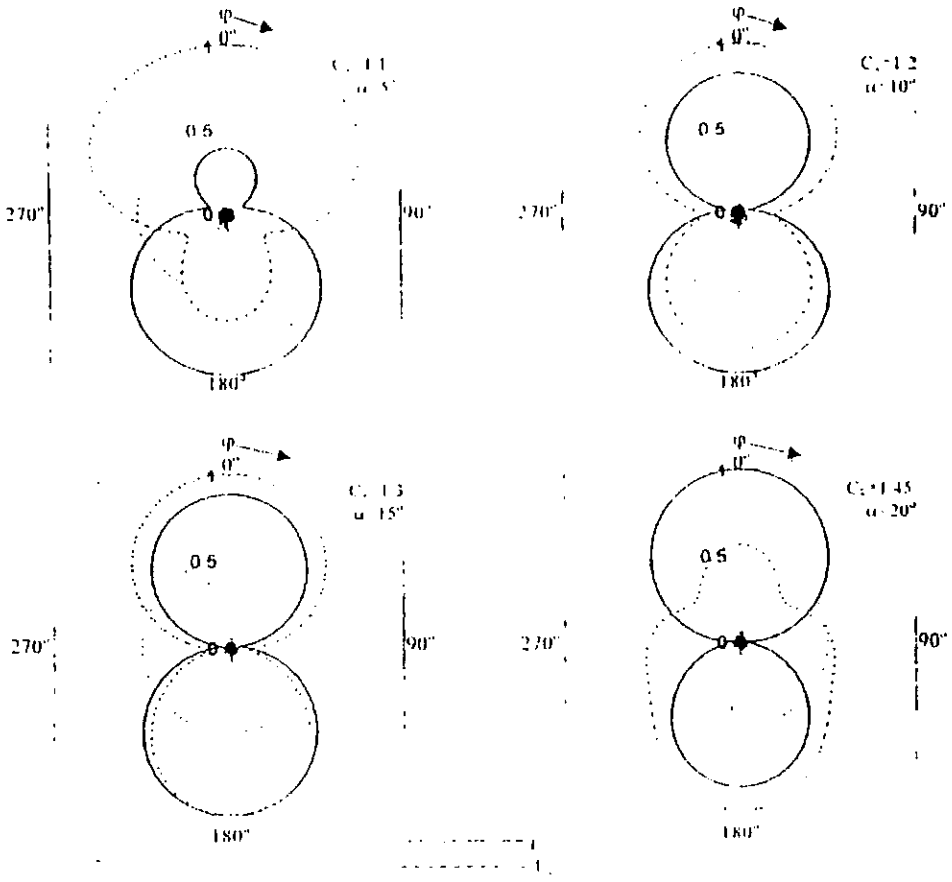

Figure 4(a): *Far-zone electric field patterns on the horizontal plane*

4.3.2 Vertical Plane

Figures 4(c) and 4(d) describe how the variations of (C_λ, α) affect the fields radiated by the helix at the vertical plane defined by $\varphi = 90°$. The vertical plane, parallel to the antenna axis, only admits E_θ, the $\hat{\theta}$- component of the electric field, as the $\hat{\varphi}$-component has been completely attenuated. It can be seen from the figures that E_θ patterns are predominantly multi-lobed.

For every value of C_λ, each figure shows how E_θ behaves with variations of pitch angle α, between 5° and 30°. Also portrayed in the figures, are the profiles of how the field behaves with variations of C_λ.

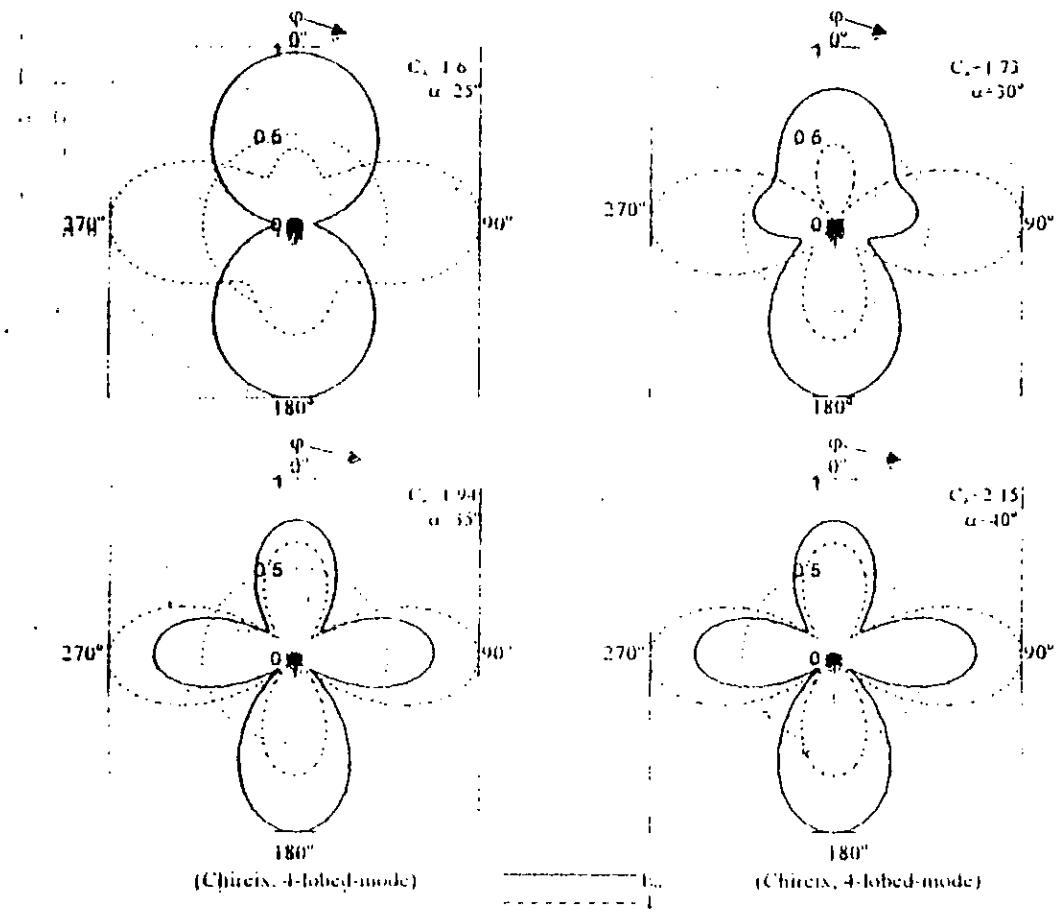

Figure 4(b): *Far-zone electric field patterns on the horizontal plane*

4.4 Input Resistance, Input Reactance and Total Power Radiated

Use is usually made of the characteristics of the input impedance of an antenna to determine how its electrical properties vary with frequency. Consequently, the determination of that parameter cannot be over-emphasized. This is what we address in this section. Although the aforementioned input impedance is a more interesting parameter as against the power radiated, nevertheless, we also present here the profile of the latter for the sake of completeness.

Based on the current distributions of Figures 3(a) and 3(b), we evaluated the input resistance, input reactance and total power radiated by a centre-fed 8-turn helical antenna, which are graphically illustrated in Figures 5, 6, and 7, respectively. Use is made of equation(23) to compute the input resistance and the input reactance while equation(24) is employed for the computation of the total power radiated. As evident

from Figure 5 the input resistance decreases from 361Ω for $C_\lambda = 1.1$ to 124Ω when $C_\lambda = 1.2$. Thereafter, it increases almost linearly when C_λ lies between 1.3 and 1.6, and drops to 277Ω for $C_\lambda = 1.73$. Beyond $C_\lambda = 1.73$, the input resistance rises steadily and attains a value of 546Ω when $C_\lambda = 2.15$. Pertaining to the input reactance shown in Figure 6, it increases exponentially with C_λ within the band $1.1 \le C_\lambda \le 1.45$, while beyond $C_\lambda > 1.45$, the input reactance undulates in a wavelike manner. The total power radiated which is graphically illustrated in Figure 7, increases nearly linearly when C_λ lies in the range $1.1 \le C_\lambda \le 1.3$ reaching a peak value of 1.64mW. It drops to 1.3mW for $C_\lambda = 1.45$ and remains approximately at this level until C_λ assumes a value of 1.6. A total power of 2mW is radiated for both $C_\lambda = 1.94$ and 2.15.

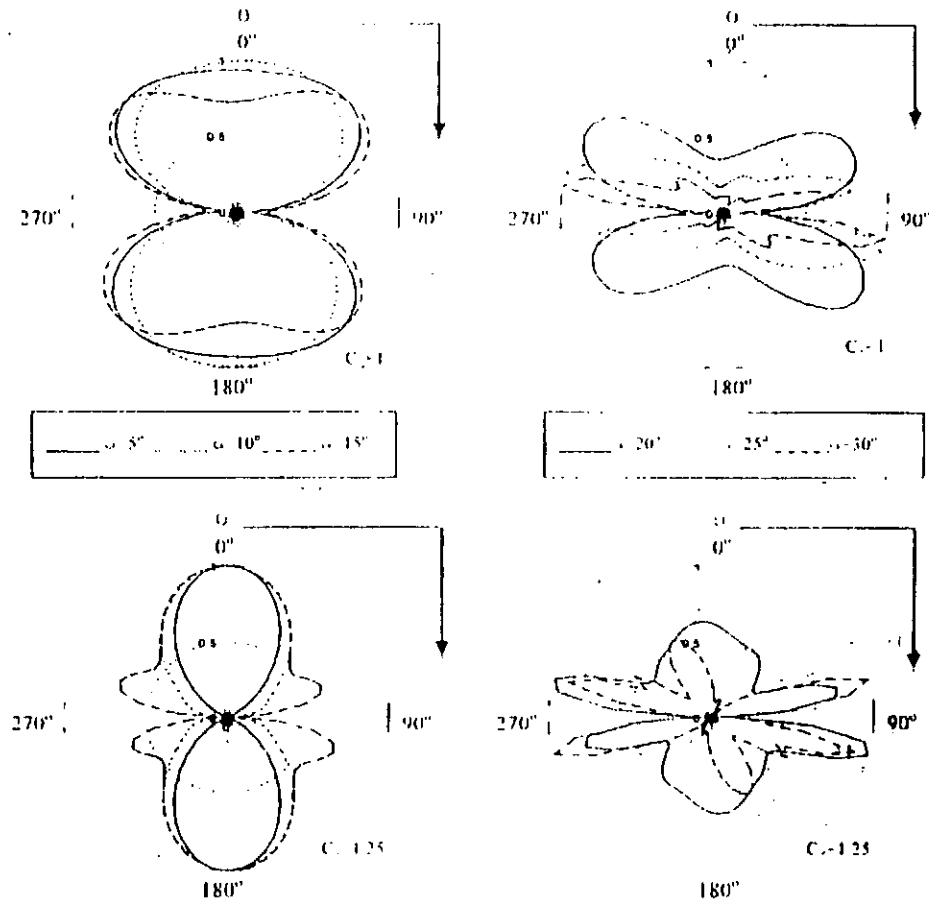

Figure 4(c): *Far-zone electric field (E_θ) on the $\phi = 90°$ plane when $C_\lambda = 1.0$ and 1.25*

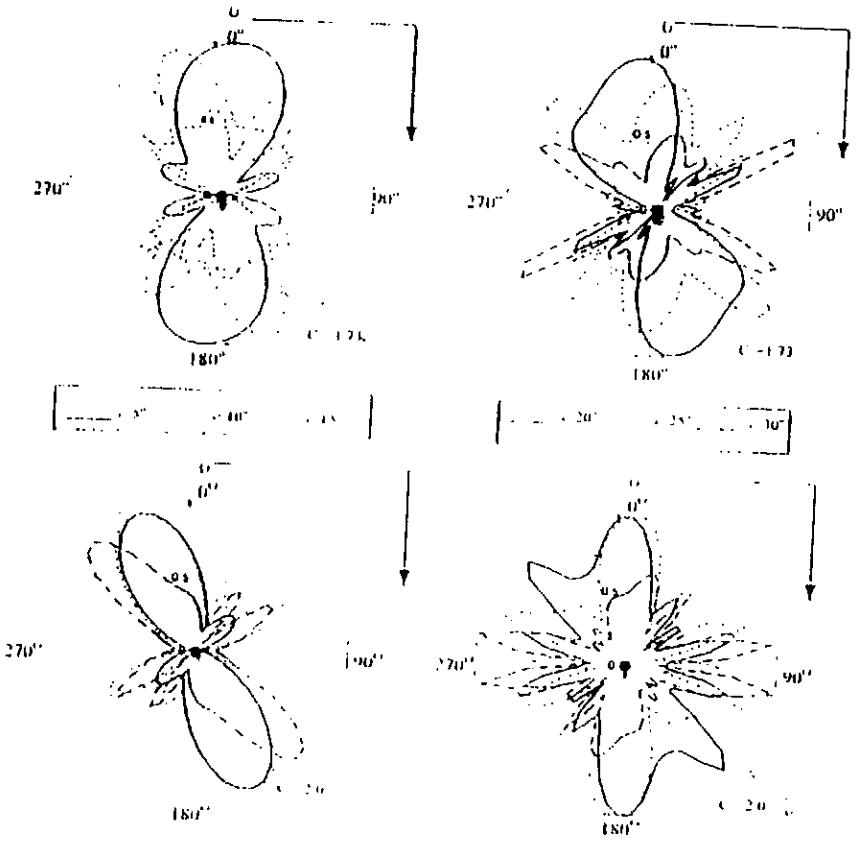

Figure 4(d): *Far-zone electric field (E_θ) on the $\phi = 90°$ plane when $C_\lambda = 1.73$ and 2.0*

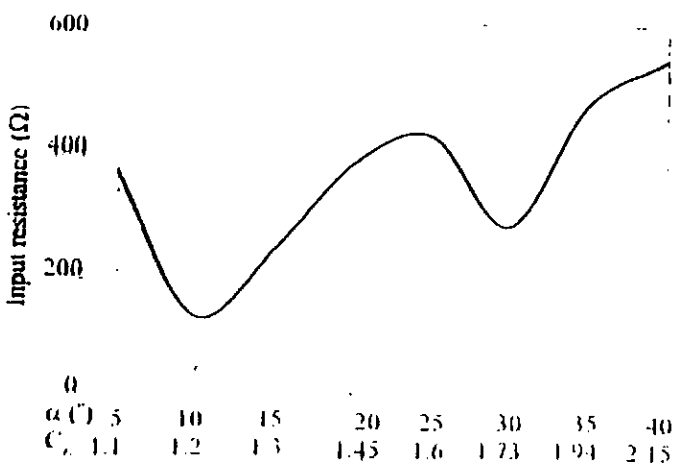

Figure 5: *Input resistance against pitch angle (α) and helix circumference (C_λ)*

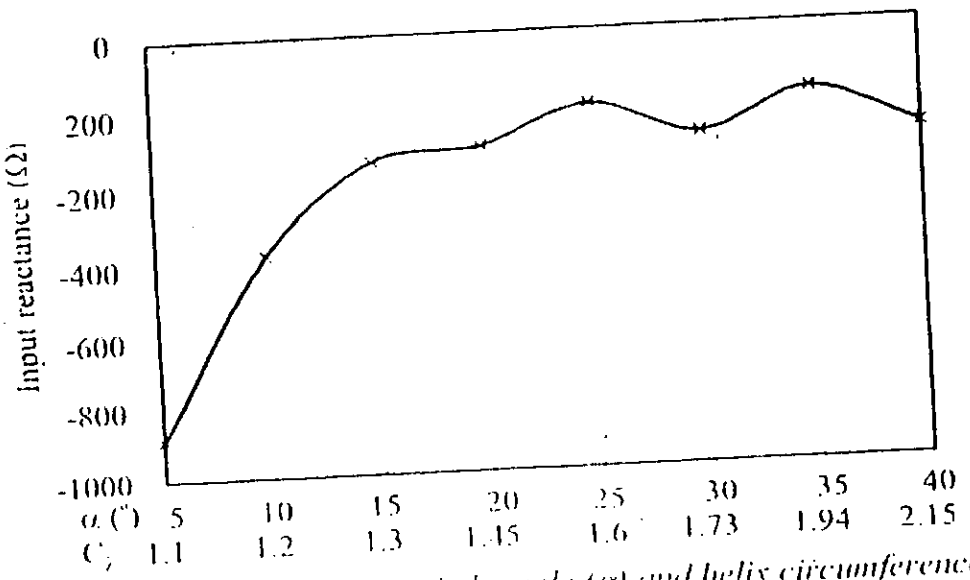

Figure 6: *Input reactance against pitch angle (α) and helix circumference (C_λ)*

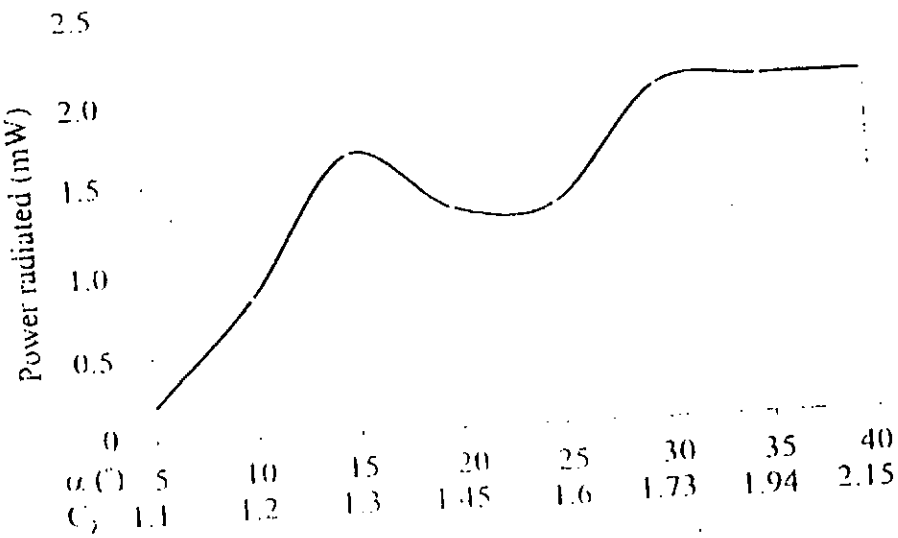

Figure 7: *Power radiated against pitch angle (α) and helix circumference (C_λ)*

5. CONCLUDING REMARKS

The electrical properties of the centre-fed helical antenna determined in this paper reveal many interesting features of engineering importance hitherto unavailable in the literature. First, the current distributions which are symmetrical about the feed-point decays exponentially towards the termination at both ends of the helix. Second, (E_θ, E_φ) patterns at the horizontal plane orthogonal to the antenna axis, enjoy an evolution from two lobes at moderate values of the parameters (C_λ, α) into multiple lobes as these parameters increase, culminating in chireix, 4-lobed modes when (C_λ, α) assume values given as (1.94, 35°) and (2.15, 40°), respectively. Here lies the novelty of the present contribution. The peaks of the patterns of the chireix lobes are normal to the helix axis. It is noted that the current distributions producing those 4-lobed patterns behave like standing waves. At moderate values of (C_λ, α) lower than the aforementioned numeric quantities, (E_θ, E_φ) exhibit their maxima in opposite directions. As (C_λ, α) increase the maxima completely reverse through 180° at (C_λ, α) = (1.45, 20°).

Third, E_θ predominates at the vertical plane parallel to the antenna axis as the E_φ field has been completely attenuated. In this case, the field radiated is completely multi-lobed. An interesting feature is the input impedance computed here in order to have an insight into how the helical antenna responds electrically to frequency variation.

The validity and accuracy of the results presented in the foregoing were tested through the use of an existing control available in the literature. In that regard, the current distribution for a 6-turn centre-fed helix operating at 600MHz, for which $C_\lambda = 1.01\lambda$, was computed, using the equations reported here. An antenna with the same dimensions had earlier been analysed by Chen, [2], who employed a Fourier series approach. The characteristic features of the profiles of current distributions obtained from these two different approaches exhibited very close similarities, thus lending credence to the validity of the formulation given in this paper.

6. REFERENCES

[1] Adekola, S.A, and Okereke O.U. (1989). "Analysis of a circular-loop antenna using moment methods". *Int. J. Electronics*, London, U.K., 66, pp. 821-834.

[2] Chen, C.L. (1967): "Theory of the balanced helical wire antenna". *Radio Science*, vol. 2, (New series), pp. 167-190.

[3] Harrington, R.F. (1968). *Field computation by moment methods*. The Macmillan Company, New York, 229pp.

[4] Kraus, J.D.(1988). *Antennas*. McGraw-Hill Inc. USA, Second Edition, chap. 7, pp.265-339.

[5] Kuo, D.C. and Strait, B.J. (1972). "Improved programs for analysis of radiation and scattering by configuration of arbitrarily bent wires". *Syracuse University Scientific report No.15*, 50pp.

[6] Lee, K.F., Wong, P.F., and Larm, K.F. (1982). "Theory of the frequency responses of uniform and quasi-taper helical antennas". *IEEE Trans.* Vol. **AP-30**, No.5, pp. 1017-1021.

[7] Nakano, H. and Yamauchi, J. (1980). "Radiation characteristics of helix antenna with parasitic elements". *Electronic Letters*, vol. 16, No. 18, pp. 687-688.

[8] Lazzi, G., and Gandhi, O.P. (1998). "On modeling and personal dosimetry of cellular telephone helical antennas with the FDTD code". *IEEE Trans.*, **AP-46**, (1), pp.525-530.

[9] Kraus, J.D. (1947). "Helical beam antenna", *Electronics*, **20**, April, pp.109-111.

[10] Kraus, J.D. (1995). "A helical-beam antenna without a ground plane". *IEEE Ant. & Prog. Mag.*, vol.37, (2), p.45.

[11] Nakano, H., and Mimaki, H. (1995). "Radiation from a short helical antenna backed by a cavity". *Electronics Letters*, vol. 31, 8, pp.602-604.

[12] Munk, B.A., and Peters Jnr., L. (1968). " A helical launcher for the helical antenna". *IEEE Trans*, **AP-16**, pp.362-363.

[13] Reference Data for Radio Engineers, (1972). 5th Edition (Howard W. Sams & Co., Inc., a subsidiary of International Telephone and Telegraph (ITT) Corporation), p.16-20.

[14] King, H.E., and Wong., J.L. (1972)."240-400 MHz Antenna system for the FleetSatCom satellites". *IEEE Int'l Symposium on Antennas and Propagation*, Stanford University, Stanford, California, U.S.A., June 20 - 22, pp. 349-352; AP-S Session 12, 1000, Tuesday June 21.

[15] Wong, J.L., and King, H.E. (1977). " A technique for broadband gain-pattern synthesis of helical antennas". *IEEE Int'l Symposium on Antennas and Propagation*, Stanford University, Stanford, California, U.S.A., June 20 - 22, pp. 234-237; AP-S Session 8, 0400, Monday, June 20.

[16] Kornhauser, E.T. (1951). "Radiation field of helical antennas with sinusoidal current". *Journal of Applied Physics*, Vol.22, No.7, pp.887-891.

APPENDIX I(d):

EXCLUSION OF GROUND PLANES IN THIN-WIRE HELICAL ANTENNAS

JER - 9, Nos. 3 & 4, 13-28 Sept. 2001

Exclusion of Ground Planes in Thin-wire Helical Antennas

S. Adeniyi Adekola, A. Ike Mowete and A. Ayotunde Ayorinde
Department of Electrical & Electronics Engineering
University of Lagos, Akoka - Yaba, Lagos, Nigeria

Abstract
This paper addresses the problem of determining the current distributions and the associated far-zone electric fields of a thin-wire helical antenna, when excited without the conventional ground plane. Use is made of the method of moments in a Galerkin's procedure, for the numerical solution of the problem. It is clearly established that the axial current distribution is significantly affected by variations in pitch angle, contrary to the approximately invariant behaviour of this axial current distribution with change in pitch angle, when a small ground-plane is included. Furthermore, it is shown that the global current distribution, together with its corresponding far-field patterns, which are predominantly in the backfire direction, can be controlled by a judicious choice of both the pitch angle and the operating frequency. Also, highlighted is the extent to which the numerical results agree with experimental data, available in the open literature.

1. INTRODUCTION

The helical antenna has found a wide variety of applications, ranging from telephony, television and data transmission in space communications, to weather and global positioning satellites, as well as tracking satellites, geostationary satellites and data-relay satellites. Indeed, the antenna has not only been utilised in exploratory ventures to the moon and mars, but also in probing other planets as well as comets [1]. As a matter of fact, Lazzi and Gandhi [2], have also recently discussed the further use of helical antennas in cellular telephony.

Historically, the discovery of helical beam antennas appears traceable to Kraus [3], who demonstrated that the applicability of the helix is not just confined within the travelling wave tube where it was merely used for amplification and as a guiding structure, but, that in addition, it is also of great practical utility as a versatile radiating element in free

space. Thus, at the beginning, the helical-beam antenna was conceived as a radiating element designed to be fed through a ground plane. Because it was well-suited in that configuration to several important practical applications, the resulting monofilar element engaged the attention of several investigators whose results provided significant insight into the radiation characteristics of the antenna [4-6]. For example, the extensive experimental results reported by King and Wong [4], suggested that when the diameter of the ground plane of the monofilar helical antenna is in excess of 0.5λ at the operating frequency in which λ is the associated wavelength, it radiates exclusively in the forward endfire direction or axial mode. These results were subjected to various theoretical analyses, notable among which are the works of Nakano and his collaborators [7], and which elucidated vital design information. In a related contribution [8], Nakano *et al.* have also carried out a numerical analysis illustrating the effect of variations in ground plane size, on the performance of helical antennas.

The results obtained in the reference just cited above indicate that when the diameter of the ground plane is decreased below 0.5λ, at the operating frequency, backward radiation becomes dominant. It then becomes possible for the monofilar helical antenna to operate in the backward endfire mode. Other backfire helical antennas have been described by Kilgus [10], and Patton [9], who confirmed an earlier prediction by Kraus [1], that the direction of the antenna's radiation will be reversed, when the ground plane is excluded. Patton [9], and Johnson and Cotton [14], describe practical methods for feeding monofilar helical antennas, without use of ground planes. To the best of our knowledge, no theoretical analyses have been reported in the open literature, on the antenna types described by Patton [9], and Johnson and Cotton [14].

This presentation, therefore, describes a moment-method analysis of the monofilar helical antenna, fed without a ground plane, using a delta-gap model for the feed arrangement prescribed by Patton [9]. Numerical results are presented for the monofilar helical antenna with pitch angles in the range $5^\circ < \alpha < 20^\circ$, and for operations in the frequency band (4.2 - 7.0) GHz. Profiles of the results computed here follow the same characteristics as those obtained through experimentation by other authors. This demonstrates the validity of the analysis proposed in this paper.

2. FORMULATION

When an electromagnetic disturbance illuminates any conducting body in free space, the resulting scattered electric field denoted by $\mathbf{E}^s$ is expressible in terms of the retarded vector magnetic potential $\mathbf{A}$ in the usual manner as [12]

$$\mathbf{E}^s = -j\omega\mathbf{A} + \frac{1}{j\omega\varepsilon_0\mu_0}\nabla(\nabla\cdot\mathbf{A}) \qquad (1(a))$$

$$\mathbf{A} = \frac{\mu_0}{4\pi}\int_{V'} \mathbf{J}(\mathbf{r}')\frac{\exp(-jk_0R)}{R}\,dV' \qquad (1(b))$$

where ∇ stands for the del operator, ω ($= 2\pi f$) the angular frequency, f the operating frequency, $\mathbf{J}(\mathbf{r}')$ the current distribution density while (ε_0, μ_0, k_0), respectively, designate free-space permittivity, permeability and the propagation constant. Moreover, as usual, $j = \sqrt{-1}$, while $R = |\mathbf{r} - \mathbf{r}'|$ is the distance between the source and field points denoted by $(\mathbf{r}', \mathbf{r})$, respectively.

A specialisation of equations (1a) and (1b) for the thin-wire helical antenna depicted in Figure 1 in which the antenna current, symbolised by $I(\ell')$, is constrained to flow along the axial direction, $\hat{\ell}'$, of the helical wire, yields the following equation [12]:

$$E_\ell^s = \frac{-j\omega\mu_0}{4\pi}\int_{\substack{\text{arm}\\\text{length}}} I(\ell')\frac{\exp(-jk_0R)}{R}\,d\ell' + \frac{1}{j4\pi\omega\varepsilon_0}\frac{d}{d\ell}\int_{\substack{\text{arm}\\\text{length}}} \frac{dI(\ell')}{d\ell'}\frac{\exp(-jk_0R)}{R}\,d\ell' \qquad (2)$$

The quantity R which appears in equation (2), now represents the distance between a source point specified by φ' on the wire axis, and an observation point identified by φ on the wire surface; that is:

$$R = a\left\{4\sin^2\left(\frac{\varphi - \varphi'}{2}\right) + \tan^2\alpha(\varphi - \varphi')^2 + \left(\frac{b}{a}\right)^2\right\}^{\frac{1}{2}} \qquad (3)$$

where $\alpha = \tan^{-1}\left(\frac{p}{2\pi a}\right)$.

In equation (3), a represents the helical cylinder radius, b the wire radius, α the pitch angle, p the pitch distance; $d\ell$ and $d\ell'$ stand for differential lengths along the wire surface and the wire axis, respectively.

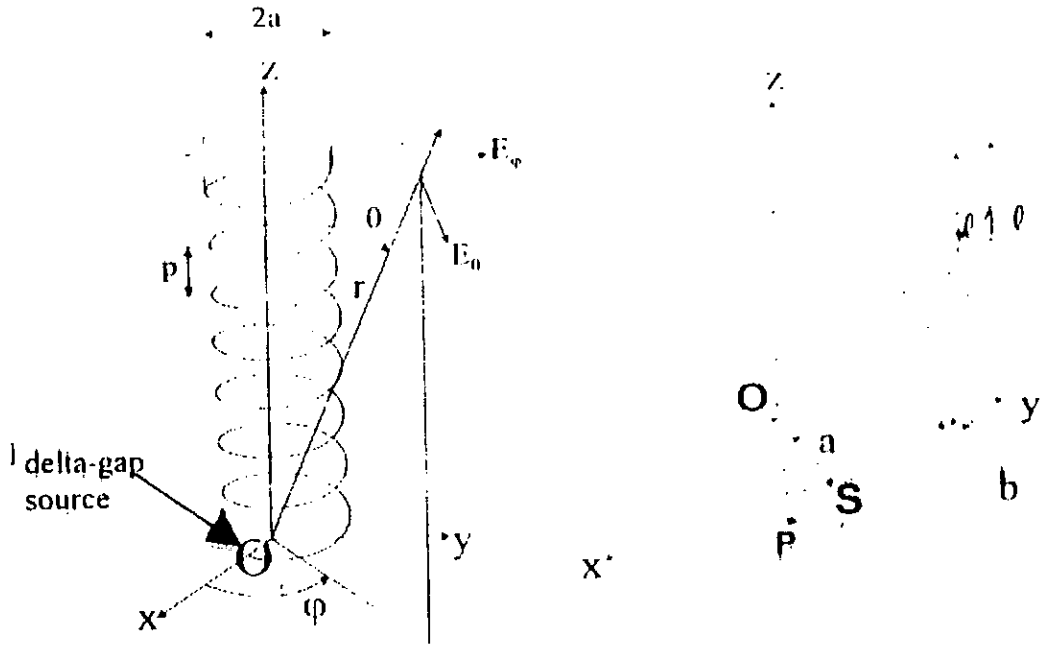

Figure 1: *(a) A 7-turn thin-wire helical antenna excited without a ground plane (b) A typical turn of the helix depicting the source point $S(\rho = a, \varphi, z)$ and observation point $P(\rho = a + b, \varphi, z)$ and the unit vectors ℓ and ℓ' along the helical surface and centreline, respectively.*

Equation (2) admits the more compact representation

$$E_\ell^s = \frac{1}{4\pi} \int_{\substack{\text{arm}\\ \text{length}}} \left\{ \left[-j\omega\mu_o I(\ell') + \frac{1}{j\omega\varepsilon_o} \frac{dI(\ell')}{d\ell'} \frac{d}{d\ell} \right] \frac{\exp(-jk_o R)}{R} \right\} d\ell' \qquad (4)$$

Physically, equation (4) relates the scattered electric field tangential to the helical surface to the current flow along the wire axis. When the boundary condition of vanishing tangential component of total electric field on the perfectly conducting helix is imposed, we find that the axial component of the incident electric field denoted by E_ℓ^I, is given by

$$E_\ell^i = \frac{1}{4\pi}\int_{\substack{\text{arm}\\ \text{length}}} \left\{ \left[j\omega\mu_o I(\ell') - \frac{1}{j\omega\varepsilon_o}\frac{dI(\ell')}{d\ell'}\frac{d}{d\ell}\right]\frac{\exp(-jk_oR)}{R}\right\} d\ell \qquad (5)$$

This gives an integrodifferential expression for the determination of the unknown axial current distribution, in terms of the prescribed incident electric field.

3. ANALYSIS

In this presentation, a numerical solution, based on the method of moments, [Harrington 1968] is obtained for the unknown current in equation (5). And in that connection, it is readily established that the generalised impedance matrix appropriate to this formulation is

$$[Z_{mn}] = \frac{1}{4\pi}\iint_{m\,n}\left[j\omega\mu_o W_m(\ell)T_n(\ell') - \frac{1}{j\omega\varepsilon_o}\frac{dT_n(\ell')}{d\ell'}\frac{dW_m(\ell)}{d\ell}\right] \times \frac{\exp(-jk_oR_{mn})}{R_{mn}}\, d\ell' d\ell \qquad (6)$$

where R_{mn} stands for the expression described as:

$$R_{mn} = a\left\{4\sin^2\left(\frac{\varphi_m - \varphi_n}{2}\right) + \tan^2\alpha\,(\varphi_m - \varphi_n)^2 + \left(\frac{b}{a}\right)^2\right\}^{\frac{1}{2}} \qquad (7)$$

following a specialisation of equation (3). It is noted that the basis functions denoted by $T_n(\ell')$ and the testing function represented by $W_m(\ell)$ are, in this case, of the same piece-wise linear variety.

With the explicit determination of the generalised impedance matrix, the numerical approximation to the generalised current distribution is then obtained through routine matrix operations as described elsewhere, [11], as

$$[I_n] = [Z_{mn}]^{-1}[V_m] \qquad (8)$$

In equation (8), $[V_m]$ is the generalised voltage matrix, which derives from the delta-gap model adopted for the feed arrangement.

Given the approximation to the antenna's current distribution as specified by equation (8), it becomes possible to obtain numerical data on the far-zone electric field radiated by the helical antenna. To that end, use is made of the classical magnetic vector potential approach, as described in what follows.

At a great distance from the antenna, the contribution of the second member of the right-hand side of equation (1a) becomes negligible, and only θ- and φ- components of the electric field are predominant. Consequently, equation (1a) passes over into

$$\mathbf{E}^s = j\omega(\hat{\theta}A_\theta + \hat{\varphi}A_\varphi) \tag{9}$$

provided $(\hat{\theta}, \hat{\varphi})$ are unit vectors in the θ- and φ- directions, respectively, and where [15]:

$$A_\theta = \mu_0 a \sec\alpha \int_0^{2\pi N} [\sin\alpha \sin\theta + \cos\alpha \cos\theta \sin(\varphi - \varphi')] \times I(\varphi') \frac{\exp(-jk_0 R)}{4\pi R} d\varphi' \tag{10(a)}$$

$$A_\varphi = \mu_0 a \int_0^{2\pi N} [\cos(\varphi - \varphi')] I(\varphi') \frac{\exp(-jk_0 R)}{4\pi R} d\varphi' \tag{10(b)}$$

in which use has been made of $d\ell' = a \sec\alpha \, d\varphi'$ and the symbol N denotes the number of helix turns. Employing the usual Cartesian coordinate system, any arbitrary source point r′ on the circular helix can be represented by

$$\mathbf{r}' = a\cos\varphi'\hat{a}_x + a\sin\varphi'\hat{a}_y + a\tan\alpha\varphi'\hat{a}_z \tag{11(a)}$$

whereas a general far-field point r is expressible as

$$\mathbf{r} = r\sin\theta\cos\varphi\,\hat{a}_x + r\sin\theta\sin\varphi\,\hat{a}_y + r\cos\theta\,\hat{a}_z \tag{11(b)}$$

Here, $\hat{a}_x$, $\hat{a}_y$ and $\hat{a}_z$ are the unit vectors in the x- , y- and z- directions, respectively. The distance measure denoted by R in equations (10(a)) and (10(b)) is given by

$$R = |\mathbf{r} - \mathbf{r}'| = \left\{(x - x')^2 + (y - y')^2 + (z - z')^2\right\}^{\frac{1}{2}} \qquad (11(c))$$

The dominant first two terms of the binomial expansion of equation (11c) give

$$R \approx r - (a \tan\alpha \cos\theta)\varphi' - a \sin\theta \cos(\varphi - \varphi') \qquad (11(d))$$

Hence, the E_θ and E_φ components of the fields radiated can be written, respectively, as [15]

$$E_\theta(\theta, \varphi) = \frac{-j\omega\mu_0 a}{4\pi r} \sum_n [\tan\alpha \sin\theta + \cos\theta \sin(\varphi - \varphi_n')][I_n]\exp(-jk_0R_n) \qquad (12(a))$$

$$E_\varphi(\theta, \varphi) = \frac{-j\omega\mu_0 a}{4\pi r} \sum_n \cos(\varphi - \varphi')[I_n]\exp(-jk_0R_n) \qquad (12(b))$$

where R_n is given by

$$R_n \approx r - (a \tan\alpha \cos\theta)\varphi_n' - a \sin\theta \cos(\varphi - \varphi_n') \qquad (13)$$

It is worth pointing out that the integrations explicit in equations (10(a)) and (10(b)) have been replaced with summations, while R in the denominator of the two equations has been approximated by r, in the usual manner of the "magnitude approximation". Numerical results obtained from the equations formulated in this section are displayed in graphical formats, and they constitute the subjects of discussions in section 4, which follows.

4. DISCUSSION

Numerical results obtained from the foregoing analytical solution are employed in this section, to describe the performance characteristics of the helical antenna whose feed mechanism does not include a ground plane. For the sake of brevity, a picturesque description of the results will be restricted to just a few figures. The discussion begins by considering the current distributions.

4.1 Current Distributions

Displayed in Figures 2 and 3 are graphical representations of the numerical results obtained for the approximate generalised current distributions when use is made of equation (8) for a monofilar helical antenna whose pitch angle variation is given by $5^o \leq \alpha \leq 20^o$, while operating in the frequency band 4.2 GHz - 7.0 GHz. In the aforementioned figures, the solid lines represent magnitude of current while the dashed lines depict the phase distributions of the current wave on the helical arm length. Figure 2(a) suggests that when the pitch angle of the helix and the operating frequency are 5° and 5.0 GHz,

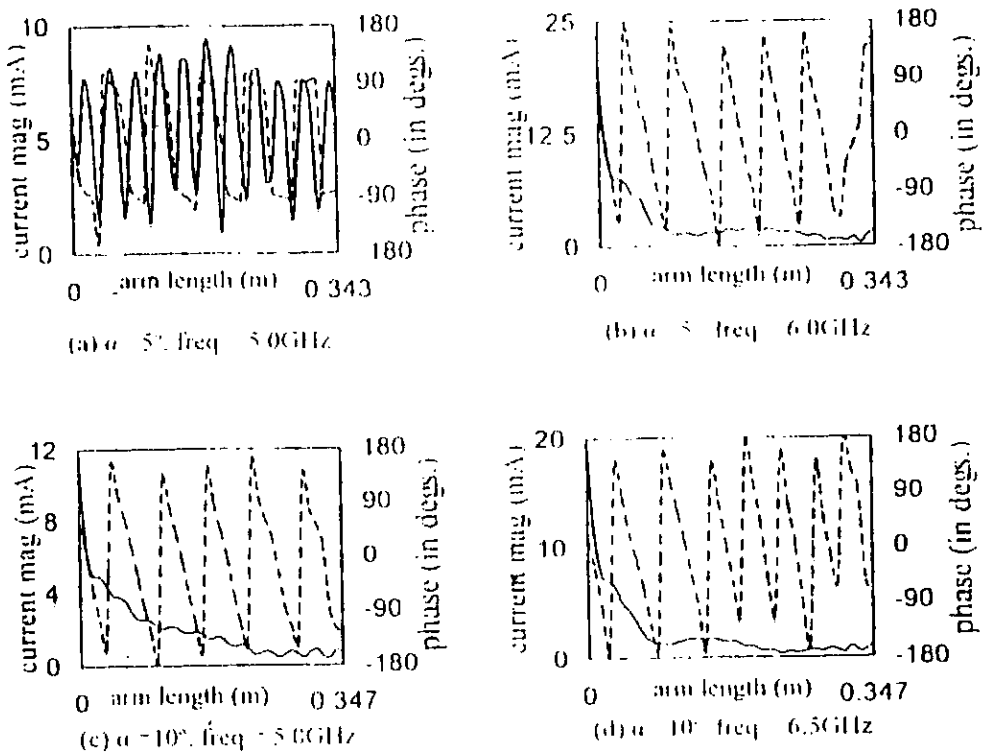

Figure 2: *Current distribution on a monofilar helical antenna without a ground plane: α (pitch angle): 5° - 10° and number of turns = 7,* ..... *current magnitude,* -------- *current phase*

respectively, the current distribution is characterised by a dominant standing wave component. Although not graphically illustrated, this characteristic is also observed

in numerical results for all other pitch angles in the lower frequency regimes 4.2 GHz - 7.0 GHz. As the pitch angle increases from 5° to 10°, the standing wave component is gradually attenuated from 5 GHz upwards, with a clearly noticeable decaying feature being displayed between 6.0 GHz and 6.5 GHz as revealed by Figures 2(c) and 2(d). When the pitch angle is 15°, Figure 3(b) reveals that the decaying characteristic of the current wave becomes more pronounced at the operating frequency of 5.0 GHz, although the standing wave component is still slightly noticeable for the current at 4.5 GHz for that value of pitch angle. It is interesting to note that, when the pitch angle assumes a value of 20° at 7.0 GHz, the current distribution assumes an approximately exponential variation over half of the helix, and sinusoidal for the other half, as depicted in Figure 3(d). The phase variation of the current distributions is typified by a negative

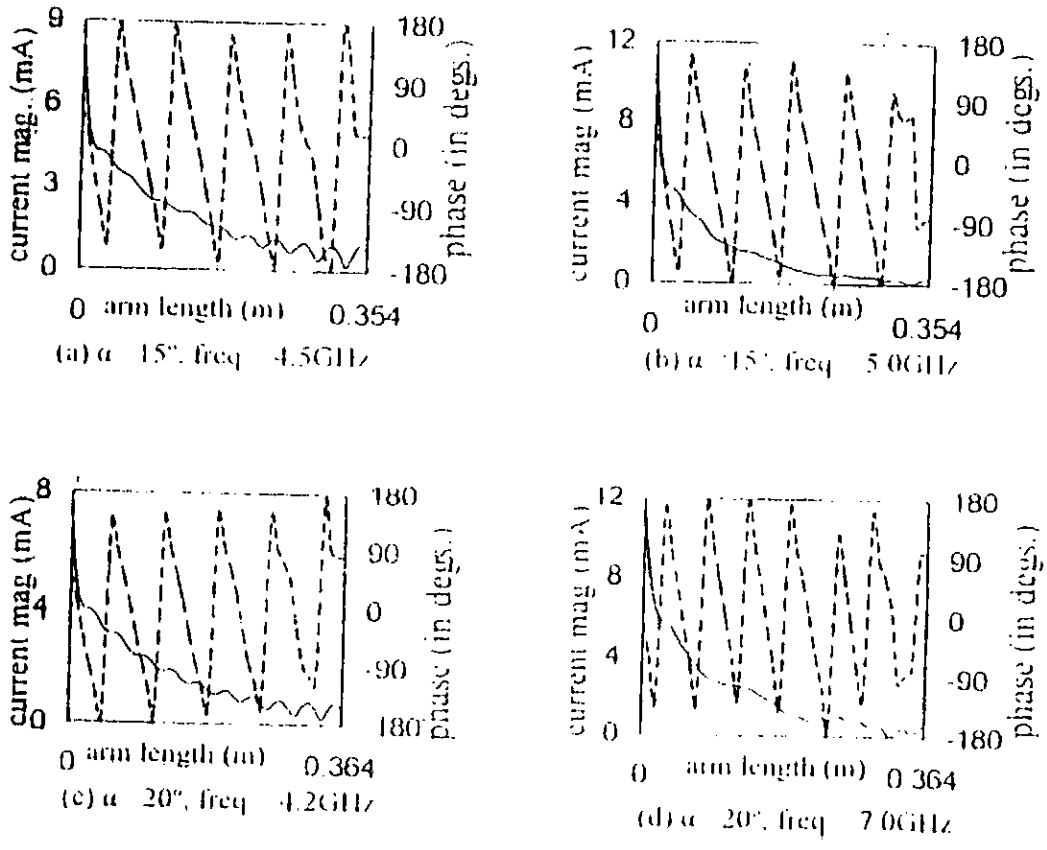

Figure 3: *Current distribution on a monofilar helical antenna without a ground plane: α (pitch angle): 15° - 20° and number of turns = 7. _____ current magnitude, -------- current phase*

slope for nearly every turn of the helix for all the frequencies and pitch angles investigated. These results indicate that unlike what obtains with the backfire helical antenna with a small ground plane as reported by Nakano *et al.* [8], current in the ground planeless helical antenna is significantly affected by the pitch angle. Indeed, it would appear that significant backward radiation can be excited at the lower frequencies, if a proper choice of pitch angle is made.

4.2 Radiation Patterns

As a means of checking the correctness of the formulation presented in this paper, the equations derived were utilised for the computation of radiation-zone data for a monofilar helical antenna, earlier experimentally investigated by Patton [9]. This antenna is characterised by the parameters: *pitch distance 3 cm, helix radius 2.847 cm, pitch angle 10.18°, wire radius 0.069 cm, operating frequency 1400 MHz.* A choice of 7, for the number of turns was made although Patton only reported that the helix should be reasonably long. Although Patton's measurements are not illustrated in this paper, the numerical results of the aforementioned exercise are graphically displayed in Figure 4 and the characteristics follow identical profiles like those of Patton [9].

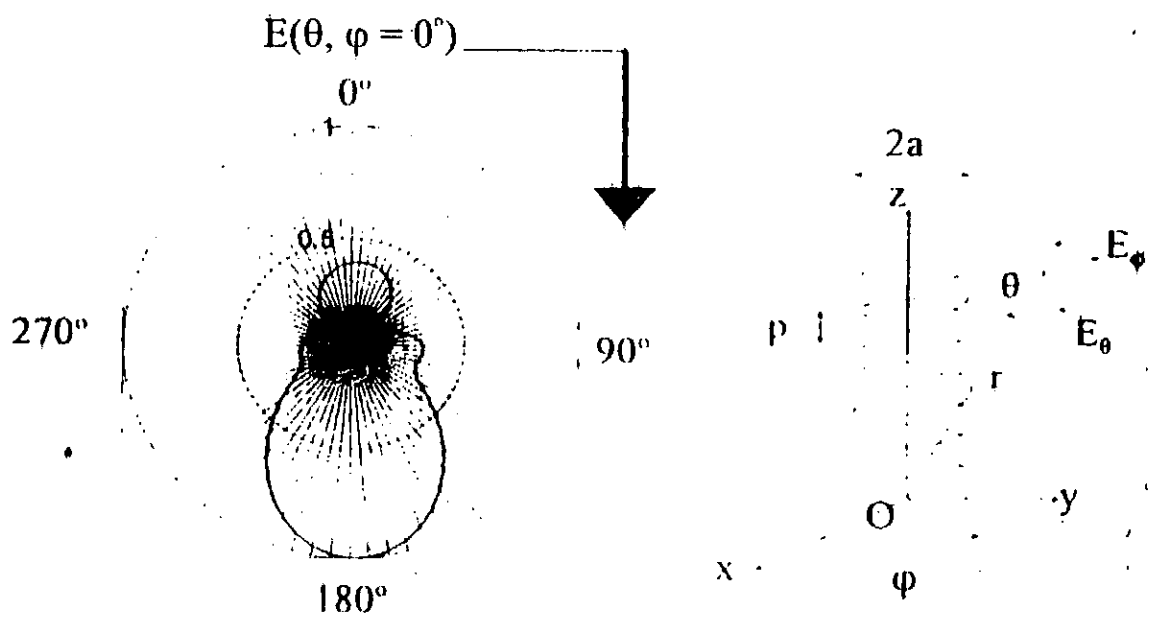

Figure 4: *Computed pattern radiated from a helix structured along an experimental model*

The far-zone radiation patterns ($E_\theta(\theta,\varphi)$ and $E_\varphi(\theta,\varphi)$) as computed from equation (12) for the $\varphi = 0°$ plane corresponding to the current distributions of Figures 2 and 3, are displayed in Figures 5 and 6, respectively. These results as well as those not shown in this paper, reveal that as expected, the monofilar helical antenna fed without a ground plane radiates predominantly in the backfire direction.

Figure 5(a) shows that the radiation in the forward direction is comparable to the backfire radiation when the pitch angle is 5° at an operating frequency of 5.0 GHz: although the field strength in the backward direction is slightly greater than that of the forward direction. This observation can be attributed to the strong standing wave nature of the antenna current shown in Figure 2(a). When the frequency is increased to 6.0 GHz at the same pitch angle, the level of the forward radiation reduces considerably as revealed in Figure 5(b), because of the marked suppression of the reflected current

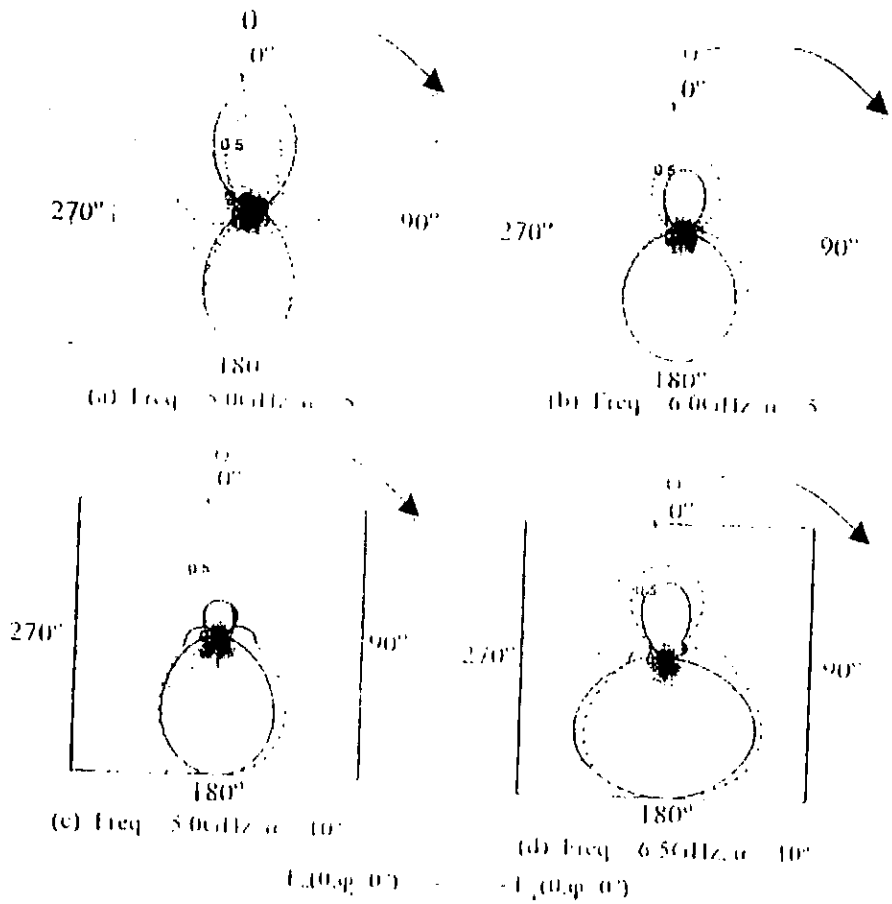

Figure 5: *Typical far-zone electric field patterns on φ = 0° plane, α: 5° – 10°*

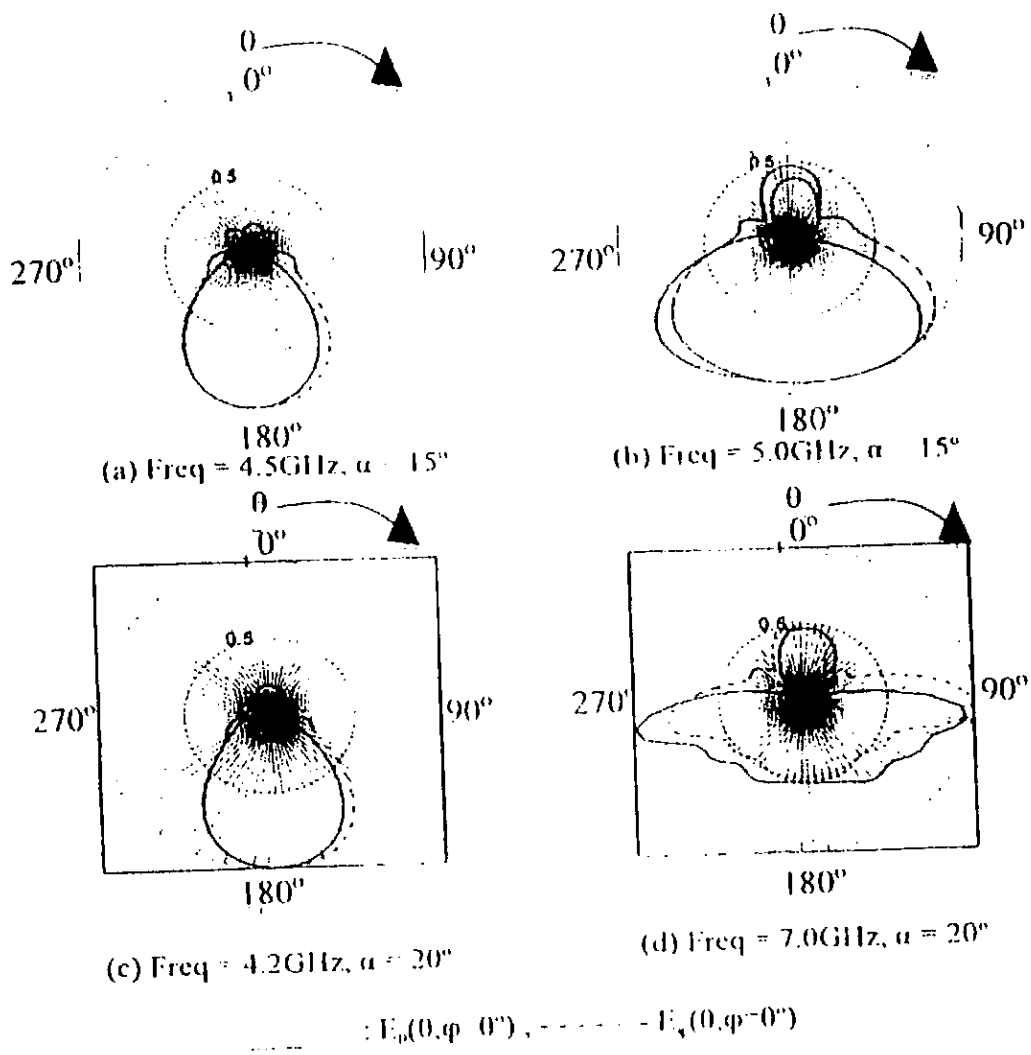

Figure 6: *Typical far-zone electric field patterns on* $\varphi = 0°$ *plane,* α, 15° - 20°

amplitude as displayed in Figure 2(b). At a pitch angle of 10°, the radiation in the forward direction at a frequency of 5.0 GHz is lower compared with that at 6.5 GHz, due to the appearance of the surface wave region in the current distribution at 6.5 GHz as shown in Figure 2(d). In addition, the half power beamwidth of the backfire radiation is smaller at 5.0 GHz than at 6.5 GHz based on Figures 6(c) -(d). We also find that for a value of $\alpha = 15°$, the patterns are mainly backward endfire; although a broader backward pattern is indicated for the frequency 5.0 GHz as against the pattern at frequency 4.5 GHz as can be seen from Figures 6(a)-(b). Interestingly, the patterns

for (frequency = 4.5 GHz, α = 15°) and (frequency = 4.2 GHz, α = 20°) are almost identical as revealed by Figures 6(a) and (c). The doughnut-shape associated with the backward radiation is severely distorted when f =7.0 GHz and α = 20° as shown in Figure 6(d), suggesting that the antenna may not be suitable as a primary feed for a paraboloidal antenna when operated at 7.0 GHz.

5. ON THE EXCITATION OF A MONOFILAR HELICAL ANTENNA WITHOUT A GROUND PLANE

Although a ground plane is conventionally employed in the feeding arrangement of a monofilar helical antenna, as first demonstrated by Kraus [1947], some means of exciting a monofilar helical antenna without a ground plane have since been devised and used in practice [9], [14]. Such antennas, for which the ground plane is excluded in the feeding configuration of a monofilar helix, were shown to radiate predominantly in the backfire direction. Among the methods conceived for feeding a monofilar helix without a ground plane are the two techniques described in what follows. First is that due to Johnson and Cotton [14], in which the helical wire is curled around a rigid coaxial transmission line and excited by a 50 Ω-transmission line via a combination of a two-stage transformer, which is embedded in the rigid coaxial transmission line, and a two-wire balun made of wires of different sizes.

The other is that due to Patton [9], where the feeding arrangement entails bonding the inner conductor of a microdot cable, used for the excitation of the antenna, to the centre of a 10cm long wire on the helix axis, while the outer conductor is connected to the helix feed-point. In the delta-gap model adopted in this presentation for that feeding arrangement, two short segments adjacent to the feed point are appended to the origin of the monofilar helix so that the peak of the first basis (triangle) function corresponds to the excitation point.

When it becomes desirable to utilise a helical antenna fed without a ground plane, it is fundamental to adequately address the problem of providing a suitable counterpoise. Different feeding arrangements have been specified for the monofilar helical antenna [Kraus, 1988]. A particularly instructive solution to the problem of providing a suitable counterpoise has been offered in a recent contribution by Kraus [1995]. In that experimental investigation, the helical antenna was mounted on a pole, and fed from a configuration of three circular loops of wire of diameter equal to that of the helix wire.

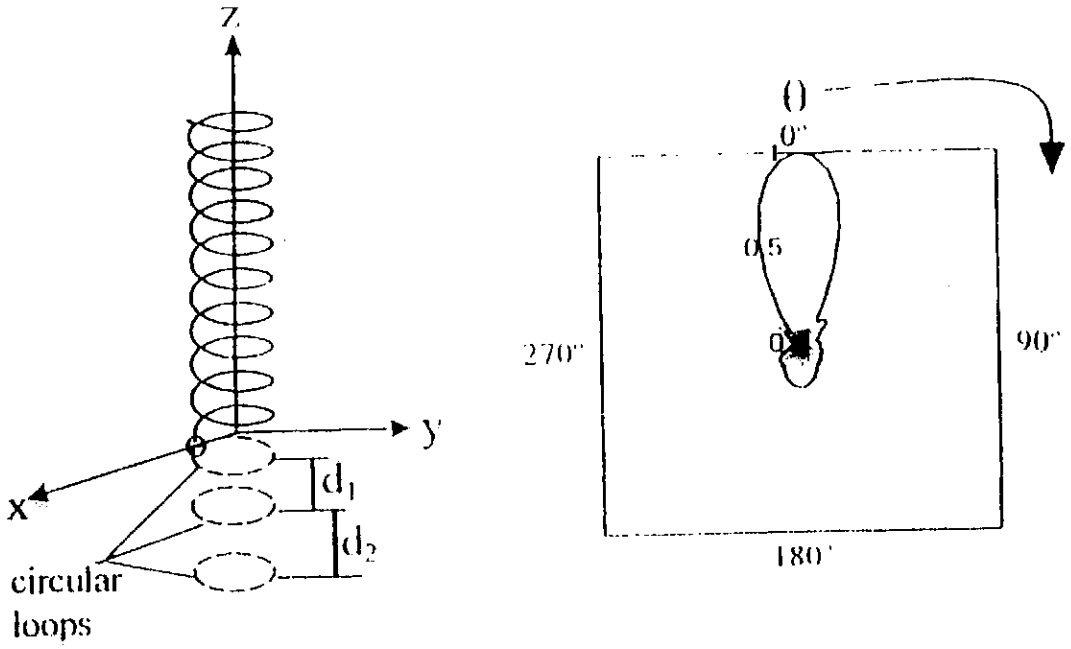

Figure 7: *A 10-turn helical antenna backed by circular loops and its radiated power pattern in the $\varphi = 0^{o}$ plane*

Kraus, [1995], reported certain advantages, which can be expected from the pole-mounted helix, and described a number of practical applications. The distances d_1 and d_2 between the loops assume the following ranges: $\frac{1}{3}\lambda \le d_1 \le \frac{1}{2}\lambda$ and $d_1 \le d_2 \le 1\lambda$ where d_1 is the separation between the first two loops while d_2 is the distance between the second and third loops, and λ denotes the wavelength at the operating frequency. Pattern measurements reported by Kraus of the helix backed by circular loops show that it performs equivalently as the helix backed by a plane reflector, in the sense that a forward endfire radiation is generated. However, the side-lobes are somewhat stronger in this case. In this paper, the moment-method based computer program developed for the analysis of a monofilar helical antenna without a ground plane was specialised to enable an analysis of the pole-mounted helical antenna, as described by Kraus [1995]. The simulated pattern of the loops-backed helix, displayed in Figure 7, shows that the antenna radiates principally in the forward endfire direction as expected, but with side lobes, which are less pronounced than the side-lobes of the experimental pattern reported by Kraus.

6. CONCLUSION

In this paper, the current distributions and the associated far-zone electric fields of a thin-wire helical antenna without a ground plane are determined using the method of moments, with piecewise linear basis and testing functions. Results reported indicate that unlike the small-ground plane monofilar helical antenna, which also radiates in the backfire direction, current distribution on the ground planeless helical antenna is significantly affected by the pitch angle. The radiated fields computed show that the antenna radiates principally in the backfire direction which is consistent with expectations due to experimental results earlier reported in the literature.

7. REFERENCES

[1] Kraus, J.D. (1988). *Antennas*, McGraw-Hill Inc. USA, Second edition, Chap. 7, pp 265-339.

[2] Lazzi, G., and Gandhi, O.P. (1998). "On modeling and personal dosimetry of cellular telephone helical antennas with the FDTD code". *IEEE Trans.*, **AP-46**, (1), pp.525-530.

[3] Kraus, J.D. (1947). "Helical beam antenna". *Electronics*, **20**, April, pp.109-111.

[4] King, H.E., and Wong, J.L. (1980). "Characteristics of 1 to 8 wavelength uniform helical antennas". *IEEE Trans.*, **AP-28**, pp. 291-296.

[5] Kraus, J.D., and Williamson, J.C. (1948). "Characteristics of helical antennas radiating in the axial mode". *Journal of Applied Physics*, **19**, pp.87-96.

[6] Kornhauser, E.T. (1951). "Radiation field of helical antennas with sinusoidal current". *Journal of Applied Physics*, **22**, pp. 887-891.

[7] Nakano, H., Samada, Y., and Yamauchi, J. (1986). "Axial mode helical antennas". *IEEE Trans.*, **AP-34**, pp. 1143-1148.

[8] Nakano,H., Yamauchi, J., and Mimaki, H. (1988). "Backfire radiation from a monofilar helix with a small ground plane". *IEEE Trans.*, **AP-36**, pp. 1359-1364.

[9] Patton, W.T. (1963). "The backfire bifilar helical antenna". *Ph.D. Thesis*, University of Illinois.

[10] Kilgus, C.C. (1968) "Multi element, fractional turn helices". *IEEE Trans.*, **AP-16**, pp. 499-500.

[11] Harrington, R.F. (1968). *Field computation by moment methods* The Macmillan Company, New York.

[12] Adekola, S.A., and Okereke, O.U. (1989). "Analysis of a circular-loop antenna using moment methods". *Int'l.J. Elec.*, **66**, pp.821-834.

[13] Kuo, D.C., and Strait, B.J. (1972). "Improved programs for analysis of radiation and scattering by configurations of arbitrarily bent wires". *Syracuse University Scientific Report* **No. 15,** 50pp.

[14] Johnson, R.C., and Cotton, R.B. (1984). "A backfire helical feed". *IEEE Trans.*, AP-32, No. 10, pp. 1126-1128.

[15] Adekola, S.A., and Ayorinde, A.A. (2001). "Effects of centre-excitation on the radiation mechanism of helical antennas employed in communication satellites". *JER-8*, Nos. 1& 2, pp 1-20.

[16] Kraus, J.D. (1995). "A helical-beam antenna without a ground plane". *IEEE A&P Mag.*, Vol.37, (2), p.45.

APPENDIX II:

FORTRAN 77 COMPUTER PROGRAMS FOR THIN-WIRE ANTENNA DESIGNS

```
C       THIS NUMERICAL ELECTROMAGNETIC CODES (NEC) COMPUTES THE CURRENT
        DISTRIBUTIONS, RADIATED FIELDS, INPUT IMPEDANCE, INPUT POWER, AXIAL
        RATIO (dB), FRONT-TO-BACK RATIO, AND DIRECTIVE GAIN (dB) OF THIN-WIRE
        HELICAL ANTENNAS OPERATING IN FREE SPACE.


          SUBROUTINE ROW(N,TH,PH,E)
C     THIS SUBROUTINE COMPUTES THE RADIATION FIELD (THETA- AND PHI
C     COMPONENTS) OF ARBITRAIRLY SHAPED THIN-WIRE ANTENNAS IN
      FREE-SPACE

      COMPLEX C(200),E(2),U,U1,U2,U3,U4,U5
      COMMON XX(270),XY(270),XZ(270),TX(270),TY(270),TZ(270),AL(270)
      COMMON T(700),TP(700),BK,RAD2(13),L(13),LR(13)/COA/C
      DIMENSION BKR(800),DT(800),DP(800)
      U=(0.0,1.0)
      ETA=376.7307
      CT=COS(TH)
      ST=SIN(TH)
      CP=COS(PH)
      SP=SIN(PH)
      S1=CT*CP
      S2=CT*SP
      BK1=BK*ST*CP
      BK2=BK*ST*SP
      BK3=BK*CT
      N2=1
      N3=-2
      DO 1 NS =1,N
      IF (L(N2)-NS)2,3,2
3     KK=1
      N3=N3+2
      N2=N2+1
      GO TO 4
2     KK=3
4     DO 5 K=KK,4
      N7=N3+K
      BKR(N7)=XX(N7)*BK1+XY(N7)*BK2+XZ(N7)*BK3
      DT(N7)=TX(N7)*S1+TY(N7)*S2-TZ(N7)*ST
      DP(N7)=-TX(N7)*SP+TY(N7)*CP
5     CONTINUE
      N3=N3+2
1     CONTINUE
      N2=1
      N3=-2
      U3=0.0
      U4=0.0
      DO 6 NS=1,N
      IF (L(N2)-NS)7,8,7
8     N3=N3+2
      N2=N2+1
7     J1=(NS-1)*4
      U1=0.0
      U2=0.0
      DO 9 JS=1,4
      J2=J1+JS
      J3=N3+JS
      S1=BKR(J3)
      U5=T(J2)*(COS(S1)+U*SIN(S1))
```

```
      U1=U1+U5*DT(J3)
      U2=U2+U5*DP(J3)
9     CONTINUE
      U3=U3+U1*C(NS)
      U4=U4+U2*C(NS)
      N3=N3+2
6     CONTINUE
      S1=0.0795774*ETA*BK
      E(1)=-U*S1*U3
      E(2)=-U*S1*U4
      RETURN
      END


      SUBROUTINE CALZ(N,N1,Z)
C     THIS SUBROUTINE CALCULATES THE GENERALIZED IMPEDANCE
      MATRIX
C     ELEMENTS OF ARBITRAILY THIN-WIRE ANTENNAS IN FREE-SPACE

      COMPLEX Z(15000),PSI(7500),U,U1,U2,U3,U4,U5,U6
      COMMON XX(270),XY(270),XZ(270),TX(270),TY(270),TZ(270),AL(270)
      COMMON T(700),TP(700),BK,RAD2(13),L(13),LR(13)
      DIMENSION DC(7500)
      U=(0.0,1.0)
      PI=3.1414593
      ETA=376.7307
      C1=0.125/PI
      C2=0.25/PI
      J1=1
      J2=-2
      DO 1 J=1,N
      IF (L(J1)-J)3,4,3
4     J2=J2+2
      J1=J1+1
3     J3=(J-1)*4
      J4=J3+1
      J5=J4+1
      J6=J5+1
      J7=J6+1
      K4=J2+1
      K5=K4+1
      K6=K5+1
      K7=K6+1
      S1=AL(K4)+AL(K5)
      S2=AL(K6)+AL(K7)
      T(J4)=AL(K4)*.5*AL(K4)/S1
      T(J5)=AL(K5)*(AL(K4)+.5*AL(K5))/S1
      T(J6)=AL(K6)*(AL(K7)+.5*AL(K6))/S2
      T(J7)=AL(K7)*.5*AL(K7)/S2
      TP(J4)=AL(K4)/S1
      TP(J5)=AL(K5)/S1
      TP(J6)=-AL(K6)/S2
      TP(J7)=-AL(K7)/S2
      J2=J2+2
1     CONTINUE
      U3=U*BK*ETA
      U4=-U/BK*ETA
      BK2=BK*BK/2.
      BK3=BK2*BK/3.
```

```
      N9=0
      N2=1
      N0=1
      N3=-2
      DO 10 NS=1,N
      IF (L(N2)-NS)12,11,12
11     KK=1
      N3=N3+2
      N2=N2+1
      GO TO 13
12     KK=3
      DO 14 NF=1,N1
      N4=NF+N1
      N5=N4+N1
      N6=N5+N1
      DC(NF)=DC(N5)
      DC(N4)=DC(N6)
      PSI(NF)=PSI(N5)
      PSI(N4)=PSI(N6)
14     CONTINUE
13     IF (N3+1-LR(N0))5,6,5
6     AA=RAD2(N0)
      N0=N0+1
5     CONTINUE
      DO 15 K=KK,4
      N7=N3+K
      K1=(K-1)*N1
      DO 16 NF=1,N1
      N8=NF+K1
      S1=XX(N7)-XX(NF)
      S2=XY(N7)-XY(NF)
      S3=XZ(N7)-XZ(NF)
      R2=S1*S1+S2*S2+S3*S3+AA
      R=SQRT(R2)
      RT=ABS(S1*TX(N7)+S2*TY(N7)+S3*TZ(N7))
      RT2=RT*RT
      RH=(R2-RT2)
      ALP=0.5*AL(N7)
      AR=ALP/R
      S1=BK*R
      U2=COS(S1)-U*SIN(S1)
      IF (AR-0.1)22,22,21
21     U2=U2*C1/ALP
      S1=RT-ALP
      S2=RT+ALP
      S3=SQRT(S1*S1+RH)
      S4=SQRT(S2*S2+RH)
      IF (S1) 18,18,19
18     AI1=ALOG((S2+S4)*(-S1+S3)/RH)
      GO TO 20
19     AI1=ALOG((S2+S4)/(S1+S3))
20     AI2=AL(N7)
      AI3=(S2*S4-S1*S3+RH*AI1)/2.0
      AI4=AI2*(RH+ALP*ALP/3.+RT2)
      S3=AI1*R
      S1=AI1-BK2*(AI3-R*(2.0*AI2-S3))
      S2=-BK*(AI2-S3)+BK3*(AI4-3.*AI3*R+R2*(3.*AI2-S3))
      GO TO 28
22     U2=U2*C2/R
```

```
      BA=BK*ALP
      BA2=BA*BA
      AR2=AR*AR
      AR3=AR2*AR
      ZR=RT/R
      ZR2=ZR*ZR
      ZR3=ZR2*ZR
      ZR4=ZR3*ZR
      H1=(3.-30.*ZR2+35.*ZR4)*AR3/40.
      A1=AR*(-1.+3.*ZR2)/6.+(3.-30.*ZR2+35.*ZR4)*AR3/40.
      A0=1.+AR*A1
      A2=-ZR2/6.-AR2*(1.-12.*ZR2+15.*ZR4)/40.
      A3=AR*(3.0*ZR2-5.*ZR4)/60.
      A4=ZR4/120.
      S1=A0+BA2*(A2+BA2*A4)
      S2=BA*(A1+BA2*A3)
28     PSI(N8)=U2*(S1+U*S2)
      DC(N8)=TX(NF)*TX(N7)+TY(NF)*TY(N7)+TZ(NF)*TZ(N7)
16     CONTINUE
15     CONTINUE
      N3=N3+2
      J3=(NS-1)*4
      J7=-2
      J9=1
      DO 25 NF=1,N
      J1=(NF-1)*4
      IF (L(J9)-NF)26,27,26
27     J9=J9+1
      J7=J7+2
26     N9=N9+1
      U5=0.0
      U6=0.0
      J5=0
      DO 23 JS=1,4
      J4=J3+JS
      J8=J5+J7
      DO 24 JF=1,4
      J6=J8+JF
      J2=J1+JF
      U5=T(J2)*T(J4)*DC(J6)*PSI(J6)+U5
      U6=TP(J2)*TP(J4)*PSI(J6)+U6
24     CONTINUE
      J5=J5+N1
23     CONTINUE
      Z(N9)=U5*U3+U6*U4
      J7=J7+2
25     CONTINUE
10     CONTINUE
      RETURN
      END

      SUBROUTINE LINEQ(N,Z)
C          THIS SUBROUTINE INVERTS THE GENERALIZED IMPEDANCE MATRIX GENERATED
         BY THE SUBROUTINE CALZ

      COMPLEX Z(15000),STOR,STO,ST,S
      DIMENSION LA(500)
      DO 20 I=1,N
      LA(I)=I
```

```
20    CONTINUE
      M1=0
      DO 18 M=1,N
      K=M
      DO 2 I=M,N
      K1=M1+I
      K2=M1+K
      IF (CABS(Z(K1))-CABS(Z(K2)))2,2,6
6     K=I
2     CONTINUE
      LS=LA(M)
      LA(M)=LA(K)
      LA(K)=LS
      K2=M1+K
      STOR=Z(K2)
      J1=0
      DO 7 J=1,N
      K1=J1+K
      K2=J1+M
      STO=Z(K1)
      Z(K1)=Z(K2)
      Z(K2)=STO/STOR
      J1=J1+N
7     CONTINUE
      K1=M1+M
      Z(K1)=1./STOR
      DO 11 I=1,N
      IF (I-M)12,11,12
12    K1=M1+I
      ST=Z(K1)
      Z(K1)=0.0
      J1=0
      DO 10 J=1,N
      K2=J1+M
      K1=J1+I
      Z(K1)=Z(K1)-Z(K2)*ST
      J1=J1+N
10    CONTINUE
11    CONTINUE
      M1=M1+N
18    CONTINUE
      J1=0
      DO 9 J=1,N
      IF (J-LA(J))14,8,14
14    LAJ=LA(J)
      J2=(LAJ-1)*N
31    DO 13 I=1,N
      K2=J2+I
      K1=J1+I
      S=Z(K2)
      Z(K2)=Z(K1)
      Z(K1)=S
13    CONTINUE
      LA(J)=LA(LAJ)
      LA(LAJ)=LAJ
      IF (J-LA(J))14,8,14
8     J1=J1+N
9     CONTINUE
      RETURN
```

```
      END


        SUBROUTINE ARATIO(N)
C       THIS SUBROUTINE DETERMINES THE AXIAL RATIO OF THE RADIATED FIELD
        WITHOUT ASSUMING TIME-PHASE QUADRATURE BETWEEN THE FIELD
        COMPONENETS

      COMPLEX E(2)
      N=N
      PIX=3.14159/180.
      TH=180.*PIX
      PH=0.*PIX
      CALL ROW(N,TH,PH,E)
      A=CABS(E(1))
      B=CABS(E(2))
      ATH=ATAN2(AIMAG(E(1)),REAL(E(1)))
      APH=ATAN2(AIMAG(E(2)),REAL(E(2)))
      ANG=0.5*ATAN((2.*A*B*COS(APH-ATH))/(A**2-B**2))
      ANU=(B**2)*(SIN(ANG))**2+(A**2)*(COS(ANG))**2+
     / A*B*COS(APH-ATH)*SIN(2.*ANG)
      ADE=(B**2)*(COS(ANG))**2+(A**2)*(SIN(ANG))**2-
     / A*B*COS(APH-ATH)*SIN(2.*ANG)
      AX=SQRT(ANU/ADE)
      ARN18=ABS(20.*ALOG10(AX))
      ANU=SQRT(0.5*(A**2+B**2+SQRT(A**4+B**4+2.*A**2*
     / B**2*COS(2.*(APH-ATH)))))
      ADE=SQRT(0.5*(A**2+B**2-SQRT(A**4+B**4+2.*A**2*
     / B**2*COS(2.*(APH-ATH)))))
      AX=ANU/ADE
      ARB18=ABS(20.*ALOG10(AX))
      AR=A/B
      AR18=ABS((ALOG10(AR)*20.))
      WRITE(6,310)AR18,ARB18,ARN18
310   FORMAT('AR180=',2X,F10.5,/,2X,'ARB180=',2X,F10.5,/,
     / 'ARN180=',2X,F10.5,3X,//)
      TH=0.0*PIX
      PH=0.0*PIX
      CALL ROW(N,TH,PH,E)
      C=CABS(E(1))
      D=CABS(E(2))
      ATH=ATAN2(AIMAG(E(1)),REAL(E(1)))
      APH=ATAN2(AIMAG(E(2)),REAL(E(2)))
      ANG=0.5*ATAN((2.*C*D*COS(APH-ATH))/(C**2-D**2))
      ANU=(D**2)*(SIN(ANG))**2+(C**2)*(COS(ANG))**2+
     / C*D*COS(APH-ATH)*SIN(2.*ANG)
      ADE=(D**2)*(COS(ANG))**2+(C**2)*(SIN(ANG))**2-
     / C*D*COS(APH-ATH)*SIN(2.*ANG)
      AX=SQRT(ANU/ADE)
      ARN0=ABS(20.*ALOG10(AX))
      ANU=SQRT(0.5*(C**2+D**2+SQRT(C**4+D**4+2.*C**2*
     / D**2*COS(2.*(APH-ATH)))))
      ADE=SQRT(0.5*(C**2+D**2-SQRT(C**4+D**4+2.*C**2*
     / D**2*COS(2.*(APH-ATH)))))
      AX1=ANU/ADE
      ARB0=ABS(20.*ALOG10(AX1))
      ARR=C/D
      AR0=ABS((ALOG10(ARR)*20.))
```

```
      WRITE(6,300)AR0,ARN0,ARB0
300   FORMAT('AR0=',2X,F10.5,2X,/,2X,'ARN0=',2X,F10.5,/
     / 'ARB0=',2X,F12.5,3X,/,/)
      RETURN
      END


      SUBROUTINE FBRATI(N)
C          THIS SUBROUTINE EVALUATES THE FRONT-TO-BACK RATIO OF THE RADIATION
           FIELD INTENSITY

      COMPLEX E(2)
      N=N
      PIX=3.14159/180.
      THF=0.*PIX
      PHF=0.*PIX
      CALL ROW(N,THF,PHF,E)
      A=CABS(E(1))
      B=CABS(E(2))
      THB=180.*PIX
      PHB=0.*PIX
      CALL ROW(N,THB,PHB,E)
      C=CABS(E(1))
      D=CABS(E(2))
      FB=(A**2+B**2)/(C**2+D**2)
      FBDB=(10.*ALOG10(FB))
      WRITE(6,301)FB,FBDB
301   FORMAT(3X,'FB=',3X,F10.5,/,3X,'FBDB=',3X,F10.5,/)
      RETURN
      END


      SUBROUTINE POGAIN(N,POWER,DIS)
C          THIS SUBROUTINE EVALUATES THE DIRECTIVE GAIN OF THE THIN-WIRE
           ANTENNA.

      COMPLEX E(2)
      PIX=3.14159/180.
      TH=180.*PIX
      PH=0.*PIX
      CALL ROW(N,TH,PH,E)
      A=CABS(E(1))
      B=CABS(E(2))
      C=A**2+B**2
      POG=C/(60.*POWER)
      POGDB=10.*ALOG10(POG)
      POG2=(C*DIS**2)/(60.*POWER)
      POG2DB=10.*ALOG10(POG2)
      WRITE(6,20)POGDB,POG2DB
20    FORMAT(//,'POWER GAIN (R NORMALIZED) =',F10.5,//,
     / 'POWER GAIN = ',2X,F10.5,//)
      RETURN
      END


      C*******************************************************************
C     THE MAIN PROGRAM FOR THE THIN WIRE HELICAL ANTENNA FED WITHOUT A
GROUND PLANE (EXCLUSION-MODE HELIX)
C*******************************************************************
```

```
      COMPLEX Z(6400),U(80),C(80),E(3),EI(2),UV(4),U1,ZL,ZIN,YIN,V
      COMMON XX(165),XY(165),XZ(165),TX(165),TY(165),TZ(165),AL(165)
      COMMON T(1600),TP(1600),BK,RAD2(10),L(5),LR(10)/COA/C
      DIMENSION PX(165),PY(165),PZ(165),LL(5),RAD(10),IFP(80),EN(80)
      DIMENSION CM(80),CP(80),ENOR(80)
      OPEN(5,FILE='JANO1.DAT')
      OPEN(6,FILE='X15F145.OUT')
C     NW--TOTAL NUMBER OF DIFFERENT WIRES IN THE PROBLEM GEOMETRY
C     NP--NUMBER OF POINTS DEFINING THE GEOMETRY OF THE WIRE
C     NR--TOTAL NUMBER OF DIFFERENT WIRE RADII ENCOUNTERED IN CONSIDERING
C     THE SEGMENTS CONSECUTIVELY
      READ(5,144)NW,NR
 144   FORMAT(2I2)
 143   FORMAT(//,'NW  NR  ',//2(I2,2X))
      PI=3.141592654
      WRITE(6,143)NW,NR
C     PX(I),PY(I),& PZ(I)  ARE THE XYZ CO-ORDINATES OF THE PTS DEFINING
C     THE PROBLEM GEOMETRY
      NTURNS=7
      PANGLE=15.
      PITAN=(PANGLE*PI)/180.0
      FREQ=14.5E+09
      WAVEL=300E+06/FREQ
      ECC=0.0
C     CIRWA=1.00
      CIRWA=(2.5E-02)/WAVEL
      CIR=CIRWA*WAVEL
      RA=CIR/(2.0*PI)
      SPAC=CIR*TAN(PITAN)
      SPAC1=CIRWA*TAN(PITAN)
      PIE=(2.*PI)/12.
      DISK=SQRT(CIR**2+SPAC**2)
      DISA=NTURNS*(SQRT(CIR**2+SPAC**2))
      DIS=(2.*DISA**2)/WAVEL
      DO 49 KK=1,2
      PX(KK)=0.0
      PY(KK)=0.0
 49   CONTINUE
      PZ(1)=-(SPAC/12.)*2.
      PZ(2)=-(SPAC/12.)*1.
      DO 46 KK=3,15
      PX(KK)=RA*COS((KK-3)*PIE)
      PY(KK)=RA*SQRT(1.0-ECC**2)*SIN((KK-3)*PIE)
      PZ(KK)=(SPAC/(2.*PI))*((KK-3)*PIE)
 46   CONTINUE
      NP=NTURNS*12+3
      NJ=NP-15
      DO 47 II=1,NJ
      NA=II+15
      PX(NA)=PX(II+3)
      PY(NA)=PY(II+3)
      PZ(NA)=PZ(II+3)+SPAC
 47   CONTINUE
      PX(3)=0.0
      PY(3)=0.0
      PZ(3)=0.0
      WRITE(6,250)CIRWA,SPAC1,PITAN,FREQ,NTURNS
 250   FORMAT(//,'CIRCUMFERENCE (IN WAVELENGTHS) =',2X,F9.5,
```

```
     1 //,'SPACING (IN WAVELENGTHS) =',2X,F9.5,
     1 //,'PITCH ANGLE (IN RADIANS) =',2X,F9.5,
     1 //,'OPERATING FREQUENCY =',2X,E13.7,
     1 //,'NUMBER OF TURNS =',2X,I2,//)
       ALEN=(SQRT(CIR**2+SPAC**2))*NTURNS
       BK=(2.*PI)/WAVEL
       WRITE(6,255)ALEN
 255   FORMAT(2X,'ARM LENGTH=',2X,F9.4,'M',//)
C      NSEG: NUMBER OF SEGMENTS PER TURN = 12
C      NP=TOTAL NUMBER OF POINTS DESCRIBING THE PROBLEM GEOMETRY
       WRITE(6,280)
 280   FORMAT(//,'COORDINATES OF THE POINTS (IN METRES) DEFINING
     1 THE PROBLEM GEOMETRY',///)
       WRITE(6,701)
 701   FORMAT(30X,'PX',//)
       WRITE(6,104)(PX(I),I=1,NP)
       WRITE(6,702)
 702   FORMAT(30X,'PY',//)
       WRITE(6,104)(PY(I),I=1,NP)
       WRITE(6,703)
 703   FORMAT(30X,'PZ',//)
       WRITE(6,104)(PZ(I),I=1,NP)
 104   FORMAT(8(F8.5,2X))
C      LL(NW+1)--A CLM. MATRIX CONTAINING THE NUMBERS OF FIRST PTS.
C      OF DIFFERENT WIRES
       READ(5,146)(LL(I),I=1,NW)
 146   FORMAT(20I2)
       WRITE(6,147)(LL(I),I=1,NW)
 147   FORMAT(/,'LL',/(1X,10I4))
       LL(NW+1)=200
C      LR(NR+1)--A CLM. MATRIX CONTAINING THE NUMBERS OF THE SEGMENTS
C      AT WHICH CHANGES IN RADIUS OCCUR
       READ(5,146)(LR(I),I=1,NR)
       WRITE(6,148)(LR(I),I=1,NR)
 148   FORMAT(/,'LR',/(1X,10I4))
       LR(NR+1)=200
C      RAD(I)--WIRE RADII
       READ(5,149)(RAD(I),I=1,NR)
 149   FORMAT(5E14.7)
       WRITE(6,150)(RAD(I),I=1,NR)
 150   FORMAT(/,'RAD',/5E14.7)
C      NUMBER OF DISCRETE LOAD IMPEDANCE
       DO 50 I=1,NR
       RAD2(I)=RAD(I)*RAD(I)
 50    CONTINUE
       J1=1
       J2=2
       N1=0
       DO 2 J=1,NP
       IF (LL(J1)-J)3,4,3
 4     J2=J2-1
       L(J1)=J2
       J1=J1+1
       GO TO 2
 3     N1=N1+1
       J3=J-1
       IF ((N1/2*2-N1).EQ. 0)J2=J2+1
C      XX,XY,&XZ--CLM. MATRICES CONTAINING THE X,Y,&Z CO-ORDINATES
C      OF THE SEGMENTS CENTER POINTS
```

```
      XX(N1)=0.5*(PX(J)+PX(J3))
      XY(N1)=0.5*(PY(J)+PY(J3))
      XZ(N1)=0.5*(PZ(J)+PZ(J3))
      S1=PX(J)-PX(J3)
      S2=PY(J)-PY(J3)
      S3=PZ(J)-PZ(J3)
      S4=SQRT(S1*S1+S2*S2+S3*S3)
C     XX,XY,& XZ--X,Y,& Z COMPONENTS OF THE UNIT TANGENTIAL VECTOR
C     AT THE MID-POINTS OF THE STRAIGHT WIRE SEGMENTS
      TX(N1)=S1/S4
      TY(N1)=S2/S4
      TZ(N1)=S3/S4
C     AL--CLM. MATRIX CONTAINING SEGMENT LENGTHS
      AL(N1)=S4
 2    CONTINUE
C     L(I)--INDICATES THAT F(L(I)) IS THE FIRST EXPANSION FUNCTION ON
C     THE I-TH WIRE
      L(J1)=J2
C     N--NUMBER OF EXPANSION FUNCTIONS
C     N1--TOTAL NUMBER OF STRAIGHT SEGMENT WIRES
C     Z--GENERALIZED IMPEDANCE MATRIX OF ORDER N
      N=J2-2
      CALL CALZ(N,N1,Z)
      READ(5,78)NL
 78   FORMAT(I2)
      WRITE(6,79)NL
 79   FORMAT(/,'NL=',2X,I2)
      IF (NL)42,42,41
 41   WRITE(6,118)NL
 118  FORMAT(1X,'NL'/I3/'LP   LOAD')
C     ZL--LOAD IMPEDANCE IN OHMS
      DO 43 I=1,NL
      READ (5,119)LP,ZL
 119  FORMAT(I3,2E13.6)
      WRITE(6,120)LP,ZL
 120  FORMAT(1X,I3,2E13.6,/)
      J2=(LP-1)*N+LP
      Z(J2)=Z(J2)+ZL
 43   CONTINUE
 42   CALL LINEQ(N,Z)
      DO 45 I=1,N
      U(I)=0.0
 45   CONTINUE
C     FP --FEED POINT
      READ(5,107)NF
      WRITE(6,108)NF
 108  FORMAT(/,'NF=',2X,I2,/'FP          VOLTAGE',/)
 107  FORMAT(I2)
      DO 51 I=1,NF
      READ(5,52)J1,V
      WRITE(6,53)J1,V
      U(J1)=V
      IFP(I)=J1
 51   CONTINUE
 52   FORMAT(I2,2E13.7)
 53   FORMAT(//,I2,3X,2(E13.7,2X))
      WRITE(6,704)
 704  FORMAT('          CURRENT  DISTRIBUTION',//)
C     WRITE(6,111)
```

```
C111   FORMAT(2X,'I',7X,' MAGNITUDE',9X,
C    1 'PHASE',4X,'IMAGE PHASE',/)
      J3=0
      J1=0
 5     J1=J1+1
      U1=0.0
      J2=0
 6     J2=J2+1
      J3=J3+1
      U1=U1+Z(J3)*U(J2)
      IF (J2-N)6,7,7
 7     C(J1)=U1
      IF (J1-N)5,8,8
 8     CONTINUE
      DO 9 I=1,N
      U1=C(I)
      CM(I)=CABS(U1)
      IF (CM(I))11,12,11
 11     CP(I)=ATAN2(AIMAG(U1),REAL(U1))*57.2858
      GO TO 10
 12     CP(I)=0.0
 10     CONTINUE
C      WRITE(6,112)I,CM,CP
C112   FORMAT(1X,I2,5X,E15.5,5X,F8.3,6X,F8.3)
 9     CONTINUE
      WRITE(6,391)
 391    FORMAT(//,2X,'I',/)
      DO 400 NB=1,N
      ARML=ALEN*FLOAT(NB-1)*2.0/(FLOAT(NP-3))
      WRITE(6,401)ARML
 401    FORMAT(2X,F9.4)
 400    CONTINUE
      WRITE(6,692)
 692    FORMAT(//,2X,'REAL COMP. OF CURRENT',/)
      DO 602 NB=1,N
      WRITE(6,603)REAL(C(NB))*1000.
 603    FORMAT(2X,F11.6)
 602    CONTINUE
      WRITE(6,604)
 604    FORMAT(//2X,'IMAGNINARY COMP OF CURRENT',/)
      DO 605 NB=1,N
      WRITE(6,606)AIMAG(C(NB))*1000.
 606    FORMAT(2X,F11.6)
 605    CONTINUE
      WRITE(6,392)
 392    FORMAT(//,2X,'CURRENT MAGNITUDE',/)
      DO 402 NB=1,N
      WRITE(6,403)CM(NB)*1000.
 403    FORMAT(2X,F11.6)
 402    CONTINUE
      WRITE(6,393)
 393    FORMAT(2X,/,'PHASE OF CURRENT DISTRIBUTION',/)
      DO 404 NB=1,N
      WRITE(6,405)CP(NB)
 405    FORMAT(3X,F9.3)
 404    CONTINUE
 55     POWER=0.0
      DO 23 I=1,NF
      J1=IFP(I)
```

```
      ZIN=U(J1)/C(J1)
      WRITE(6,122)J1,ZIN
122   FORMAT(1X,'INPUT IMPEDANCE AT POSITION',I3,'=(',2(E14.7,2X),')'
     1 ,/1X,/)
      GM=CABS(ZIN)
      IF (GM-0.1E-6)24,24,25
25    YIN=1.0/ZIN
      WRITE(6,123)J1,YIN
123   FORMAT(1X,'INPUT ADMITTANCE AT POSITION',I3,'=(',2(E14.7,2X),')'
     1 ,///)
24    S1=REAL(ZIN)
      S2=CABS(C(J1))
      POWER=POWER+0.5*S2*S2*S1
23    CONTINUE
      WRITE(6,124)POWER
124   FORMAT(1X,'TOTAL POWER INPUT=',E14.7,1X,'W',/)
      WRITE(6,113)
113   FORMAT(1X,'EM-MODE FIELD PATTERN',//1X,'K=1 FOR THETA COMPONENT'
     1,//1X, 'K=2 FOR PHI COMPONENT',//,1X,'THETA',4X,'PHI',4X,'K',7X,
     1'MAGNITUDE',8X,'PHASE',/)
      WRITE(6,1131)
1131  FORMAT(//,1X,'THETA',4X,'PHI',12X,6X,
     1'MAGNITUDE',8X,'PHASE',//)
      DO 83 LK=1,91,90
      PHI=FLOAT(LK-1)
      DO 16 K=1,2
      KK=1
      PH=PHI*0.0174533
      DO 17 ITH=1,361,5
      THE=FLOAT(ITH-1)
      TH=THE*0.0174533
      CALL ROW (N,TH,PH,E)
      U1=E(K)
      GM=CABS(U1)
      EN(KK)=GM
      IF (GM) 13,13,14
14    EP=ATAN2(AIMAG(U1),REAL(U1))
      GO TO 15
13    EP=0.0
15    GP=EP*57.2858
      KK=KK+1
C     WRITE(6,114)THE,PHI,K,GM,GP
114   FORMAT(1X,F6.2,2X,F6.2,2X,I3,3X,E12.7,3X,F8.3)
17    CONTINUE
      EMAX=EN(1)
      DO 18 I=2,KK-1
      IF(EMAX-EN(I))19,18,18
19    EMAX=EN(I)
18    CONTINUE
      WRITE(6,60)EMAX
C     WRITE(6,29)
C29   FORMAT(/,'PHI',2X,'THETA',2X,'NORMALIZED E-FIELD',2X,'NORMALIZED
C    1 E-FIELD (dB)',3X,'K')
C99   FORMAT(/,'THETA',1X,'PHI',2X,'NORMALIZED E-FIELD',2X,'NORMALIZED
C    1 E-FIELD (dB)',3X,'K')
60    FORMAT('E-FIELD MAXIMUM VALUE=',2X,E13.7,/)
      DO 21 II=1,KK-1
      ENOR(II)=EN(II)/EMAX
      IF (ENOR(II)) 80,80,81
```

```
81    ENORDB=20.*ALOG10(ENOR(II))
      GO TO 82
80    ENORDB=0.0000001
      GO TO 82
82    KM=10*(II-1)
C     WRITE(6,28)PHI,KM,ENOR,ENORDB,K
C28    FORMAT(F5.1,2X,I3,5X,F12.7,6X,F14.8,3X,I3)
21    CONTINUE
      WRITE(6,394)PHI
394    FORMAT(2X,'PHI=',2X,F7.3,'PLANE',/)
      WRITE(6,395)K
395    FORMAT(2X,'THETA',5X,'K=',I2,'(K=1 THETA COMP., K=2 PHI COM.)')
      DO 407 NV=1,73
      NVB=5*(NV-1)
      WRITE(6,408)NVB
408    FORMAT(2X,I6)
407    CONTINUE
      WRITE(6,396)
396    FORMAT(2X,'NORMALIZED E-FIELD MAGNITUDE',//)
      DO 409 NV=1,73
      WRITE(6,410)ENOR(NV)
410    FORMAT(2X,F12.7)
409    CONTINUE
16    CONTINUE
83    CONTINUE
      DO 63 K=1,2
      KK=1
      THE=90.0
      TH=THE*0.0174533
      DO 64 ITH=1,361,5
      PHI=FLOAT(ITH-1)
      PH=PHI*0.0174533
      CALL ROW(N,TH,PH,E)
      U1=E(K)
      GM=CABS(U1)
      EN(KK)=GM
      IF (GM) 65,65,66
66    EP=ATAN2(AIMAG(U1),REAL(U1))
      GO TO 67
65    EP=0.0
67    GP=EP*57.2858
      KK=KK+1
C     WRITE(6,194)THE,PHI,K,GM,GP
194    FORMAT(1X,F6.2,2X,F6.2,2X,I3,E12.7,3X,F8.3)
64    CONTINUE
      EMAX=EN(1)
      DO 68 I=2,KK-1
      IF(EMAX-EN(I))69,68,68
69    EMAX=EN(I)
68    CONTINUE
      WRITE(6,309)EMAX
309    FORMAT('E-FIELD MAXIMUM VALUE=',2X,E13.7,//)
      DO 70 II=1,KK-1
      ENOR(II)=EN(II)/EMAX
      ENORDB=20.*ALOG10(ENOR(II))
      KM=10*(II-1)
C     WRITE(6,88)THE,KM,ENOR,ENORDB,K
C88    FORMAT(F5.1,2X,I3,5X,F12.7,8X,F14.8,3X,I3)
70    CONTINUE
```

```
      WRITE(6,357)THE
357   FORMAT(2X,'THETA-',3X,F7.3,2X,'PLANE',/)
      WRITE(6,358)K
358   FORMAT('PHI',4X,'K=',I2,3X,'(K=1 THETA COMP., K=2 PHI COMP.)',/)
      DO 413 NV=1,73
      NVB=(NV-1)*5
      WRITE(6,414)NVB
414   FORMAT(I4)
413   CONTINUE
      WRITE(6,353)
353   FORMAT(1X,'NORMALIZED E-FIELD MAGNITUDE',/)
      DO 415 NV=1,73
      WRITE(6,416)ENOR(NV)
416   FORMAT(2X,F12.7)
415   CONTINUE
63    CONTINUE
      CALL ARATIO(N)
      CALL FBRATI(N)
      CALL POGAIN(N,POWER,DIS)
      STOP
      END


C*************************************************************************
C     THE MAIN PROGRAM FOR THE THIN-WIRE HELICAL ANTENNA FITTED WITH A
C          A SMALL GROUND PLANE MODELLED BY WIRE GRIDS (COMPOSITE STRUCTURE)
C*************************************************************************

      COMPLEX Z(15000),U(200),C(200),E(2),EI(3),UV(4),UI,ZL,ZIN
      COMPLEX YIN,V
      COMMON XX(270),XY(270),XZ(270),TX(270),TY(270),TZ(270),AL(270)
      COMMON T(700),TP(700),BK,RAD2(13),L(13),LR(13)/COA/C
       DIMENSION PX(250),PY(250),PZ(250),LL(13),RAD(13)
       DIMENSION IFP(250),EN(250)
       DIMENSION CM(200),CP(200),ENOR(200)
       OPEN(5,FILE='JANO2.DAT')
       OPEN(6,FILE='W15F140.OUT')
C      NW--TOTAL NUMBER OF DIFFERENT WIRES IN THE PROBLEM GEOMETRY
C      NP--NUMBER OF POINTS DEFINING THE GEOMETRY OF THE WIRE
C      NR--TOTAL NUMBER OF DIFFERENT WIRE RADII ENCOUNTERED IN CONSIDERING
C      THE SEGMENTS CONSECUTIVELY
C      READ(5,144)NW,NR
      NW=11
      NR=11
 144   FORMAT(2I2)
 143   FORMAT(//,'NW  NR  ',//2(I2,2X))
      PI=3.141592654
      PI2=2.0*PI
      WRITE(6,143)NW,NR
C      PX(I),PY(I),& PZ(I)  ARE THE XYZ CO-ORDINATES OF THE PTS DEFINING
C      THE PROBLEM GEOMETRY
      NTURNS=7
      PANGLE=15.0
      PITAN=(PANGLE*PI)/180.0
      FREQ=14.0E+09
      WAVEL=300E+06/FREQ
C      CIRWA=1.00
      CIRWA=(2.5E-02)/WAVEL
      CIR=CIRWA*WAVEL
```

```
      RA=CIR/(2.0*PI)
      RAO=0.8*RA
      SPAC=CIR*TAN(PITAN)
      SPAC1=CIRWA*TAN(PITAN)
      PIE=(2.*PI)/12.
      DISK=SQRT(CIR**2+SPAC**2)
      DISA=NTURNS*(SQRT(CIR**2+SPAC**2))
      DIS=(2.*DISA**2)/WAVEL
      DO 49 KK=1,2
      PX(KK)=0.0
      PY(KK)=0.0
49    CONTINUE
      PZ(1)=-(SPAC/12.)*2.
      PZ(2)=-(SPAC/12.)*1.
      PZZ=-(SPAC/12.)*2.
      DO 46 KK=3,15
      PX(KK)=RA*COS((KK-3)*PIE)
      PY(KK)=RA*SIN((KK-3)*PIE)
      PZ(KK)=(SPAC/(2.*PI))*((KK-3)*PIE)
46    CONTINUE
      NP1=NTURNS*12+3
      NJ=NP1-15
      DO 47 II=1,NJ
      NA=II+15
      PX(NA)=PX(II+3)
      PY(NA)=PY(II+3)
      PZ(NA)=PZ(II+3)+SPAC
47    CONTINUE
      PX(3)=0.0
      PY(3)=0.0
      PZ(3)=0.0
      KG=NP1+1
      DO 30 KS=NP1+1,NP1+19,1
      PX(KS)=RAO*COS((KS-KG)*PI2/16.)
      PY(KS)=RAO*SIN((KS-KG)*PI2/16.)
      PZ(KS)=PZZ
30    CONTINUE
      NP2=NP1+19
      KG=NP1+20
      DO 31 KS=NP2+1,NP2+19,1
      PX(KS)=0.75*RAO*COS((KS-KG)*PI2/16.)
      PY(KS)=0.75*RAO*SIN((KS-KG)*PI2/16.)
      PZ(KS)=PZZ
31    CONTINUE
      NP3=NP2+19
      KG=NP2+20
      DO 32 KS=NP3+1,NP3+19,1
      PX(KS)=0.5*RAO*COS((KS-KG)*PI2/16.)
      PY(KS)=0.5*RAO*SIN((KS-KG)*PI2/16.)
      PZ(KS)=PZZ
32    CONTINUE
      NP4=NP3+19
      KG=NP3+20
      DO 33 KS=NP4+1,NP4+19,1
      PX(KS)=0.25*RAO*COS((KS-KG)*PI2/16.)
      PY(KS)=0.25*RAO*SIN((KS-KG)*PI2/16.)
      PZ(KS)=PZZ
33    CONTINUE
      NP5=NP4+19
```

```
      KM=NP5
      DO 34 KS=4,-4,-1
      KM=KM+1
      PX(KM)=RAO*COS(0.0)*FLOAT(KS)/4.0
      PY(KM)=RAO*SIN(0.0)*FLOAT(KS)/4.0
      PZ(KM)=PZZ
34    CONTINUE
      KM=NP5+9
      DO 35 KS=4,-4,-1
      KM=KM+1
      PX(KM)=RAO*COS(PI/6.)*FLOAT(KS)/4.0
      PY(KM)=RAO*SIN(PI/6.)*FLOAT(KS)/4.0
      PZ(KM)=PZZ
35    CONTINUE
      KM=NP5+9+9
      DO 36 KS=4,-4,-1
      KM=KM+1
      PX(KM)=RAO*COS(PI/3.)*FLOAT(KS)/4.
      PY(KM)=RAO*SIN(PI/3.)*FLOAT(KS)/4.
      PZ(KM)=PZZ
36    CONTINUE
      KM=NP5+9+9+9
      DO 37 KS=4,-4,-1
      KM=KM+1
      PX(KM)=RAO*COS(PI/2.)*FLOAT(KS)/4.
      PY(KM)=RAO*SIN(PI/2.)*FLOAT(KS)/4.
      PZ(KM)=PZZ
37    CONTINUE
      KM=NP5+9+9+9+9
      DO 38 KS=4,-4,-1
      KM=KM+1
      PX(KM)=RAO*COS(2.*PI/3.)*FLOAT(KS)/4.
      PY(KM)=RAO*SIN(2.*PI/3.)*FLOAT(KS)/4.
      PZ(KM)=PZZ
38    CONTINUE
      KM=NP5+9+9+9+9+9
      DO 39 KS=4,-4,-1
      KM=KM+1
      PX(KM)=RAO*COS(5.*PI/6.)*FLOAT(KS)/4.
      PY(KM)=RAO*SIN(5.*PI/6.)*FLOAT(KS)/4.
      PZ(KM)=PZZ
39    CONTINUE
      KM=NP5+9+9+9+9+9+9
      NP=NP5+9+9+9+9+9+9
      WRITE(6,250)CIRWA,SPACI,PITAN,FREQ,NTURNS
250   FORMAT(//,'CIRCUMFERENCE (IN WAVELENGTHS) =',2X,F9.5,
     1 //,'SPACING (IN WAVELENGTHS) =',2X,F9.5,
     1 //,'PITCH ANGLE (IN RADIANS) =',2X,F9.5,
     1 //,'OPERATING FREQUENCY =',2X,E13.7,
     1 //,'NUMBER OF TURNS =',2X,I2,//)
      ALEN=(SQRT(CIR**2+SPAC**2))*NTURNS
      BK=(2.*PI)/WAVEL
      WRITE(6,255)ALEN
255   FORMAT(2X,'ARM LENGTH=',2X,F9.4,'M',//)
C     NSEG: NUMBER OF SEGMENTS PER TURN = 12
C     NP=TOTAL NUMBER OF POINTS DESCRIBING THE PROBLEM GEOMETRY
      WRITE(6,280)
280   FORMAT(//,'COORDINATES OF THE POINTS (IN METRES) DEFINING
     1 THE PROBLEM GEOMETRY',///)
```

```
      WRITE(6,701)
701   FORMAT(30X,'PX',//)
      WRITE(6,104)(PX(I),I=1,NP)
      WRITE(6,702)
702   FORMAT(30X,'PY',//)
      WRITE(6,104)(PY(I),I=1,NP)
      WRITE(6,703)
703   FORMAT(30X,'PZ',//)
      WRITE(6,104)(PZ(I),I=1,NP)
104   FORMAT(8(F8.5,2X))
C     LL(NW+1)--A CLM. MATRIX CONTAINING THE NUMBERS OF FIRST PTS.
C     OF DIFFERENT WIRES
      LL(1)=1
      LL(2)=88
      LL(3)=107
      LL(4)=126
      LL(5)=145
      LL(6)=164
      LL(7)=173
      LL(8)=182
      LL(9)=191
      LL(10)=200
      LL(11)=209
146   FORMAT(2012)
      WRITE(6,147)(LL(I),I=1,NW)
147   FORMAT(/,'LL',/(1X,10I4))
      LL(NW+1)=250
C     LR(NR+1)--A CLM. MATRIX CONTAINING THE NUMBERS OF THE SEGMENTS
C     AT WHICH CHANGES IN RADIUS OCCUR
      LR(1)=1
      LR(2)=87
      LR(3)=105
      LR(4)=123
      LR(5)=141
      LR(6)=159
      LR(7)=167
      LR(8)=175
      LR(9)=183
      LR(10)=191
      LR(11)=199
      WRITE(6,148)(LR(I),I=1,NR)
148   FORMAT(/,'LR',/(1X,10I4))
      LR(NR+1)=250
C     RAD(I)--WIRE RADII
      ASECP=1./COS(PITAN)
      WRAD=CIRWA*ASECP*WAVEL/60.
      RAD(1)=WRAD
      DO 149 NN=2,NR
      RAD(NN)=(WRAD)*0.25
149   CONTINUE
      WRITE(6,150)(RAD(I),I=1,NR)
150   FORMAT(/,'RAD',/5E14.7)
C     NUMBER OF DISCRETE LOAD IMPEDANCE
      DO 50 I=1,NR
      RAD2(I)=RAD(I)*RAD(I)
50    CONTINUE
      J1=1
      J2=2
      N1=0
```

```
      DO 2 J=1,NP
      IF (LL(J1)-J)3,4,3
 4     J2=J2-1
      L(J1)=J2
      J1=J1+1
      GO TO 2
 3     N1=N1+1
      J3=J-1
      IF ((N1/2*2-N1).EQ. 0)J2=J2+1
C      XX,XY,&XZ--CLM. MATRICES CONTAINING THE X,Y,&Z CO-ORDINATES
C      OF THE SEGMENTS CENTER POINTS
      XX(N1)=0.5*(PX(J)+PX(J3))
      XY(N1)=0.5*(PY(J)+PY(J3))
      XZ(N1)=0.5*(PZ(J)+PZ(J3))
      S1=PX(J)-PX(J3)
      S2=PY(J)-PY(J3)
      S3=PZ(J)-PZ(J3)
      S4=SQRT(S1*S1+S2*S2+S3*S3)
C      XX,XY,& XZ--X,Y,& Z COMPONENTS OF THE UNIT TANGENTIAL VECTOR
C      AT THE MID-POINTS OF THE STRAIGHT WIRE SEGMENTS
      TX(N1)=S1/S4
      TY(N1)=S2/S4
      TZ(N1)=S3/S4
C      AL--CLM. MATRIX CONTAINING SEGMENT LENGTHS
      AL(N1)=S4
 2     CONTINUE
C      L(I)--INDICATES THAT F(L(I)) IS THE FIRST EXPANSION FUNCTION ON
C      THE I-TH WIRE
      L(J1)=J2
C      N--NUMBER OF EXPANSION FUNCTIONS
C      N1--TOTAL NUMBER OF STRAIGHT SEGMENT WIRES
C      Z--GENERALIZED IMPEDANCE MATRIX OF ORDER N
      N=J2-2
      CALL CALZ(N,N1,Z)
      READ(5,78)NL
 78     FORMAT(I2)
      WRITE(6,79)NL
 79     FORMAT(/,'NL=',2X,I2)
      IF (NL)42,42,41
 41     WRITE(6,118)NL
 118    FORMAT(1X,'NL'/I3/'LP   LOAD')
C      ZL--LOAD IMPEDANCE IN OHMS
      DO 43 I=1,NL
      READ (5,119)LP,ZL
 119    FORMAT(I3,2E13.6)
      WRITE(6,120)LP,ZL
 120    FORMAT(1X,I3,2E13.6,/)
      J2=(LP-1)*N+LP
      Z(J2)=Z(J2)+ZL
 43     CONTINUE
 42     CALL LINEQ(N,Z)
      DO 45 I=1,N
      U(I)=0.0
 45     CONTINUE
C      FP --FEED POINT
      READ(5,107)NF
      WRITE(6,108)NF
 108    FORMAT(/,'NF=',2X,I2,/'FP          VOLTAGE'/)
 107    FORMAT(I2)
```

```
      DO 51 I=1,NF
      READ(5,52)J1,V
      WRITE(6,53)J1,V
      U(J1)=V
      IFP(I)=J1
 51   CONTINUE
 52   FORMAT(I2,2E13.7)
 53   FORMAT(//,I2,3X,2(E13.7,2X))
      WRITE(6,704)
 704  FORMAT('            CURRENT  DISTRIBUTION',//)
C     WRITE(6,111)
C111  FORMAT(2X,'I',7X,' MAGNITUDE',9X,
C    1 'PHASE',4X,'IMAGE PHASE',/)
      J3=0
      J1=0
 5    J1=J1+1
      U1=0.0
      J2=0
 6    J2=J2+1
      J3=J3+1
      U1=U1+Z(J3)*U(J2)
      IF (J2-N)6,7,7
 7    C(J1)=U1
      IF (J1-N)5,8,8
 8    CONTINUE
      DO 9 I=1,N
      U1=C(I)
      CM(I)=CABS(U1)
      IF (CM(I))11,12,11
 11   CP(I)=ATAN2(AIMAG(U1),REAL(U1))*57.2858
      GO TO 10
 12   CP(I)=0.0
 10   CONTINUE
C     WRITE(6,112)I,CM,CP
C112  FORMAT(1X,I2,5X,E15.5,5X,F8.3,6X,F8.3)
 9    CONTINUE
      WRITE(6,391)
 391  FORMAT(//,2X,'I',/)
      NV=(NP1-3)/2
      DO 400 NB=1,NV
      ARML=ALEN*FLOAT(NB-1)*2.0/(FLOAT(NP1-3))
      WRITE(6,401)ARML
 401  FORMAT(2X,F9.4)
 400  CONTINUE
      WRITE(6,692)
 692  FORMAT(//,2X,'REAL COMP. OF CURRENT',/)
      DO 602 NB=1,NV
      WRITE(6,603)REAL(C(NB))*1000.
 603  FORMAT(2X,F11.6)
 602  CONTINUE
      WRITE(6,604)
 604  FORMAT(//2X,'IMAGNINARY COMP OF CURRENT',/)
      DO 605 NB=1,NV
      WRITE(6,606)AIMAG(C(NB))*1000.
 606  FORMAT(2X,F11.6)
 605  CONTINUE
      WRITE(6,392)
 392  FORMAT(//,2X,'CURRENT MAGNITUDE',/)
      DO 402 NB=1,NV
```

```
      WRITE(6,403)CM(NB)*1000.
403   FORMAT(2X,F11.6)
402   CONTINUE
      WRITE(6,393)
393   FORMAT(2X,/,'PHASE OF CURRENT DISTRIBUTION',/)
      DO 404 NB=1,NV
      WRITE(6,405)CP(NB)
405   FORMAT(3X,F9.3)
404   CONTINUE
55    POWER=0.0
      DO 23 I=1,NF
      J1=IFP(I)
      ZIN=U(J1)/C(J1)
      AZIN=CABS(ZIN)
      PZIN=ATAN2(IMAG(ZIN),REAL(ZIN))*(180./PI)
      WRITE(6,122)J1,ZIN,AZIN,PZIN
122   FORMAT(1X,'INPUT IMPEDANCE AT POSITION',I3,'=(',2(E14.7,2X),')'
     1 ,/1X,//,'IMP MAG=',2X,F7.2,4X,'IMP PHA.=',2X,F7.2,//)
      GM=CABS(ZIN)
      IF (GM-0.1E-6)24,24,25
25    YIN=1.0/ZIN
      WRITE(6,123)J1,YIN
123   FORMAT(1X,'INPUT ADMITTANCE AT POSITION',I3,'=(',2(E14.7,2X),')'
     1 ,///)
24    S1=REAL(ZIN)
      S2=CABS(C(J1))
      POWER=POWER+0.5*S2*S2*S1
23    CONTINUE
      WRITE(6,124)POWER
124   FORMAT(1X,'TOTAL POWER INPUT=',E14.7,1X,'W',/)
      WRITE(6,113)
113   FORMAT(1X,'EM-MODE FIELD PATTERN',//1X,'K=1 FOR THETA COMPONENT'
     1,//1X, 'K=2 FOR PHI COMPONENT',//,1X,'THETA',4X,'PHI',4X,'K',7X,
     1 'MAGNITUDE',8X,'PHASE',/)
      WRITE(6,1131)
1131  FORMAT(//,1X,'THETA',4X,'PHI',12X,6X,
     1'MAGNITUDE',8X,'PHASE',//)
      DO 83 LK=1,91,90
      PHI=FLOAT(LK-1)
      DO 16 K=1,2
      KK=1
      PH=PHI*0.0174533
      DO 17 ITH=1,361,5
      THE=FLOAT(ITH-1)
      TH=THE*0.0174533
      CALL ROW (N,TH,PH,E)
      U1=E(K)
      GM=CABS(U1)
      EN(KK)=GM
      IF (GM) 13,13,14
14    EP=ATAN2(AIMAG(U1),REAL(U1))
      GO TO 15
13    EP=0.0
15    GP=EP*57.2858
      KK=KK+1
C     WRITE(6,114)THE,PHI,K,GM,GP
114   FORMAT(1X,F6.2,2X,F6.2,2X,I3,3X,E12.7,3X,F8.3)
17    CONTINUE
      EMAX=EN(1)
```

```
      DO 18 I=2,KK-1
      IF(EMAX-EN(I))19,18,18
 19    EMAX=EN(I)
 18    CONTINUE
      WRITE(6,60)EMAX
C      WRITE(6,29)
C29    FORMAT(/,'PHI',2X,'THETA',2X,'NORMALIZED E-FIELD',2X,'NORMALIZED
C   1 E-FIELD (dB)',3X,'K')
C99    FORMAT(/,'THETA',1X,'PHI',2X,'NORMALIZED E-FIELD',2X,'NORMALIZED
C   1 E-FIELD (dB)',3X,'K')
 60    FORMAT('E-FIELD MAXIMUM VALUE=',2X,E13.7,/)
      DO 21 II=1,KK-1
      ENOR(II)=EN(II)/EMAX
      IF (ENOR(II)) 80,80,81
 81    ENORDB=20.*ALOG10(ENOR(II))
      GO TO 82
 80    ENORDB=0.0000001
      GO TO 82
 82    KM=10*(II-1)
C      WRITE(6,28)PHI,KM,ENOR,ENORDB,K
C28    FORMAT(F5.1,2X,I3,5X,F12.7,6X,F14.8,3X,I3)
 21    CONTINUE
      WRITE(6,394)PHI
 394   FORMAT(2X,'PHI=',2X,F7.3,'PLANE',/)
      WRITE(6,395)K
 395   FORMAT(2X,'THETA',5X,'K=',I2,'(K=1 THETA COMP., K=2 PHI COM.)')
      DO 407 NV=1,73
      NVB=5*(NV-1)
      WRITE(6,408)NVB
 408   FORMAT(2X,I6)
 407   CONTINUE
      WRITE(6,396)
 396   FORMAT(2X,'NORMALIZED E-FIELD MAGNITUDE',//)
      DO 409 NV=1,73
      WRITE(6,410)ENOR(NV)
 410   FORMAT(2X,F12.7)
 409   CONTINUE
 16    CONTINUE
 83    CONTINUE
      DO 63 K=1,2
      KK=1
      THE=90.0
      TH=THE*0.0174533
      DO 64 ITH=1,361,5
      PHI=FLOAT(ITH-1)
      PH=PHI*0.0174533
      CALL ROW(N,TH,PH,E)
      U1=E(K)
      GM=CABS(U1)
      EN(KK)=GM
      IF (GM) 65,65,66
 66    EP=ATAN2(AIMAG(U1),REAL(U1))
      GO TO 67
 65    EP=0.0
 67    GP=EP*57.2858
      KK=KK+1
C      WRITE(6,194)THE,PHI,K,GM,GP
 194   FORMAT(1X,F6.2,2X,F6.2,2X,I3,E12.7,3X,F8.3)
 64    CONTINUE
```

```
      EMAX=EN(1)
      DO 68 I=2,KK-1
      IF(EMAX-EN(I))69,68,68
 69    EMAX=EN(I)
 68    CONTINUE
      WRITE(6,309)EMAX
 309   FORMAT('E-FIELD MAXIMUM VALUE=',2X,E13.7,//)
      DO 70 II=1,KK-1
      ENOR(II)=EN(II)/EMAX
      ENORDB=20.*ALOG10(ENOR(II))
      KM=10*(II-1)
C     WRITE(6,88)THE,KM,ENOR,ENORDB,K
C88    FORMAT(F5.1,2X,I3,5X,F12.7,8X,F14.8,3X,I3)
 70    CONTINUE
      WRITE(6,357)THE
 357   FORMAT(2X,'THETA=',3X,F7.3,2X,'PLANE',/)
      WRITE(6,358)K
 358   FORMAT('PHI',4X,'K=',I2,3X,'(K=1 THETA COMP., K=2 PHI COMP.)',/)
      DO 413 NV=1,73
      NVB=(NV-1)*5
      WRITE(6,414)NVB
 414   FORMAT(I4)
 413   CONTINUE
      WRITE(6,353)
 353   FORMAT(1X,'NORMALIZED E-FIELD MAGNITUDE',/)
      DO 415 NV=1,73
      WRITE(6,416)ENOR(NV)
 416   FORMAT(2X,F12.7)
 415   CONTINUE
 63    CONTINUE
      CALL ARATIO(N)
      CALL FBRATI(N)
      CALL POGAIN(N,POWER,DIS)
      STOP
      END


C ***********************************************************************
C     THE MAIN PROGRAM FOR A CENTRE-FED THIN-WIRE HELICAL ANTENNA
C     OPERATING IN FREE SPACE
C***********************************************************************

      COMPLEX Z(6400),U(80),C(80),E(3),EI(2),UV(4),U1,ZL,ZIN,YIN,V
      COMMON XX(165),XY(165),XZ(165),TX(165),TY(165),TZ(165),AL(165)
      COMMON T(1600),TP(1600),BK,RAD2(10),L(5),LR(10)/COA/C
      DIMENSION PX(165),PY(165),PZ(165),LL(5),RAD(10),IFP(80),EN(80)
      DIMENSION CM(80),CP(80),ENOR(80)
      OPEN(5,FILE='CENHEL.DAT')
      OPEN(6,FILE='CC13P15.OUT')
C     NW--TOTAL NUMBER OF DIFFERENT WIRES IN THE PROBLEM GEOMETRY
C     NP--NUMBER OF POINTS DEFINING THE GEOMETRY OF THE WIRE
C     NR--TOTAL NUMBER OF DIFFERENT WIRE RADII ENCOUNTERED IN CONSIDERING
C     THE SEGMENTS CONSECUTIVELY
      READ(5,144)NW,NR
 144   FORMAT(2I2)
 143   FORMAT(//,'NW  NR  ',//2(I2,2X))
      PI=3.141592654
      WRITE(6,143)NW,NR
```

```
C     PX(I),PY(I),& PZ(I)  ARE THE XYZ CO-ORDINATES OF THE PTS DEFINING
C     THE PROBLEM GEOMETRY
      NTURNS=8
      PITAND=25.0
      PITAN=(PITAND*PI)/180.
      FREQ=3000E+06
      WAVEL=300E+06/FREQ
C     CIRWA=(5.0E-02)/WAVEL
      CIRWA=1.60
      CIR=CIRWA*WAVEL
      RA=CIR/(2.0*PI)
      SPAC=CIR*TAN(PITAN)
      SPAC1=CIRWA*TAN(PITAN)
      PIE=(2.*PI)/12.
      DISA=NTURNS*(SQRT(CIR**2+SPAC**2))
      DIS=(2.*DISA**2)/WAVEL
      DO 46 KK=1,13
      PX(KK)=RA*COS((KK-1)*PIE)
      PY(KK)=RA*SIN((KK-1)*PIE)
      PZ(KK)=(-SPAC*FLOAT(NTURNS))/2.+((KK-1)*SPAC)/12.
 46   CONTINUE
      NP=NTURNS*12+1
      NJ=NP-13
      DO 47 II=1,NJ
      NA=II+13
      PX(NA)=PX(II+1)
      PY(NA)=PY(II+1)
      PZ(NA)=PZ(II+1)+SPAC
 47   CONTINUE
      WRITE(6,250)CIRWA,SPAC1,PITAND,FREQ,NTURNS
 250  FORMAT(//,'CIRCUMFERENCE (IN WAVELENGTHS) =',2X,F9.5,
     1 //,'SPACING (IN WAVELENGTHS) =',2X,F9.5,
     1 //,'PITCH ANGLE (IN DEGREES) =',2X,F9.5,
     1 //,'OPERATING FREQUENCY =',2X,E13.7,
     1 //,'NUMBER OF TURNS =',2X,I2,//)
      ALEN=(SQRT(CIR**2+SPAC**2))*NTURNS
      BK=(2.*PI)/WAVEL
      WRITE(6,255)ALEN
 255  FORMAT(2X,'ARM LENGTH=',2X,F9.4,'M',//)
C     NSEG: NUMBER OF SEGMENTS PER TURN = 12
C     NP=TOTAL NUMBER OF POINTS DESCRIBING THE PROBLEM GEOMETRY
      WRITE(6,280)
 280  FORMAT(//,'COORDINATES OF THE POINTS (IN METRES) DEFINING
     1 THE PROBLEM GEOMETRY',///)
      WRITE(6,701)
 701  FORMAT(30X,'PX',//)
      WRITE(6,104)(PX(I),I=1,NP)
      WRITE(6,702)
 702  FORMAT(30X,'PY',//)
      WRITE(6,104)(PY(I),I=1,NP)
      WRITE(6,703)
 703  FORMAT(30X,'PZ',//)
      WRITE(6,104)(PZ(I),I=1,NP)
 104  FORMAT(8(F8.5,2X))
C     LL(NW+1)--A CLM. MATRIX CONTAINING THE NUMBERS OF FIRST PTS.
C     OF DIFFERENT WIRES
      READ(5,146)(LL(I),I=1,NW)
 146  FORMAT(20I2)
      WRITE(6,147)(LL(I),I=1,NW)
```

```
147   FORMAT(/,'LL',/(1X,10I4))
      LL(NW+1)=200
C     LR(NR+1)--A CLM. MATRIX CONTAINING THE NUMBERS OF THE SEGMENTS
C     AT WHICH CHANGES IN RADIUS OCCUR
      READ(5,146)(LR(I),I=1,NR)
      WRITE(6,148)(LR(I),I=1,NR)
148   FORMAT(/,'LR',/(1X,10I4))
      LR(NR+1)=200
C     RAD(I)--WIRE RADII
      READ(5,149)(RAD(I),I=1,NR)
149   FORMAT(5E14.7)
      WRITE(6,150)(RAD(I),I=1,NR)
150   FORMAT(/,'RAD',/5E14.7)
C     NUMBER OF DISCRETE LOAD IMPEDANCE
      DO 50 I=1,NR
      RAD2(I)=RAD(I)*RAD(I)
50    CONTINUE
      J1=1
      J2=2
      N1=0
      DO 2 J=1,NP
      IF (LL(J1)-J)3,4,3
4     J2=J2-1
      L(J1)=J2
      J1=J1+1
      GO TO 2
3     N1=N1+1
      J3=J-1
      IF ((N1/2*2-N1).EQ. 0)J2=J2+1
C     XX,XY,&XZ--CLM. MATRICES CONTAINING THE X,Y,&Z CO-ORDINATES
C     OF THE SEGMENTS CENTER POINTS
      XX(N1)=0.5*(PX(J)+PX(J3))
      XY(N1)=0.5*(PY(J)+PY(J3))
      XZ(N1)=0.5*(PZ(J)+PZ(J3))
      S1=PX(J)-PX(J3)
      S2=PY(J)-PY(J3)
      S3=PZ(J)-PZ(J3)
      S4=SQRT(S1*S1+S2*S2+S3*S3)
C     XX,XY,& XZ--X,Y,& Z COMPONENTS OF THE UNIT TANGENTIAL VECTOR
C     AT THE MID-POINTS OF THE STRAIGHT WIRE SEGMENTS
      TX(N1)=S1/S4
      TY(N1)=S2/S4
      TZ(N1)=S3/S4
C     AL--CLM. MATRIX CONTAINING SEGMENT LENGTHS
      AL(N1)=S4
2     CONTINUE
C     L(I)--INDICATES THAT F(L(I)) IS THE FIRST EXPANSION FUNCTION ON
C     THE I-TH WIRE
      L(J1)=J2
C     N--NUMBER OF EXPANSION FUNCTIONS
C     N1--TOTAL NUMBER OF STRAIGHT SEGMENT WIRES
C     Z--GENERALIZED IMPEDANCE MATRIX OF ORDER N
      N=J2-2
      CALL CALZ(N,N1,Z)
      READ(5,78)NL
78    FORMAT(I2)
      WRITE(6,79)NL
79    FORMAT(/,'NL=',2X,I2)
      IF (NL)42,42,41
```

```
41    WRITE(6,118)NL
118   FORMAT(1X,'NL'/I3/'LP   LOAD')
C     ZL--LOAD IMPEDANCE IN OHMS
      DO 43 I=1,NL
      READ (5,119)LP,ZL
119   FORMAT(I3,2E13.6)
      WRITE(6,120)LP,ZL
120   FORMAT(1X,I3,2E13.6,/)
      J2=(LP-1)*N+LP
      Z(J2)=Z(J2)+ZL
43    CONTINUE
42    CALL LINEQ(N,Z)
      DO 45 I=1,N
      U(I)=0.0
45    CONTINUE
C     FP --FEED POINT
      READ(5,107)NF
      WRITE(6,108)NF
108   FORMAT(/,'NF=',2X,I2,/'FP          VOLTAGE',/)
107   FORMAT(I2)
      J1=3*NTURNS
      DO 51 I=1,NF
      READ(5,52)V
      WRITE(6,53)J1,V
      U(J1)=V
      IFP(I)=J1
51    CONTINUE
52    FORMAT(2E13.7)
53    FORMAT(//,I2,3X,2(E13.7,2X))
      WRITE(6,704)
704   FORMAT('            CURRENT  DISTRIBUTION',//)
C     WRITE(6,111)
C111  FORMAT(2X,'I',7X,' MAGNITUDE',9X,
C    1 'PHASE',4X,'IMAGE PHASE',/)
      J3=0
      J1=0
5     J1=J1+1
      U1=0.0
      J2=0
6     J2=J2+1
      J3=J3+1
      U1=U1+Z(J3)*U(J2)
      IF (J2-N)6,7,7
7     C(J1)=U1
      IF (J1-N)5,8,8
8     CONTINUE
      DO 9 I=1,N
      U1=C(I)
      CM(I)=CABS(U1)
      IF (CM(I))11,12,11
11    CP(I)=ATAN2(AIMAG(U1),REAL(U1))*57.2858
      GO TO 10
12    CP(I)=0.0
10    CONTINUE
C     WRITE(6,112)I,CM,CP
C112  FORMAT(1X,I2,5X,E15.5,5X,F8.3,6X,F8.3)
9     CONTINUE
      WRITE(6,499)ALEN/2.0
499   FORMAT(2X,'CENTRE POINT =',4X,F10.5)
```

```
      WRITE(6,391)
391   FORMAT(//,2X,'I',/)
      QQ=0.
      ARML=(-1.*ALEN)/2.
      DO 400 NB=1,N+2
      ARML=QQ+ARML
      WRITE(6,401)ARML
401   FORMAT(2X,F9.4)
      QQ=(2.*ALEN)/FLOAT(NP-1)
400   CONTINUE
      WRITE(6,692)
692   FORMAT(//,2X,'REAL COMP. OF CURRENT',/)
      DO 602 NB=1,N
      WRITE(6,603)REAL(C(NB))*1000.
603   FORMAT(2X,F11.6)
602   CONTINUE
      CREAL=0.000
      WRITE(6,603)CREAL
      WRITE(6,604)
604   FORMAT(//2X,'IMAGNINARY COMP OF CURRENT',/)
      DO 605 NB=1,N
      WRITE(6,606)AIMAG(C(NB))*1000.
606   FORMAT(2X,F11.6)
605   CONTINUE
      CAIMAG=0.0000
      WRITE(6,606)CAIMAG
      WRITE(6,392)
392   FORMAT(//,2X,'CURRENT MAGNITUDE',/)
      DO 402 NB=1,N
      WRITE(6,403)CM(NB)*1000.
403   FORMAT(2X,F11.6)
402   CONTINUE
      CMZ=0.000
      WRITE(6,403)CMZ
      WRITE(6,393)
393   FORMAT(2X,/,'PHASE OF CURRENT DISTRIBUTION',/)
      DO 404 NB=1,N
      WRITE(6,405)CP(NB)
405   FORMAT(3X,F9.3)
404   CONTINUE
      CPZ=0.00
      WRITE(6,405)CPZ
55    POWER=0.0
      DO 23 I=1,NF
      J1=IFP(I)
      ZIN=U(J1)/C(J1)
      WRITE(6,122)J1,ZIN
122   FORMAT(1X,'INPUT IMPEDANCE AT POSITION',I3,'=(',2(E14.7,2X),')'
     1 ,/1X,/)
      GM=CABS(ZIN)
      IF (GM-0.1E-6)24,24,25
25    YIN=1.0/ZIN
      WRITE(6,123)J1,YIN
123   FORMAT(1X,'INPUT ADMITTANCE AT POSITION',I3,'=(',2(E14.7,2X),')'
     1 ,///)
24    S1=REAL(ZIN)
      S2=CABS(C(J1))
      POWER=POWER+0.5*S2*S2*S1
23    CONTINUE
```

```
      WRITE(6,124)POWER
124   FORMAT(1X,'TOTAL POWER INPUT=',E14.7,1X,'W',/)
      WRITE(6,113)
113   FORMAT(1X,'EM-MODE FIELD PATTERN',//1X,'K=1 FOR THETA COMPONENT'
     1,//1X, 'K=2 FOR PHI COMPONENT',//,1X,'THETA',4X,'PHI',4X,'K',7X,
     1'MAGNITUDE',8X,'PHASE',/)
      WRITE(6,1131)
1131  FORMAT(//,1X,'THETA',4X,'PHI',12X,6X,
     1'MAGNITUDE',8X,'PHASE',//)
      DO 83 LK=1,91,90
      PHI=FLOAT(LK-1)
      DO 16 K=1,2
      KK=1
      PH=PHI*0.0174533
      DO 17 ITH=1,361,5
      THE=FLOAT(ITH-1)
      TH=THE*0.0174533
      CALL ROW (N,TH,PH,E)
      U1=E(K)
      GM=CABS(U1)
      EN(KK)=GM
      IF (GM) 13,13,14
14    EP=ATAN2(AIMAG(U1),REAL(U1))
      GO TO 15
13    EP=0.0
15    GP=EP*57.2858
      KK=KK+1
C     WRITE(6,114)THE,PHI,K,GM,GP
114   FORMAT(1X,F6.2,2X,F6.2,2X,I3,3X,E12.7,3X,F8.3)
17    CONTINUE
      EMAX=EN(1)
      DO 18 I=2,KK-1
      IF(EMAX-EN(I))19,18,18
19    EMAX=EN(I)
18    CONTINUE
      WRITE(6,60)EMAX
C     WRITE(6,29)
C29   FORMAT(/,'PHI',2X,'THETA',2X,'NORMALIZED E-FIELD',2X,'NORMALIZED
C    1 E-FIELD (dB)',3X,'K')
C99   FORMAT(/,'THETA',1X,'PHI',2X,'NORMALIZED E-FIELD',2X,'NORMALIZED
C    1 E-FIELD (dB)',3X,'K')
60    FORMAT('E-FIELD MAXIMUM VALUE ',2X,E13.7,/)
      DO 21 II=1,KK-1
      ENOR(II)=EN(II)/EMAX
      IF (ENOR(II)) 80,80,81
81    ENORDB=20.*ALOG10(ENOR(II))
      GO TO 82
80    ENORDB=0.0000001
      GO TO 82.
82    KM=10*(II-1)
C     WRITE(6,28)PHI,KM,ENOR,ENORDB,K
C28   FORMAT(F5.1,2X,I3,5X,F12.7,6X,F14.8,3X,I3)
21    CONTINUE
      WRITE(6,394)PHI
394   FORMAT(2X,'PHI=',2X,F7.3,'PLANE',/)
      WRITE(6,395)K
395   FORMAT(2X,'THETA',5X,'K=',I2,'(K=1 THETA COMP., K=2 PHI COM.)')
      DO 407 NV=1,73
      NVB=5*(NV-1)
```

```
      WRITE(6,408)NVB
408   FORMAT(2X,I6)
407   CONTINUE
      WRITE(6,396)
396   FORMAT(2X,'NORMALIZED E-FIELD MAGNITUDE',//)
      DO 409 NV=1,73
      WRITE(6,410)ENOR(NV)
410   FORMAT(2X,F12.7)
409   CONTINUE
16    CONTINUE
83    CONTINUE
      DO 63 K=1,2
      KK=1
      THE=90.0
      TH=THE*0.0174533
      DO 64 ITH=1,361,5
      PHI=FLOAT(ITH-1)
      PH=PHI*0.0174533
      CALL ROW(N,TH,PH,E)
      U1=E(K)
      GM=CABS(U1)
      EN(KK)=GM
      IF (GM) 65,65,66
66    EP=ATAN2(AIMAG(U1),REAL(U1))
      GO TO 67
65    EP=0.0
67    GP=EP*57.2858
      KK=KK+1
C     WRITE(6,194)THE,PHI,K,GM,GP
194   FORMAT(1X,F6.2,2X,F6.2,2X,I3,E12.7,3X,F8.3)
64    CONTINUE
      EMAX=EN(1)
      DO 68 I=2,KK-1
      IF(EMAX-EN(I))69,68,68
69    EMAX=EN(I)
68    CONTINUE
      WRITE(6,309)EMAX
309   FORMAT('E-FIELD MAXIMUM VALUE=',2X,E13.7,//)
      DO 70 II=1,KK-1
      ENOR(II)=EN(II)/EMAX
      ENORDB=20.*ALOG10(ENOR(II))
      KM=10*(II-1)
C     WRITE(6,88)THE,KM,ENOR,ENORDB,K
C88   FORMAT(F5.1,2X,I3,5X,F12.7,8X,F14.8,3X,I3)
70    CONTINUE
      WRITE(6,357)THE
357   FORMAT(2X,'THETA=',3X,F7.3,2X,'PLANE',/)
      WRITE(6,358)K
358   FORMAT('PHI',4X,'K=',I2,3X,'(K=1 THETA COMP., K=2 PHI COMP.)',/)
      DO 413 NV=1,73
      NVB=(NV-1)*5
      WRITE(6,414)NVB
414   FORMAT(I4)
413   CONTINUE
      WRITE(6,353)
353   FORMAT(1X,'NORMALIZED E-FIELD MAGNITUDE',/)
      DO 415 NV=1,73
      WRITE(6,416)ENOR(NV)
416   FORMAT(2X,F12.7)
```

```
415   CONTINUE
63    CONTINUE
      CALL ARATIO(N)
      CALL FBRATI(N)
      CALL POGAIN(N,POWER,DIS)
      CALL WATT(N)
      STOP
      END


C     ********************************************************************
C      THE MAIN PROGRAM FOR THE THIN-WIRE HELICAL ANTENNA BACKED BY
C          RESONANT LOOPS
C          ********************************************************************

      COMPLEX Z(10900),U(200),C(200),E(3),EI(3),UV(4),U1,ZL,ZIN,YIN,V
      COMMON XX(250),XY(250),XZ(250),TX(250),TY(250),TZ(250),AL(250)
      COMMON T(500),TP(500),BK,RAD2(10),L(5),LR(10)/COA/C
      DIMENSION PX(250),PY(250),PZ(250),LL(5),RAD(10),IFP(50),EN(100)
      DIMENSION CM(200),CP(200),ENOR(100)
      COMPLEX U2
      DIMENSION BX(250),BY(250),BZ(250),PN(80),PNOR(80),PNORDB(80)
      OPEN(5,FILE='H3LDF.DAT')
      OPEN(6,FILE='HHHH.OUT')
C      NW--TOTAL NUMBER OF DIFFERENT WIRES IN THE PROBLEM GEOMETRY
C      NP--NUMBER OF POINTS DEFINING THE GEOMETRY OF THE WIRE
C      NR--TOTAL NUMBER OF DIFFERENT WIRE RADII ENCOUNTERED IN CONSIDERING
C      THE SEGMENTS CONSECUTIVELY
      READ(5,144)NW,NR
144   FORMAT(2I2)
143   FORMAT(//,'NW  NR  ',//2(I2,2X))
      PI=3.141592654
      WRITE(6,143)NW,NR
C      PX(I),PY(I),& PZ(I)  ARE THE XYZ CO-ORDINATES OF THE PTS DEFINING
C      THE PROBLEM GEOMETRY
      NTURNS=10
      PADEG=15.11
      PITAN=(PADEG*PI)/180.0
      FREQ=1680E+06
      WAVEL=300E+06/FREQ
      CIRWA=1.20
      CIR=CIRWA*WAVEL
      RA=CIR/(2.0*PI)
      SPAC=CIR*TAN(PITAN)
      SPAC1=CIRWA*TAN(PITAN)
      PIE=(2.*PI)/16.
      DISA=NTURNS*(SQRT(CIR**2+SPAC**2))
      DIS=(2.*DISA**2)/WAVEL
      DO 46 KK=1,17
      PX(KK)=RA*COS((KK-1)*PIE)
      PY(KK)=RA*SIN((KK-1)*PIE)
      PZ(KK)=(SPAC/(2.*PI))*((KK-1)*PIE)
46    CONTINUE
      NP1=NTURNS*16+1
      NJ=NP1-17
      DO 47 II=1,NJ
      NA=II+17
      PX(NA)=PX(II+1)
      PY(NA)=PY(II+1)
```

```
      PZ(NA)=PZ(II+1)+SPAC
47    CONTINUE
      I=1
      DO 30 KC=NP1,1,-1
      BX(I)=PX(KC)
      BY(I)=PY(KC)
      BZ(I)=PZ(KC)
      I=I+1
30    CONTINUE
      DO 36 I=1,NP1,1
      PX(I)=BX(I)
      PY(I)=BY(I)
      PZ(I)=BZ(I)
36    CONTINUE
      VC=0.00001
      VC1=0.00000
      DO 235 KZ=NP1+1,NP1+2,1
      PX(KZ)=PX(NP1)+VC
      PY(KZ)=PY(NP1)+VC1
      PZ(KZ)=PZ(NP1)+VC1
      VC=VC+0.00001
235   CONTINUE
      JG1=NP1+3
      DO 32 JG=JG1,JG1+18,1
      PX(JG)=RA*COS(PIE*(JG-JG1))
      PY(JG)=RA*SIN(PIE*(JG-JG1))
      PZ(JG)=-0.0028*WAVEL
32    CONTINUE
C     PX(NP1+20)=RA*COS(PI/180.)
C     PX(NP1+21)=RA*COS((2.*PI)/180.)
C     PY(NP1+20)=RA*SIN(PI/180.)
C     PY(NP1+21)=RA*SIN((2.*PI)/180.)
C     PZ(NP1+20)=-0.003
C     PZ(NP1+21)=-0.003
      JG2=NP1+22
      DO 362 MJ=JG2,JG2+18,1
      PX(MJ)=RA*COS(PIE*(MJ-JG2))
      PY(MJ)=RA*SIN(PIE*(MJ-JG2))
      PZ(MJ)=(-1.0*WAVEL)/2.
362   CONTINUE
C     PX(NP1+39)=RA*COS(PI/180.)
C     PX(NP1+40)=RA*COS((2.*PI)/180.)
C     PY(NP1+39)=RA*SIN(PI/180.)
C     PY(NP1+40)=RA*SIN((2.*PI)/180.)
C     PZ(NP1+39)=(-1.0*WAVEL)/2.
C     PZ(NP1+40)=(-1.0*WAVEL)/2.
      JG3=NP1+41
      DO 363 MJ=JG3,JG3+18,1
      PX(MJ)=RA*COS(PIE*(MJ-JG3))
      PY(MJ)=RA*SIN(PIE*(MJ-JG3))
      PZ(MJ)=(-10.0*WAVEL)/10.0
363   CONTINUE
C     PX(NP1+58)=RA*COS(PI/180.)
C     PX(NP1+59)=RA*COS((2.*PI)/180.)
C     PY(NP1+58)=RA*SIN(PI/180.)
C     PY(NP1+59)=RA*SIN((2.*PI)/180.)
C     PZ(NP1+58)=(-10.0*WAVEL)/10.0
C     PZ(NP1+59)=(-10.0*WAVEL)/10.0
      NP=NP1+2+19+19+19
```

```
      WRITE(6,250)CIRWA,SPACI,PADEG,FREQ,NTURNS
250   FORMAT(//,'CIRCUMFERENCE (IN WAVELENGTHS) =',2X,F9.5,
     1 //,'SPACING (IN WAVELENGTHS) =',2X,F9.5,
     1 //,'PITCH ANGLE (IN DEGREES) =',2X,F9.5,
     1 //,'OPERATING FREQUENCY =',2X,E13.7,
     1 //,'NUMBER OF TURNS =',2X,I2,//)
      ALEN=(SQRT(CIR**2+SPAC**2))*NTURNS
      BK=(2.*PI)/WAVEL
      WRITE(6,255)ALEN
255   FORMAT(2X,'ARM LENGTH=',2X,F9.4,'M',//)
C     NSEG: NUMBER OF SEGMENTS PER TURN = 16
C     NP=TOTAL NUMBER OF POINTS DESCRIBING THE PROBLEM GEOMETRY
      WRITE(6,280)
280   FORMAT(//,'COORDINATES OF THE POINTS (IN METRES) DEFINING
     1 THE PROBLEM GEOMETRY',///)
      WRITE(6,701)
701   FORMAT(30X,'PX',//)
      WRITE(6,104)(PX(I),I=1,NP)
      WRITE(6,702)
702   FORMAT(30X,'PY',//)
      WRITE(6,104)(PY(I),I=1,NP)
      WRITE(6,703)
703   FORMAT(30X,'PZ',//)
      WRITE(6,104)(PZ(I),I=1,NP)
104   FORMAT(8(F8.5,2X))
C     LL(NW+1)--A CLM. MATRIX CONTAINING THE NUMBERS OF FIRST PTS.
C     OF DIFFERENT WIRES
      LL(1)=1
      LL(2)=NTURNS*16+4
      LL(3)=NTURNS*16+23
      LL(4)=NTURNS*16+42
      WRITE(6,147)(LL(I),I=1,NW)
147   FORMAT(/,'LL',/(1X,10I4))
      LL(NW+1)=270
C     LR(NR+1)--A CLM. MATRIX CONTAINING THE NUMBERS OF THE SEGMENTS
C     AT WHICH CHANGES IN RADIUS OCCUR
      LR(1)=1
      LR(2)=NTURNS*16+3
      LR(3)=NTURNS*16+21
      LR(4)=NTURNS*16+39
      WRITE(6,148)(LR(I),I=1,NR)
148   FORMAT(/,'LR',/(1X,10I4))
      LR(NR+1)=270
C     RAD(I)--WIRE RADII
      RAD(1)=0.0028*WAVEL
      RAD(2)=0.0028*WAVEL
      RAD(3)=0.0028*WAVEL
      RAD(4)=0.0028*WAVEL
      WRITE(6,150)(RAD(I),I=1,NR)
150   FORMAT(/,'RAD',/5E14.7)
C     NUMBER OF DISCRETE LOAD IMPEDANCE
      DO 50 I=1,NR
      RAD2(I)=RAD(I)*RAD(I)
50    CONTINUE
      J1=1
      J2=2
      N1=0
      DO 2 J=1,NP
      IF (LL(J1)-J)3,4,3
```

```
4     J2=J2-1
      L(J1)=J2
      J1=J1+1
      GO TO 2
3     N1=N1+1
      J3=J-1
      IF ((N1/2*2-N1).EQ. 0)J2=J2+1
C     XX,XY,&XZ--CLM. MATRICES CONTAINING THE X,Y,&Z CO-ORDINATES
C     OF THE SEGMENTS CENTER POINTS
      XX(N1)=0.5*(PX(J)+PX(J3))
      XY(N1)=0.5*(PY(J)+PY(J3))
      XZ(N1)=0.5*(PZ(J)+PZ(J3))
      S1=PX(J)-PX(J3)
      S2=PY(J)-PY(J3)
      S3=PZ(J)-PZ(J3)
      S4=SQRT(S1*S1+S2*S2+S3*S3)
C     XX,XY,& XZ--X;Y,& Z COMPONENTS OF THE UNIT TANGENTIAL VECTOR
C     AT THE MID-POINTS OF THE STRAIGHT WIRE SEGMENTS
      TX(N1)=S1/S4
      TY(N1)=S2/S4
      TZ(N1)=S3/S4
C     AL--CLM. MATRIX CONTAINING SEGMENT LENGTHS
      AL(N1)=S4
2     CONTINUE
C     L(I)--INDICATES THAT F(L(I)) IS THE FIRST EXPANSION FUNCTION ON
C     THE I-TH WIRE
      L(J1)=J2
      DO 441 KQ=1,3
      WRITE (6,442)L(KQ)
442     FORMAT(2X,'L(J1)=',2X, I3,/)
441     CONTINUE
C     N--NUMBER OF EXPANSION FUNCTIONS
C     N1--TOTAL NUMBER OF STRAIGHT SEGMENT WIRES
C     Z--GENERALIZED IMPEDANCE MATRIX OF ORDER N
      N=J2-2
      WRITE(6,743)N,N1
743     FORMAT(2X,'N=',2X,I3,2X,'N1=',2X,I3,/)
      CALL CALZ(N,N1,Z)
      READ(5,78)NL
78      FORMAT(I2)
      WRITE(6,79)NL
79      FORMAT(/,'NL=',2X,I2)
C     NX=(NTURNS*12-2)/2+1
C     N=NX
      IF (NL)42,42,41
41      WRITE(6,118)NL
118     FORMAT(1X,'NL'/I3/'LP   LOAD')
C     ZL--LOAD IMPEDANCE IN OHMS
      DO 43 I=1,NL
      READ (5,119)LP,ZL
119     FORMAT(I3,2E13.6)
      WRITE(6,120)LP,ZL
120     FORMAT(1X,I3,2E13.6,/)
      J2=(LP-1)*N+LP
      Z(J2)=Z(J2)+ZL
43      CONTINUE
42      F=0.0
      CALL LINEQ(N,Z)
      DO 45 I=1,N
```

```
      U(I)=0.0
 45   CONTINUE
C     FP --FEED POINT
      READ(5,107)NF
      WRITE(6,108)NF
 108  FORMAT(/,'NF=',2X,I2,/'FP          VOLTAGE',/)
 107  FORMAT(I2)
C     J1=(16*NTURNS)/2
      DO 51 I=1,NF
      READ(5,52)J1,V
      WRITE(6,53)J1,V
      U(J1)=V
      IFP(I)=J1
 51   CONTINUE
 52   FORMAT(I3,2E13.7)
 53   FORMAT(//,I2,3X,2(E13.7,2X))
      WRITE(6,704)
 704  FORMAT('            CURRENT  DISTRIBUTION',//)
C     WRITE(6,111)
C111  FORMAT(2X,'I',7X,' MAGNITUDE',9X,
C    1 'PHASE',4X,'IMAGE PHASE',/)
      J3=0
      J1=0
 5    J1=J1+1
      U1=0.0
      J2=0
 6    J2=J2+1
      J3=J3+1
      U1=U1+Z(J3)*U(J2)
      IF (J2-N)6,7,7
 7    C(J1)=U1
      IF (J1-N)5,8,8
 8    CONTINUE
      DO 9 I=1,N
      U1=C(I)
      CM(I)=CABS(U1)
      IF (CM(I))11,12,11
 11   CP(I)=ATAN2(AIMAG(U1),REAL(U1))*57.2858
      GO TO 10
 12   CP(I)=0.0
 10   CONTINUE
C     WRITE(6,112)I,CM,CP
C112  FORMAT(1X,I2,5X,E15.5,5X,F8.3,6X,F8.3)
 9    CONTINUE
      WRITE(6,391)
 391  FORMAT(//,2X,'I',/)
      NX=(NTURNS*16-2)/2+1
      ARML1=0.00
      WRITE(6,401)ARML1
      DO 400 NB=1,NX
      ARML=ALEN*FLOAT(NB)*2.0/(FLOAT(NP1-1))
      WRITE(6,401)ARML
 401  FORMAT(2X,F9.4)
 400  CONTINUE
      WRITE(6,692)
 692  FORMAT(//,2X,'REAL COMP. OF CURRENT',/)
      DO 602 NB=NX,1,-1
      WRITE(6,603)REAL(C(NB))*1000.0
 603  FORMAT(2X,F9.4)
```

```
602   CONTINUE
      CREAL=0.00
      WRITE(6,603)CREAL
      WRITE(6,604)
604   FORMAT(//2X,'IMAGNINARY COMP OF CURRENT',/)
      DO 605 NB=NX,1,-1
      WRITE(6,606)AIMAG(C(NB))*1000.0
606   FORMAT(2X,F9.4)
605   CONTINUE
      CIMAG=0.00
      WRITE(6,606)CIMAG
      WRITE(6,392)
392   FORMAT(//,2X,'CURRENT MAGNITUDE',/)
      DO 402 NB=NX,1,-1
      WRITE(6,403)CM(NB)*1000.0
403   FORMAT(2X,F9.4)
402   CONTINUE
      CMAG=0.00
      WRITE(6,403)CMAG
      WRITE(6,393)
393   FORMAT(2X,/,'PHASE OF CURRENT DISTRIBUTION',/)
      DO 404 NB=NX,1,-1
      WRITE(6,405)CP(NB)
405   FORMAT(3X,F9.3)
404   CONTINUE
      CPHASE=0.00
      WRITE(6,405)CPHASE
55    POWER=0.0
      DO 23 I=1,NF
      J1=IFP(I)
      ZIN=U(J1)/C(J1)
      WRITE(6,122)J1,ZIN
122   FORMAT(1X,'INPUT IMPEDANCE AT POSITION',I3,'=(',2(E14.7,2X),')'
     1 ,/1X,/)
      GM=CABS(ZIN)
      IF (GM-0.1E-6)24,24,25
25    YIN=1.0/ZIN
      WRITE(6,123)J1,YIN
123   FORMAT(1X,'INPUT ADMITTANCE AT POSITION',I3,'=(',2(E14.7,2X),')'
     1 ,///)
24    S1=REAL(ZIN)
      S2=CABS(C(J1))
      POWER=POWER+0.5*S2*S2*S1
23    CONTINUE
      WRITE(6,124)POWER
124   FORMAT(1X,'TOTAL POWER INPUT=',E14.7,1X,'W',/)
      WRITE(6,113)
113   FORMAT(1X,'EM-MODE FIELD PATTERN',//1X,'K=1 FOR THETA COMPONENT'
     1,//1X, 'K=2 FOR PHI COMPONENT',//,1X,'THETA',4X,'PHI',4X,'K',7X,
     1'MAGNITUDE',8X,'PHASE',/)
      WRITE(6,1131)
1131  FORMAT(//,1X,'THETA',4X,'PHI',12X,6X,
     1'MAGNITUDE',8X,'PHASE',//)
      DO 83 LK=1,91,90
      PHI=FLOAT(LK-1)
      DO 16 K=1,2
      KK=1
      PH=PHI*0.0174533
      DO 17 ITH=1,361,5
```

```
      THE=FLOAT(ITH-1)
      TH=THE*0.0174533
      CALL ROW (N,TH,PH,E)
      U1=E(K)
      GM=CABS(U1)
      EN(KK)=GM
      IF (GM) 13,13,14
 14    EP=ATAN2(AIMAG(U1),REAL(U1))
      GO TO 15
 13    EP=0.0
 15    GP=EP*57.2858
      KK=KK+1
C      WRITE(6,114)THE,PHI,K,GM,GP
 114   FORMAT(1X,F6.2,2X,F6.2,2X,I3,3X,E12.7,3X,F8.3)
 17    CONTINUE
      EMAX=EN(1)
      DO 18 I=2,KK-1
      IF(EMAX-EN(I))19,18,18
 19    EMAX=EN(I)
 18    CONTINUE
      WRITE(6,60)EMAX
C      WRITE(6,29)
C29    FORMAT(/,'PHI',2X,'THETA',2X,'NORMALIZED E-FIELD',2X,'NORMALIZED
C    1 E-FIELD (dB)',3X,'K')
C99    FORMAT(/,'THETA',1X,'PHI',2X,'NORMALIZED E-FIELD',2X,'NORMALIZED
C    1 E-FIELD (dB)',3X,'K')
 60    FORMAT('E-FIELD MAXIMUM VALUE=',2X,E13.7,/)
      DO 21 II=1,KK-1
      ENOR(II)=EN(II)/EMAX
      IF (ENOR(II)) 80,80,81
 81    ENORDB=20.*ALOG10(ENOR(II))
      GO TO 82
 80    ENORDB=0.0000001
      GO TO 82
 82    KM=10*(II-1)
C      WRITE(6,28)PHI,KM,ENOR,ENORDB,K
C28    FORMAT(F5.1,2X,I3,5X,F12.7,6X,F14.8,3X,I3)
 21    CONTINUE
      WRITE(6,394)PHI
 394   FORMAT(2X,'PHI=',2X,F7.3,'PLANE',/)
      WRITE(6,395)K
 395   FORMAT(2X,'THETA',5X,'K=',I2,'(K=1 THETA COMP., K=2 PHI COM.)')
      DO 407 NV=1,73
      NVB=5*(NV-1)
      WRITE(6,408)NVB
 408   FORMAT(2X,I6)
 407   CONTINUE
      WRITE(6,396)
 396   FORMAT(2X,'NORMALIZED E-FIELD MAGNITUDE',//)
      DO 409 NV=1,73
      WRITE(6,410)ENOR(NV)
 410   FORMAT(2X,F12.7)
 409   CONTINUE
 16    CONTINUE
 83    CONTINUE
      DO 63 K=1,2
      KK=1
      THE=90.0
      TH=THE*0.0174533
```

```
      DO 64 ITH=1,361,5
      PHI=FLOAT(ITH-1)
      PH=PHI*0.0174533
      CALL ROW(N,TH,PH,E)
      U1=E(K)
      GM=CABS(U1)
      EN(KK)=GM
      IF (GM) 65,65,66
66    EP=ATAN2(AIMAG(U1),REAL(U1))
      GO TO 67
65    EP=0.0
67    GP=EP*57.2858
      KK=KK+1
C     WRITE(6,194)THE,PHI,K,GM,GP
194   FORMAT(1X,F6.2,2X,F6.2,2X,I3,E12.7,3X,F8.3)
64    CONTINUE
      EMAX=EN(1)
      DO 68 I=2,KK-1
      IF(EMAX-EN(I))69,68,68
69    EMAX=EN(I)
68    CONTINUE
      WRITE(6,309)EMAX
309   FORMAT('E-FIELD MAXIMUM VALUE=',2X,E13.7,//)
      DO 70 II=1,KK-1
      ENOR(II)=EN(II)/EMAX
      ENORDB=20.*ALOG10(ENOR(II))
      KM=10*(II-1)
C     WRITE(6,88)THE,KM,ENOR,ENORDB,K
C88   FORMAT(F5.1,2X,I3,5X,F12.7,8X,F14.8,3X,I3)
70    CONTINUE
      WRITE(6,357)THE
357   FORMAT(2X,'THETA=',3X,F7.3,2X,'PLANE',/)
      WRITE(6,358)K
358   FORMAT('PHI',4X,'K=',I2,3X,'(K=1 THETA COMP., K=2 PHI COMP.)',/)
      DO 413 NV=1,73
      NVB=(NV-1)*5
      WRITE(6,414)NVB
414   FORMAT(I4)
413   CONTINUE
      WRITE(6,353)
353   FORMAT(1X,'NORMALIZED E-FIELD MAGNITUDE',/)
      DO 415 NV=1,73
      WRITE(6,416)ENOR(NV)
416   FORMAT(2X,F12.7)
415   CONTINUE
63    CONTINUE
C     FAR-FIELD POWER COMPUTATION IN dB
C     ***************************************************
      WRITE(6,193)
193   FORMAT('*************************************',//)
      DO 230 KA=1,91,90
      PHI=FLOAT(KA-1)
      KK=1
      PH=PHI*0.0174533
      DO 231 ITH=1,361,5
      THE=FLOAT(ITH-1)
      TH=THE*0.0174533
      CALL ROW(N,TH,PH,E)
      U1=E(1)
```

```
      U2=E(2)
      GM=(CABS(U1))**2+(CABS(U2))**2
      PN(KK)=GM
      KK=KK+1
231   CONTINUE
      PMAX=PN(1)
      DO 232 I=2,KK-1
      IF(PMAX-PN(I))233,232,232
233   PMAX=PN(I)
232   CONTINUE
      DO 96 II=1,KK-1
      PNOR(II)=PN(II)/PMAX
      IF(PNOR(II))34,34,35
35    PNORDB(II)=10.*ALOG10(PNOR(II))
      GO TO 95
34    PNORDB(II)=0.0000001
      GO TO 95
95    LK=1
96    CONTINUE
      WRITE(6,394)PHI
      DO 236 NV=1,73
      NVB=5*(NV-1)
      WRITE(6,408)NVB
236   CONTINUE
      WRITE(6,37)
37    FORMAT(2X,'NORMALIZED FAR-FIELD POWER IN DB',//)
      DO 38 NV=1,73
      WRITE(6,416)PNOR(NV)
38    CONTINUE
      DO 39 NV=1,73
      WRITE(6,416)PNORDB(NV)
39    CONTINUE
230   CONTINUE
      CALL ARATIO(N)
      CALL FBRATI(N)
      CALL POGAIN(N,POWER,DIS)
      CALL WATT(N)
      STOP
      END


C     ****************************************************************
C     THE MAIN PROGRAM FOR THE THIN-WIRE HELICAL ANTENNA BONDED TO AN
C         INFINITE GROUND PLANE
C         ****************************************************************

      COMPLEX Z(16500),U(140),C(140),E(3),EI(3),UV(4),U1,ZL,ZIN,YIN,V
      COMMON XX(270),XY(270),XZ(270),TX(270),TY(270),TZ(270),AL(270)
      COMMON T(700),TP(700),BK,RAD2(10),L(5),LR(10)/COA/C
      DIMENSION PX(270),PY(270),PZ(270),LL(5),RAD(10),IFP(50),EN(100)
      DIMENSION CM(200),CP(200),ENOR(100)
      DIMENSION BX(270),BY(270),BZ(270)
      OPEN(5,FILE='BJAN.DAT')
      OPEN(6,FILE='GPH130.OUT')
C     NW--TOTAL NUMBER OF DIFFERENT WIRES IN THE PROBLEM GEOMETRY
C     NP--NUMBER OF POINTS DEFINING THE GEOMETRY OF THE WIRE
C     NR--TOTAL NUMBER OF DIFFERENT WIRE RADII ENCOUNTERED IN CONSIDERING
C     THE SEGMENTS CONSECUTIVELY
```

```
      READ(5,144)NW,NR
144   FORMAT(2I2)
143   FORMAT(//,'NW  NR  ',//2(I2,2X))
      PI=3.141592654
      WRITE(6,143)NW,NR
C     PX(I),PY(I),& PZ(I)  ARE THE XYZ CO-ORDINATES OF THE PTS DEFINING
C     THE PROBLEM GEOMETRY
      NTURNS=8
      PADEG=12.5
      PITAN=(PADEG*PI)/180.0
      FREQ=3.0E+09
      WAVEL=3.0E+08/FREQ
C     CIRWA=(5.0E-02)/WAVEL
      CIRWA=1.0
      CIR=CIRWA*WAVEL
      RA=CIR/(2.0*PI)
      SPAC=CIR*TAN(PITAN)
      SPAC1=CIRWA*TAN(PITAN)
      PIE=(2.*PI)/16.
      DISA=NTURNS*(SQRT(CIR**2+SPAC**2))
      DIS=(2.*DISA**2)/WAVEL
      DO 46 KK=1,17
      PX(KK)=RA*COS((KK-1)*PIE)
      PY(KK)=RA*SIN((KK-1)*PIE)
      PZ(KK)=(SPAC/(2.*PI))*((KK-1)*PIE)
46    CONTINUE
      NP1=NTURNS*16+1
      NJ=NP1-17
      DO 47 II=1,NJ
      NA=II+17
      PX(NA)=PX(II+1)
      PY(NA)=PY(II+1)
      PZ(NA)=PZ(II+1)+SPAC
47    CONTINUE
      I=1
      DO 30 KC=NP1,1,-1
      BX(I)=PX(KC)
      BY(I)=PY(KC)
      BZ(I)=PZ(KC)
      I=I+1
30    CONTINUE
      DO 36 I=1,NP1,1
      PX(I)=BX(I)
      PY(I)=BY(I)
      PZ(I)=BZ(I)
36    CONTINUE
      VC=0.00001
      VC1=0.00000
      DO 235 KZ=NP1+1,NP1+2,1
      PX(KZ)=PX(NP1)+VC
      PY(KZ)=PY(NP1)+VC1
      PZ(KZ)=PZ(NP1)+VC1
      BX(KZ)=BX(NP1)+VC
      BY(KZ)=BY(NP1)+VC1
      BZ(KZ)=BZ(NP1)+VC1
      VC=VC+0.00001
235   CONTINUE
      NN=NP1+2
      DO 32 JG=NP1+3,(2*NTURNS*16+6),1
```

```
      PX(JG)=BX(NN)
      PY(JG)=BY(NN)
      PZ(JG)=-BZ(NN)
      NN=NN-1
 32    CONTINUE
      NP=(NP1+2)*2
      WRITE(6,250)CIRWA,SPAC1,PADEG,FREQ,NTURNS
 250   FORMAT(//,'CIRCUMFERENCE (IN WAVELENGTHS) =',2X,F9.5,
     1 //,'SPACING (IN WAVELENGTHS) =',2X,F9.5,
     1 //,'PITCH ANGLE (IN DEGREES) =',2X,F9.5,
     1 //,'OPERATING FREQUENCY =',2X,E13.7,
     1 //,'NUMBER OF TURNS =',2X,I2,//)
      ALEN=(SQRT(CIR**2+SPAC**2))*NTURNS
      BK=(2.*PI)/WAVEL
      WRITE(6,255)ALEN
 255   FORMAT(2X,'ARM LENGTH=',2X,F9.4,'M',//)
C      NSEG: NUMBER OF SEGMENTS PER TURN = 12
C      NP=TOTAL NUMBER OF POINTS DESCRIBING THE PROBLEM GEOMETRY
      WRITE(6,280)
 280   FORMAT(//,'COORDINATES OF THE POINTS (IN METRES) DEFINING
     1 THE PROBLEM GEOMETRY',///)
      WRITE(6,701)
 701   FORMAT(30X,'PX',//)
      WRITE(6,104)(PX(I),I=1,NP)
      WRITE(6,702)
 702   FORMAT(30X,'PY',//)
      WRITE(6,104)(PY(I),I=1,NP)
      WRITE(6,703)
 703   FORMAT(30X,'PZ',//)
      WRITE(6,104)(PZ(I),I=1,NP)
 104   FORMAT(8(F8.5,2X))
C      LL(NW+1)--A CLM. MATRIX CONTAINING THE NUMBERS OF FIRST PTS.
C      OF DIFFERENT WIRES
      LL(1)=1
      LL(2)=4+NTURNS*16
      WRITE(6,147)(LL(I),I=1,NW)
 147   FORMAT(/,'LL',/(1X,10I4))
      LL(NW+1)=270
C      LR(NR+1)--A CLM. MATRIX CONTAINING THE NUMBERS OF THE SEGMENTS
C       AT WHICH CHANGES IN RADIUS OCCUR
      LR(1)=1
      LR(2)=3+NTURNS*16
      WRITE(6,148)(LR(I),I=1,NR)
 148   FORMAT(/,'LR',/(1X,10I4))
      LR(NR+1)=270
C      RAD(I)--WIRE RADII
      RAD(1)=0.5E-03
      RAD(2)=0.5E-03
      WRITE(6,150)(RAD(I),I=1,NR)
 150   FORMAT(/,'RAD',/5E14.7)
C      NUMBER OF DISCRETE LOAD IMPEDANCE
      DO 50 I=1,NR
      RAD2(I)=RAD(I)*RAD(I)
 50    CONTINUE
      J1=1
      J2=2
      N1=0
      DO 2 J=1,NP
      IF (LL(J1)-J)3,4,3
```

```
4     J2=J2-1
      L(J1)=J2
      J1=J1+1
      GO TO 2
3     N1=N1+1
      J3=J-1
      IF ((N1/2*2-N1).EQ. 0)J2=J2+1
C      XX,XY,&XZ--CLM. MATRICES CONTAINING THE X,Y,&Z CO-ORDINATES
C      OF THE SEGMENTS CENTER POINTS
      XX(N1)=0.5*(PX(J)+PX(J3))
      XY(N1)=0.5*(PY(J)+PY(J3))
      XZ(N1)=0.5*(PZ(J)+PZ(J3))
      S1=PX(J)-PX(J3)
      S2=PY(J)-PY(J3)
      S3=PZ(J)-PZ(J3)
      S4=SQRT(S1*S1+S2*S2+S3*S3)
C      XX,XY,& XZ--X,Y,& Z COMPONENTS OF THE UNIT TANGENTIAL VECTOR
C      AT THE MID-POINTS OF THE STRAIGHT WIRE SEGMENTS
      TX(N1)=S1/S4
      TY(N1)=S2/S4
      TZ(N1)=S3/S4
C      AL--CLM. MATRIX CONTAINING SEGMENT LENGTHS
      AL(N1)=S4
2     CONTINUE
C      L(I)--INDICATES THAT F(L(I)) IS THE FIRST EXPANSION FUNCTION ON
C      THE I-TH WIRE
      L(J1)=J2
      DO 441 KQ=1,3
      WRITE (6,442)L(KQ)
442     FORMAT(2X,'L(J1)=',2X, I3,/)
441     CONTINUE
C      N--NUMBER OF EXPANSION FUNCTIONS
C      N1--TOTAL NUMBER OF STRAIGHT SEGMENT WIRES
C      Z--GENERALIZED IMPEDANCE MATRIX OF ORDER N
      N=J2-2
      WRITE(6,743)N,N1
743     FORMAT(2X,'N=',2X,I3,2X,'N1=',2X,I3,/)
      CALL CALZ(N,N1,Z)
      READ(5,78)NL
78     FORMAT(I2)
      WRITE(6,79)NL
79     FORMAT(/,'NL=',2X,I2)
C      NX=(NTURNS*16-2)/2+1
C      N=NX
      IF (NL)42,42,41
41     WRITE(6,118)NL
118     FORMAT(1X,'NL=',I3/'LP  LOAD')
C      ZL--LOAD IMPEDANCE IN OHMS
      DO 43 I=1,NL
      READ (5,119)LP,ZL
119     FORMAT(I3,2E13.6)
      WRITE(6,120)LP,ZL
120     FORMAT(1X,I3,2E13.6,/)
      J2=(LP-1)*N+LP
      Z(J2)=Z(J2)+ZL
43     CONTINUE
42     F=0.0
C      NZ=1
C      DO 200 K1=1,N
```

```
C     DO 201 K2=1,N
C     Z1(K1,K2)=Z(NZ)
C     NZ=NZ+1
C201  CONTINUE
C200  CONTINUE
C     K5=1
C     DO 202 K4=1,N/2
C     DO 203 K3=1,N/2
C     Z(K5)=Z1(K4,K3)+Z1(K4,K3+N/2)
C     K5=K5+1
C203  CONTINUE
C202  CONTINUE
C     N=N/2
      CALL LINEQ(N,Z)
      DO 45 I=1,N
      U(I)=0.0
 45   CONTINUE
C     FP --FEED POINT
      READ(5,107)NF
      WRITE(6,108)NF
 108  FORMAT(/,'NF=',2X,I2,/'FP          VOLTAGE',/)
 107  FORMAT(I2)
      J1=((((16*NTURNS+1)-3))/2)+1
      DO 51 I=1,NF
      READ(5,52)V
      WRITE(6,53)J1,V
      U(J1)=V
      IFP(I)=J1
 51   CONTINUE
 52   FORMAT(2E13.7)
 53   FORMAT(//,I2,3X,2(E13.7,2X))
      WRITE(6,704)
 704  FORMAT('            CURRENT  DISTRIBUTION',//)
C     WRITE(6,111)
C111  FORMAT(2X,'I',7X,' MAGNITUDE',9X,
C    1 'PHASE',4X,'IMAGE PHASE',/)
      J3=0
      J1=0
 5    J1=J1+1
      U1=0.0
      J2=0
 6    J2=J2+1
      J3=J3+1
      U1=U1+Z(J3)*U(J2)
      IF (J2-N)6,7,7
 7    C(J1)=U1
      IF (J1-N)5,8,8
 8    CONTINUE
      DO 9 I=1,N
      U1=C(I)
      CM(I)=CABS(U1)
      IF (CM(I))11,12,11
 11   CP(I)=ATAN2(AIMAG(U1),REAL(U1))*57.2858
      GO TO 10
 12   CP(I)=0.0
 10   CONTINUE
C     WRITE(6,112)I,CM,CP
C112  FORMAT(1X,I2,5X,E15.5,5X,F8.3,6X,F8.3)
 9    CONTINUE
```

```
      WRITE(6,391)
391   FORMAT(//,2X,'I',/)
      NX=(NTURNS*16-2)/2+1
      ARML1=0.00
      WRITE(6,401)ARML1
      DO 400 NB=1,NX
      ARML=ALEN*FLOAT(NB)*2.0/(FLOAT(NP1-1))
      WRITE(6,401)ARML
401   FORMAT(2X,F9.4)
400   CONTINUE
      WRITE(6,692)
692   FORMAT(//,2X,'REAL COMP. OF CURRENT',/)
      DO 602 NB=NX,1,-1
      WRITE(6,603)REAL(C(NB))*1000.0
603   FORMAT(2X,F9.4)
602   CONTINUE
      CREAL=0.00
      WRITE(6,603)CREAL
      WRITE(6,604)
604   FORMAT(//2X,'IMAGNINARY COMP OF CURRENT',/)
      DO 605 NB=NX,1,-1
      WRITE(6,606)AIMAG(C(NB))*1000.0
606   FORMAT(2X,F9.4)
605   CONTINUE
      CIMAG=0.00
      WRITE(6,606)CIMAG
      WRITE(6,392)
392   FORMAT(//,2X,'CURRENT MAGNITUDE',/)
      DO 402 NB=NX,1,-1
      WRITE(6,403)CM(NB)*1000.0
403   FORMAT(2X,F9.4)
402   CONTINUE
      CMAG=0.00
      WRITE(6,403)CMAG
      WRITE(6,393)
393   FORMAT(2X,/,'PHASE OF CURRENT DISTRIBUTION',/)
      DO 404 NB=NX,1,-1
      WRITE(6,405)CP(NB)
405   FORMAT(3X,F9.3)
404   CONTINUE
      CPHASE=0.00
      WRITE(6,405)CPHASE
55     POWER=0.0
      DO 23 I=1,NF
      J1=IFP(I)
      ZIN=U(J1)/C(J1)
      WRITE(6,122)J1,ZIN
122   FORMAT(1X,'INPUT IMPEDANCE AT POSITION',I3,'=(',2(E14.7,2X),')'
     1 ,/1X,/)
      GM=CABS(ZIN)
      IF (GM-0.1E-6)24,24,25
25     YIN=1.0/ZIN
      WRITE(6,123)J1,YIN
123   FORMAT(1X,'INPUT ADMITTANCE AT POSITION',I3,'=(',2(E14.7,2X),')'
     1 ,///)
24     S1=REAL(ZIN)
      S2=CABS(C(J1))
      POWER=POWER+0.5*S2*S2*S1
23    CONTINUE
```

```
      WRITE(6,124)POWER
124   FORMAT(1X,'TOTAL POWER INPUT=',E14.7,1X,'W',/)
      WRITE(6,113)
113   FORMAT(1X,'EM-MODE FIELD PATTERN',//1X,'K=1 FOR THETA COMPONENT'
     1,//1X, 'K=2 FOR PHI COMPONENT',//,1X,'THETA',4X,'PHI',4X,'K',7X,
     1'MAGNITUDE',8X,'PHASE',/)
      WRITE(6,1131)
1131  FORMAT(//,1X,'THETA',4X,'PHI',12X,6X,
     1'MAGNITUDE',8X,'PHASE',//)
      DO 83 LK=1,91,90
      PHI=FLOAT(LK-1)
      DO 16 K=1,2
      KK=1
      PH=PHI*0.0174533
      DO 17 ITH=1,361,5
      THE=FLOAT(ITH-1)
      TH=THE*0.0174533
      CALL ROW (NX,TH,PH,E)
      U1=E(K)
      GM=CABS(U1)
      EN(KK)=GM
      IF (GM) 13,13,14
14    EP=ATAN2(AIMAG(U1),REAL(U1))
      GO TO 15
13    EP=0.0
15    GP=EP*57.2858
      KK=KK+1
C     WRITE(6,114)THE,PHI,K,GM,GP
114   FORMAT(1X,F6.2,2X,F6.2,2X,I3,3X,E12.7,3X,F8.3)
17    CONTINUE
      EMAX=EN(1)
      DO 18 I=2,KK-1
      IF(EMAX-EN(I))19,18,18
19    EMAX=EN(I)
18    CONTINUE
      WRITE(6,60)EMAX
C     WRITE(6,29)
C29   FORMAT(/,'PHI',2X,'THETA',2X,'NORMALIZED E-FIELD',2X,'NORMALIZED
C    1 E-FIELD (dB)',3X,'K')
C99   FORMAT(/,'THETA',1X,'PHI',2X,'NORMALIZED E-FIELD',2X,'NORMALIZED
C    1 E-FIELD (dB)',3X,'K')
60    FORMAT('E-FIELD MAXIMUM VALUE=',2X,E13.7,/)
      DO 21 II=1,KK-1
      ENOR(II)=EN(II)/EMAX
      IF (ENOR(II)) 80,80,81
81    ENORDB=20.*ALOG10(ENOR(II))
      GO TO 82
80    ENORDB=0.0000001
      GO TO 82
82    KM=10*(II-1)
C     WRITE(6,28)PHI,KM,ENOR,ENORDB,K
C28   FORMAT(F5.1,2X,I3,5X,F12.7,6X,F14.8,3X,I3)
21    CONTINUE
      WRITE(6,394)PHI
394   FORMAT(2X,'PHI=',2X,F7.3,'PLANE',/)
      WRITE(6,395)K
395   FORMAT(2X,'THETA',5X,'K=',I2,'(K=1 THETA COMP., K=2 PHI COM.)')
      DO 407 NV=1,73
      NVB=5*(NV-1)
```

```
      WRITE(6,408)NVB
408   FORMAT(2X,I6)
407   CONTINUE
      WRITE(6,396)
396   FORMAT(2X,'NORMALIZED E-FIELD MAGNITUDE',//)
      DO 409 NV=1,73
      WRITE(6,410)ENOR(NV)
410   FORMAT(2X,F12.7)
409   CONTINUE
16    CONTINUE
83    CONTINUE
      DO 63 K=1,2
      KK=1
      THE=90.0
      TH=THE*0.0174533
      DO 64 ITH=1,361,5
      PHI=FLOAT(ITH-1)
      PH=PHI*0.0174533
      CALL ROW(NX,TH,PH,E)
      U1=E(K)
      GM=CABS(U1)
      EN(KK)=GM
      IF (GM) 65,65,66
66    EP=ATAN2(AIMAG(U1),REAL(U1))
      GO TO 67
65    EP=0.0
67    GP=EP*57.2858
      KK=KK+1
C     WRITE(6,194)THE,PHI,K,GM,GP
194   FORMAT(1X,F6.2,2X,F6.2,2X,I3,E12.7,3X,F8.3)
64    CONTINUE
      EMAX=EN(1)
      DO 68 I=2,KK-1
      IF(EMAX-EN(I))69,68,68
69    EMAX=EN(I)
68    CONTINUE
      WRITE(6,309)EMAX
309   FORMAT('E-FIELD MAXIMUM VALUE=',2X,E13.7,//)
      DO 70 II=1,KK-1
      ENOR(II)=EN(II)/EMAX
      ENORDB=20.*ALOG10(ENOR(II))
      KM=10*(II-1)
C     WRITE(6,88)THE,KM,ENOR,ENORDB,K
C88   FORMAT(F5.1,2X,I3,5X,F12.7,8X,F14.8,3X,I3)
70    CONTINUE
      WRITE(6,357)THE
357   FORMAT(2X,'THETA=',3X,F7.3,2X,'PLANE',/)
      WRITE(6,358)K
358   FORMAT('PHI',4X,'K=',I2,3X,'(K=1 THETA COMP., K=2 PHI COMP.)',/)
      DO 413 NV=1,73
      NVB=(NV-1)*5
      WRITE(6,414)NVB
414   FORMAT(I4)
413   CONTINUE
      WRITE(6,353)
353   FORMAT(1X,'NORMALIZED E-FIELD MAGNITUDE',/)
      DO 415 NV=1,73
      WRITE(6,416)ENOR(NV)
416   FORMAT(2X,F12.7)
```

```
415   CONTINUE
63    CONTINUE
      CALL ARATIO(NX)
      CALL FBRATI(NX)
      CALL POGAIN(NX,POWER,DIS)
      STOP
      END
```

References

Abd-Alhameed, R.A., and Excell, P.S., (1999): *"Analysis of a normal-mode helical antenna including non-uniform wire surface current effects," IEE Proc.-Microw. Ant. & Prop., vol.146, No.1, pp. 1-5.*

Abramowitz, M., and Stegun, I.A., (1964): *"Handbook of Mathematical Functions," (Washington D.C.: Natl. Bur. Stand., U.S. GPO), p.589.*

Adekola, S.A., (1983): *"On the excitation of a circular loop antenna by travelling- and standing-wave current distributions," Int'l Jour. Electronics, 54, pp. 705-732.*

Adekola, S.A., and Okereke, O.U., (1989): *"Analysis of a circular-loop antenna using moment methods, Int'l Jour. Electronics, vol.66, No.5, pp. 821-834.*

Adekola, S.A., and Okereke, O.U., (1997): *"Moment-method analysis of an end-fire Yagi-antenna array of circular loop elements," Journal of Engineering Research (JER) 5, No.2, pp. 1-28.*

Adekola, S.A., Mowete, A.I., and Ayorinde, A.A., (2001): *"Exclusion of ground planes in thin-wire helical antennas," JER, vol. 9, Nos. 3&4, pp. 13-28.*

Awadalla, K.H., and Maclean, T.S.M., (1978): *"Input impedance of a monopole antenna at the center of a finite ground plane," IEEE Trans. Ant. & Prop., vol.26, No.2, pp. 244-248.*

Balanis, C.A., (1982): *"Antenna Theory: Analysis and Design," John Wiley & Sons, New York, 2nd Edition, pp.1-512.*

Best, S.R., (2004): *"The radiation properties of electrically small folded spherical helix antennas," IEEE Trans. Ant. & Prop., vol. 52, No. 4, pp.953-960.*

Carver, K.R., (1967): *"The helicone - a circularly polarized antenna with low sidelobe level," Proc. IEEE, April, p. 559.*

Chan, K.Y., Hui, H.T., and Yung, E.K.N., (2001): *"Central-fed hemispherical helical antenna," Ant. & Prog. Soc. Int'l Symposium, vol. 4, pp. 545-548.*

Chatterjee, J.S., (1953): *"Radiation field of a conical helix," Jour. Appl. Phys., vol. 24, No.5, pp. 550-559.*

Chen, C.L., (1967): *"Theory of the balanced helical wire antenna," Radio Science, vol.2, No.2, pp 167-190.*

Chow, Y.W., Yung, E.K.N., and Hui, H.T., (2001): *"Bandwidth enhancement of the monopole antenna by using a parasitic normal-mode helix, Int'l J. Electronics, vol. 88, No.5, pp. 587-593.*

Cooper, R., (2001): *"Use of circular polarization to minimize multi-path distortion of signals," Institution of Electrical Engineers (IEE) News, April, p.6.*

Dobbins, J., and Rogers, R.L., (2001): *"An electrically small folded conical helix antenna suitable for HF to VHF communications," IEEE Trans. Ant. & Prop., vol. 49, No. 12, pp.1777-1781.*

Gataullin, Y.V., Zahidova, D.V., and Gataullin, V. Kh., (2004): *"Cost effective application of the helical antenna array for high resolution pictures reception from NOAA polar-orbiting satellites, 55th Int'l Astronautical Congress 2004 – Vancouver, Canada, pp. 1-7.*

Gerst, C.W., and Worden, R.A., (1966): *"Helix antennas take turn for better," Electronics, Aug. 1966, pp. 100-110.*

Glasser, O.J., and Kraus, J.D., (1948): *"Measured impedances of helical beam antennas," Jour. Appl. Phys., Feb., vol. 19, pp. 193-197.*

Hansen, R.C., and Ridgley, R.D., (2001): *"Fields of contra-wound toroidal helix antenna," IEEE Trans. Ant. and Prop., vol.49, No.8, pp. 1138-1141.*

Harrington, R.F., (1961): *"Time-harmonic electromagnetic fields," McGraw- Hill, New York, pp. 1-365.*

Harrington, R.F., (1967): *"Matrix methods for field problems," Proc. IEEE, vol. 55, pp.136-149.*

Harrington, R.F., (1968): *"Field computation by moment methods," The Macmillian Book Company, New York, 125pp.*

Harrington, R.F., and Mautz, M.S., (1968): *"Electromagnetic behaviour of circular wire loops with arbitrary excitation and loading," Proc. IEE, Vol. 115, No.1, pp. 68-77.*

Hayt, W.H., Jr., (1988): *"Engineering Electromagnetics," McGraw-Hill, Inc., USA, 5nd Edition, pp.14-22.*

Hill, D.A., and Wait, J.R., (1977): *"Electromagnetic surface wave propagation over a bonded wire mesh," IEEE Trans. Electromagnetic Compatibility, vol. EMC 19, No.1, pp. 1-7.*

Holtum, A.G., (1960): *"Improving the helical beam antenna," Electronics, Apr. 1960, pp. 99-101.*

Hui, H.T., Chan, K.Y., and Yung, E.K.N., (2001): *"The input impedance and the antenna gain of the spherical helical antenna," IEEE Trans. Ant. and Prop., vol.49, No.8, pp. 1235-1237.*

Hui, H.T., Chan, K.Y., and Yung, E.K.N., (2003): *"The low-profile hemispherical helical antenna with circular polarization radiation over a wide angular range," IEEE Trans. Ant. & Prop., vol. 51, No. 6, pp.1415-1418.*

Hui, H.T., Yung, E.K.N., Law, C.L., Koh, Y.S., and Koh, W.L., (2004): *"Design of a small and low-profile 2 x 2 hemispherical helical antenna array for mobile satellite communications," IEEE Trans. Ant. & Prop., vol. 52, No. 1, pp.346-348.*

IEEE Standard Definitions of Terms for Antennas, (1983): *IEEE Trans. Ant. & Prop., vol. 31, No.6, pp.3-29.*

Johnson, R.C., and Cotton, R.B., (1984): *"A backfire helical feed," IEEE Trans. Ant. & Prop., vol. 32, No.10, pp. 1126-1128.*

Jones, D.S., (1974): *"Numerical methods for antenna problems," Proc. IEE, vol.121, No.7, pp. 573-582.*

Jordan, E.C., and Balmain, K.G., (1968): *"Electromagnetic waves and radiating systems," Prentice-Hall, Inc., New Jersey, Inc., 2nd Edition, pp.1-456.*

Kilgus, C.C., (1969): *"Resonant quadrifilar helix," IEEE Trans. Ant. & Prop., May, pp. 349-351.*

King, H.E., and Wong, J.L., (1975): *"Directivity of a uniformly excited N x N array of directive elements", IEEE Trans. Ant. & Prop., May, pp. 401-404.*

King, H.E., and Wong, J.L., (1980): *"Characteristics of 1 to 8 wavelength uniform helical antennas," IEEE Trans. Ant. & Prop., vol.28, No.2, pp. 291-296.*

King, R.W.P., (1945): *"Electromagnetic Engineering," Mc-Graw-Hill Book Company, Inc., New York, vol. 1, p.271.*

Knudsen, H.L., (1952): *"Radiation field of a square, helical beam antenna," Jour. App. Phys., Apr., vol. 23, No.4, pp. 483-491.*

Kornhauser, E.T., (1951): *"Radiation field of helical antennas with sinusoidal current," Jour. Appl. Phys., Jul., vol.22, No.7, pp. 887-891.*

Kraus, J.D, (1995): *"A helical-beam antenna without a ground plane," IEEE Ant. & Prop. Magazine, vol.37, No.2, p. 45.*

Kraus, J.D., (1947): *"Helical beam antenna," Electronics, Apr., pp. 109- 111.*

Kraus, J.D., (1948): *"Helical beam antennas for wide-band applications," Proc. IRE, Oct., pp. 1236 - 1242.*

Kraus, J.D., (1950): *"Antennas," McGraw-Hill, Inc., USA, 1st Edition, Chapter 7.*

Kraus, J.D., (1988): *"Antennas," McGraw-Hill, Inc., USA, 2nd Edition, pp.1-85, 265-339, 388-408.*

Kraus, J.D., and Williamson, J.C., (1948): *"Characteristics of helical antenna radiating in the axial mode," Jour. Appl. Phys., Jan., vol. 19, pp. 87 - 96.*

Kuo, D.C., and Strait, B.J., (1972): *"Improved programs for analysis of radiation and scattering by configuration of arbitrarily bent wires", Syracuse University Scientific Report No.15, 50pp.*

Leach, S.M., Agius, A.A., and Saunders, S.R., (2000): *"Intelligent quadrifilar helix antenna," IEE Proc. Microw. Ant. & Prop., vol. 147, No.3, pp. 219-223.*

Leat, C.J., (2002): *"Resistively loaded helical antennas for ground-penetrating radar," IEE Proc. Microw. Ant. & Prop., vol. 149, No.4, pp. 204-210.*

Lee, K.F., and Wong, P.F., (1984): *"Directivities of helical antennas radiating in the axial mode," IEE Proc. Microw. Ant. & Prop., vol. 131, No.2, pp. 121-122.*

Letestu, Y., and Sharaiha, A., (2006): *"Broadband folded printed quadrifilar helical antenna," IEEE Trans. Ant. & Prop., vol. 54, No.5, pp.1600-1604.*

Li, L.-W., Jiao, P.-N., Shi, X.-W., and Kong, J.A., (2004): *"Closed-form solution to electromagnetic fields in far zone radiated by toroidal antennas," IEEE Trans. Ant. & Prop., vol. 52, No. 9, pp.2381-2390.*

Lin, Y.T., and Richmond, J.H., (1975): *"EM modeling of aircraft at low frequencies," IEEE Trans. Ant. & Prop., vol.23, No.1, pp. 53-56.*

Markov, G., (1965): *"Antennas," Progress Publishers, Moscow, 1st Edition, pp 355-360.*

Marsh, J.A., (1951): *"Current distributions on helical antennas," Proc. IRE, Jun., pp. 668- 675.*

Maxwell, J.C., (1873): *"A treatise on electricity and magnetism," vol. 1, Dover Publication Inc., New York, USA, pp. 441-445.*

Mei, K.K., (1965): *"On the integral equations of thin wire antennas," IEEE Trans., AP-13, pp. 374-378.*

Miller, E.K., and Burke, G.J., (1992): *"Low-frequency computational electromagnetics for antenna analysis," Proceedings of the IEEE, Vol. 80, No.1, pp. 24-43.*

Miron, D.B., (2001): *"A study of the CTIA based on analytical models," IEEE Trans. Ant. & Prop., vol. 49, No. 8, pp.1130-1137.*

Munk, B.A, and Peters, Jr., L., (1968): *"A helical launcher for the helical antenna," IEEE Trans. Ant. & Prop., May, pp. 362-363.*

Nakano, H., and Mimaki, H, (1997): *"Axial ratio of a curl antenna," IEE Proc. Microw. Ant. & Prop., vol. 144, No.6, pp.488-490.*

Nakano, H., and Mimaki, H., (1995): *"Radiation from a short helical antenna backed by a cavity," Electronics Letters, vol.31, No. 8, pp.602-604.*

Nakano, H., and Nakayama, K., (1999): *"A curved spiral antenna above a conducting cylinder," IEEE Trans. Ant. & Prop., vol.47, No.1, pp. 3-8.*

Nakano, H., and Yamauchi, J., (1980): *"Radiation characteristics of helix antenna with parasitic elements," Electronics Letters, vol.16, No.18, pp. 687-688.*

Nakano, H., and Yamauchi, J., (1982): *"Characteristics of modified spiral and helical antennas," IEE Proc. Microw. Ant. & Prop., vol.129, No. 5, pp. 232-237.*

Nakano, H., Hitosugi, K., Tatsuzawa, N., Togashi, D., Mimaki, H., and Yamauchi, J., (2005): *"Effects on the radiation characteristics of using a corrugated reflector with a helical antenna and an electromagnetic band-gap reflector with a spiral antenna," IEEE Trans. Ant. & Prop., vol. 53, No. 1, pp.191-199.*

Nakano, H., Iio, S., and Yamauchi, J., (1984): *"Frequency characteristics of tapered backfire helical antenna with loaded termination," IEE Proc. Microw. Ant. & Prop., vol.131, No.3, pp. 147-152.*

Nakano, H., Iio, S., and Yamauchi, J., (1993): *"Improvement in front-to-back ratio of a bifilar backfire helix by a flared open end," IEEE Trans. Ant. & Prop., vol.41, No.11, pp. 1591-1595.*

Nakano, H., Ikeda, N., Wu, Y.-Y., Suzuki, R., Mimaki, H., and Yamauchi, J., (1998): *"Realization of dual-frequency and wide-band VSWR performances using normal-mode helical and inverted-F antennas," IEEE Trans. Ant. & Prop., vol.46, No.6, pp. 788-793.*

Nakano, H., Mikawa, T., and Yamauchi, J., (1985): *"Investigation of a short conical helix antenna," IEEE Trans. Ant. & Prop., vol. 33, No.10, pp. 1157-1160.*

Nakano, H., Okabe, Y., Mimaki, H., and Yamauchi, J., (2003): *"A monfilar spiral antenna excited through a helical wire," IEEE Trans. Ant. & Prop., vol. 51, No. 3, pp.661-664.*

Nakano, H., Samada, Y., and Yamauchi, J., (1986): *"Axial mode helical antennas," IEEE Trans. Ant. & Prop., vol. 34, No.9, pp. 1143-1148.*

Nakano, H., Yamane, T., and Yamauchi, J., (1983): *"Directive properties of parasitic helix and its application to circularly polarized antenna," IEE Proc. Microw. Ant. & Prop., vol.130, No. 6, pp. 391-396.*

Nakano, H., Yamauchi, J., and Iio, S., (1982): *"Tapered backfire helical antenna with loaded termination," Electronics Letters, vol.18, No.4, pp.158-159.*

Nakano, H., Yamauchi, J., and Mimaki, H., (1988): *"Backfire radiation from a monofilar helix with a small ground plane," IEEE Trans. Ant. & Prop., vol.36, No.10, pp. 1359-1364.*

Nakano, H., Yamauchi, J., Mimaki, H., and Iio, S., (1983): *"Backfire bifilar helical antenna with tapered feed end," Int'l.J. Electronics, vol.54, No.2, pp. 279-286.*

Nakano, N., Asaka, N, and Yamauchi, J., (1984): *"Short helical antenna array fed from a waveguide," IEEE Trans. Ant. & Prop., vol.-32, No.8, pp. 836-840.*

Patton, W.T., (1963): *"The backfire bifilar helical antenna," Ph.D. Thesis, University of Illinois, 113pp.*

Pertl, F.A., Smith, J.E., and Nutter, R.S., Jr., (2005): *"An analysis of the CTHA's resonance currents and the resulting radiation shapes," IEEE Trans. Ant. & Prop., vol. 53, No. 1, pp.377-385.*

Phongcharoenpanich, C., Levtwiviyaprapa, T., Lamultree, S., Wounchoum, P., Kosulvit, S., and Krairiksh, M., (2002): *"Characteristics of a helical array antenna radiating circularly polarized conical beam," Jour. KMITNB, vol. 12, No. 1, pp. 52-58.*

Pierce, J.R., and Field, L.M., (1947): *"Traveling-wave tubes," Proceedings of the I.R.E., Feb., pp. 108-123.*

Pocklington, H.C., (1897): *"Electrical oscillations in wire," Camb. Philos. Soc. Proc., vol. 9, pp. 324-332.*

Richmond, J.H., (1965): *"Digital computer solutions of the rigorous equations for scattering problems," Proceedings of the IEEE, August, pp. 796-804.*

Richmond, J.H., (1966): *"A wire-grid model for scattering by conducting bodies," IEEE Trans. Ant. & Prop., vol. AP-14, pp. 782-786.*

Rogers, S.D., and Butler, C.M., (2002): *"Wide-band sleeve-cage and sleeve-helical antennas," IEEE Trans. Ant. & Prop., vol. 50, No. 10, pp.1409-1444.*

Rowley, J.T., Waterhouse, R.B., and Joyner, K.H., (2002): *"Modeling of normal-mode helical antennas at 900MHz and 1.8GHz for mobile communications handsets using the FDTD technique," IEEE Trans. Ant. & Prop., vol. 50, No.6, pp. 812-819.*

Roy, M.N., (1969): *"Radiation characteristics of a helical ground plane antenna," Int'l Jour. Electronics, vol.27, No.2, pp. 177-183.*

Rumsey, V.H., (1954): *"Reaction concept in electromagnetic theory," Phys. Rev., Vol. 94, No. 6, pp. 1483-1491.*

Safaai-Jazi, A., and Cardoso, J.C., (1996): *"Radiation characteristics of a spherical helical antenna," IEE Proc.- Microw. Ant. Prop., vol. 143, No. 1, pp. 7-12.*

Schrank, H., (1986): *"A centennial of electromagnetics", IEEE Ant. & Prop. Society Newsletter, Dec., pp. 35-38.*

Sengupta, D.L., (1958): *"The radiation characteristics of a zig-zag antenna," IRE Trans. Ant & Prop., April, pp. 191-194.*

Sharaiha, A., and Terret, C., (1993): *"Analysis of quadrifilar resonant printed helical antenna for mobile communications," IEE Proc. Microw. Ant. & Prop., vol.140, No.4, pp. 269-273.*

Shumaker, P.K., Ho, C.H., and Smith, K.B., (1996): *"Printed half-wavelength quadrifilar helix antenna for GPS marine applications," Electronics Letters, vol. 32, No.3, pp. 153-154.*

Stutzman, W.L., and Thiele, G.A., (1981): *"Antenna theory and design," John Wiley & Sons, New York, pp.306-374.*

Sun, J., Wang, C.-F., Li, L.-W., and Leong, M.-S., (2004): *Characterizing helical microstrip antenna mounted on a dielectric-coated circular cylinder using MoM and closed-form Green's function, 2004, IEEE Trans. Ant. & Wir. Prop. Letters, vol. 3, pp.15-18.*

Taylor, C.D. and Harrison, C.W., (1974): *"On thin-wire multiturn loop antennas," IEEE Trans. Ant. & Prop., vol. 22, No. 3, pp. 407- 413.*

Tranquilla, J.M., and Best, S.R., (1990): *"A study of the quadrifilar helix antenna for global positioning system (GPS) applications," IEEE Trans. Ant. & Prop., vol.38, No.10, pp. 1545-1550.*

Tsandoulas, G.N., (1969): *"Radiation from elliptic current rings," IEEE Trans. Ant. & Prop., vol. 17, No. 1, pp. 31-36.*

Volakis, J.L., Chatterjee, A., Kempel, L.C., (1998): *"Finite element method for electromagnetics: antennas, microwave circuits, and scattering applications," Wiley-IEEE Press, 368pp.*

Walter, C.H., (1970): *"Traveling wave antennas," Dover, New York, pp. 331-333.*

Wang, D.X., Yung, E.K.N., and Chen, R.S., (2003): *"Efficient analysis of wire antennas and scatterers with arbitrary shape," IEEE Antennas & Wireless Propagation Letters, vol. 2, pp. 107-110.*

Wettergren, J., and Slättman, P., (1996): *"Electric field integral equation for cylindrical structures," IEE Proc. Microw. Ant. & Prop., vol. 143, No.2, pp. 147-151.*

Wheeler, H.A., (1947): *"A helical antenna for circular polarization," Proc. IRE, 35, pp. 1484-1488.*

Williamson, M., (2002): *"Disaster watch," IEE Review, July, pp. 19-24.*

Wong, J.Y., and Loh, S.C., (1959): *"Radiation field of an elliptical helical antenna," IRE Trans. Ant. & Prop., Jan., vol.7, pp.46-52.*

Yamauchi, J., and Nakano, H., (1981): *"Axial ratio of balanced helical antenna and ellipticity measurement of incident wave," Electronics Letters, vol.17, No.11, pp. 365-366.*

Zimmerman, Jr., R.K., (2000): *"Traveling-wave analysis of a bifilar scanning helical antenna," IEEE Trans. Ant. & Prop., vol.48, No.6, pp. 1007-1009.*